MN DEPT OF TRANSPORTATION
3 0314 00023 7171

91-04

Vibration Spectroscopy For Rigid Pavement Joint Assessment

CTS
TE
251.5
P35
1990

Minnesota Department of Transportation

Dept. of Civil and Mineral Engineering
University of Minnesota

REPORT DOCUMENTATION PAGE	1. Report No. MN/RD - 91/04	2.	3. Recipient's Accession No.
4. Title and Subtitle Vibration Spectroscopy For Rigid Pavement Joint Assessment			5. Report Date August, 1990
			6.
7. Author(s) Lucio Palmieri, Prof. Theodor Krauthammer			8. Performing Organization Rept. No. 9RD0004
9. Performing Organization Name and Address University of Minnesota Dept. of Civil and Mineral Engineering 122 Civil and Mineral Engineering Bldg. 500 Pillsbury Drive, S.E. Minneapolis, MN 55455-0220			10. Project/Task/Work Unit No. 11. Contract(C) or Grant(G) No. (C) 64988 (G)
12. Sponsoring Organization Name and Address Minnesota Department of Transportation Materials and Research Laboratory 1400 Gervais Avenue Maplewood, Minnesota 55109			13. Type of Report & Period Covered Final Report 1988-1990 14.

15. Supplementary Notes

16. Abstract (Limit: 200 words)

This study was conducted with the aim of improving the state of knowledge on the behavior of joints in concrete pavements, and to explore the feasibility of developing a non-destructive testing technique based on the frequency response of dynamically loaded joints. One of the objectives of the present study was to experimentally investigate the existence of a relationship between load transfer capacity of a joint in rigid pavements and its dynamic response. the experimental study involved the application of an impact testing approach for the evaluation of two test systems. One system represented an ideal condition of full load transfer across a joint, while the other system was used to simulate variable load transfer conditions. Acceleration-time histories captured from both sides of the joint, under short load pulses, were used for analysis both in the time and frequency domains. These results provided a comprehensive description of the joint response characteristics, and enabled the derivation of a clear relationship between the response frequencies and the joint's shear transfer capabilities. These results may be used as the starting point for the development of a precise non-destructive testing method for a wide range of cases in which shear transfer across discontinuities in concrete systems is a principal load resisting mechanism. Specific conclusions and recommendations on future developments have been provided.

17. Document Analysis a.Descriptors
Frequency Analysis
Impact Testing
Pavement Joints

b.Identifiers/Open-Ended Terms

c.COSATI Field/Group

18. Availability Statement No restrictions. This document is available through the National Technical Information Services, Springfield, VA 22161	19. Security Class (This Report) Unclassified	21. No. of Pages 211
	20. Security Class (This Page) Unclassified	22. Price

VIBRATION SPECTROSCOPY FOR RIGID PAVEMENT JOINT ASSESSMENT

Final Report

Prepared by

Lucio Palmieri

Prof. Theodor Krauthammer

Department of Civil and Mineral Engineering
University of Minnesota

Submitted to

Research Administration and Development Section
Office of Materials and Research
Minnesota Department of Transportation

August 1990

This report represents the results of research conducted by the authors and does not necessarily reflect the official views or policy of Mn/DOT. This report does not contain a standard or specified technique.

ACKNOWLEDGEMENTS

The authors wish to acknowledge the assistance and cooperation of the staff at the Minnesota Department of Transportation, which administered contract MNDOT/64988 T.O #39 under which most of the work was performed.

Also the authors wish to express their thanks to Mr. Kevin P. Hoostal, of Trask Engineering Inc., and to Mr. Greg Sherar, of the computer group in the department of Civil and Mineral Engineering at the University of Minnesota, for their helpful assistance in many technical problems.

EXECUTIVE SUMMARY

This study was conducted for the Minnesota Department of Transportation with the aim of improving the state of knowledge on the behavior of joints in concrete pavements, and to explore the feasibility of developing a non-destructive testing technique based on the frequency response of dynamically loaded joints. One of the objectives of the present study was to experimentally investigate the existence of a relationship between load transfer capacity of a joint in rigid pavements and its dynamic response, and the obtained results confirm the existence of such a relationship.

The experimental study involved the application of an impact testing approach for the evaluation of two test systems. One system represented an ideal condition of full load transfer across a joint, while the other system was used to simulate variable load transfer conditions. Acceleration-time histories captured from both sides of the joint, under short load pulses, were used for analysis both in the time and frequency domains. These results provided a comprehensive description of the joint response characteristics, and enabled the derivation of a clear relationship between the response frequencies and the joint's shear transfer capabilities. These results may be used as the starting point for the development of a precise non-destructive testing method for a wide range of cases in which shear transfer across discontinuities in concrete systems is a principal load resisting mechanism.

Specific conclusions and recommendations on future developments and corresponding parametric studies have been provided.

TABLE OF CONTENTS

LIST OF TABLES

LIST OF FIGURES

CHAPTER 1

INTRODUCTION

1.1 Objectives

Pavement maintenance for insuring acceptable serviceability conditions, is one of the major tasks for highway engineers. The assessment of a pavement's internal conditions is a problem without an easy solution. The determination of such conditions is usually simple for cases exhibiting severe damages, but it becomes more difficult to assess pavements when the aim is to detect the internal conditions of a pavement prior to the extensive damage state. In rigid pavements, the most critical points are the joints. These are geometrical discontinuities in the pavement structure, where usually spalling of concrete, cracking and pumping of the underneath soil occur. In the last decades significant efforts have been undertaken for the development of non-destructive testing techniques for pavements evaluation, as indicated by a rich bibliography. Most of these techniques provide information on pavement deflections, a parameter largely used for the pavement structural evaluation. However, deflection measurements are particularly suitable for the analysis of flexible pavements, or layered systems, and they can be used for estimating the layer stiffnesses. The behavior of rigid pavements is different, and the deflections are mostly due to compressibility of the base rather than of the concrete slab. Furthermore, deflections depends on the modality of loading and on the magnitude of the load, and one of the major problems is to identify an experimental loading mode representative of traffic loads.

The objective of this study is to initiate the development of a non-destructive testing (NDT) method for the assessment of shear transfer conditions in a rigid pavement joint, based on the frequency analysis of its dynamic response. The ultimate goal of this phase of study is to support the development of a new testing device, and a testing approach, for non destructive evaluations of pavement joints and bridge decks. Development and implementation of this approach is expected to save significant resources in the continuous effort of managing bridge and roadway maintenance.

1.2 Scope

The initial part of the study was devoted to exploring the feasibility of the approach, to a careful assessment of the theoretical aspects of the problem and to laboratory tests for demonstrating the proposed approach.

The study reported here, however, focuses on the experimental observations of the relationship between shear transfer capabilities across a simulated pavement joint and the frequency response in terms of range of frequencies and amplitude of vibrations transmitted from one side of the joint to the other. The analysis of the data recorded during the tests is performed both in the time domain and in the frequency domain, and a correlation between the results obtained in these two domains is presented. Also conclusion are presented about the proposed approach and the findings.

Chapter 2

BACKGROUND

2.1 General Classification of Pavements

A general classification of road and airfield pavements distinguishes between rigid and flexible pavements; their behavior is different under loading, as are the corresponding nature of the materials. The main component of a rigid pavement is concrete with a higher modulus of elasticity than the subgrade soil, and with an appreciable tensile strength. The goal of designing a rigid pavement is the realization of a stiff and strong structure able to transmit and to distribute vertical loads to the subgrade, in a manner that insures acceptable stresses in the subgrade. On the other hand a flexible pavement is a layered system, the pavement material is softer than concrete, and the effect of loading is progressively reduced with depth.

A more accurate classification of pavements has to include the so called semi-rigid or semi-flexible pavements. This group includes pavements that have cement-treated base (CTB). This type of base guarantees a very good load-spreading ability, and for this reason they are often used for roads with heavy traffic. However, the use of cement-treated bases, together with a stiffer pavement structure, introduces problems stemming from the brittle nature of concrete.

From the point of view of the general behavior, a pavement (flexible, rigid or semirigid) must provide, together with a capability to transfer vertical loads, the ability to transfer horizontal loads induced by the wheel-road interaction. It must be durable under the extremes of weather and chemical effects (such as de-icing salt), and it should retain its desired properties over the years. It must guarantee a good riding standard in terms of comfort and safety.

2.2 Concrete Properties

Concrete is a construction material that associates compressive and tensile strength; the latter being usually less than 20% of the compressive strength. Although concrete is seldom subjected to only uniaxial stress, the parameters characterizing its properties are generally obtained on the bases of uniaxial tests. According to Park and Paulay (1975), once that the compressive strength of concrete f'_c is known from tests on standard cylinders specimens, it is possible evaluate the modulus of elasticity E_c using the following relation

$$E_c = 57000 \sqrt{f'_c} \ \text{psi} \tag{2.1}$$

The modulus of elasticity of concrete is also a function of the strain rate; according to Newmark and Rosenblueth (1971) in dynamic analysis, the modulus of elasticity can be up to 1.3 times the static value. As reported by Park and Paulay (1975), the influence of the strain rate is related to the concrete strength: for low strength concrete (2.5 ksi) the ratio of the dynamic modulus of elasticity to the static one is about 1.62, for higher strength concrete (6.5 ksi) this ratio is 1.4.

<u>The tensile strength in flexure</u>, or modulus of rupture f_r, can be obtained from the approximate relation

$$f_r = K \sqrt{f'_c} \ \text{psi} \tag{2.2}$$

where the constant K can range between 7 and 13; a value of 7.5 is often assumed.

<u>The Poisson's coefficient</u>, defined as the ratio in condition of uniaxial loading between the transverse strain and the strain in the direction of application of the load, can be assumed to be between 0.10 and 0.30. The value of the Poisson's ratio can be determined both with static or dynamic tests.

2.2.1 Shear Friction

Application of shear to planes of discontinuity (cracks, interfaces between different materials, interfaces between concretes casted at different times), causes relative slip between the two sides of the discontinuity. Different is the behavior according to the presence or not of reinforcement crossing the interface. As reported by MacGregor (1988), if reinforcement is present, the shear is transferred across the interface mainly by two mechanisms:

1. Under the shear action the surfaces tend to separate and/or to slip; in both cases the reinforcement is subjected to tension, for equilibrium the concrete is subjected to compression. Consequent to these compressive stresses, friction develops in the interface.
2. Aggregate interlock between the particles of concrete and by dowel action of the reinforcement crossing the surface.

According to Mattock and Hawkins (1972), the shear strength V_n when shear friction reinforcement is perpendicular to the shear plane, can be evaluated from

$$V_n = 0.8\ A_{vf} f_y + A_c K_1 \tag{2.3}$$

where A_{vf} : area of reinforcement crossing the surface,

A_c : area of concrete surface resisting the friction,

K_1 : constant equal to 400 for normal-weight concrete,

f_y : yield strength of reinforcement.

The first term represents mechanism 1 (friction), and the coefficient of friction 0.8 is taken for concrete sliding on concrete; the last term represents mechanism 2.

2.3 Concrete Pavements

In concrete roads the pavements acts as the main structural layer and at the same time provides the running surface. Because of the modality of construction associated with the characteristic of the materials, concrete roads do not have a uniform continuous running surface like those of flexible roads. The continuity of the surface is frequently interrupted by longitudinal and transverse joints that are needed to accommodate the expansion (thermal) or contraction (thermal, shrinkage,..) of concrete. Such joints prevent the development of excessively high stresses in the material. In general, the structural performance of a well designed concrete road is excellent; the defects are usually confined to minor construction failures, such as cracking or spalling at joints. Some of the features that have been criticized in concrete roads are:

- Poor riding quality;
- High initial cost;
- Poor ability to retain a surface texture that gives satisfactory

resistance to skidding without generating excessive noise.

Concrete pavements can be built using reinforced or unreinforced concrete. As reported by Williams (1986), in unreinforced concrete pavements the slabs are required to be relatively thick and short; where the thickness reduces the stresses and the short length ensures that cracks do not develop between the closely spaced joints. In reinforced concrete pavements, however, the slabs are longer, transverse cracks are allowed to form, but the reinforcement, usually in the form of a steel mesh, will control the width of the cracks.

According to Williams (1986) and Yoder and Witczak (1975), who discussed design procedures, several parameters must be taken into account to determine the structural characteristics. For example the slab thickness, presence and amount of reinforcement, type of joints and their spacing, type of sub-base, mix details, etc. Among the main aspects to consider are traffic conditions, subgrade conditions and environmental effects.

2.3.1 Stresses in Concrete Pavements

The structural performance of concrete pavements is governed by tensile stresses and, in certain high temperature conditions by compressive stresses.

Various causes induce stresses in concrete, among them:

Wheel-loading effect: A fundamental study of this problem was done by Westergaard (1926), (1929), (1947). Among the findings from Westergaard's analysis are the location and magnitude of tensile stresses in the slab, and these results are summarized by Westergaard's formula that had been modified based on field experience, as reported by Williams (1986):

$$f_i = 0.275(1+\sigma)(P/h^2)[\log_{10}(Eh^3/kb^4) - 54.54(l/n)^2N] \quad (2.4)$$

$$f_e = 0.529(1+0.54\sigma)(P/h^2)[\log_{10}(Eh^3/kb^4)+\log_{10}(b/(1-\sigma^2))-1.0792] \quad (2.5)$$

$$f_c = (3P/h^2)\{1-[12(1-\sigma^2)k/Eh^3]^{0.3}(a\sqrt{2})^{1.2}\} \quad (2.6)$$

where:

f_i = stress developed under a wheel-load applied at the interior of a slab, lb f/in^2;

f_e = stress developed under a wheel load-applied at the edge of a slab, lb f/in^2;

f_c = stress developed in a slab when a wheel-load is applied at a corner, lb f/in^2;

σ = Poisson's ratio for concrete;

P = wheel-load, lb f;

h = slab thickness, inches;

E = modulus of elasticity of concrete, lb f/in^2;

k = modulus of subgrade reaction, lb f/in^2/in;

b = radius of equivalent distribution of pressure, inches

= a, the radius of tire contact if $a \geq 1.724$ h

= $(1.6a^2+h^2)^{0.5}-0.675h$ if $a < 1.724$ h;

l = $[(Eh^3)/12(1-\sigma^2)k]^{1/4}$, a factor known as the radius of relative stiffness which occurs repeatedly in the theory;

n = a factor, with a suggested value of 51, governed by the maximum distance from the center of the load within which a redistribution of subgrade reaction occurs;

N = a factor, with a suggested value of 0.2, related to the ratio in the reduction of maximum deflection.

These equations indicate that the magnitude of the stresses are dependent on the thickness of the slab, however, the induced stress is relatively insensitive to the bearing capacity of the subgrade.

A good design should preclude edge stresses. This can be obtained in several ways; among the most common are the presence of a 'sleeper' beams under the joints and flat curbs on the slab preventing the vehicles to run on the edges.

Temperature effects: There are two main effects to be taken into account:

- Changes in length of the slab due to seasonal temperature fluctuation, that are opposed by friction against the supporting layer.
- Temperature gradient through the depth of a slab as a consequence of quick change, day-night, in temperature. This phenomenon can cause a curling of the slab which is opposed by the weight of the slab itself and by friction at joints.

An analytical approach for this problem was given by Westergaard (1927); a linear temperature variation with depth was assumed for deriving the following expression:

$$f_w = \frac{E\alpha t}{2(1-\sigma)} \tag{2.7}$$

where f_W = maximum warping stress

E = modulus of elasticity of concrete

σ = Poisson's ratio for concrete

α = thermal coefficient for concrete

t = temperature difference between the top and bottom of the slab.

Numerical evaluation of these stresses can show that they are capable of inducing cracking. They can be reduced by providing closely spaced joints, but they always remain at a level such that they must be taken into account.

As a general rule, unreinforced concrete slabs must be thick enough to resist traffic induced load cracking, and short enough to ensure that thermal stresses do not increase significantly the traffic stresses.

2.3.2 Joints

Joints are locations where geometric discontinuities are introduced in the slab, and they are the weakest part of a concrete pavement. A classification given by Williams (1986), defines the type of joint on the basis of their functions:

- Free Joints: to allow longitudinal movements.
- Tied Joints: to prevent longitudinal movements.
- Warping Joints: to allow some longitudinal movements and some rotations.
- Dowelled Joints, or Keyed Joints: to prevent vertical movements.

A classification given By Yoder and Witczak (1975) divides joints into the following four basic groups, as illustrated in Figure 2.1:

Contraction Joint : This joint creates a weaker section in the concrete slab, determining a position were cracking consequent to shrinkage and contraction will probably occur. Once the crack has occurred the load transfer capability is assured by aggregate interlock, if no dowel bars have been used, or by aggregate interlock and dowel bars in the case of dowelled joints. A contraction joint consists of a grove at the pavement surface. This grove can be created by sawing the concrete once it is hard enough, or placing a separating strip in the uncured concrete and removing it as soon as the initial setting of the concrete has taken place.

Expansion Joint : It is a clean break through the depth of the slab to permit expansion. Since in this joint aggregate interlock cannot take place, it is necessary to provide some type of a load transfer device. This is usually provided in the form of dowel bars bonded in one slab and allowed to move in the other side of the joint by mean of expansion caps embedded in the concrete. Expansion joints allow expansion and contraction to take place. Today they are often omitted because they are more difficult to provide and more expensive than contraction joints. Furthermore, with the omission of this type of joint the possibility to have aggregate interlock is increased. The absence of this joint does not allow an excessive opening of contraction joints. Often, instead of expansion joints, aggregates with low coefficient of thermal expansion are used, but this can cause blow-ups under high expansion stresses. The expansion of the concrete slab under high temperature gradients, that is not permitted because of the absence of this type of joint, determines a lifting of the slab from the subbase.

<u>Construction Joint :</u> It is usually of keyed type and contains dowel bars for the transfer of the load across the joint. It is built at the transition between the old and the new construction.

<u>Hinge or Warping Joint :</u> This kind of joint controls cracking along the center line of the pavement. The characteristics of the joint change according to the method of pouring the concrete slab.

2.3.3 Load Transfer

The provision of load transfer has to be one of the main concerns in concrete pavements design. Load transfer is provided by shear forces across a discontinuity between adjacent edges. In the case of a crack the action of transferring the load across the crack by interaction of the irregular faces is called aggregate interlock, as illustrated in Figure 2.2. In reinforced concrete pavements one of the functions of the reinforcing steel mesh is to resist the opening of the cracks, and to preserve the aggregate interlock. This mechanism is essentially the same as the one that develops in reinforced concrete beams described, together with others, in the ACI-ASCE Committee 426 report (1973).

The development of good aggregate interlock can greatly prevent the development of critical edge stresses. In the case of joints where, because of the regularity of the edge's faces, it is not possible to develop aggregate interlock, the loads must be transferred in some other way. A widely accepted solution is to provide steel dowel bars across the discontinuity, as shown in Figure 2.3: the edge stress that develops is about one half of the value it would have otherwise reached.

2.3.4 Load Transfer Efficiency

Load transfer efficiency is defined as the ratio of the deflection of the unloaded side of the joint divided by the deflection of the loaded side of the joint. For convenience this ratio is usually expressed as a percentage. This parameter is clearly related to the joint shear transfer capacity. From the study by Foxworthy (1985) it has been shown that the load transfer efficiency of a joint is closely related to the stresses that are developed on the bottom of the slab and, therefore, on the performance of the slab under loading. To measure the load transfer efficiency several devices are available; one, the Falling Weight Deflectometer (FWD), will be described in Section 2.7. Previous analysis by Tabaytaie and Barenberg (1980) have showed that the load transfer efficiency across a joint affects both the maximum stresses in the slab, especially under edge and corner loading conditions.

Figure 2.4 shows the effect of the load transfer efficiency of a joint on the stresses at the joint when the load is applied near the joint. Since the stress transmitted to the subgrade is the deflection times K, the subgrade stress will be affected in the same manner as the deflection. The critical point to note in the in Figure 2.4 is that just a small reduction from a full joint efficiency results in a significant change in the stress ratio. Many benefits could be gained by designing joints with higher load transfer efficiency. For example Barenberg and Arntzen (1981) showed (see Table 1) a relationship between maximum stresses and joint efficiency for a plain jointed pavement slab 21 inches thick with 6 inches of asphalt-concrete (AC) subbase for several loading conditions indicated.

Joint efficiency is dependent on many factors: temperature, moisture, frost but not on the load magnitude. It has been shown by Foxwhorty (1985) that this factor does not affect appreciably the joint efficiency (at least in the load range of the FWD testing).

As structural systems, rigid pavements can be supported by a base or by a subgrade soil; in both case this leads one to model pavements as plates on elastic foundations. Often, finite element analyses are performed on rigid and flexible pavements for capturing non-linear behaviors of such systems. In general, plate theories and finite-elements approaches are used in rigid pavement design.

2.4 Theory of Plate on Elastic Foundation

The theory of plate on elastic foundation, as presented by Timoshenko and Woinowsky-Krieger (1959), includes a basic assumption that the reaction of the subgrade is at every point proportional to the deflection w of the plate. The assumption, good for incoherent types of soil, can lead to crude approximations in the case of coherent types of soil where the pressure in a certain point is affected by the pressure in the adjacent positions.

With this hypothesis the reaction of the subgrade can be evaluated as k*w where k, called Modulus of Foundation and expressed as a pressure per unit length, is a parameter depending on the physical properties of the subgrade and its conditions. A diagram with values of k for different types of soil is given in Timoshenko and Woinowsky-Krieger (1959).

In the case of rectangular plates the differential equation for the deflections, as given by Timoshenko and Woinowsky-Krieger (1959), is

$$\frac{\partial^4 w}{\partial x^4} + 2\frac{\partial^4 w}{\partial x^2 \partial y^2} + \frac{\partial^4 w}{\partial y^4} = \frac{q}{D} - \frac{kw}{D} \tag{2.8}$$

with q : intensity of the lateral load

h : thickness of the plate

v : Poisson's Ratio

$D = E\ h^2\ /\ 12(1-\nu)$

In the particular case of one vertical load P acting on an infinitely large plate the maximum deflection can be found to be

$$w_{max} = \frac{P\ \lambda^2}{\pi\ k\ 2\sqrt{\ }2}\int_0^\infty \frac{1}{\sqrt{2}}\ \frac{du}{1+u^2} \approx \frac{P\ \lambda^2}{8\ k} \tag{2.9}$$

where

$$\lambda^4 = k\ /\ D$$

Once the magnitude of the deflection has been obtained, the pressure on the subgrade is obtained as

$$p_{max} = k\ w_{max} = P\ \lambda^2\ /\ 8 = (P/8) * (\sqrt{(k/D)}) \tag{2.10}$$

In this derivation the hypothesis of independence of the pressure at one point from the pressure at adjacent points has been adopted. If this condition is not acceptable (i.e. in coherent subgrades) a more accurate computation can be performed with the following assumptions:

- The foundation has the properties of a semi-infinite elastic body.
- The plate rests on the subgrade without friction.
- A perfect contact between the plate and the foundation also exists in the case of a negative mutual pressure.

With these assumptions Timoshenko and Woinowsky-Krieger (1959) derived another solution for an infinitely large plate in conditions of axial symmetry; in the derivation polar coordinates r, φ have been used, and the plate equation in this case is

$$D \Delta \Delta w(r) = q(r) - p(r) \tag{2.11}$$

where $q(r)$: given surface loading.

$p(r)$: reaction of the subgrade.

Equation (2.11) is satisfied by the expression

$$w(r) = \int_0^\infty \frac{Q(\alpha)\ K(\alpha)\ J_0(\alpha r)\ \alpha}{1 + D\ \alpha^4\ K(\alpha)}\ d\alpha \tag{2.12}$$

where J_0 = Bessel function of order zero.

$K(\alpha)$ = term depending on the nature of the subgrade:

$$K(\alpha) = \int_0^\infty 2\ \pi\ s\ K_0(s)\ J_0(\alpha s)\ ds \tag{2.13}$$

here

$$K_0(s) = K_0\ [(r^2 + \rho^2 - 2\rho r\cos\varphi)^{1/2}] \tag{2.14}$$

with s distance between points $(r,0)$ and (ρ,φ).

$$Q(\alpha) = P\ J_1(\alpha c)\ /\ \pi\ c\ \alpha \tag{2.15}$$

here J_1 = Bessel function of order 1.

c : radius of the circular area over which the load P is assumed to be uniformly distributed.

The problem of a large plate resting on an elastic foundation and loaded with vertical forces acting at equidistant points along the longitudinal axis has also been discussed by Westergaard (1926), (1929), (1933). Using the thick plate theory he obtained the following relations

$$(\sigma)_{max} = 0.275\ (1+\nu)\ (p/h^2)\ \log_{10}(Eh^3/Kb^4) \tag{2.16}$$

where

$$b = \sqrt{(0.5\ u^2 + h^2)} - 0.675\ h \qquad \text{if} \quad u < 3.025\ h$$

$$b = 0.57\ u \qquad \text{if} \quad u > 3.025\ h$$

here u is the length of the side of the square over which the load P is assumed to be uniformly distributed.

These solutions were proposed for static loading conditions. However, the problem studied here is that of a dynamically loaded pavement. Under such conditions the loads are expected to be applied in an impulsive manner, and the effects will propagate in the pavement. For this reason, it is essential to review some aspects of wave propagation.

2.5 Wave Propagation

In the study of wave propagation in an infinite, elastic, isotropic medium with no boundaries, according to Kolsky (1963) two main types of waves can be identified:

Irrotational or dilatation waves : Mainly associated with changes in volume of the medium, they travel through, but to some extent they also involve a distortion of the medium. In the propagation of these waves the medium is subjected to compression and shear. The propagation velocity c of these waves can be expressed as:

$$c = \sqrt{\frac{\lambda + 2\mu}{\rho}} \tag{2.17}$$

where

λ , μ are the Lamé's constants, they define completely the elastic behavior of an isotropic solid;

ρ is the density.

Equivoluminal or distortion waves : This kind of waves has no dilatational components, only rotational. This means that an element of the medium is subjected to a rotation but its volume will not change. The velocity of these waves is:

$$c = \sqrt{\frac{\mu}{\rho}} \tag{2.18}$$

When the medium has to be considered semi-infinite, a surface or more surfaces are present, then several kinds of waves can be identified:

Primary waves or P-waves: Also called longitudinal waves, are mainly associated with the compression of the medium. These waves can be included in the group of the dilatational waves;

Secondary waves or S-waves: Defined also as shear waves. They belong to the category of the distortion waves;

Rayleigh waves : These waves propagate only close to the surface, their effect decreases rapidly with depth, thus the definition of skin effect; their path is elliptical, and one of their most important characteristics is that they propagate without energy loss. Rayleigh waves have both horizontal and vertical components;

Love waves : These waves have no vertical component and they propagate with vibrations parallel to the front of the wave.

The velocity of propagation of these waves is dependent on the physical properties of the media they are travelling through; one of the factors that has a great influence on wave velocity is the Poisson's ratio as pointed by Yoder and Witczak (1975).

2.5.1 Reflection and Refraction of Waves

The phenomena associated with the propagation of waves through boundary between different media cannot be listed in one group; the characteristics of these phenomena will be different depending on the nature of the two media and on the types of waves being considered. In general when a wave hits a boundary four different waves are generated, a wave of each type (dilatation and distortion) is reflected and one of each type is refracted.

In the case of a dilatation wave hitting a free surface it can be found that both a dilatation wave and a distortion wave are reflected. The angle α_2 that the reflected dilatation wave will form with the normal to the surface is the same as the angle α_1 of incidence of the original wave; the angle β_2 of the reflected distortion wave is given by Kolsky (1963):

$$\frac{\sin \alpha_1}{\sin \beta_2} = \frac{c_1}{c_2} \tag{2.19}$$

where c_1 and c_2 are the velocities of dilatation and distortion waves.

Similar relations are given by Kolsky (1963) for the case of a distortion wave incident on a free boundary and for the cases of distortion and dilatation waves incident on the interface between two media.

2.5.2 Reflection and Transmission of Wave in Bounded Elastic Media

Considering the case of wave propagation in thin rods and bars, three types of vibrations can occur: longitudinal, torsional and lateral.

For longitudinal vibrations of elastic rods, with conservation of plane sections, assuming uniform distribution of stresses over the cross section and lateral dimension of the bar smaller then the length of the elastic wave, the following results can be obtained.

Introducing the following definitions:

$r_\sigma = \sigma_r / \sigma_i$: reflection factor for stresses;

$t_\sigma = \sigma_t \,/\, \sigma_i$: transmission factor for stresses;

$r_v = v_r \,/\, v_i$: reflection factor for velocities;

$t_v = v_t \,/\, v_i$: transmission factor for velocities;

where: σ is the stress, v the velocity and the subscripts i, r and t refer to incident, reflected and refracted waves respectively.

If the rod is constituted by two media, the Boundary Conditions at the interface are:

$$\sigma_1 = \sigma_2 \qquad ; \qquad u_1 = u_2 \tag{2.20}$$

where: σ is the stress, u the displacement, subscript 1 refers to the medium where the incident wave travels and subscript 2 refers to the medium where the transmitted wave travels.

Assuming for the incident wave

$$u_i = A_1 \exp[-ik_1(x-c_1t)] \tag{2.21}$$

it can be found for the reflected wave

$$u_r = B_1 \exp[-ik_1(x+c_1t)] \tag{2.22}$$

and for the transmitted wave

$$u_t = A_2 \exp[-ik_2(x-c_2t)] \tag{2.23}$$

where: A_1, B_1, A_2 are constants, k is the Bulk Modulus, c_1 and c_2 are defined by $\sqrt{(E/\rho)}$ with E Young's Modulus and ρ density.

Applying the Boundary Conditions it can be obtained:

$$r_\sigma = (J_2 - J_1) / \Sigma J \quad ; \quad t_\sigma = 2\, J_2 / \Sigma J$$
$$r_v = (J_1 - J_2) / \Sigma J \quad ; \quad t_v = 2\, J_1 / \Sigma J \tag{2.24}$$

where: $J_1=\rho_1 c_1$ and $J_2=\rho_2 c_2$ called Acoustic Impedances of the Materials, define the resistances to the waves propagation.

In the case of free end ($\rho_2 c_2=0$):

- The reflected stress is equal to the incident but with opposite sign (if the incident is compressive the reflected is tensile);
- The reflected velocity is equal to the incident velocity;
- The transmitted velocity is twice the incident one.

In the case of fixed end ($\rho_2 c_2 \to \infty$):

- The reflected stress is identical to the incident with the same sign;
- The transmitted stress is twice the incident one and has the same sign;
- The reflected velocity is equal to the incident but with opposite sign;
- The transmitted velocity is zero.

These two cases correspond to limit situations and can be considered as an upper and lower bound for the other cases. Many behavioral aspects observed experimentally can be explained based on the relatively simple model presented above, as will be discussed later herein.

2.6 Fourier Techniques

Data acquired during tests represent the time history of a certain variable. If the set or sequence of data satisfies the conditions to have a non infinite integral and a non infinite number of discontinuities, then it can be represented as a summation over all frequencies of sinusoidal functions of that variable. Signals that appear random in nature can be resolved into a summation of single frequency components.

A discrete time signal is defined as a signal whose time and amplitude are discrete. In the analysis of discrete time signals the utilization of sinusoidal and complex exponential sequences has a great importance. This is particularly true for the category of the linear, shift-invariant systems. According to Oppenheim and Schafer (1975) a system is defined mathematically as a unique transformation that maps an input sequence $X(n)$ into an output sequence $Y(n)$:

$$Y(n) = T\,[\,X(n)\,] \tag{2.25}$$

A system can be considered Linear if the Principle of Superposition applies; calling $Y_1(n)$ and $Y_2(n)$ the responses to the inputs $X_1(n)$ and $X_2(n)$, then the necessary and sufficient condition for the system to be linear is that

$$T[aX_1(n) + bX_2(n)] = aT[X_1(n)] + bT[X_2(n)] =$$

$$= a\,Y_1(n) + b\,Y_2(n) \tag{2.26}$$

where a and b are arbitrary constants.

The system is defined as Shift Invariant if the following property applies: if Y(n) is the response to X(n) then Y(n-k) is the response to X(n-k) where K is a positive or negative integer. When the index n is associated with time, a Shift Invariant System becomes a Time Invariant System.

The property of Linear, Shift Invariant System is that the steady state response to a sinusoidal input is sinusoidal with amplitude and phase determined by the system, but with a frequency that is the same as that of the input.

This is the property that makes sinusoidal and complex exponential representations of discrete time signals so important. The following example is taken from Oppenheim and Schafer (1975): supposing the input sequence is a complex exponential of radian frequency ω :

$$X(n) = e^{j\omega n} \qquad \text{for} \quad -\infty < n < +\infty \tag{2.27}$$

the output can be expressed in the form :

$$Y(n) = \sum_{k=-\infty}^{\infty} h(k)\, e^{j\omega(n-k)} \tag{2.28}$$

where h(k) is the unit sample response.

$$Y(n) = e^{j\omega n} \sum_{k=-\infty}^{\infty} h(k)\, e^{-j\omega k} \tag{2.29}$$

Defining

$$H(e^{j\omega}) = \sum_{k=-\infty}^{\infty} h(k)\, e^{-j\omega k} \tag{2.30}$$

it is possible write

$$Y(n) = H(e^{j\omega})\ e^{j\omega n} \tag{2.31}$$

The function $H(e^{j\omega})$ describes the change in complex amplitude of the complex exponential as a function of the frequency ω. This function is called frequency response of the system whose unit sample is h(n). It is a continuous function of ω and periodic in ω with period 2π; this property follows from Eq. (2.30) of the function $H(e^{j\omega})$ since

$$e^{j(\omega+2\pi)k} = e^{j\omega k} \tag{2.32}$$

Since $H(e^{j\omega})$ is a periodic function of ω, it can be represented by a Fourier Series; Equation (2.30), definition of $H(e^{j\omega})$, is a Fourier Series whose Fourier Coefficients correspond to the unit sample response h(n). It follows that h(n) can be obtained from $H(e^{j\omega})$ using the relations that give the Fourier coefficients of a periodic function:

$$h(n) = \frac{1}{2\pi}\int_{-\pi}^{\pi} H(e^{j\omega})\ e^{j\omega n}\ d\omega \tag{2.33}$$

where

$$H(e^{j\omega}) = \sum_{n=-\infty}^{\infty} h(n)\ e^{-j\omega n} \tag{2.34}$$

Equations (2.33) and (2.34) are called Fourier Transform Pair for the sequence h(n). The general expressions of the Transform Pair for a function of time f(t) are

$$f(t) = \frac{1}{2\pi}\int_{-\pi}^{\pi} F(\omega)\ e^{j\omega t}\ d\omega \tag{2.35}$$

where

$$F(\omega) = \int_{-\infty}^{\infty} f(t)\ e^{-j\omega t}\ dt \qquad (2.36)$$

Equation (2.35) is called Inverse Fourier Transform, it transforms a function of frequency $F(\omega)$ into its equivalent function of time $f(t)$ (Fourier Synthesis). Equation (2.36) is called Direct Fourier Transform, it transforms a function of time $f(t)$ into its equivalent function of frequency $F(\omega)$ (Fourier Analysis). Fourier Analysis and Fourier Synthesis are the two basic techniques used to transform data into and from the frequency domain. In general the Fourier Transform $F(\omega)$ is a complex function; calling $F_1(\omega)$ and $F_2(\omega)$ its real and imaginary parts:

$$F(\omega) = F_1(\omega) + j\ F_2(\omega) \qquad (2.37)$$

Any function of time $f(t)$ can be divided into its even $f_e(t)$ and odd $f_o(t)$ parts:

$$f(t) = f_e(t) + f_o(t) \qquad (2.38)$$

The Transform, given by equation (2.36), can be divided into its even and odd parts:

$$F(\omega) = \int_{-\infty}^{\infty} f_e(t)\ e^{-j\omega t}\ dt + \int_{-\infty}^{\infty} f_o(t)\ e^{-j\omega t}\ dt \qquad (2.39)$$

using the relation

$$e^{-j\omega t} = \cos\omega t - j\sin\omega t \qquad (2.40)$$

it becomes

$$F(\omega) = \int_{-\infty}^{\infty} f_e(t)(\cos\omega t - j\sin\omega t)dt + \int_{-\infty}^{\infty} f_o(t)(\cos\omega t - j\sin\omega t)dt \qquad (2.41)$$

But sine is an odd function and cosine is an even function; the integrals over the interval $-\infty$ to $+\infty$ of odd function multiplied by an even function are equal to zero:

$$F(\omega) = \int_{-\infty}^{\infty} f_e(t)\cos\omega t\ dt + j\int_{-\infty}^{\infty} f_o(t)\sin\omega t\ dt \qquad (2.42)$$

Equating with Eq. (2.37):

$$F_1(\omega) = \int_{-\infty}^{\infty} f_e(t)\cos\omega t\ dt = 2\int_{0}^{\infty} f_e(t)\cos\omega t\ dt \qquad (2.43)$$

$$F_2(\omega) = \int_{-\infty}^{\infty} f_o(t)\sin\omega t\ dt = 2\int_{0}^{\infty} f_o(t)\sin\omega t\ dt \qquad (2.44)$$

the real part of the Fourier Transform is even and it is based only on the even part of f(t); the imaginary part of the Fourier Transform is odd and is based only on the odd part of f(t). With a similar procedure, one can show that even and odd parts of the time function are depending only on the even and odd parts of the transform:

$$f_o(t) = -\frac{1}{\pi}\int_{0}^{\infty} F_2(\omega)\sin\omega t\ d\omega \qquad (2.45)$$

$$f_e(t) = \frac{1}{\pi}\int_{0}^{\infty} F_1(\omega)\cos\omega t\ d\omega \qquad (2.46)$$

Because every time function can be divided into an odd and an even part and because at a time less than zero these two parts must cancel one another, the odd and the even parts must be equal and opposite. At a time greater than zero they must add and be equal:

$$f_e(t) = f_o(t) \qquad \text{for } t > 0 \tag{2.47}$$

and

$$f(t) = 2\, f_e(t) = 2\, f_o(t) \qquad \text{for } t > 0 \tag{2.48}$$

Equations (2.43) and (2.44) reduce to:

$$F_1(\omega) = \int_0^{\infty} f(t)\cos\omega t \, dt \tag{2.49}$$

$$F_2(\omega) = \int_0^{\infty} f(t)\sin\omega t \, dt \tag{2.50}$$

In this study the Fast Fourier Transform (FFT) has been used to gain into the mechanism of shear transfer across pavement joints, as will be discussed later herein.

2.7 Non-destructive Evaluation Techniques for Pavements

Non-destructive techniques are methods to evaluate the characteristics of a system, not compromising the serviceability of the system itself. In general the interest is focused on the determination of the structural strength of the pavement, intended as its ability to limit strains. The deflection of a pavement under loading is generally due to compression of the soil rather then to compression of the pavement layers. The goal is to never reach values of deformations in the pavement, and consequently of pressure on the soil, able to result in permanent deformations of the soil. The value of maximum allowable stress without permanent deformations varies with the characteristics of the soil, according to Barenberg and Arntzen (1981) it is between 12 and 18 psi. Pavement deflections are dependent on the modality of loading (static, dynamic, etc.) and on the magnitude of the load; the ideal testing procedure is the one closely representing a design moving load. According to a classification by Moore et al. (1978), four major categories of non-destructive structural evaluation of pavements can be individuated:

1. Static Deflections. These methods consist of the application of a static or quasi-static load to the pavement, and in the measurement of the corresponding deflections. A quasi-static load corresponds to a vehicle moving slowly in the proximity of the place of the measurements. Once the displacements are known, several approaches are available to obtain information on the structural capacity of the pavement. These type of technique is mainly used for flexible pavements; in the case of rigid pavements the change in shape due to thermal variations makes difficult obtain an immovable reference point for the displacement measurements.

2. Steady State Deflections. In these techniques a steady state sinusoidal vibration is induced in the pavement and the consequent deflections are measured by means of accelerometers or velocity sensors. The major advantage respect to the static deflection method is that an immovable reference point is not required for the measurements. Varying the force applied to the pavement, the difference between the amplitude of two consecutive peaks in the displacement records can be related with the change in the applied force. Among the major concerns with these kinds of

techniques are:

- Only little information is available in the low frequency range, this because of the low output of the inertial motion sensors at these frequencies;
- Not much information on the parameters that characterize plastic deformations;
- In the case of layered system, the difficulties to quantify the contribution of each single layer to the general behavior.

3. Impact Load Response. A transient load is applied to the pavement and the response, usually in terms of displacements is measured. To obtain a short duration loading, a weight is dropped on a plate resting on the pavement surface. According to Moore (1978) the duration of the pulse should not exceed 1 msec for the loading to be considered transient; this is because the rise time, defined as the time the pavement needs to deflect from 10 to 90 percent of its maximum deflection after being subjected to a step loading, can vary between 3 and 6 msec. The response to longer loadings will not contain only information on the steady-state frequencies but also on the frequencies characteristic of the loading function. It is difficult to obtain in the field such short pulses, in general the devices today used for impact load tests have pulses with duration of 20 msec or longer. Like before the response obtained is the one of the entire structure, with no information about the contributes of the single layers.

Falling Weight Deflectometer: The testing procedure consists of dropping vertically a large mass on a plate resting on the pavement surface. A spring-damping system is interposed between the mass and the plate. Weight of the mass, dimensions of the plate and height of dropping can vary depending on different versions of the device. The followings are referred to the Phoenix FWD: mass 330 pounds, height 15.7 in, 11.8 in diameter circular plate. The response of the pavement is measured through its deflection using LVDT (Linear Variable Differential Transformer). The pulse obtained has a duration of about 26 msec and the magnitude of the peak, that can be obtained equating the initial potential energy to the strain energy stored in the spring at its maximum compression, is of the order of 5.5 tons. The magnitude of the maximum force can be varied by changing either the spring constant or the mass of the weight or dropping height.

Different types of FWD present pulses of different duration but always in the interval 20-40 msec. The theoretical accelerations transmitted to the pavement by the FWD devices are of the order of 10-30 g (where g is the acceleration of gravity). For example, the accelerations measured in the field by Hoffman and Thompson (1982) are about 4 g; this difference is probably due to the interaction FWD-pavement and to the rubber mat interposed between loading plate and pavement surface. Even considering the 4 g peak accelerations, they are about 10 times higher than those due to traffic, as pointed out by Sebaaly et al. (1985). The same authors noticed that typical pulses from traffic loading are of the order of several hundred msec. Despite these discrepancies, the deflections measured by Hoffman and Thompson (1982) using the FWD were consistent with the ones due to traffic. Better results with the FWD are obtained using velocity transducers instead of LVDT; this is because geophones, like accelerometers, do not need an immovable reference system as required by a LVDT.

4. Wave propagation. These techniques are particularly suitable for layered pavement systems, because they are able to supply information about the individual layers. These methods can be based on steady state vibrations or on impulsive loading. Usually the velocities of propagation of the waves are measured, then using relations similar to the ones presented in Section 2.4, information is obtained on the parameters characterizing the media.

For more information, a detailed description of non-destructive techniques is given by Moore et al. (1978).

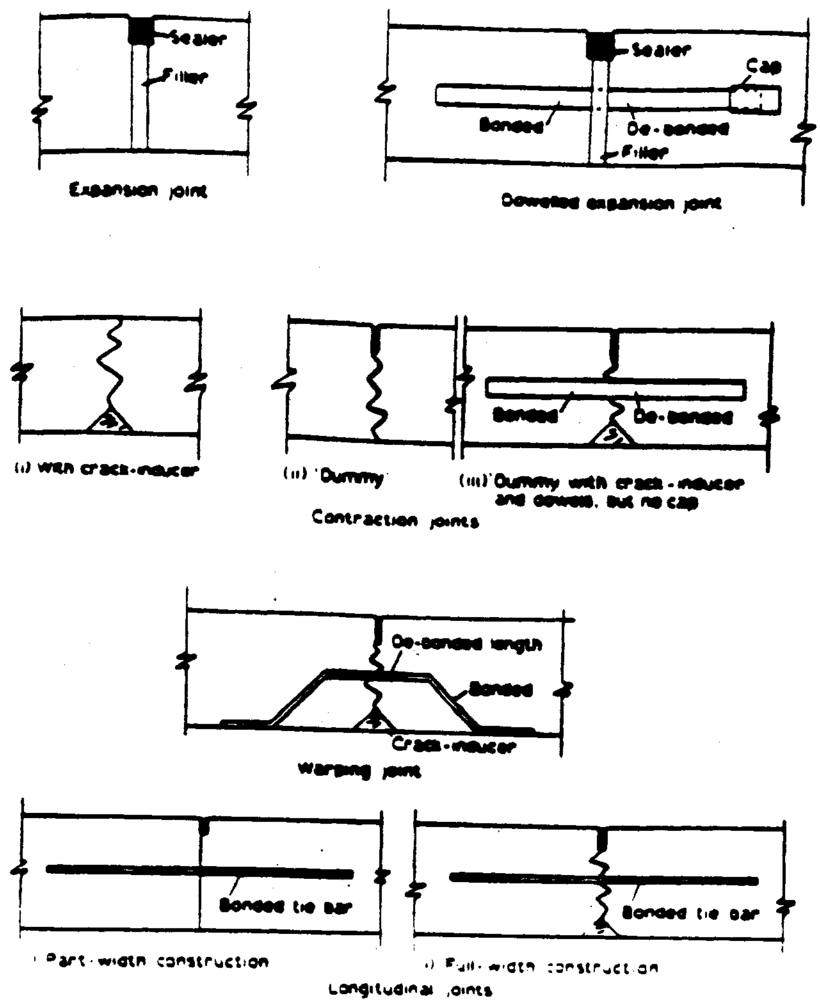

Figure 2.1 Types of joint. (Moore, 1986)

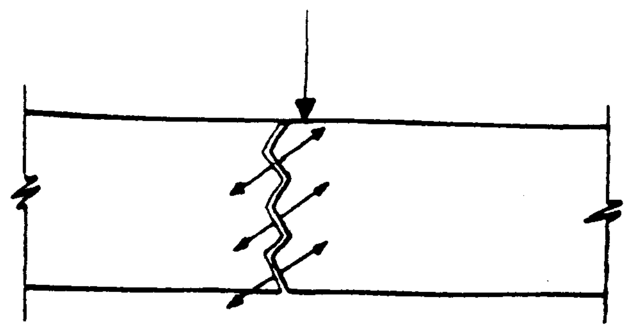

Figure 2.2 Aggregate Interlock Mechanism. (Moore, 1986)

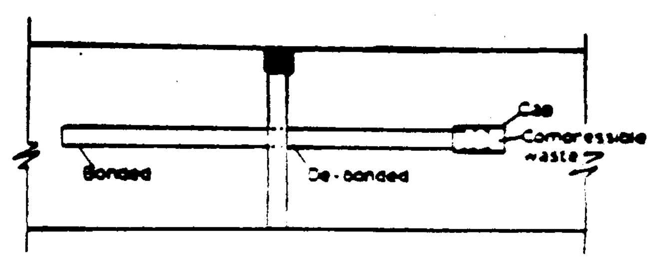

Figure 2.3 Dowelled Expansion Joint. (Moore, 1986)

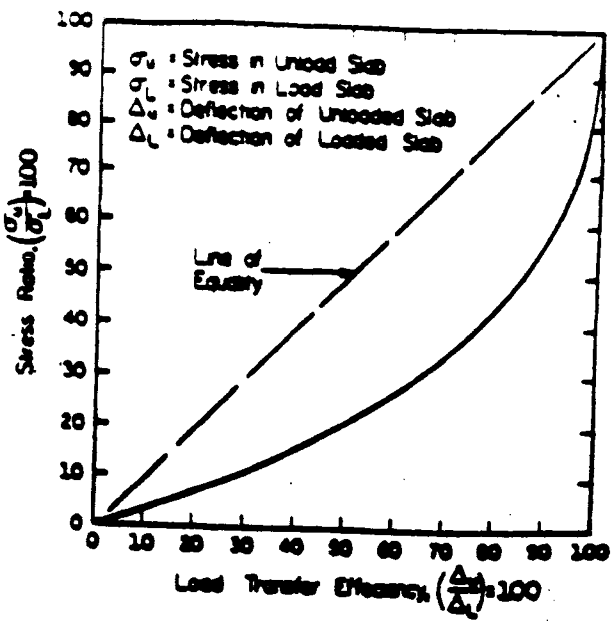

Figure 2.4 Relation Joint Efficiency - Joint Stresses. (Barenberg and Arntzen, 1981)

Aircraft	Loading Descriptive (kips)	Max Stress (Edge Load) Joint Efficiency	
		<10%	>90%
747	Max Ramp (778)	360	220
	Max Landing (600)	280	[illegible]5
DC-10-30	Max Ramp (558)	425	270
	Max Landing (403)	235	185

Table 2.1 Stress under loading in different conditions of Joint Efficiency. (Barenberg and Arntzen, 1981)

CHAPTER 3

APPROACH OF THE STUDY

3.1 General

Following the general concept for developing a non destructive method for pavement joint evaluation, as presented by Foxworty (1985) and Western and Krauthammer (1988), and following the basic concepts that can be found in Moore et al. (1978), the present study is aimed at developing an experimental procedure for evaluating joint shear transfer capabilities.

In studies of pavements performance a parameter called "joint efficiency", defined as the ratio between the pavement's deflections on two sides of a joint when one side is loaded, is widely used. This parameter can be obtained by different measurement methods; one of the most commonly used is the Falling Weight Deflectometer method (FWD).

Krauthammer and Western (1988) showed that the shear transfer can be described accurately by a shear stress versus a shear slip relationship. A deterioration in the joint shear transfer capability was correlated to a reduction in the joint shear stiffness. In that study the joint efficiency was related to the joint shear transfer capacity and to the joint shear transfer mechanism. Based on those relationships it was possible to assess the joint conditions very accurately by comparing FWD data with results from the numerical study.

It was then proposed to explore the feasibility of detecting the joint deterioration by measuring the joint's response frequency. This was based on the anticipated finding of a relationship between the frequency response of a joint to dynamic loading and the joint shear transfer capability. If a relationship between the internal shear transfer conditions of the joint and its response frequencies exists, then it would be possible, by measuring a corresponding frequency shift "in situ", to determine the joint's internal condition in a unique manner. Such information would then be used to decide on the required corrective measures, and enhance roadway management procedures.

3.2 Construction of the Model

For the present study two reinforced concrete slab systems were employed in modelling the pavement-joint system as shown in Figure 3.1:

1. System 1: One reinforced concrete slab with the dimensions of 60 inches long, 30 inches wide, and 6 inches deep (Figure 3.2).
2. System 2: Two reinforced concrete slabs, each with the dimensions of 30 inches long, 30 inches wide, and 6 inches deep (Figure 3.3).

All the slabs have been reinforced with a 6 inches by 6 inches steel mesh with cross sectional area of 0.012 in^2. The mesh was positioned at one inch from the bottom of the slabs for preventing tensile damage to the concrete while the slabs were moved to and from the test. System 1 represents the ideal case of full shear transfer across an imaginary joint, while the two slabs of System 2 represent a realistic joint interface in a pavement. The two Systems were placed on a one foot deep sand bed, as showed in Figure 3.4, for simulating an underlaying base material.

3.2.1 Simulation of Different Conditions of Joint Shear Transfer

The simulation of different conditions of joint shear transfer in System 2 was done by applying to the system the in-plane compressive force N, as shown in Figure 3.1. The application of this force was realized by means of two 1-inch-diameter steel rods connected to steel angles placed at the ends of the slabs. When the nuts at the end of the rods were torqued, tensile forces were induced in the rods and a corresponding compressive force was induced in the plane of the slabs, as shown in Figures 3.5 and in Figure 3.6 is a detail of one rod edge with the nut. Under loading, when the vertical force F(t) is applied, the two slabs are forced to move relative to each other, and a frictional force T develops on the interface opposing this relative movement. Under static conditions, the force T is constant and its magnitude is proportional to the product of the resultant compressive force N and the coefficient of friction μ. According to the ACI 318-89 specifications, the coefficient μ can be assumed equal to 0.6.

A precise evaluation of the coefficient μ is difficult under dynamic loading, but following an approximate (but well accepted) rule μ can be considered one half of its static values. Thus, for dynamic loading the force T can be assumed to be:

$$T = \mu N / 2 \tag{3.1}$$

Varying the values of the force N, the values of T changes accordingly, as will the total resultant forces acting on the two side of the interface. Neglecting the friction between the slabs and the sand, this force will be close to F(t)-T on the loaded side of the joint, while on the unloaded side it will be T. Neglecting the base resistance can be an acceptable assumption because of the modality used in applying the in-plane compressive force, as it will be discussed later herein. Changing the magnitude of these resultant forces causes a difference in the corresponding displacements of the two sides of the joint, hence, the value of joint efficiency can be computed. This approach permits one to vary the value of N for simulating different shear transfer conditions and corresponding joint efficiencies.

The axial forces in the rods were calculated from the measured strains. These strain measurements were obtained from two strain gages that were mounted on a 1-foot smooth section at 2/3 of the length of each rod, as shown in Figure 3.7. The strain gages were mounted diametrically opposite and their readings were averaged for removing possible bending effects. The average strain in each rod was multiplied by the steel modulus of elasticity and by the cross-sectional area for computing the axial force, as discussed further in Section 3.6.

For a later reference, facing the joint from the point of load application (Figure 3.7), the rod on the left will be identified as rod # 1, and the rod on the right will be identified as rod # 2. The strain gages located on rod # 1 will be identified as gages 1 and 2, respectively, and the ones on rod #2 as gages 3 and 4, respectively.

3.2.2 Loading Device

The dynamic loading was delivered by a 30 pounds weight (composed of 6 circular steel plates of 5 pounds each bonded together) dropped from an height of 3 feet. The weight had a 2 inch-diameter circular hole in its center so that it could be guided by a, nearly, frictionless 5-foot high pole, with a diameter of 1 and 7/8 inches. The pole was connected at its base to a 12 x 12 x 3/8 inches steel plate. Thus the impact load was uniformly distributed over an area of 144 square inches to prevent cracking and breaking of the concrete. The plate was positioned along the major axis of symmetry of the slab at a distance of 3 inches from the joint, and firmly attached to the slab by four steel bolts for preventing rebound.

Two rubber pads were interposed between the plate and the concrete slab and between the plate and the weight. One 1/16-inch thick rubber mat covered the square plate for preventing a steel-to-steel high acceleration impact. A second 1/8-inch thick rubber mat was interposed between the plate and the slab with the double purpose to keep the accelerations under the maximum value of 500 g's (where g is the acceleration of gravity), and to obtain a more even distribution of the load from the steel plate onto the concrete slab; the corners of this mat were cut to allow the passage of the bolts. This approach ensured that almost the same impact conditions would exist for all tests. Only in three records, out of a total of 52 tests, the maximum acceleration exceed the value of 500 g's, and reached about 580 g's.

The impulsive force obtained in this manner had a recorded maximum amplitude of 22,500 lbs and a duration of about 1.6 msec, as shown in Figure 3.8. These pulse characteristics were chosen for maintaining the duration of the pulse close to the limit of 1 msec (following the reasons described in Chapter 2) and, at the same time, to obtain a high value of the peak for simulating an FWD test.

3.3 Properties of the Materials

The properties of the steel mesh and concrete are the following :

STEEL MESH	:	$E = 29000$ Ksi
CONCRETE	:	$f'_c = 3900$ Ksi for System 1.
		$f'_c = 3200$ Ksi for System 2.
		$E = 57000 \sqrt{(f'_c)}$ psi

The properties of steel rods and steel angles are the following:

STEEL ANGLES	:	L 4 x 4 x 3/4
		$F_y = 36$ Ksi
		$F_u = 58\text{-}80$ Ksi
		$E = 29000$ Ksi
STEEL RODS	:	Diameter rod # 1 = 0.793 inch
		Diameter rod # 2 = 0.790 inch
		$F_y = 36$ Ksi
		$F_u = 58\text{-}80$ Ksi
		$E = 29000$ Ksi

The properties of the sand, as obtained from laboratory tests, are the following:

γ = 105 lbs/ft^3

E = 10500 psi

where: E = Young Modulus;

F_y = Minimum Yield Stress;

F_u = Ultimate Strength;

f'_c = compressive cylinder strength in psi;

γ = Density.

3.4 Instrumentation and Data Acquisition System

Experimental data consisted of acceleration-time histories obtained from accelerometers glued to the reinforced concrete slabs. The accelerometers were positioned at 2.5 inches from the joint along the major axis of symmetry of the slab, on both sides of the joint.

The accelerometers were 8620 Piezotron by Kistler Instruments Corporation, that are designed to minimize the effects of noise, handling, temperature gradients and other environmental effects. They can be considered as general purpose shock and vibration measuring instruments. Characteristics of the 8620 Piezotron are:

Range	=	+-500 g
Sensitivity	≈	10 mV/g
Transverse Sensitivity	≈	2.4 %
Mounted Resonant Frequency	=	50 kHz

where g is the acceleration of gravity assumed equal to 9.807 m/sec^2.

The accelerometers were connected to the data acquisition system through a channel coupler (Model 5122 by Kistler Instruments Corporation). The data was acquired by a high-speed (up to 1x10^6 samples per second) DAS-50 Data Acquisition and Control board by MetraByte Corporation. The acquisition was performed at the maximum sampling rate allowed by the system (1 MHz) for insuring that all pertinent characteristic responses of the system are captured. Since two accelerometers were used, the effective sampling rate per each channel was 500 kHz. The number of samples acquired by each channel was 5000; this determined an acquisition of data covering an interval of time, Δt, of 10 msec. This Δt was sufficient for capturing the vibrations of the systems under the main impact. The trigger was given by the weight itself shortly before its contact with the steel plate. The experimental data was then transferred for analysis by the scientific software Asystant+ (Asyst Software Technologies, 1987).

3.5 Tests on System 1

A set of eight tests was conducted on System 1 that represented an ideal situation of full shear transfer. Each test is marked by the Letter B followed by a number from 1 to 8. The data resulting from each test are the acceleration-time histories on both sides of the joint in the positions previously described. Plots, tables and in general every quantity related to these data is individuated by the Letter and Number of the test followed by a suffix IN or OUT depending if they refer to the Loaded Side of the joint or to the Unloaded Side, respectively. All these tests were conducted without applying any compression to the slab through the rods, thus representing an ideal condition of full shear transfer.

3.5.1 Preliminary Tests

In order to meet the objective of this study, it was required to eliminate all influences on the results by any test parameter, except the joint shear transfer. One such parameter was that the change in stiffness of the structure due to the application of the axial force could affect the response. If this was true then a comparison between the results obtained from System 1 and the results obtained from System 2 could be done only at parity of conditions. The response of System 2, when a compressive force of a certain value was acting, should have been compared with the response of a System 1 where the same compressive force was acting. The effects of the induced axial force on the frequency had to be evaluated, and this was done as follows. System 1 was tested with a value of axial force of 10,000 pounds in each rod; (a value bigger than the maximum thrust applied to System 2). A set of three tests denominated SB1, SB2 and SB3 was conducted. The response frequencies were compared with the results from the set B1,....,B8 (tests without axial thrust), and no appreciable differences were noted, as discussed in Chapter 4.

A second parameter was that various possible external disturbances could interfere with the tests, overlapping external frequencies to the ones typical of the structure's response, and leading to erroneous evaluations of the system's behavior. This was checked conducting a set of four tests denominated U1, U2, U3 and U4 with no loading of the structure, but the external noises were recorded. Also in this case the results showed no influence: i.e., the power spectrum of the sequences of data recorded during these tests are absolutely negligible when compared with the ones obtained during the main tests (100 versus 10E9), as shown by the plots in Appendix C.

3.6 Tests on System 2

This System is the one representing a joint with variable shear transfer conditions, that were induced by applying tension to the steel rods on both sides of the slabs. To decide what torque had to be applied to the nuts for obtaining a certain value of shear transfer capacity, a relation between the axial force in each rod and the joint shear transfer must be established.

A preliminary theoretical evaluation was performed considering instead of the real structure a one-dimensional system: a strip of the slabs with cross sectional area 12 x 12 in^2 and 60 inches long was considered as beams on elastic foundation with a joint in middle of the length. The loaded beam was subjected to a vertical force acting statically, near the joint, with magnitude F(t)-T, and the other beam to the force T, as discussed in section 3.2.1. It should be noted that the value T, assumed proportional to the in plane compressive force N, is the parameter related to the axial force in the rods. The underlying sand was assumed as a Winkler soil capable of reacting vertically both in compression and tension. This hypothesis is acceptable for cohesive types of soil but, in general, not applicable to sands and uncohesive soils. Nevertheless in this case the weight of the structure itself, large if compared to the assumed dimensions, opposing to a vertical lifting movement could be considered as a substitution for the vertical tensile reaction of the soil, as indicated by Timoshenko and Woinowsky-Krieger (1959).

In the same reference the authors suggested possible values of the Modulus of Subgrade K, a parameter that characterizes the response of the soil to vertical disturbances. Here according to Timoshenko and Woinowsky-Krieger (1959) and Belluzzi (1984) it was assumed that $K = 144$ lbs/in^3. The analytical procedure that followed was the classical one of short beams on elastic foundation, as described by Belluzzi (1984) and Pozzati (1986). Given the short length of the beam, the displacements occurring on one edge are influenced also by the phenomena occurring on the opposite edge; an iterative procedure is adopted to evaluate the displacement in the point of application of the load. The value of N, and consequently the value of T, was varied until the ratio of the displacements on the two sides of the joint gave the desired relative displacement (i.e. joint efficiencies).

The values of displacements obtained, considering the structure as one-dimensional, were considerably different from the ones obtained in the laboratory. This result was obtained probably because of the assumption of static loading, and also because that structure should have been considered as three-dimensional. As a result, it was decided to proceed in the following manner: Different values of force were applied to the steel rods, tests were conducted and the corresponding values of joint efficiency calculated. Once a sufficient amount of information was available, values of axial force had to be chosen to represent three different joint conditions: new joint, deteriorated joint and dead joint, according to the classification given by Krauthammer and Western (1988) as presented in Table 3.1:

Table 3.1 Joint Efficiencies.

	Material Strength				
	Excellent	Good	Fair	Poor	Experimental
New	0.93	0.87	0.84	0.80	0.86
Deteriorated	0.88	0.80	0.76	0.71	na
Dead	0.70	0.60	0.57	0.53	na

Thus, it was decided to keep a wider range for the values of joint efficiency (JE) corresponding to different joint conditions, and the following values were assumed:

Table 3.2 Assumed Joint Efficiency conditions.

	J E
New Joint	≥ 0.9
Deteriorated Joint	≈ 0.6
Dead Joint	< 0.4

Six values of the force, N, to be applied in each rod were chosen to represent these different joint conditions. Corresponding to these values, six sets of three tests each were conducted on System 2. Every test is marked by two letters followed by a number that goes from 1 to 3. The values of the forces and the corresponding denominations of the tests are given Table 3.3.

Table 3.3 Test cases on System 2.

TEST SET	Axial Force in Each Rod, (lbs)
ST	2,000
SU	4,000
SV	5,000
SP	6,000
SQ	8,800
SR	9,500

The data resulting from each test are the acceleration-time histories on both sides of the joint in the positions previously described. Plots, tables and in general every quantity related to these data is individuated by the Letters and number of the test followed by a suffix IN or OUT depending if they refer to the Loaded Side of the joint or to the Unloaded Side.

Having defined the in-plane forces to be applied, the values of the corresponding strains in the rods had been calculated using the basic relations:

$$\sigma = N / A \qquad ; \qquad \epsilon = \sigma / E \tag{3.2}$$

where σ = tensile stress;

ϵ = strain;

A = cross-sectional area of the rod;

E = Modulus of Elasticity.

According to these relations the following values of the strains should be obtained:

Table 3.4 Values of strain (in microstrain) in the rods corresponding to the axial force N.

SET	N (lbs)	Strain LR	Strain RR
ST	2000	139	140
SU	4000	279	281
SV	5000	349	351
SP	6000	418	422
SQ	8800	614	619
SR	9500	663	668

LR = Left Rod ; RR = Right Rod ; N = Axial Force in each rod.

Because the slab edges of the slabs were not perfectly straight, and because of the twisting of the steel angles, the rods were subjected not only to axial force but also to bending moment. Torsion in the angles was due to the fact that the force N was not applied to the shear center of the shapes, causing a torque and a consequent twist. The values of the strains registered by the strain indicators were in some cases very different from the theoretical values reported in Table 3.4, as shown in Table 3.5. In all the cases the average value from the two gages on each rod was assumed as the value of uniform strain in the cross section of the rod. The same Table 3.5 shows that these average values are always very close to the theoretical ones.

Table 3.5 Values of strain (in microstrain) in the rods in the sets of tests ST, SU, SV, SP, SQ and SR.

SET	GAGE	TEST # 1		TEST # 2		TEST # 3		Theoretical
		Rdg.	Avg.	Rdg.	Avg.	Rdg.	Avg.	Value
ST	1	149	140	135	123	154	133	139
	2	131		112		112		
	3	87	138	88	137	135	151	140
	4	190		186		168		
SU	1	330	278	355	286	322	277	279
	2	227		218		233		
	3	250	280	237	281	231	270	281
	4	311		325		310		
SV	1	415	350	389	350	377	349	349
	2	286		311		322		
	3	224	349	228	350	228	350	351
	4	474		473		472		
SP	1	543	419	544	421	534	398	418
	2	296		299		263		
	3	533	427	534	427	529	430	422
	4	322		321		332		
SQ	1	871	616	867	611	868	612	614
	2	361		356		357		
	3	796	619	795	621	800	626	619
	4	442		448		452		
SR	1	958	661	951	657	962	662	663
	2	364		363		363		
	3	901	686	894	685	894	686	668
	4	471		477		478		

Rdg. = Value from strain indicator ; Avg. = Average value

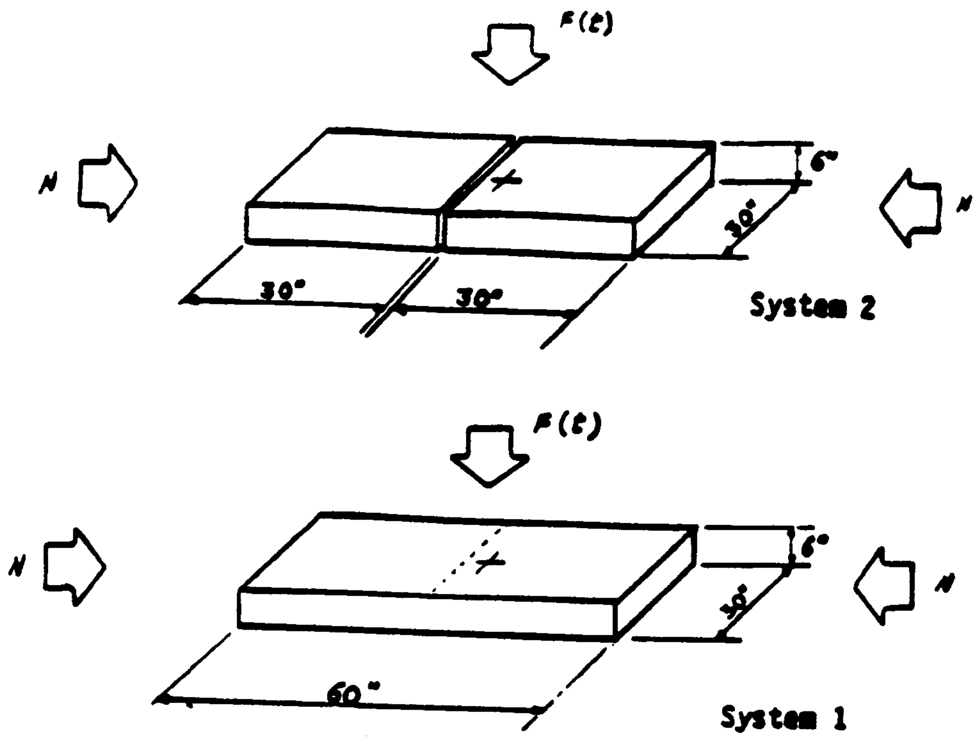

Figure 3.1 Slabs and Force Systems

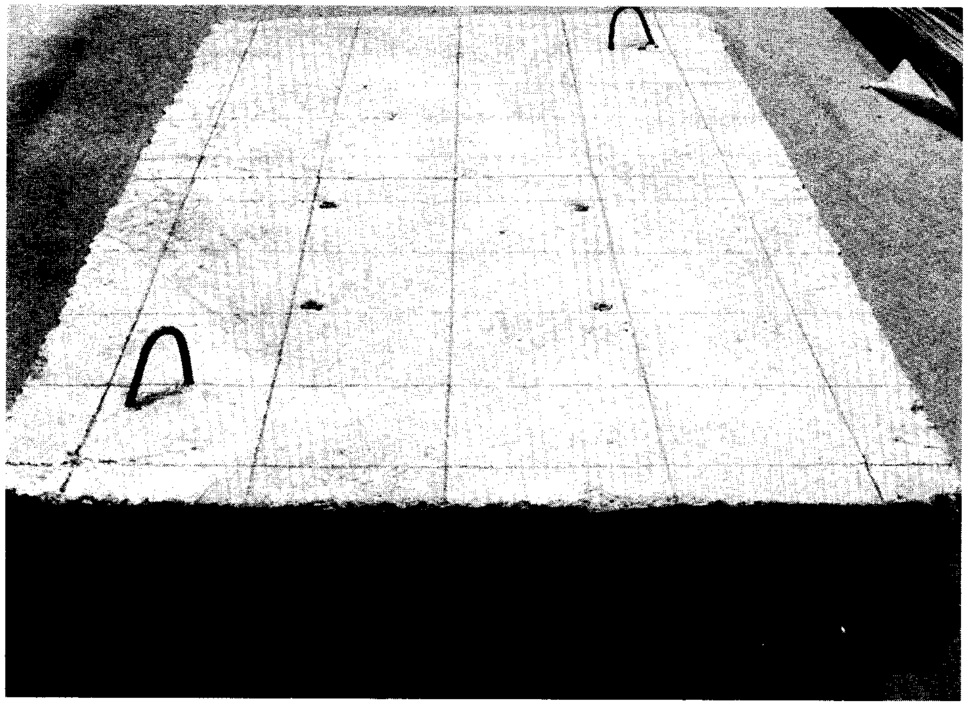

Figure 3.2 System 1.

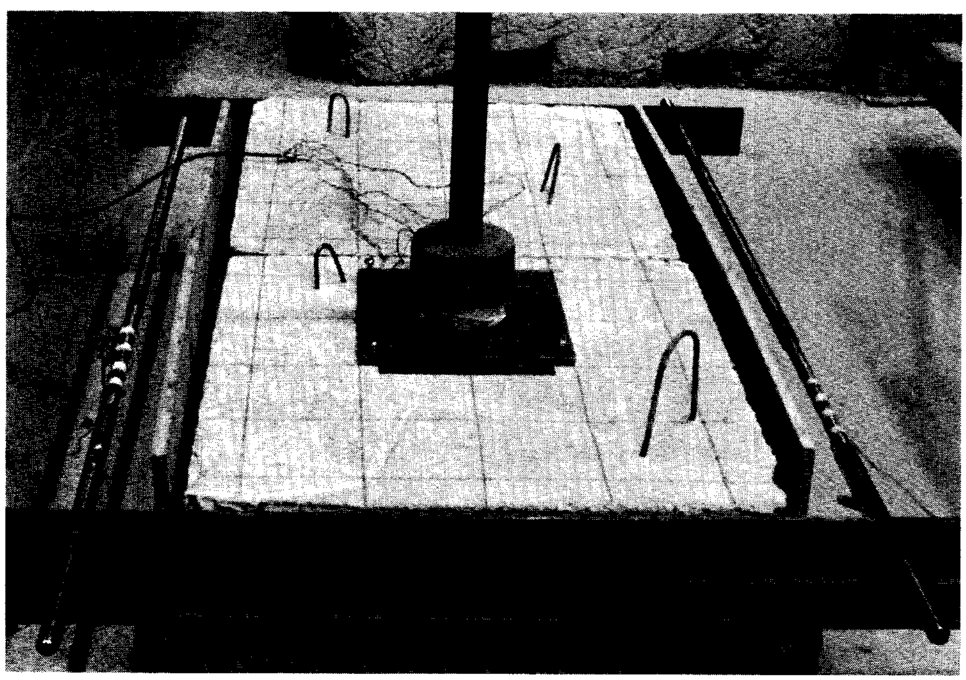

Figure 3.3 System 2.

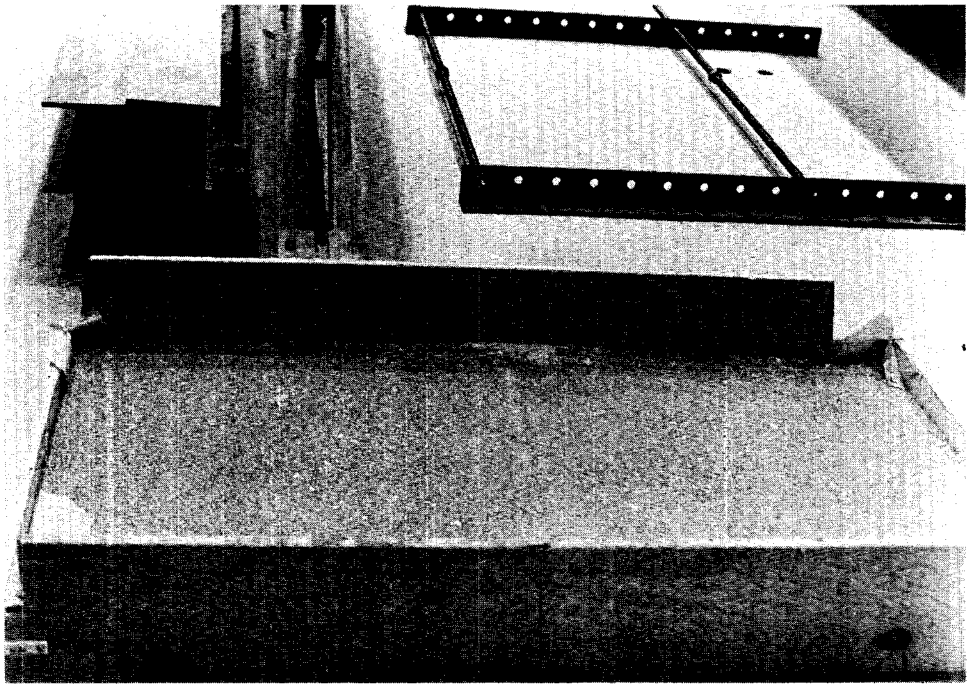

Figure 3.4 Sand bed.

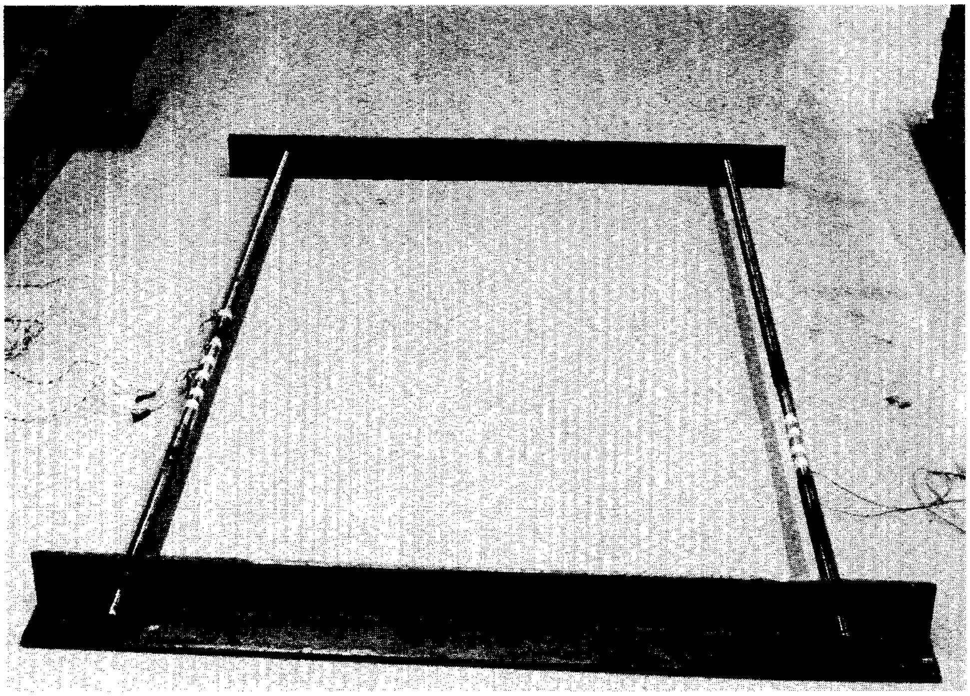

Figure 3.5 Device to apply in-plane compression to the slabs.

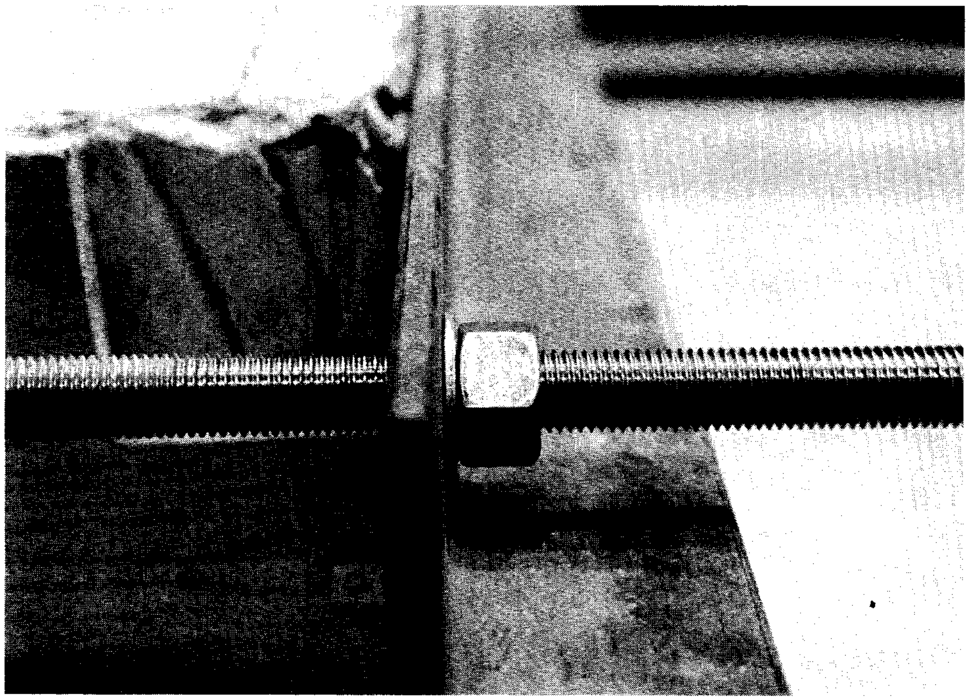

Figure 3.6 Detail of rod edge with the nut.

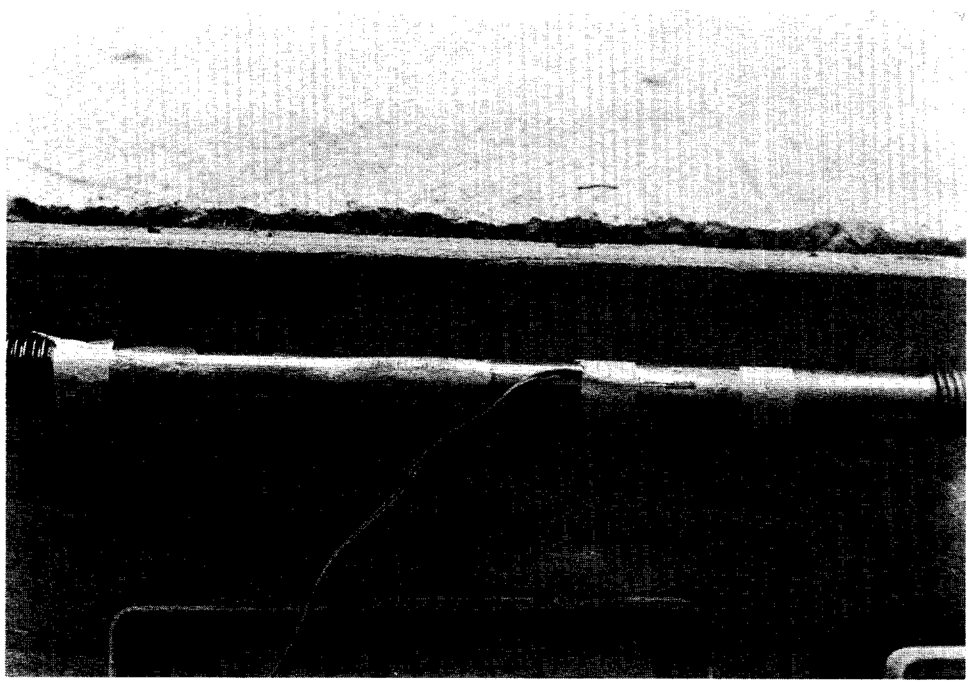

Figure 3.7 Point of application of strain gages on the rod.

Figure 3.8 Loading Pulse

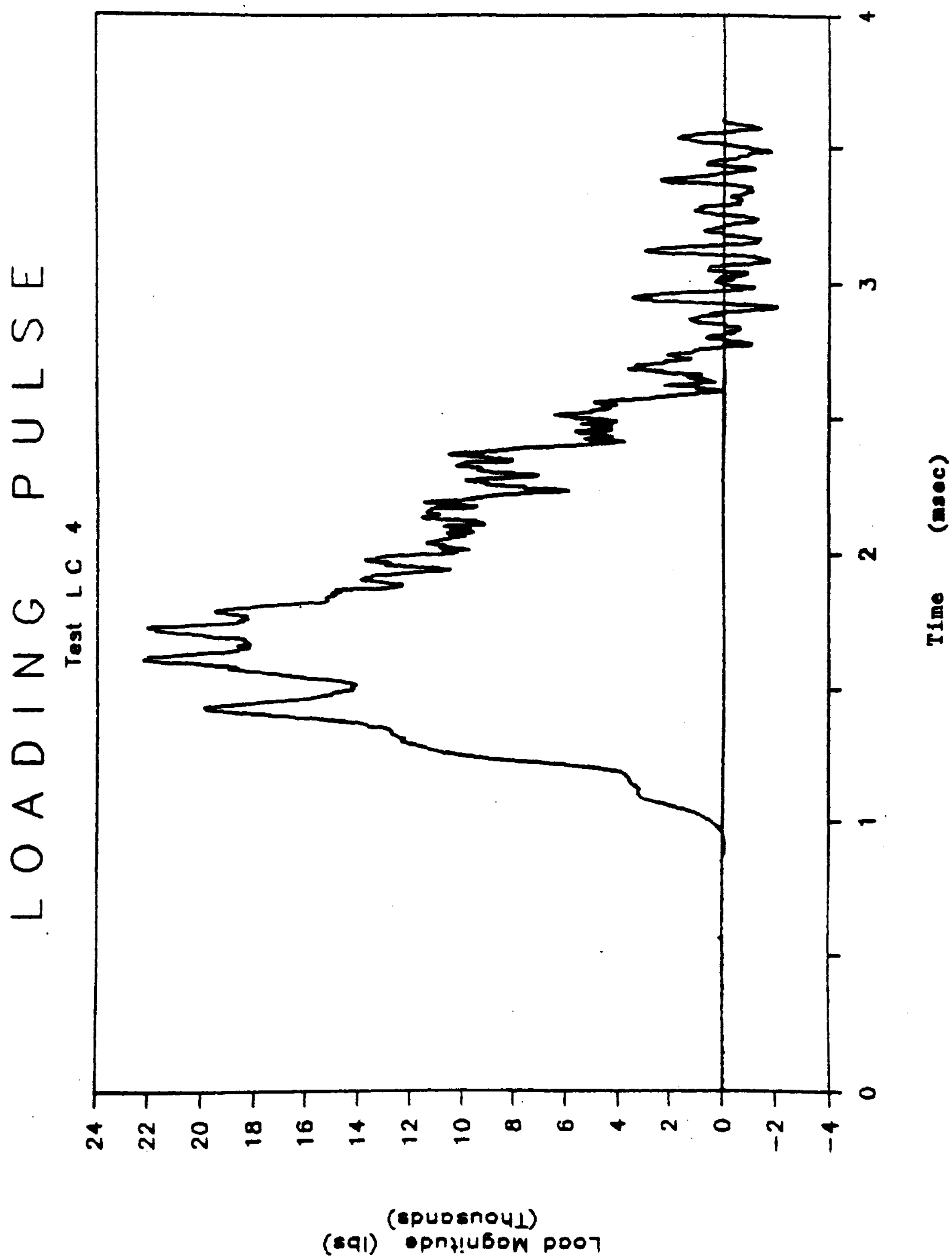

CHAPTER 4

RESULTS AND DISCUSSION

4.1 General

Experimental data consisted of acceleration-time histories obtained from the accelerometers attached to the reinforced concrete slabs in the positions previously described. A sample of plot of the accelerations for each test case is provided in Appendix A. The displacement-time histories of the same positions were obtained by integrating twice these acceleration records, and they are provided in Appendix B.

In general, signals that appear random in nature can be resolved into a summation of single frequency components as discussed in Chapter 2. A very useful tool for obtaining such components are the Fourier techniques. The approach provides a summation over all frequencies of sinusoidal functions of a given variable based on acquired experimental data. Analysis in the frequency domain was done employing Fast Fourier Transform techniques (FFT), as discussed by Oppenheim and Schafer (1975). The FFT operation as applied through the scientific software Asistant+ (1987), is defined by the following formula:

$$f(k) = \Sigma_{j\,0}^{\,n-1} f(j)e^{-2\pi ijk/n} \qquad (k = 0,\ 1, \ldots, n-1) \quad ; \quad i = \sqrt{-1} \qquad (4.1)$$

This operation takes the Discrete Fourier Transform of an input variable and returns a complex value. In fact, what was actually done is the Power Spectrum operation, defined as the square magnitude of the Fast Fourier Transform.

The results obtained from the application of the FFT to all the sequences of data showed that no interesting phenomena occurred for frequencies higher than 35000 Hz. For this reason the plots of Power Spectrum reported in Appendix C, refer to the range of frequencies 0-35000 Hz (with the exception of the tests B1 to B5 for which the range is 0-16000 Hz; the reason of this difference is that this was the range initially chosen for analysis and then extended to 0-35000 Hz because of the presence of peaks for frequencies greater than 16000 Hz. Because of the latter decision to concentrate the analysis in the range 0-5000 Hz, for the reasons that will follow, it was not necessary update these plots). Because of the very large amount of information and because already the analysis in the low frequency range gave substantial information on the system's behavior, it was decided to concentrate the analysis in the frequency range 0-5000 Hz.

The frequencies at which the main peaks in the plots occur were identified and the information was tabulated, as shown in Appendix D. Because of the uniqueness of each test, it was not possible to establish a value of the Power Spectrum common to all the tests above which the peaks in the plots should have been considered, however, for these cases the value varies from $2*10^7$ to $2*10^8$.

The following steps in the testing procedure were performed for all the tests on System 2:

1. A torque was applied to the nuts until the two slabs were in complete contact along the entire length of the common edge.
2. The nuts were then released until a zero axial force existed in the

rods (i.e., the readings from the strain indicators shifted to zero).

3. The nuts were again subjected to torque until the desired value of tension in each rod was reached.
4. The weight was lifted up to an height of three feet and dropped.
5. The data were acquired and then transferred for analysis.

The testing procedure for System 1 is composed of the last two steps only, since the axial force was found not to have an influence on the behavior (see Section 4.2).

4.2 Results for System 1

Preliminary Tests: As described in Chapter 3, a set of three tests was conducted on System 1 applying a compressive force, to see if this would alter the response of the system. During this set of tests the axial force in each rod was 10,000 pounds. These results are presented in Tables 4.1 and 4.2, and it is noted that these frequencies are the same as the ones in the Tables 4.4 and 4.5, relative to the main set of tests. It was concluded, therefore, that the presence of a compressive force applied to the big slab does not change its behavior, and because of this observation such a force was not applied during the main set of tests.

Table 4.1 System 1 with rods: loaded side of the joint.

TEST #	**Frequencies (Hz) at which peaks in Power Spectrum plots occur**								
BS 1	366	1098	1708	2196	/	/	3904	4148	4392
BS 2	366	/	1708	2928	/	/	3904	/	4392
BS 3	366	1220	1708	2196	/	3660	/	4148	/

/ = Peak too small to be significant

Table 4.2 System 1 with rods: unloaded side of the joint.

TEST #	Frequencies (Hz) at which peaks in Power Spectrum plots occur								
BS 1	366	/	1708	1952	2440	2806	/	3904	/
BS 2	366	1098	1708	2196	2440	2928	/	3904	4392
BS 3	366	1220	1708	1952	/	3172	/	/	4392

/ = Peak too small to be significant

<u>Main Tests:</u> The assumption that System 1 represents an ideal condition of full shear transfer capability is confirmed by the test results. From the initial assumptions the value of joint efficiency that was assumed to be representative of a condition of new joint is, according to Table 3.2, about 0.9. Table 4.3 gives for the tests conducted on the big slab, the values of the maximum displacements, the time at which they occur and the ratio between the displacements on the loaded side and on the unloaded side of the imaginary joint, that is the joint efficiency:

Table 4.3 System 1: Values of maximum displacements, time at which they occur and resulting joint efficiency.

TEST #	LOADED NODE		UNLOADED NODE		J.E.
	Max. Displ. / g	Time (msec)	Max. Displ. / g	Time (msec)	
B 1	-5.200 E-5	7.76	-4.680 E-5	7.77	0.900
B 2	-5.000 E-5	6.30	-4.200 E-5	6.38	0.840
B 3	-5.240 E-5	6.99	-3.288 E-5	6.55	0.628
B 4	-4.720 E-5	6.74	-4.040 E-5	6.61	0.856
B 5	-3.864 E-5	6.49	-3.440 E-5	6.51	0.890
B 6	-3.780 E-5	6.63	-4.280 E-5	6.77	1.132
B 7	-3.528 E-5	8.25	-2.924 E-5	8.19	0.829
B 8	-3.024 E-5	7.16	-2.872 E-5	7.05	0.950

J.E. = Joint Efficiency ; g = Acceleration of Gravity

At first it can be noted that for all the cases but one these values are all very close to 0.9; only during the test B 3 a value of 0.628 is obtained, probably due to a non perfect adherence between one of the accelerometers and the slab. It can be useful to recall here that the accelerometers were attached to the slab by means of an adhesive material that very rarely during the tests did not perform properly, causing the detachment of the accelerometers from the slabs. Case B 3 was included here to demonstrate this point. In case B 6 a joint efficiency bigger than 1 is obtained; there are two possible explanations, the first is a possible mistake during the transfer of the records for analysis and the exchange of the files IN and OUT; the second, again a non good performance of the adhesive.

From Table 4.3 and from the plots reported in Appendix B it can be seen that the maximum displacements on both side of the joint occur at the same time. In general for every test, all time histories of these displacements almost overlap each other: the two sides of the imaginary joint move at the same time and with displacements of the same amplitude. This indicates that the load is properly transferred from one side of the ideal joint to the other, as expected.

Once that data were available for all the cases, as reported in Appendix D, it was possible obtain a description of the main events in the frequency domain for all the cases. A summary of these is presented in Tables 4.4 and 4.5 for the loaded and the unloaded sides of the joint, respectively.

Table 4.4 System 1: Peak Frequencies on loaded side of the joint.

TEST #	Frequencies (Hz) at which peaks in Power Spectrum plots occur								
B 1	366	1098	/	2196	2684	/	/	/	/
B 2	366	1220	1708	/	/	/	/	/	/
B 3	366	/	1708	2196	/	/	/	4148	4392
B 4	366	/	1708	2196	2562	/	/	/	/
B 5	366	1098	1708	2196	2440	/	/	3904	4392
B 6	366	/	/	2196	2440	/	3660	3904	/
B 7	488	1098	1708	2196	2684	/	/	/	4270
B 8	366	1098	1708	2196	2684	/	3660	3904	/

/ = Peak too small to be significant, or no peak response at that frequency.

Table 4.5 System 1: Peak Frequencies on unloaded side of the joint.

TEST #	Frequencies (Hz) at which peaks in Power Spectrum plots occur								
B 1	366	1220	/	2196	2684	/	3660	/	/
B 2	366	1220	1708	/	/	/	/	/	4392
B 3	366	/	1708	2074	/	/	/	4148	4392
B 4	366	/	1708	2074	2684	2928	/	/	/
B 5	366	1098	1708	2074	2684	/	3904	/	/
B 6	366	/	/	2196	2684	2928	3904	/	/
B 7	488	1220	1708	2074	2684	/	/	/	4392
B 8	366	1220	1708	/	2684	2928	3904	/	/

/ = Peak too small to be significant, or no peak response at that frequency.

4.3 Results for System 2

System 2 represents the variable joint conditions through the applications of different values of axial force N in the rods. Table 4.6 contains the values of the maximum displacements, the time at which they occur and the ratio between the displacements on the loaded side and on the unloaded side of the joint, that is the joint efficiency.

Table 4.6 System 2: Values of maximum displacements, time at which they occur and resulting joint efficiency.

TEST #	LOADED NODE		UNLOADED NODE		J.E.
	Max. Displ. / g	Time (msec)	Max. Displ. / g	Time (msec)	
ST 1	-8.00 E-5	5.82	-2.216 E-5	7.21	0.277
ST 2	-6.80 E-5	6.48	-0.476 E-5	6.99	0.070
ST 3	-7.28 E-5	6.03	-1.896 E-5	7.09	0.260
SU 1	-7.16 E-5	5.77	-2.816 E-5	6.67	0.393
SU 2	-6.84 E-5	4.93	-2.408 E-5	5.83	0.352
SU 3	-5.44 E-5	5.50	-1.852 E-5	5.98	0.340
SV 1	-7.56 E-5	5.44	-4.240 E-5	7.62	0.561
SV 2	-5.64 E-5	5.83	-2.792 E-5	6.30	0.495
SV 3	-5.12 E-5	5.67	-2.660 E-5	6.25	0.520
SP 1	-5.04 E-5	5.23	-4.400 E-5	6.08	0.873
SP 2	-5.60 E-5	5.60	-3.712 E-5	5.76	0.663
SP 3	-5.04 E-5	5.23	-3.348 E-5	5.62	0.664
SQ 1	-4.520 E-5	5.72	-4.160 E-5	5.86	0.920
SQ 2	-3.916 E-5	6.05	-3.732 E-5	5.69	0.953
SQ 3	-3.844 E-5	5.70	-3.656 E-5	5.78	0.951
SR 1	-4.160 E-5	5.17	-3.988 E-5	5.19	0.959
SR 2	-3.944 E-5	5.37	-3.976 E-5	5.49	1.008
SR 3	-3.848 E-5	5.88	-3.668 E-5	5.88	0.953

J.E. = Joint Efficiency ; g = Acceleration of Gravity

The choice of the N values reported in Table 3.3 as representative of these different conditions is confirmed to be correct by the test results. Comparing the assumed values of Joint Efficiency given by Table 3.2, with the ones obtained in the laboratory, given by Table 4.6, it can be seen that the pairs of sets ST-SU, SV-SP and SQ-SR, effectively represent the cases of dead, deteriorated and new joint respectively. From the data in Table 4.6 and from the plots in Appendix B it can be seen that the interval of time between the peaks in the displacement plots decreases as the value of axial force in the rods increases. Also increasing the force, the amplitude of the displacements decreases and so does the difference between the values of the displacements on the two sides of the joint at any time. In other words, the application to the slabs of an in-plane variable compressive force effectively leaded to the simulation of different shear transfer conditions. As the value of this force increases, the two slabs tend to behave more as one. For high values of applied force (for example, sets SQ and SR), the two sides of the interface move almost simultaneously and with displacements of almost same amplitude. This fact demonstrates a good shear transfer capability across the joint interface.

This trend can be observed also from the plots in Appendix A, relative to the accelerations: increasing the value of the axial force, the difference between the accelerations of the points on the two sides of the joint, decreases.

The data for all cases, as shown in Appendix D, was transformed into the frequency domain, and the main component of the responses are summarized in Tables 4.7 and 4.8 for the loaded and unloaded sides, respectively.

Table 4.7 System 2: Peak Frequencies on loaded side of the joint.

TEST #	Frequencies (Hz) at which peaks in Power Spectrum plots occur								
ST 1	244	1098	1586	/	2440	3538	/	/	/
ST 2	244	1098	1586	/	2440	3660	3904	4270	/
ST 3	244	1098	1586	/	2440	3538	3904	/	/
SU 1	244	976	1586	2318	2562	3660	3904	4270	4758
SU 2	244	976	1586	2318	2562	3660	3904	4270	4758
SU 3	244	1098	1586	/	2562	3660	3904	4270	/
SV 1	244	1098	1586	2196	2562	3660	/	/	/
SV 2	366	1098	1586	/	2440	3660	/	4270	/
SV 3	244	1098	1586	/	2440	3660	/	4270	4758
SP 1	244	1098	1586	/	2562	3538	/	4270	4758
SP 2	244	1098	/	/	2318	/	/	4270	/
SP 3	244	1098	1586	/	/	/	/	4026	/
SQ 1	244	1220	1586	/	2318	3782	/	4270	4758
SQ 2	244	1220	1708	/	2440	3660	/	4026	4758
SQ 3	244	1220	1586	/	2562	3782	/	4270	/
SR 1	244	1220	1830	/	2440	3660	/	/	4758
SR 2	244	1220	/	/	/	3660	3904	4270	/
SR 3	244	/	1952	/	2318	/	/	/	4758

/ = Peak too small to be significant, or no peak response at that frequency.

Table 4.8 System 2: Peak Frequencies on unloaded side of the joint.

TEST #	Frequencies (Hz) at which peaks in Power Spectrum plots occur								
ST 1	244	488	1098	/	1708	2562	3782	/	/
ST 2	244	488	854	1220	1586	2440	3660	/	4880
ST 3	244	488	976	/	/	2562	3660	/	/
SU 1	244	610	976	/	1708	2440	3660	/	4880
SU 2	244	610	1098	/	1586	2562	/	4270	4880
SU 3	244	610	1098	/	1708	2562	3660	/	4880
SV 1	244	732	1098	/	1586	2440	/	/	4880
SV 2	244	732	1098	/	1586	2440	3660	/	/
SV 3	244	732	1098	/	1586	2562	3660	/	/
SP 1	244	/	1098	1586	/	2684	3660	4270	4880
SP 2	244	/	1098	/	/	/	3660	/	/
SP 3	244	/	1098	1586	/	/	/	4270	/
SQ 1	244	/	1098	1708	2440	2684	3782	/	4880
SQ 2	244	/	/	1708	2440	/	3660	/	/
SQ 3	244	/	1098	1708	2440	2684	3660	4392	/
SR 1	244	/	1220	1708	2440	/	3660	/	4758
SR 2	244	/	1098	/	/	/	3660	4270	4880
SR 3	244	/	1098	1830	/	/	/	/	/

/ = Peak too small to be significant, or no peak response at that frequency.

4.4 Comparison of the Results

To proceed with a comparison of the results, the data previously presented have been summarized in the Tables 4.9 and 4.10, where for every set, the recurrent values of frequency have been chosen as representative of the set. The Tables are referred to the loaded and unloaded side of the joint respectively.

Table 4.9 Frequency variations on loaded side of joint. For each test the frequencies reported are the more recurrent from the ones of the respective sets as given in the Tables 4.4 and 4.7.

TEST #	Frequencies (Hz) at which peaks in Power Spectrum plots occur							
ST	244	1098	1586	2440		3538	3904	
SU	244	976	1586	2318	2562	3660	3904	4270
SV	244	1098	1586	2440	2562	3660		4270
SP	244	1098	1586		2562			4270
SQ	244	1220	1586	2440	2562	3660		4270
SR	244	1220				3660		4758
B	366	1098	1708	2196	2684	3660	3904	

Table 4.10 Frequency variations on unloaded side of joint. For each test the frequencies reported are the more recurrent from the ones of the respective sets as given in the Tables 4.5 and 4.8.

TEST #	Frequencies (Hz) at which peaks in Power Spectrum plots occur								
ST	244	488	976	1586		2562	3660		
SU	244	610	976	1586	2440	2562	3660	4880	
SV	244	732	1098	1586	2440	2562	3660		
SP	244	1098		1586		2684	3660	4270	
SQ	244	1098		1708	2440	2684	3660		
SR	244	1098		1708	2440		3660	4270	
B	366	1220		1708	2074	2684		3904	4392

The following observations are made on the results presented in Tables 4.9 and 4.10:

1. The data indicates that the second response frequency is affected by the shear transfer capability of the joint. An increase in the quality of the contact across the joint increases the second response frequency, as shown in Figure 4.1. This observation is true based on the data in Table 4.10 from readings on the unloaded side.

   A similar trend can be observed from readings on the loaded side with one exception: the set of tests ST presents a second frequency of 1098 Hz, a value bigger than 976 Hz, the second frequency of the set SU.
   A further increase in the axial force caused the second frequency to reach and remain at the value 1098 Hz in the unloaded side and 1220 Hz

in the loaded side.

2. The response of the larger slab (System 1) is very close to the response of the two slabs (System 2) subjected to a large axial force. The main difference is in the first frequency, that is a function of the slab's dimensions and dynamic characteristics. This difference, observable for both the sides of the joint, indicates that the large slab has a rigid body motion that is different from the two smaller slabs.

3. For higher values of frequencies not appreciable differences can be related to changes in the quality of the contact between the two sides of the joint; on both sides the values that appear remain almost constant for all the tests.

   Exceptions are the fourth and sixth frequencies: the first shifting from 1586 Hz to 1708 Hz when the axial force increases, the latter from 2562 Hz to 2684 Hz. This shift is particularly evident on Table 4.10 relative to the unloaded side of the joint. But in these cases the trend is not as well defined as in the case of the second frequency.

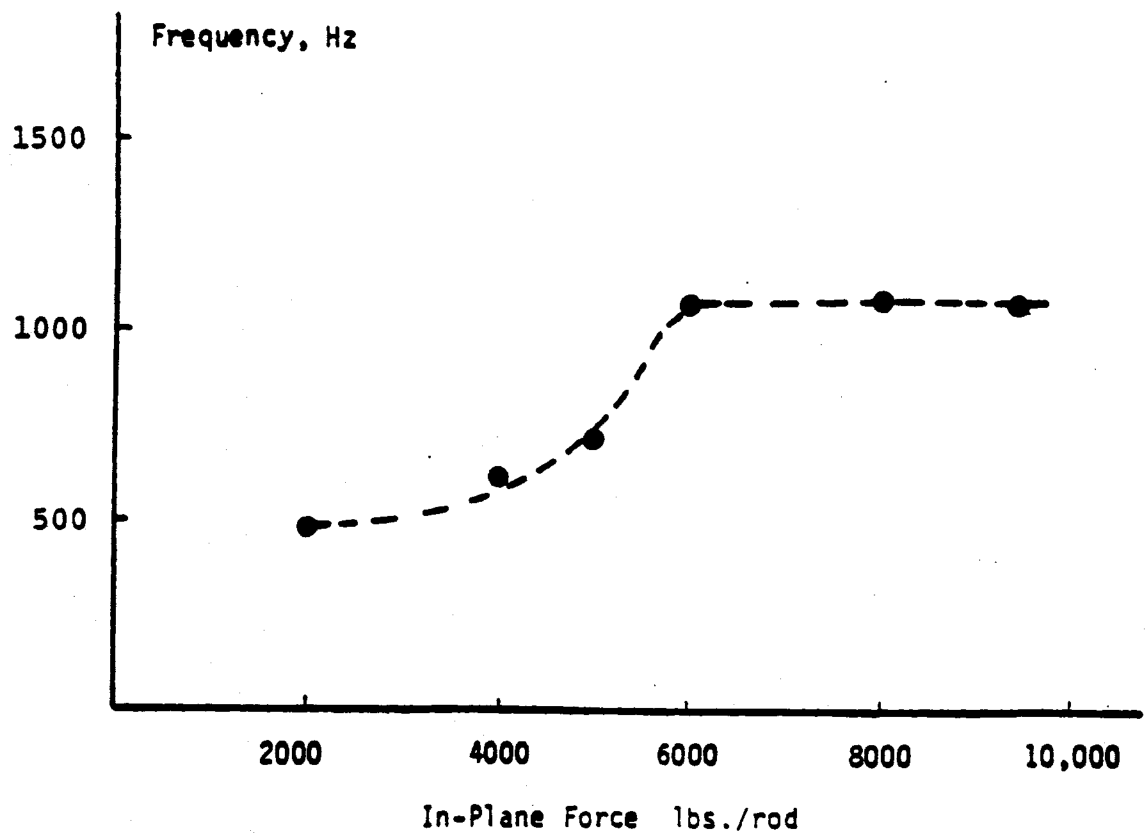

Figure 4.1 2nd Frequency vs. Interface Contact Conditions.

CHAPTER 5

CONCLUSIONS AND RECOMMENDATIONS

5.1 Conclusions

An experimental approach has been presented for non-destructive testing of pavements joints. Experimental data have been acquired on models representing different shear transfer capabilities across concrete pavements joints. That data were analyzed both in the time domain and in the frequency domain utilizing the Fourier Analysis Technique. The results obtained confirm the initial expectations that response frequencies in the dynamically loaded structure are closely related to the shear transfer capacity of the joint. In turn, this parameter is represented also by the Joint Efficiency, a commonly used indicator of a pavement joint condition. The following conclusions are drawn from this study:

1. The model that has been adopted to simulate different joint shear transfer conditions is reliable, and it has been confirmed by experimental data.
2. The utilization of the Fourier Analysis technique was effective for this investigation. The information obtained from the analysis in the frequency domain was essential for understanding the overall behavior.
3. On the basis of the obtained results, frequency variation of modal response is an excellent tool for deciphering the internal conditions of pavements joints, and vibrations of different frequency are representative of different values of joint shear transfer.
4. Specifically, the first natural frequency of the pavement joint system is not affected by changes in the joint conditions, however, the second

response frequency exhibited noticeable variation corresponding to different joint shear transfer capabilities. A change in the internal joint conditions can be correlated to a precise shift of the second frequency.

Based on these results it is concluded that this approach can be employed for the determination of the internal shear transfer capabilities of interfaces in pavement joints and bridge decks.

5.2 Recommendations

Based on the present findings, the following recommendations are made:

1. To improve the present approach for developing a more sophisticated device based on the same principles; taking into consideration all the characteristics necessary for building an instrument that could easily be used in the field.
2. To continue the present study by performing corresponding field tests on pavement joints and bridge decks, combined with FWD testing.
3. To develop a clear relationship between FWD data and the frequency response approach.
4. To determine and to define the effects of site conditions on such comparisons. The parameters to be included are: type of base and subgrade, type of pavement and joint, structural parameters of bridge and type of bridge deck, and environmental effects (i.e. temperature gradients, both seasonal and daily, moisture, frost).

5. To develop a "Handbook" for pavement engineers that correlates the observed frequency with the internal conditions of a pavement joint, and/or a joint in a bridge deck.
6. To develop and produce a simple testing device, based on the proposed approach, for quick assessment of pavement joints and bridge decks. That device could be mounted on FWD testing systems, and/or operate independently as a stand alone testing device.

REFERENCES

1. ACI 318-89, Building Code Requirement For Reinforced Concrete.

2. ACI-ASCE Commitee 426, "The Shear Strength of Reinforced Concrete Members", ASCE Journal of Structural Division, Vol. 99, June 1973.

3. "Asystant+, Scientific Software for Data Acquisition and Analysis", Asyst Software Technologies, Inc., Rochester, NY.

4. Barenberg, E.J., Arntzen, D.M., "Design of Airport Pavements as Affected by Load Transfer and Support Conditions", Proceedings of 2nd International Conference on Concrete Pavement Design, Purdue University, April 1981.

5. Belluzzi, O., (1984) "Scienza delle Costruzioni", Vol.1, Zanichelli.

6. Blouin, E.S., and Wolfe, H.S., (August 1976) "Analysis of Explosively Generated Ground Motions Using Fourier Techniques", CRREL Report 76-28.

7. Foxworty, P.T., "Concepts for the Development of a Nondestructive Testing Evaluation System for Rigid Airfield Pavements", Ph.D. Thesis, Department of Civil Engineering, University of Illinois at Urbana-Champaign, June 1985.

8. Hoffman, M.S., and Thompson, M.R., "Comparative Study of Selected Nondestructive Testing Devices", Record 852, Transportation Research Board, 1982.

9. Khanlarzadeh, H., and Krauthammer,T., (October 1986) "Analysis of Minnesota Test Section",Structural Engineering, Report ST-86-03.

10. Kolsky, H., (1963) "Stress Waves in Solids", Dover.

11. Krauthammer, T., and Western, K.L., (September 1988) "Joint Shear Transfer Effects on Pavement Behavior", Journal of Transportation Engineering, ASCE, Vol. 114, No. 5, pp. 505-529.

12. Mac Gregor, G. J., (1988) "Reinforced Concrete, Mechanics and Design", Prentice Hall.

13. Mattock, H.A., and Hawkins, M.N., "Shear Transfer in Reinforced Concrete-Recent Research", Journal of Prestressed Concrete Institute, Vol. 17, No. 2, March-April 1972.

13. Moore, W. M., Hanson, D.I., and Hall, J.W., "An Introduction to Non-destructive Structural Evaluation of Pavements", Circular 189, Transportation Research Board, Jan.,1978.

14. Newmark, N.M., and Rosenblueth, E., (1971) "Foundamentals of Earthquake Engineering", Prentice-Hall.

15. Oppenheim, A.V., and Schafer, R.W., (1975) "Digital Signal Processing", Prentice-Hall.

16. Park, R., and Paulay, T., (1975) "Reinforced Concrete Structures", Wiley-Interscience Pubblication.

17. Pozzati, P., (1986) "Teoria e Tecnica delle Strutture", Vol.2, Parte 1, Unione Tipografico-Editrice Torinese.

18. Sebaaly, B., Davis, T.G., and Mamlouk, M.S., "Dynamics of Falling Weight Deflectometer", Journal of Transportation Engineering, Vol. 111, No. 6, November 1985.

19. Tabataie, A.M., Barenberg, E.J., (September 1980) "Structural Analysis of Concrete Pavement Systems", Journal, ASCE, Vol.106, No. TE5.

20. Timoshenko, S., Woinowsky-Krieger, S., (1959) "Theory of Plates and Shells", McGraw-Hill.

21. Westergaard, H.M., "Stresses in Concrete Pavements Computed by Theoretical Analysis", Public Roads, Vol. 7, 1926.

22. Westergaard, H.M., "Analysis of Stresses in Concrete Roads Caused by Variations in Temperature", Public Roads, Vol. 8, 1927.

23. Westergaard, H.M., "Mechanics of Progressive Cracking in Concrete Pavements", Public Roads, Vol. 10, 1929.

24. Westergaard, H.M., "Analytical Tools for Judging Results of Structural Tests of Concrete Pavements", Public Roads, Vol. 14, 1933.

25. Westergaard, H.M., "New Formulas for Stresses in Concrete Pavements of Airfields", Transaction, ASCE, Vol. 73, 1947.

26. Western, K.L., and Krauthammer, T., (September 1988) "Joint Shear Transfer Effects on Pavement Performance", Structural Engineering, Report ST-86-02.

27. Williams, R.I.T., (1986) "Cement-Treated Pavements", Elsevier Applied Science Publishers.

28. Yoder, E.J., and Witczak, M.W., (1975) "Principles of Pavement Design".

APPENDIX A

Acceleration - Time Plots

The plots in the Appendix are the ones from the following tests:

B 3 :	Inside Node, Outside Node
ST 1 :	"
SU 3 :	"
SV 2 :	"
SP 2 :	"
SQ 3 :	"
SR 3 :	"

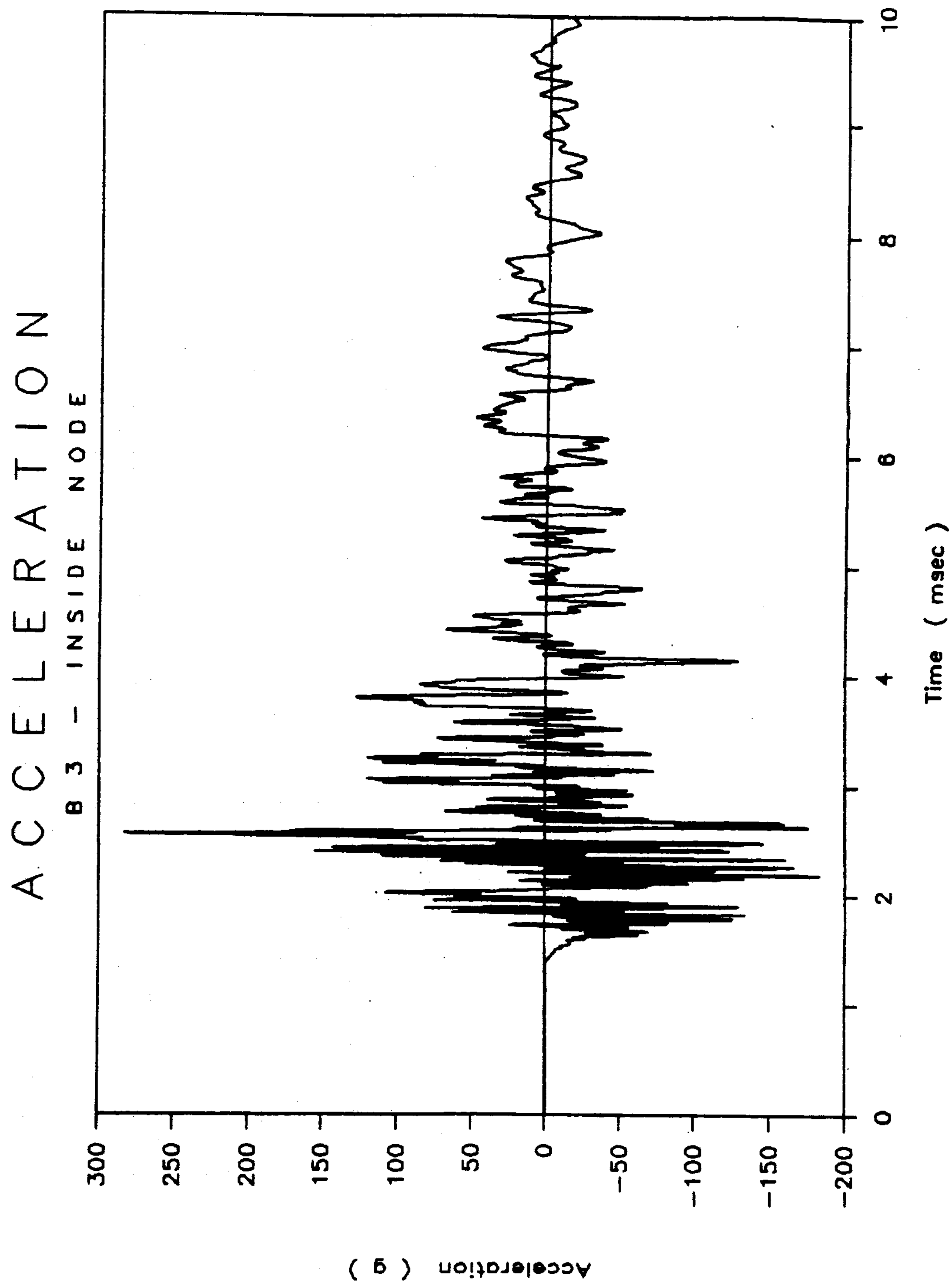
ACCELERATION
B 3 – INSIDE NODE
Acceleration (g)
300
250
200
150
100
50
0
−50
−100
−150
−200
Time (msec)
0
2
4
6
8
10

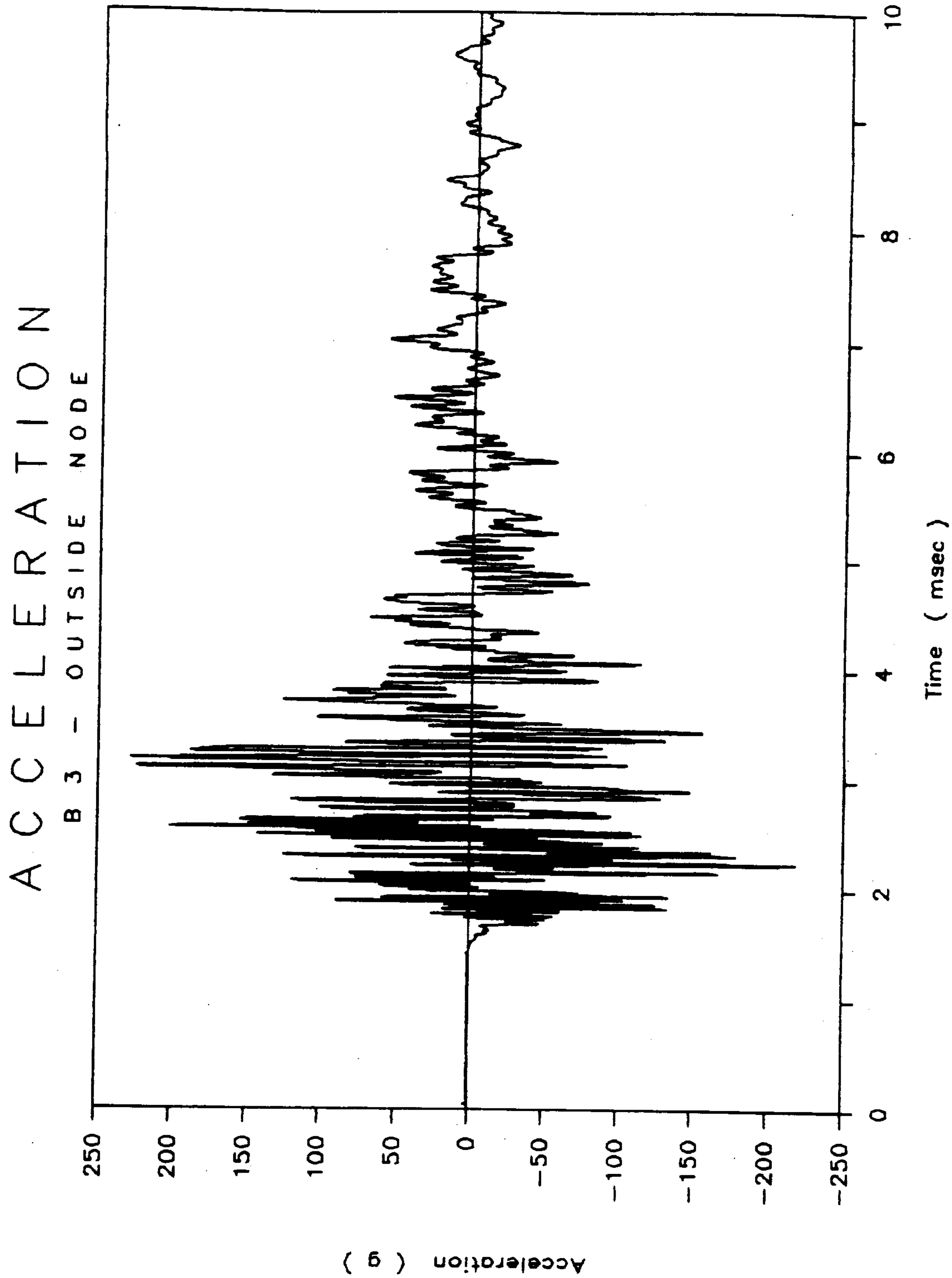
ACCELERATION
B 3 - OUTSIDE NODE
Acceleration (g)
250
200
150
100
50
0
-50
-100
-150
-200
-250
Time (msec)
0
2
4
6
8
10

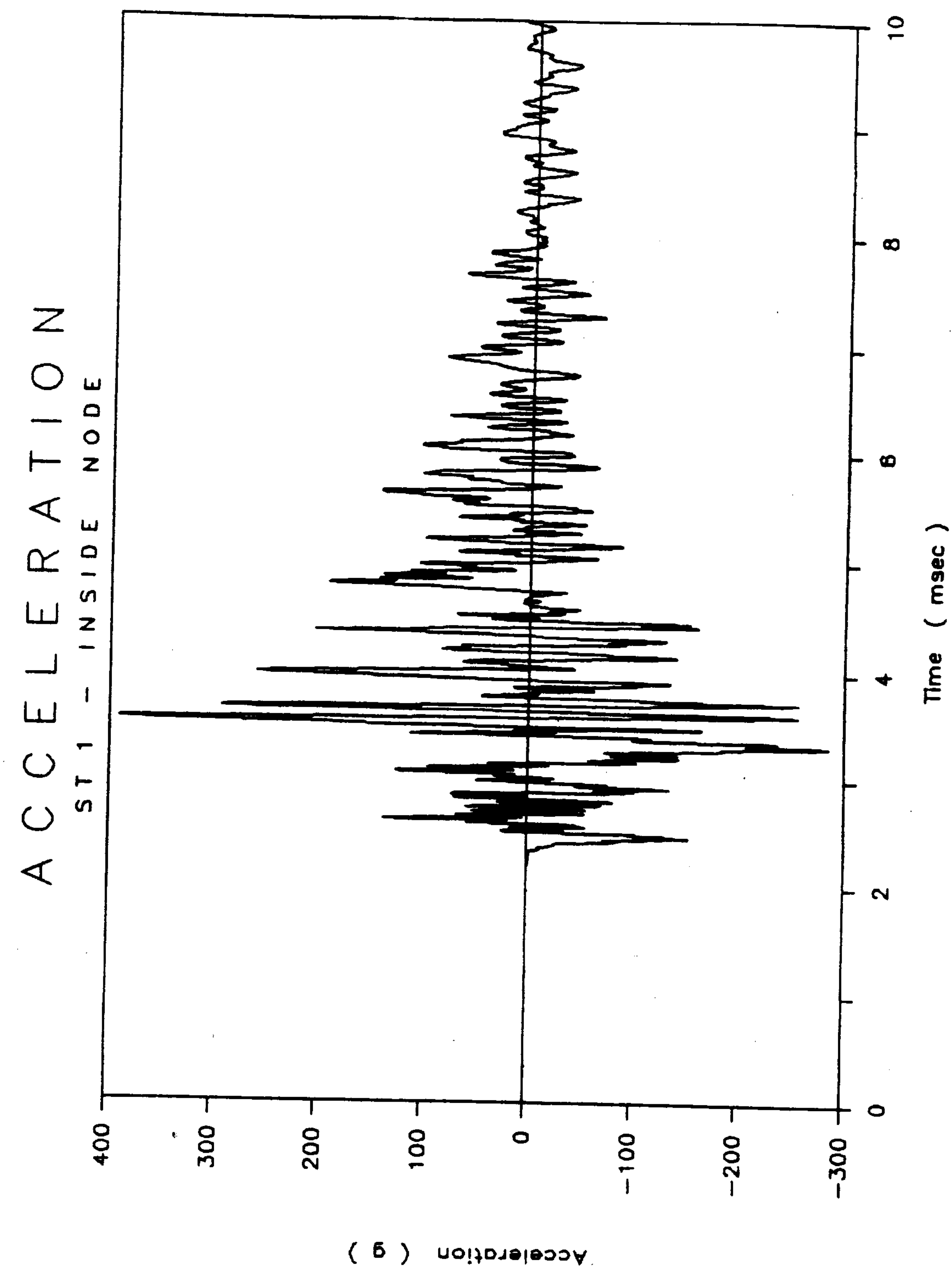

ACCELERATION
ST 1 – INSIDE NODE
Acceleration (g)
Time (msec)
400
300
200
100
0
-100
-200
-300
0
2
4
6
8
10

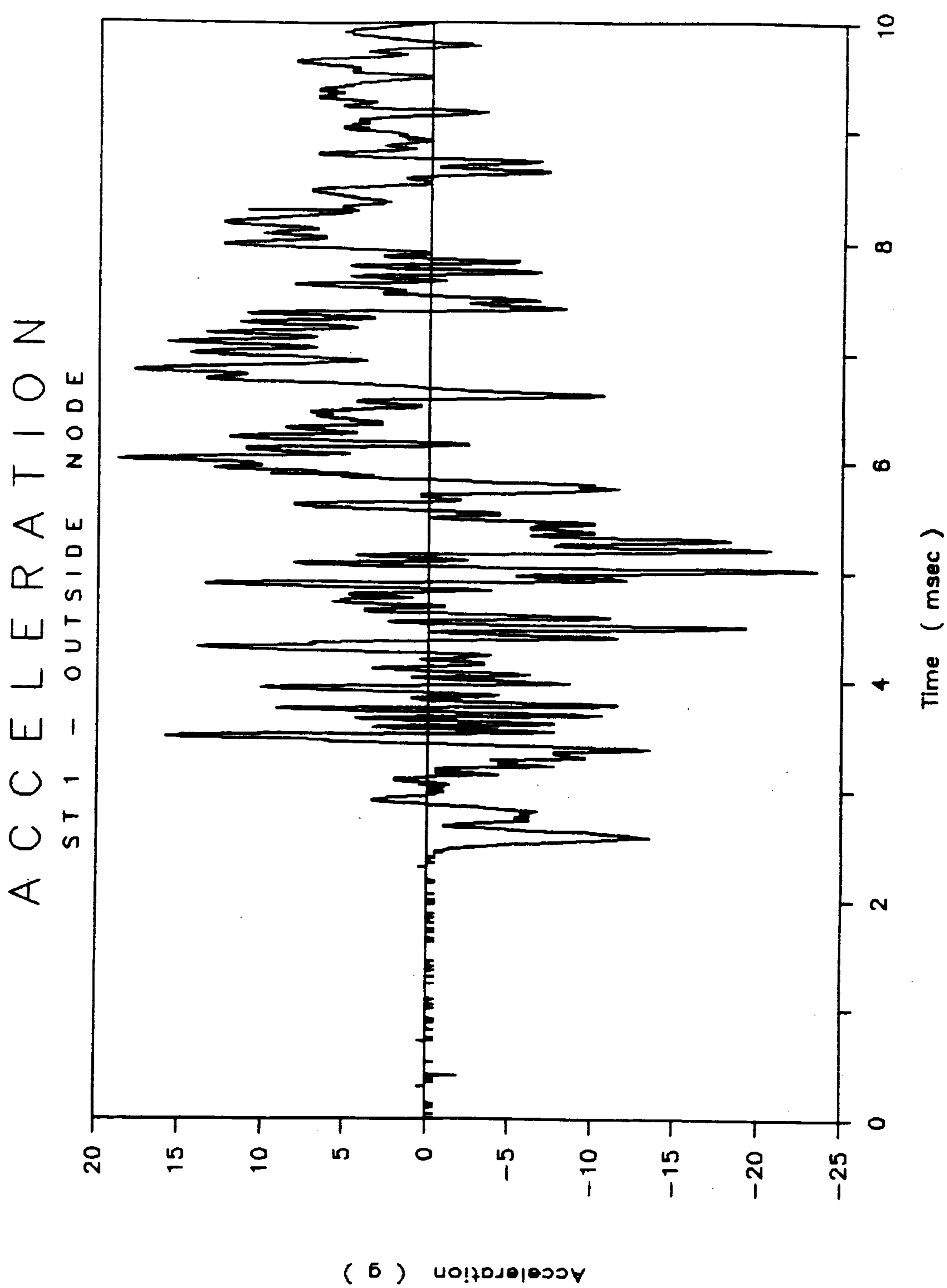

ACCELERATION
ST1 - OUTSIDE NODE
Acceleration (g)
20
15
10
5
0
-5
-10
-15
-20
-25
Time (msec)
0
2
4
6
8
10

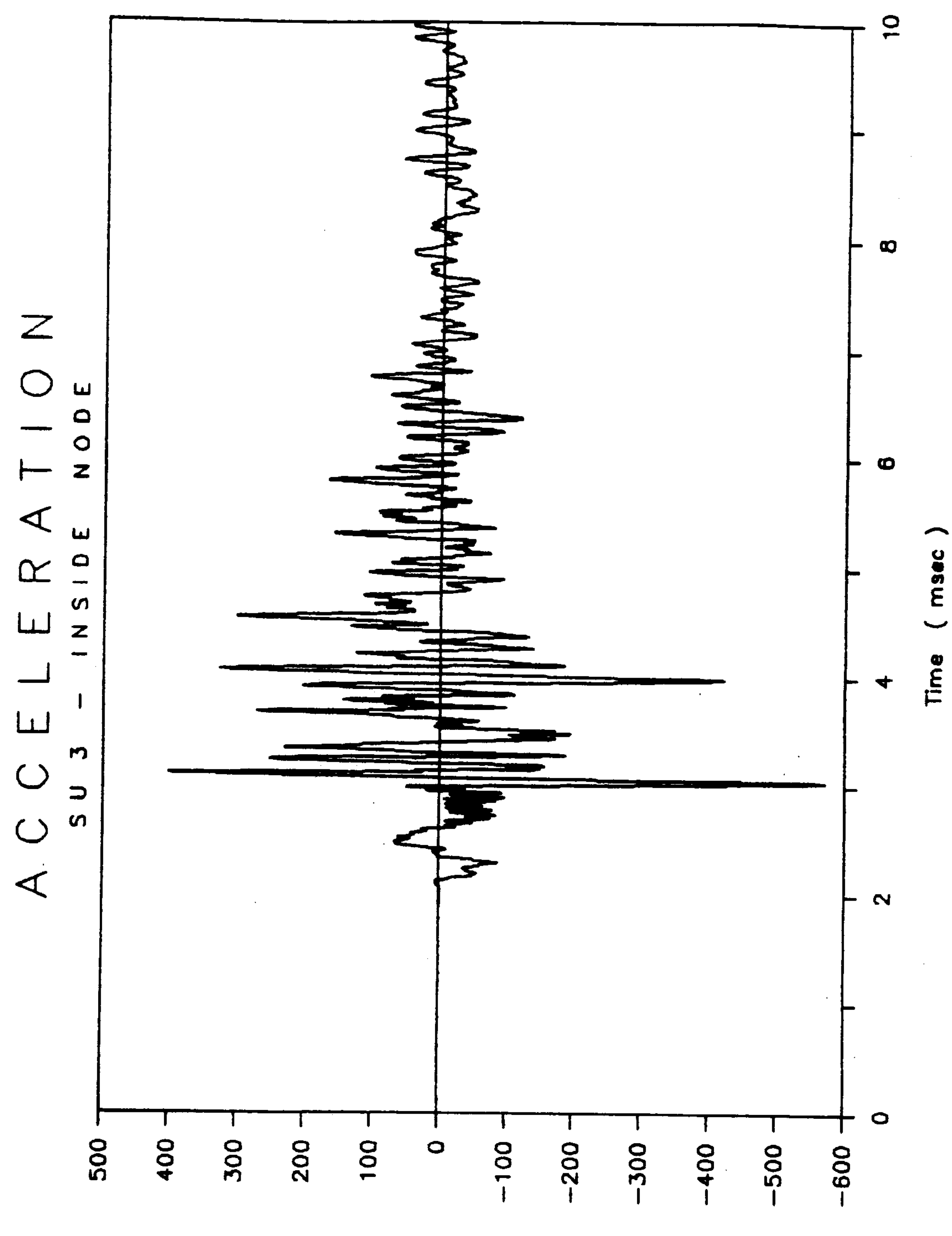
ACCELERATION
SU 3 - INSIDE NODE
Acceleration (g)
500
400
300
200
100
0
-100
-200
-300
-400
-500
-600
Time (msec)
0
2
4
6
8
10

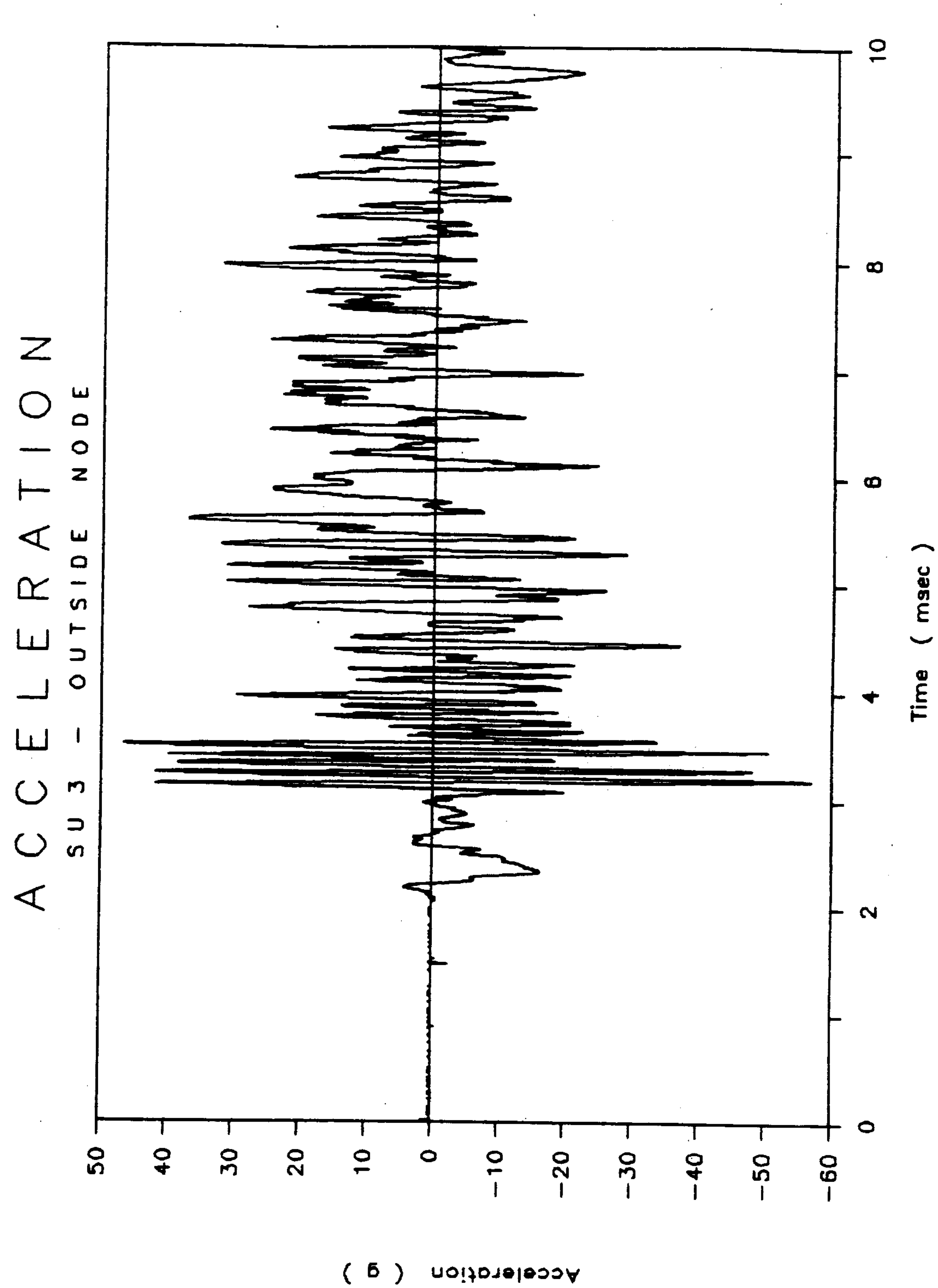

ACCELERATION
SU3 - OUTSIDE NODE
Time (msec)
Acceleration (g)
0
2
4
6
8
10
50
40
30
20
10
0
-10
-20
-30
-40
-50
-60

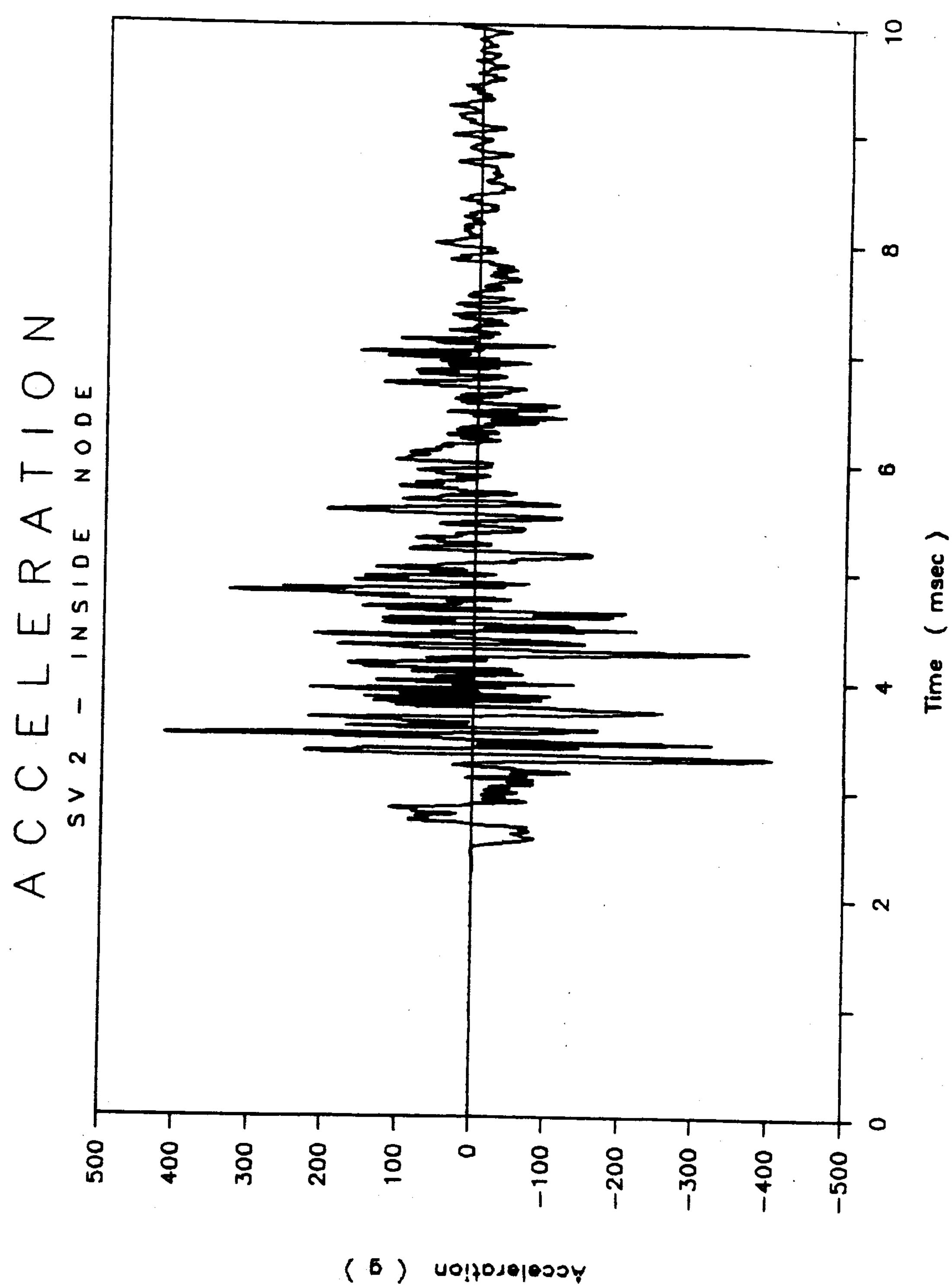
ACCELERATION
SV 2 - INSIDE NODE
Acceleration (g)
500
400
300
200
100
0
-100
-200
-300
-400
-500
Time (msec)
0
2
4
6
8
10

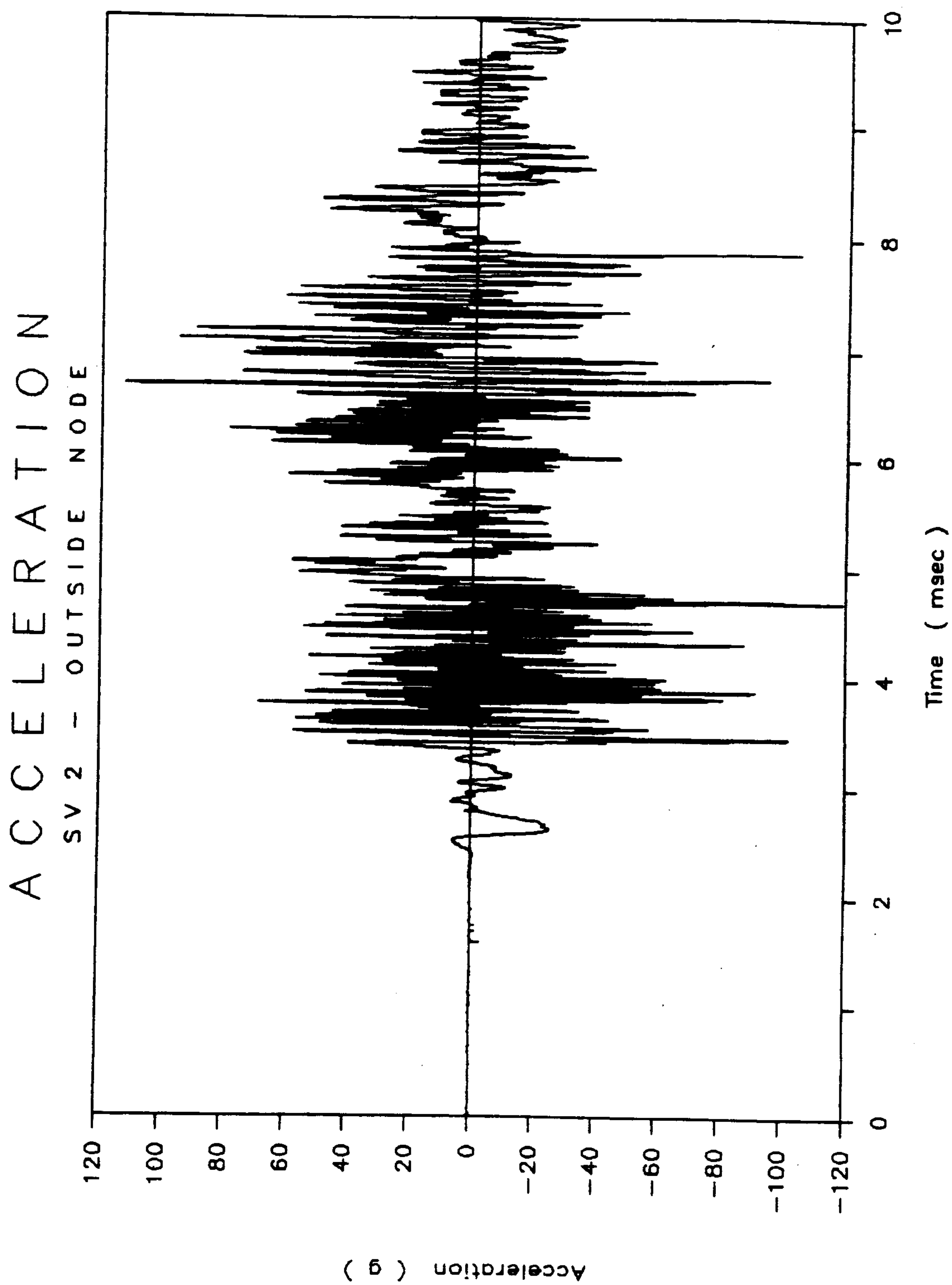
ACCELERATION
SV 2 - OUTSIDE NODE
Acceleration (g)
Time (msec)
120
100
80
60
40
20
0
-20
-40
-60
-80
-100
-120
0
2
4
6
8
10

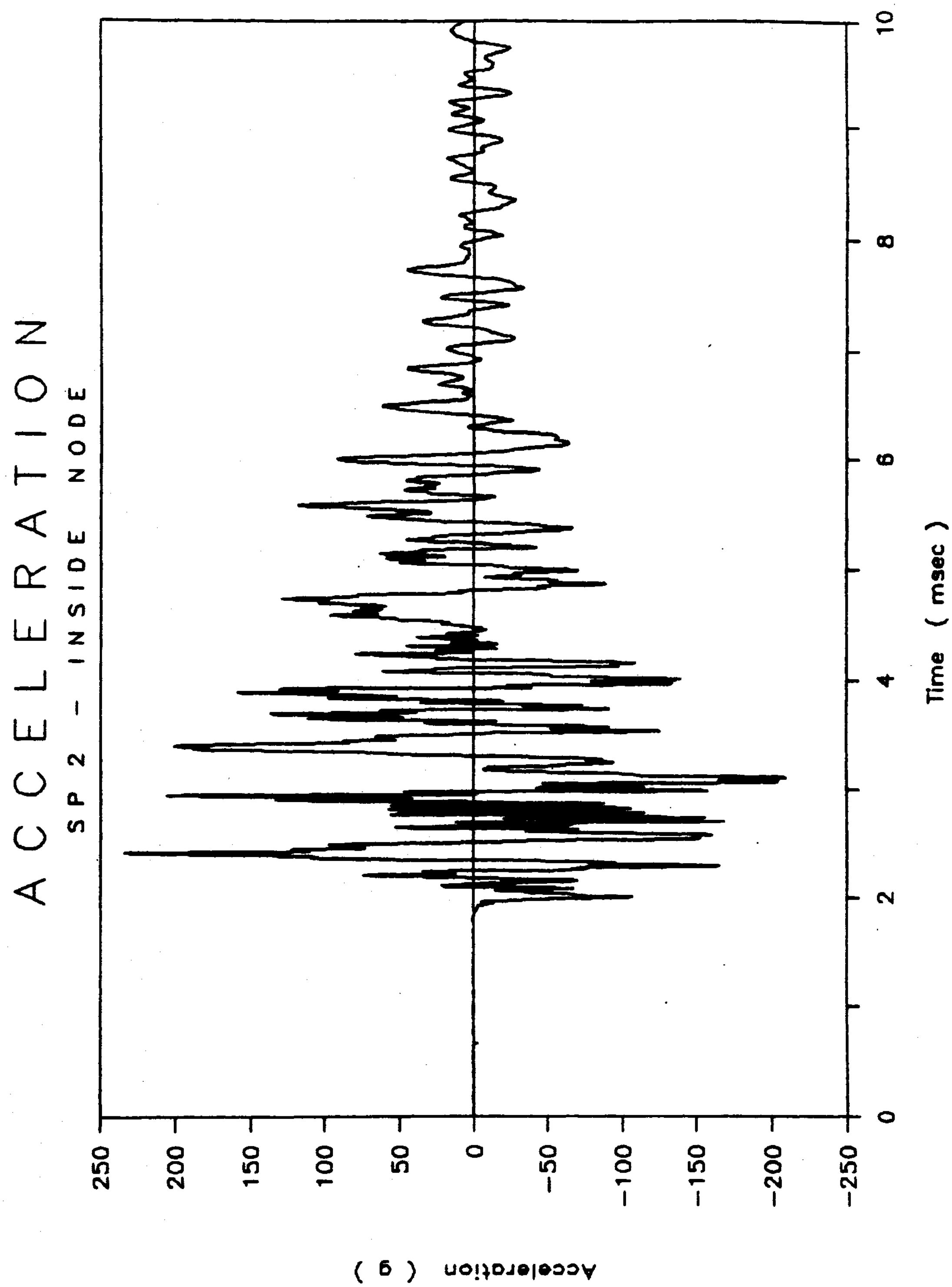
ACCELERATION
SP 2 - INSIDE NODE
250
200
150
100
50
0
-50
-100
-150
-200
-250
Acceleration (g)
0
2
4
6
8
10
Time (msec)

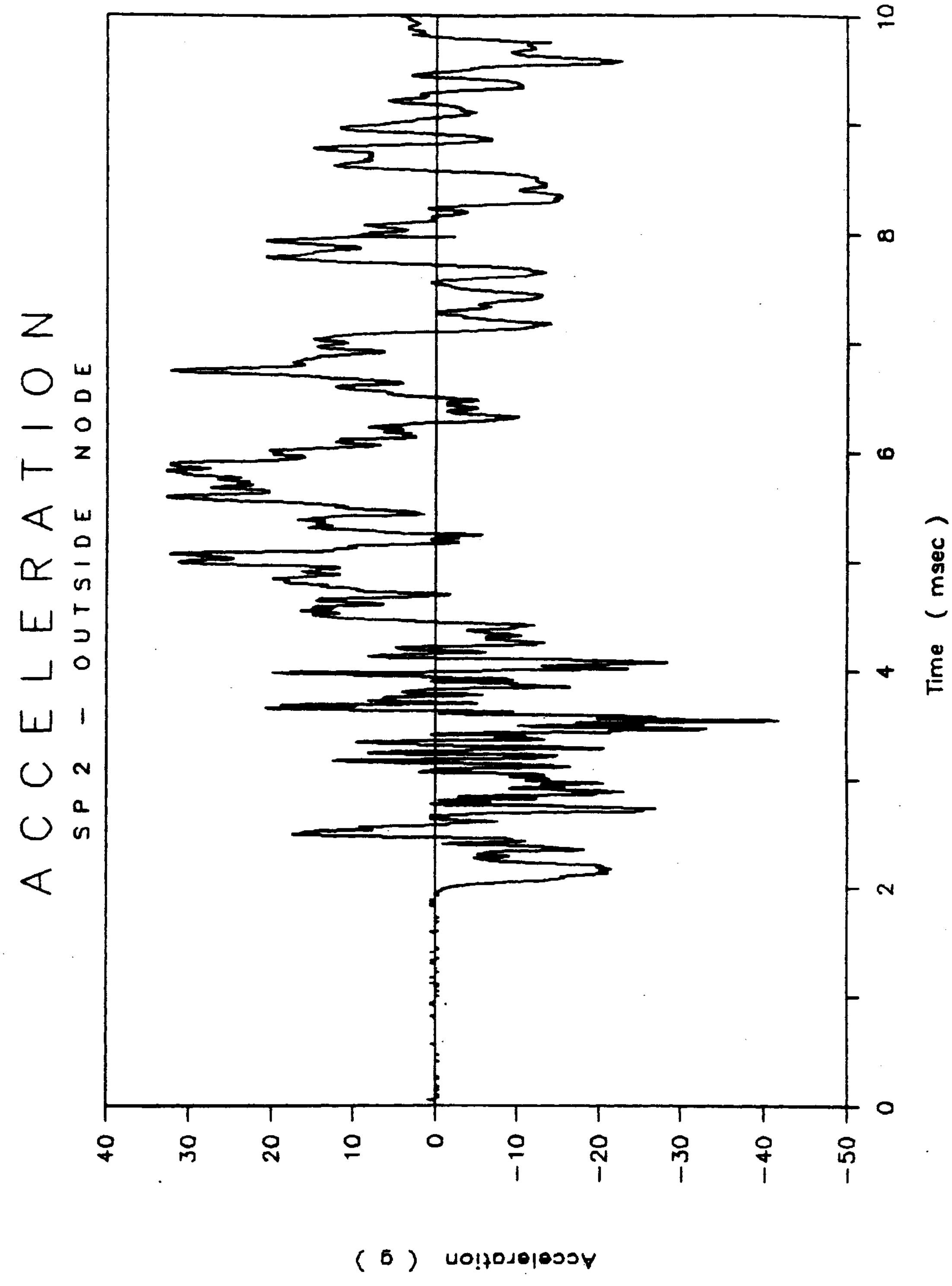
ACCELERATION
SP 2 – OUTSIDE NODE
Time (msec)
Acceleration (g)
0
2
4
6
8
10
40
30
20
10
0
-10
-20
-30
-40
-50

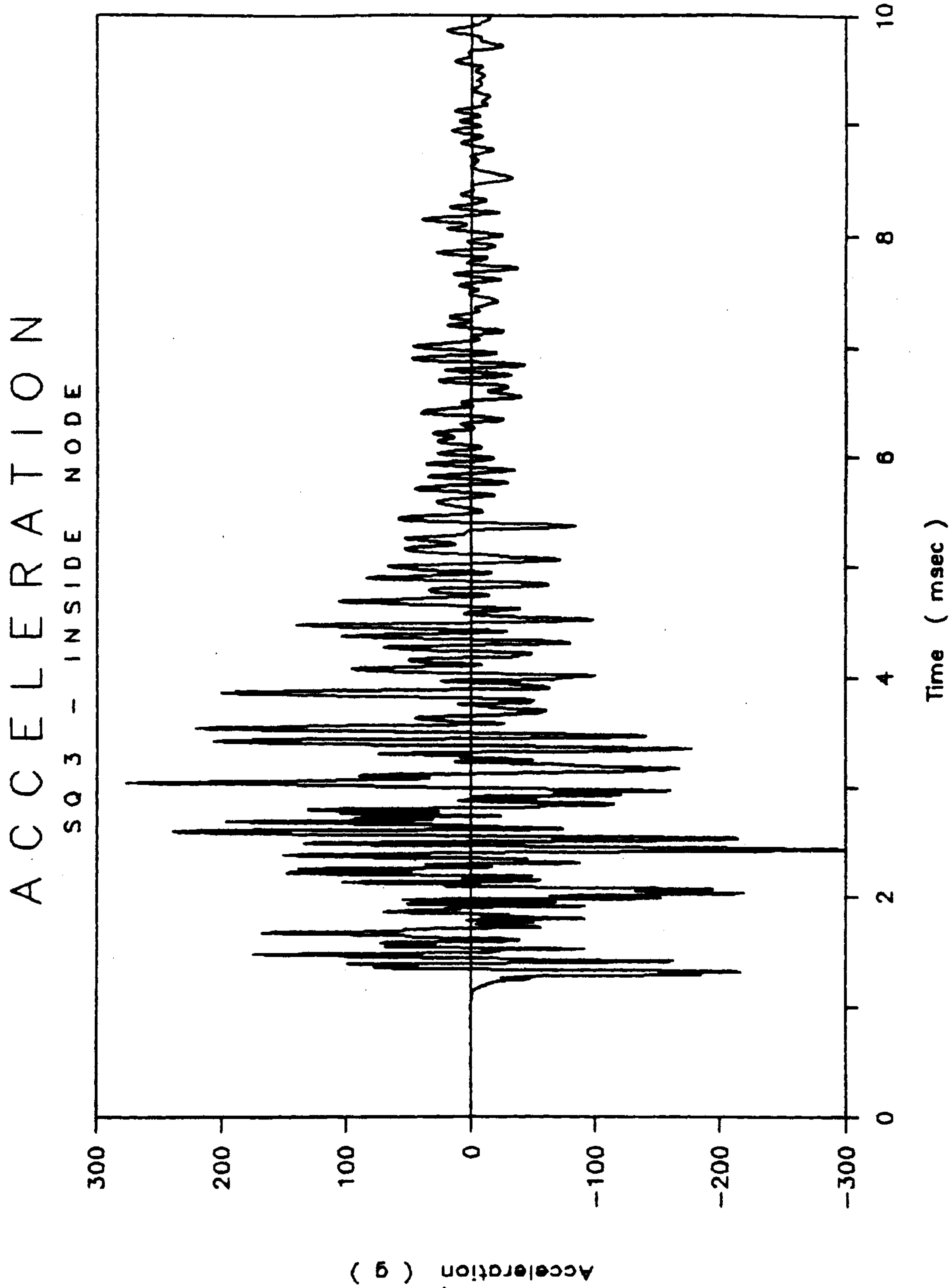
ACCELERATION
SQ 3 - INSIDE NODE
300
200
100
0
-100
-200
-300
Acceleration (g)
0
2
4
6
8
10
Time (msec)

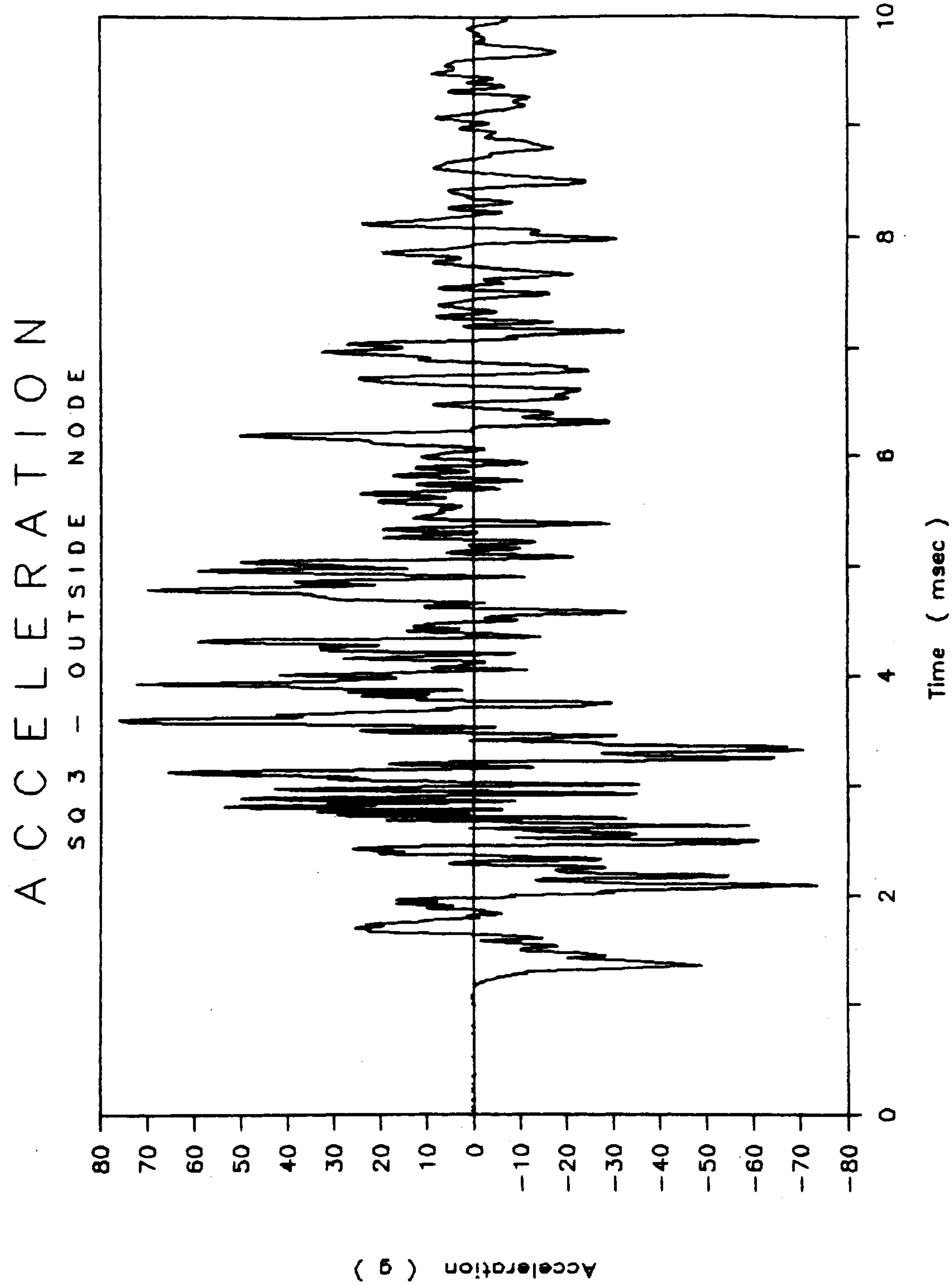
ACCELERATION
SQ 3 - OUTSIDE NODE
Time (msec)
Acceleration (g)
0
2
4
6
8
10
80
70
60
50
40
30
20
10
0
-10
-20
-30
-40
-50
-60
-70
-80

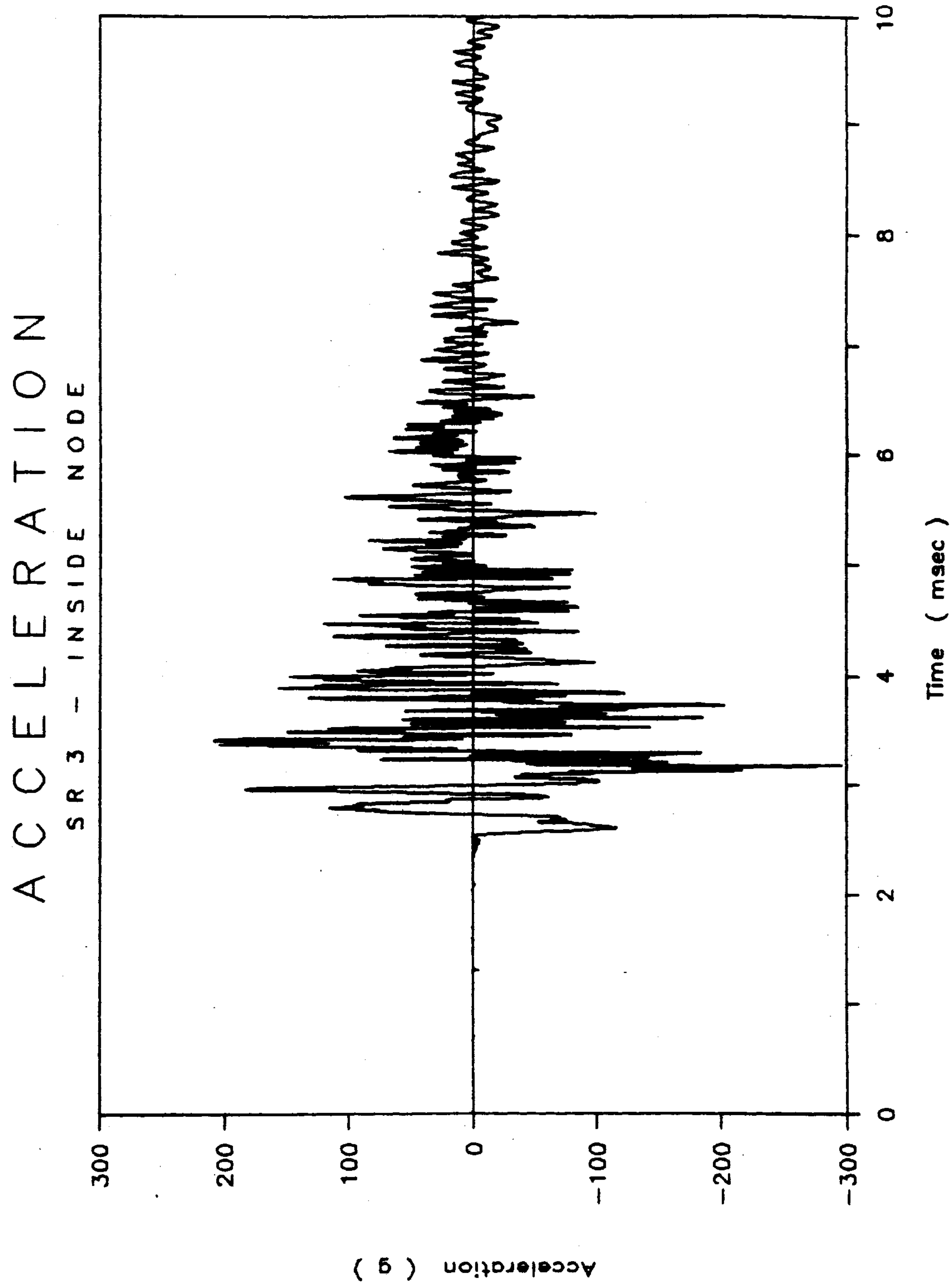
ACCELERATION
SR 3 – INSIDE NODE
Acceleration (g)
Time (msec)
300
200
100
0
−100
−200
−300
0
2
4
6
8
10

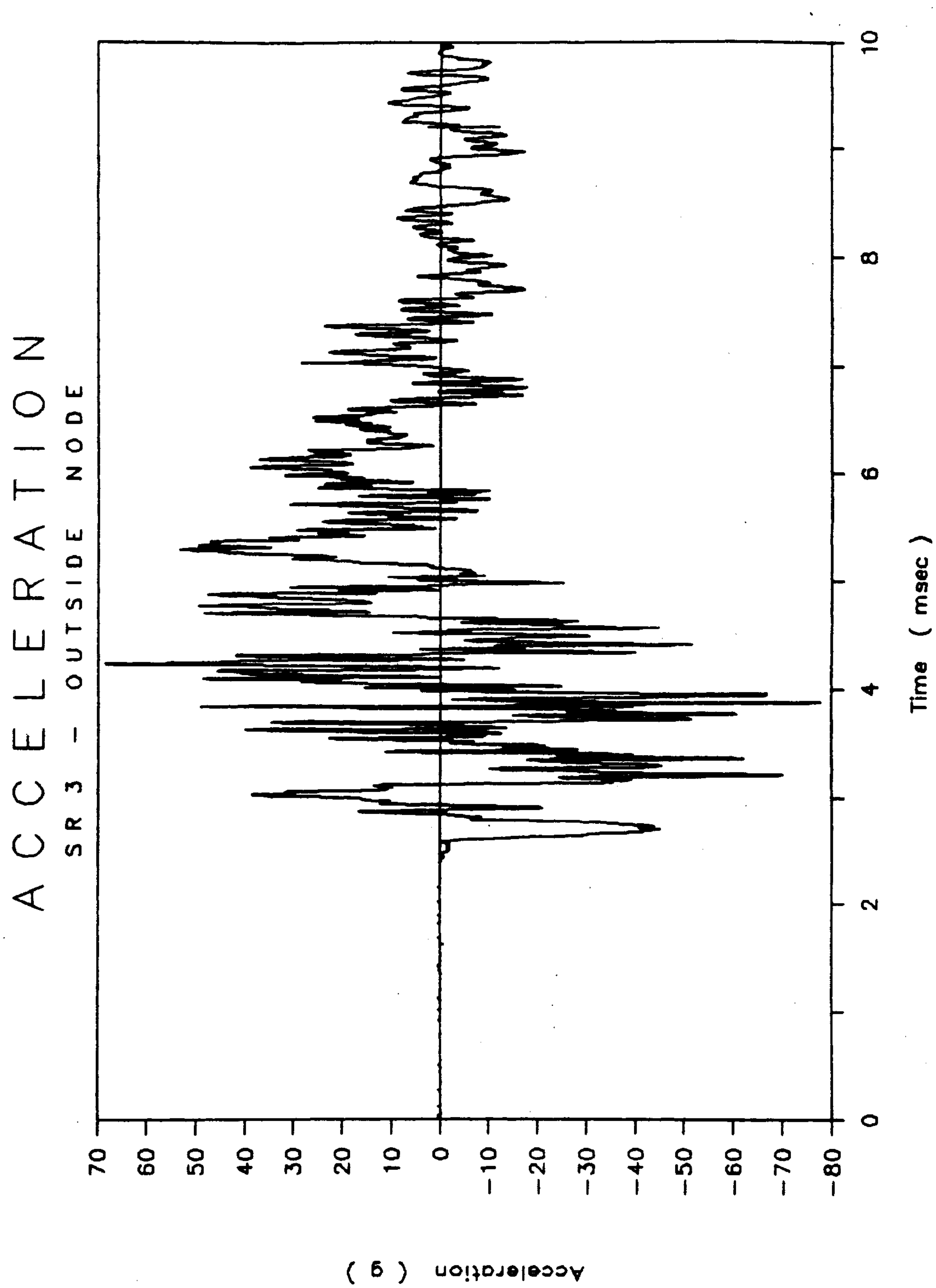

ACCELERATION
SR 3 - OUTSIDE NODE
Acceleration (g)
70
60
50
40
30
20
10
0
-10
-20
-30
-40
-50
-60
-70
-80
Time (msec)
0
2
4
6
8
10

APPENDIX B

Displacement - Time Plots

The plots in the Appendix are the ones from the following tests:

B 1	: Inside Node, Outside Node	;	B 5	: Inside Node, Outside Node	
B 2	: "	;	B 6	: "	
B 3	: "	;	B 7	: "	
B 4	: "	;	B 8	: "	
ST 1	: Inside Node, Outside Node	;	SP 1	: Inside Node, Outside Node	
ST 2	: "	;	SP 2	: "	
ST 3	: "	;	SP 3	: "	
SU 1	: Inside Node, Outside Node	;	SQ 1	: Inside Node, Outside Node	
SU 2	: "	;	SQ 2	: "	
SU 3	: "	;	SQ 3	: "	
SV 1	: Inside Node, Outside Node	;	SR 1	: Inside Node, Outside Node	
SV 2	: "	;	SR 2	: "	
SV 3	: "	;	SR 3	: "	

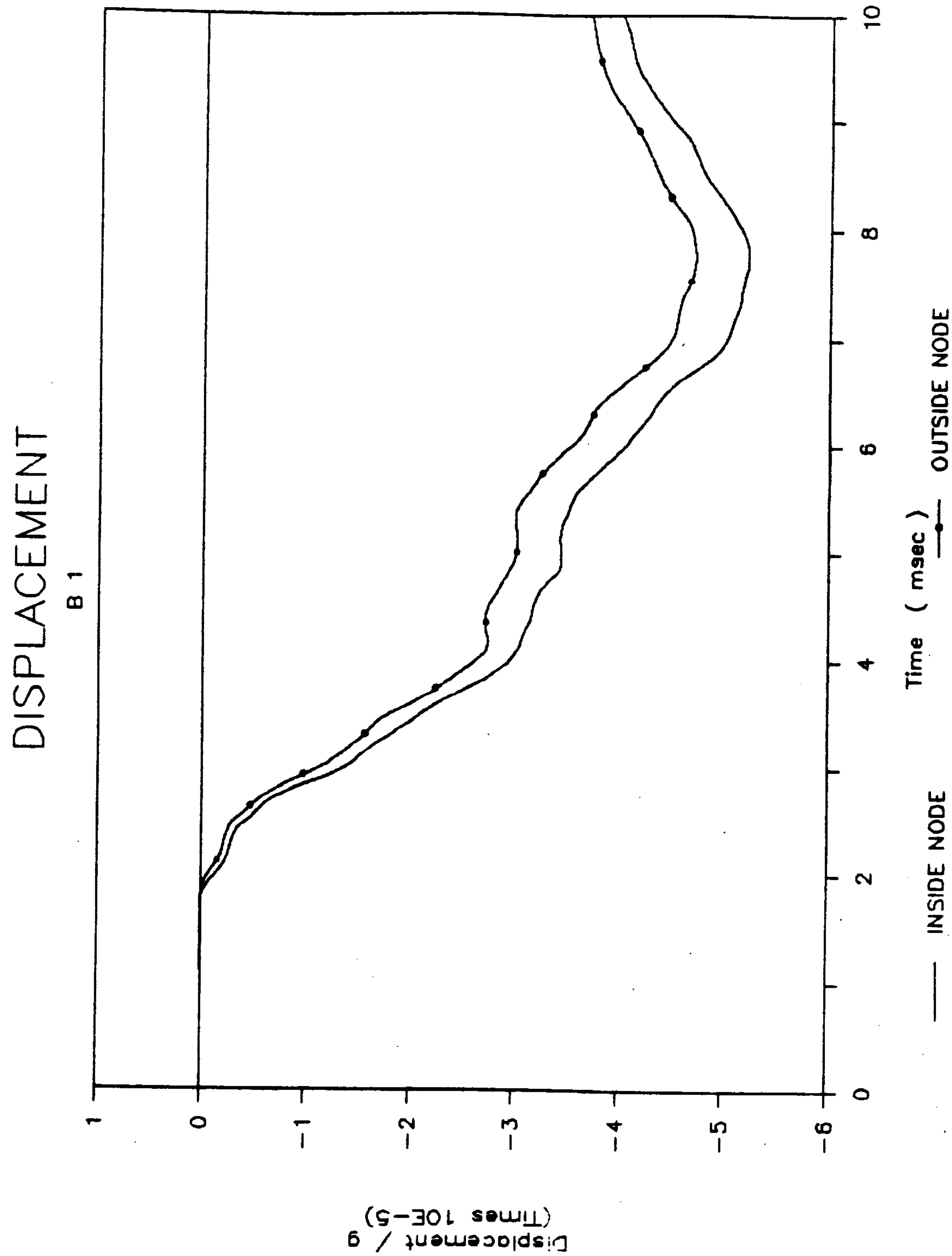
DISPLACEMENT
B 1
Displacement / g
(Times 10E-5)
1
0
-1
-2
-3
-4
-5
-6
0
2
4
6
8
10
Time (msec)
INSIDE NODE
OUTSIDE NODE

DISPLACEMENT

B 2

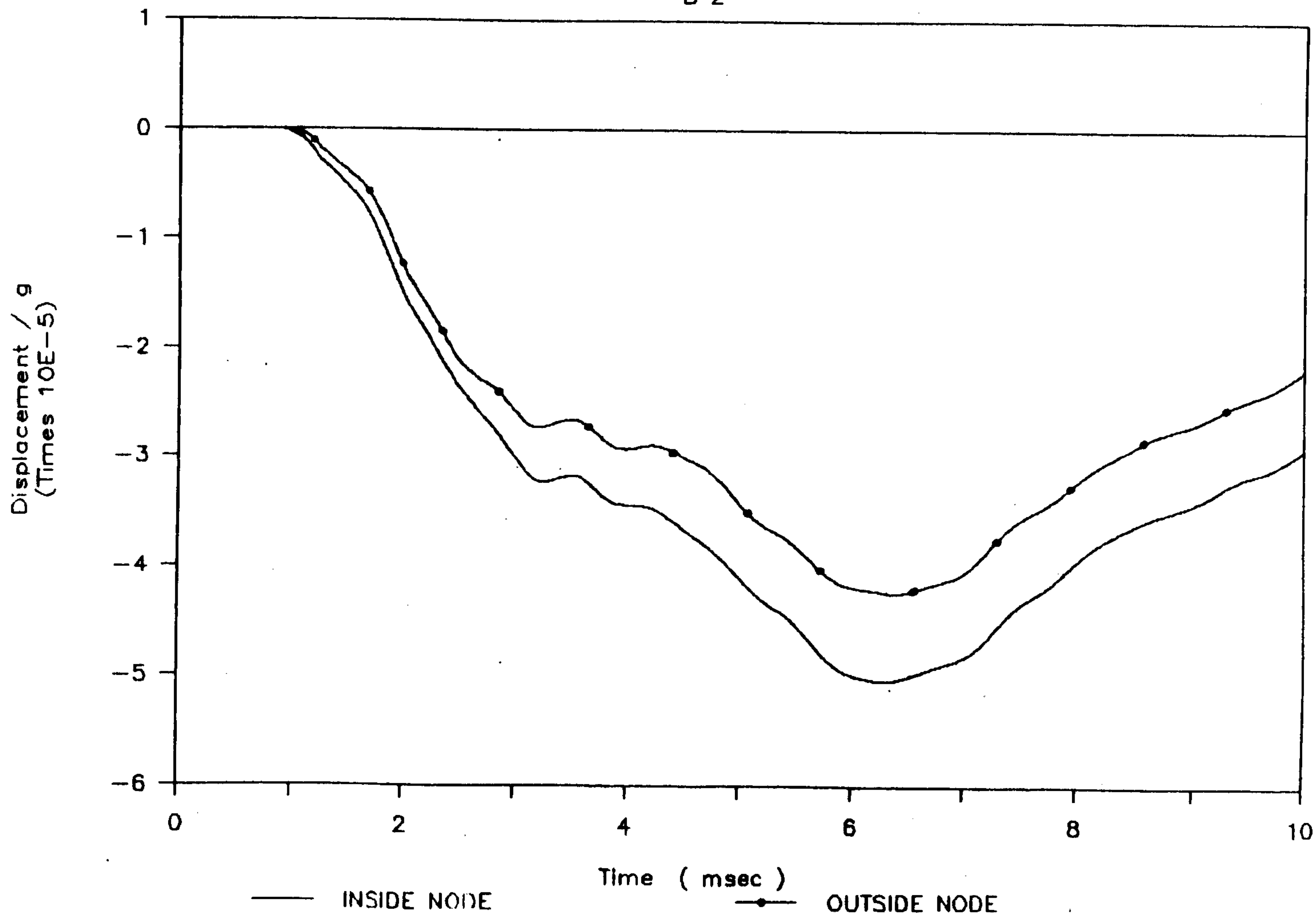

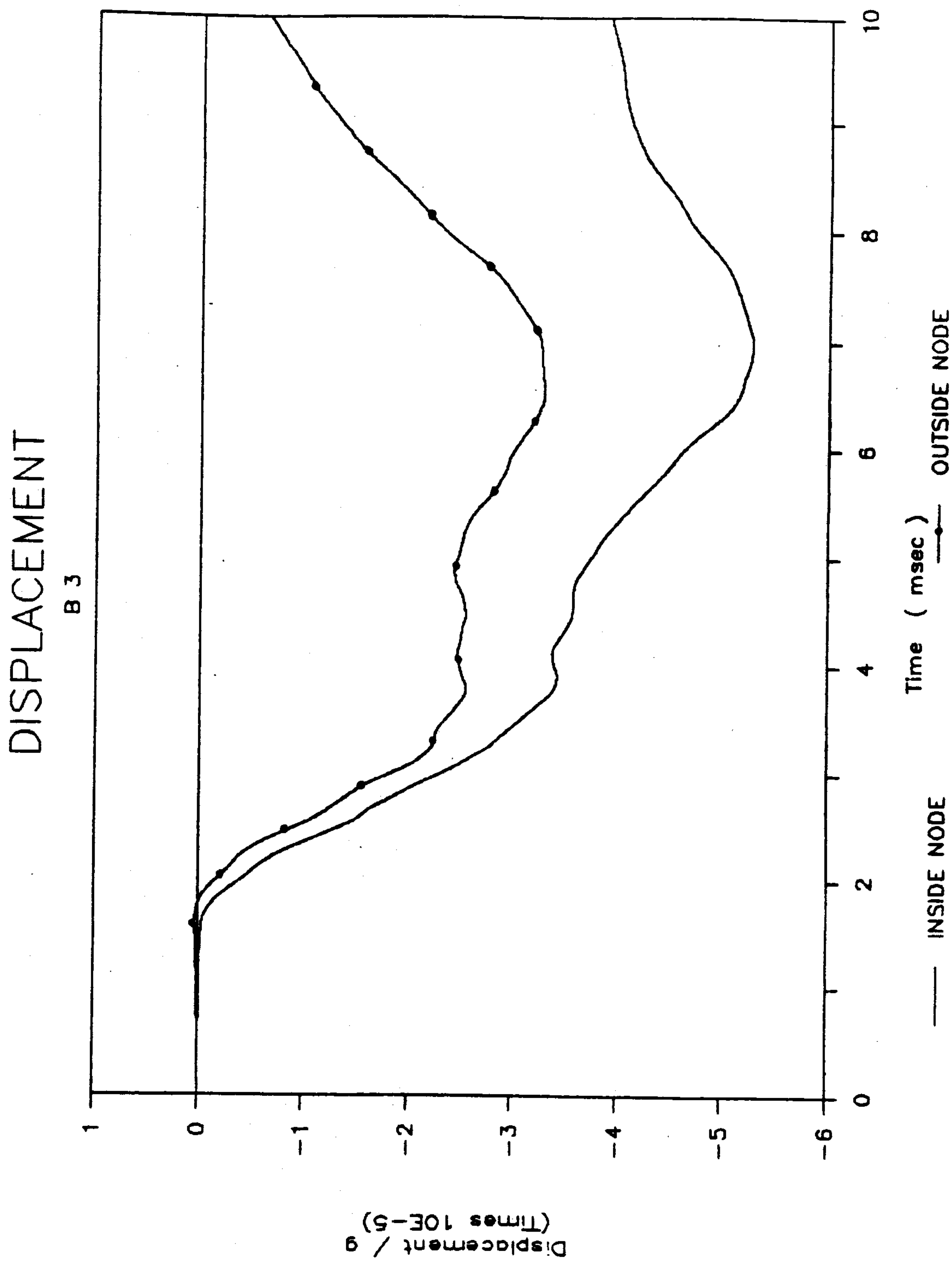
DISPLACEMENT
B 3
Displacement / g
(Times 10E-5)
Time (msec)
INSIDE NODE
OUTSIDE NODE
1
0
-1
-2
-3
-4
-5
-6
0
2
4
6
8
10

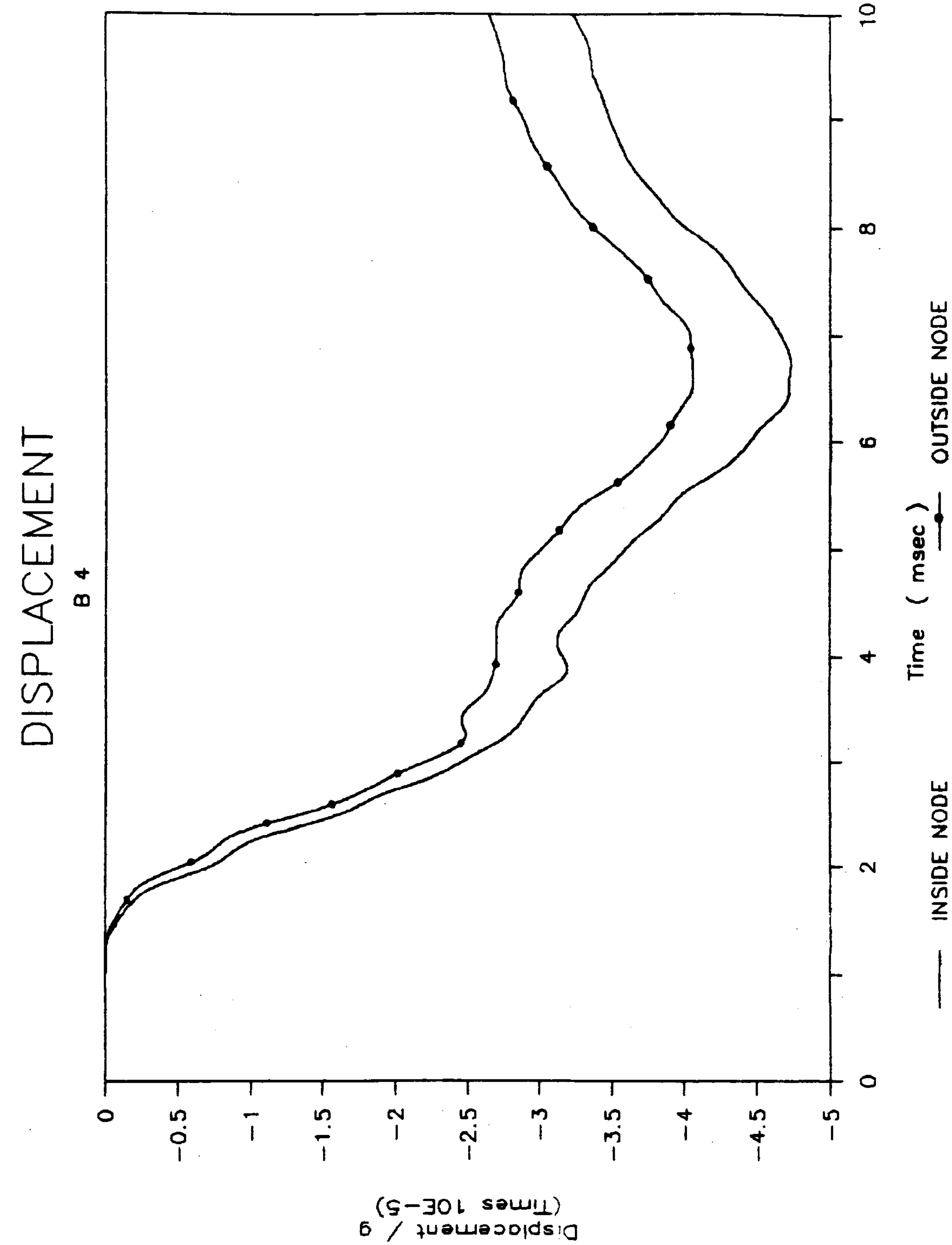

DISPLACEMENT
B 4
Displacement / g
(Times 10E-5)
0
-0.5
-1
-1.5
-2
-2.5
-3
-3.5
-4
-4.5
-5
0
2
4
6
8
10
Time (msec)
INSIDE NODE
OUTSIDE NODE

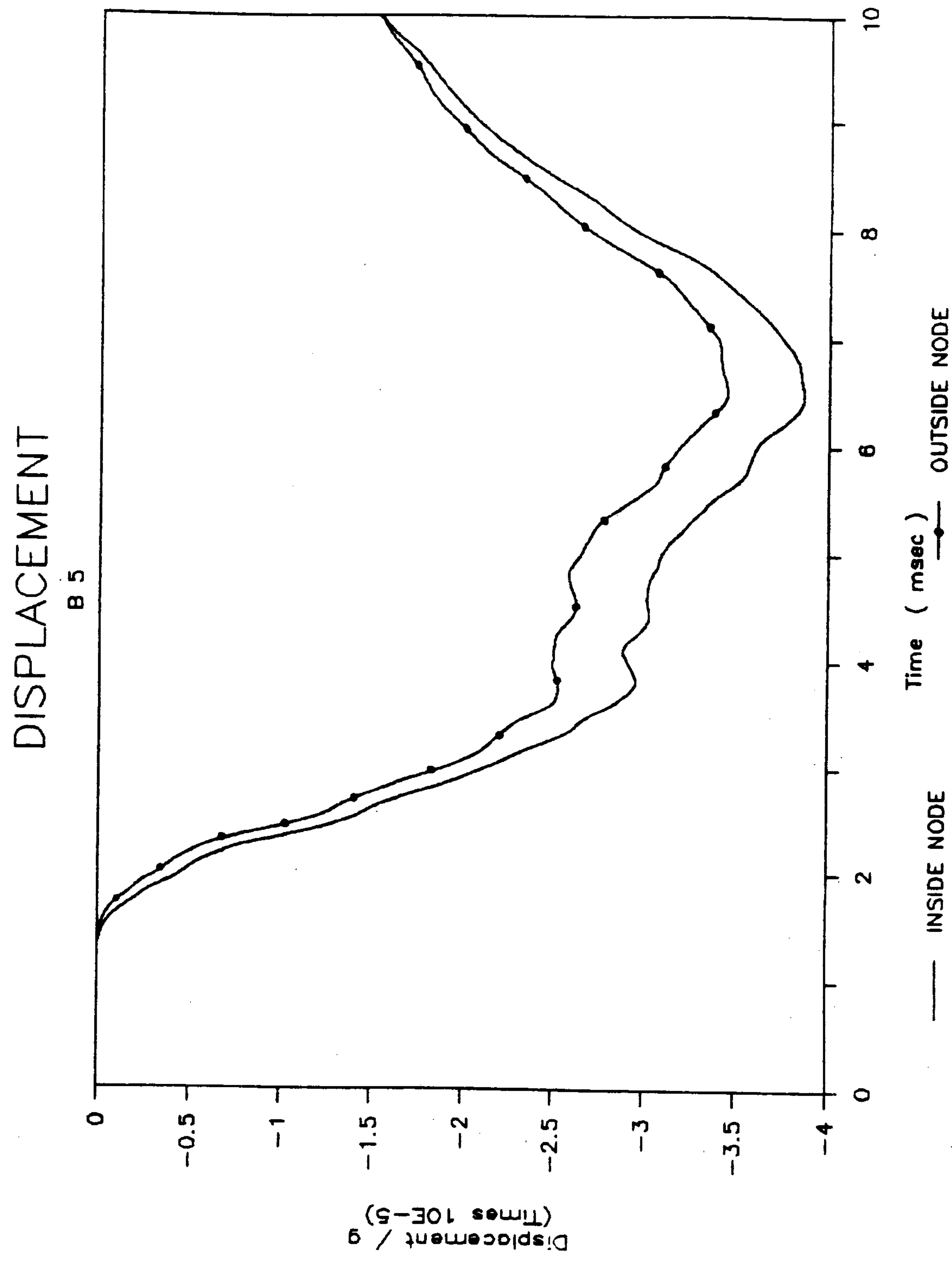
DISPLACEMENT
B 5
Displacement / g
(Times 10E-5)
0
-0.5
-1
-1.5
-2
-2.5
-3
-3.5
-4
0
2
4
6
8
10
Time (msec)
INSIDE NODE
OUTSIDE NODE

DISPLACEMENT

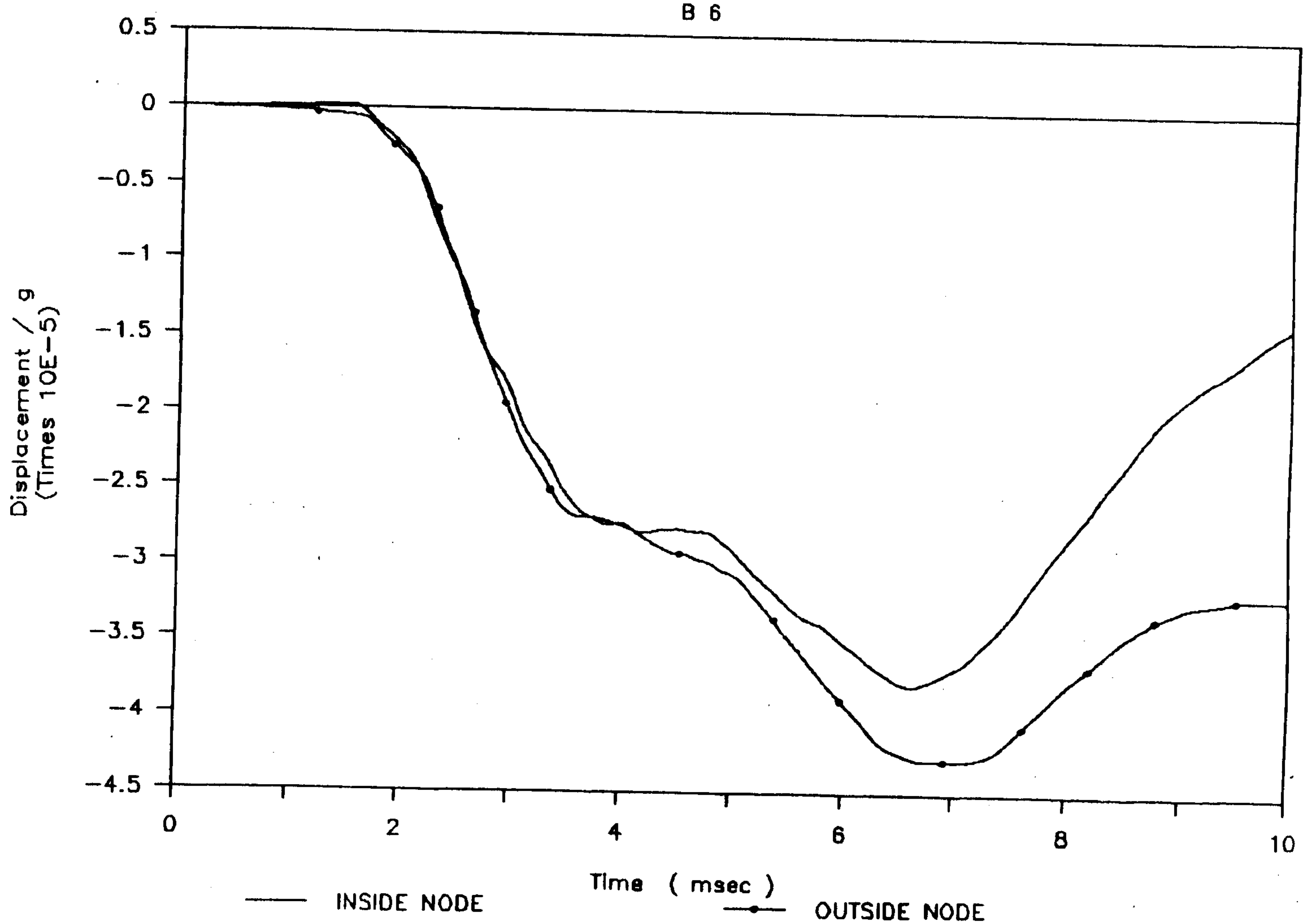

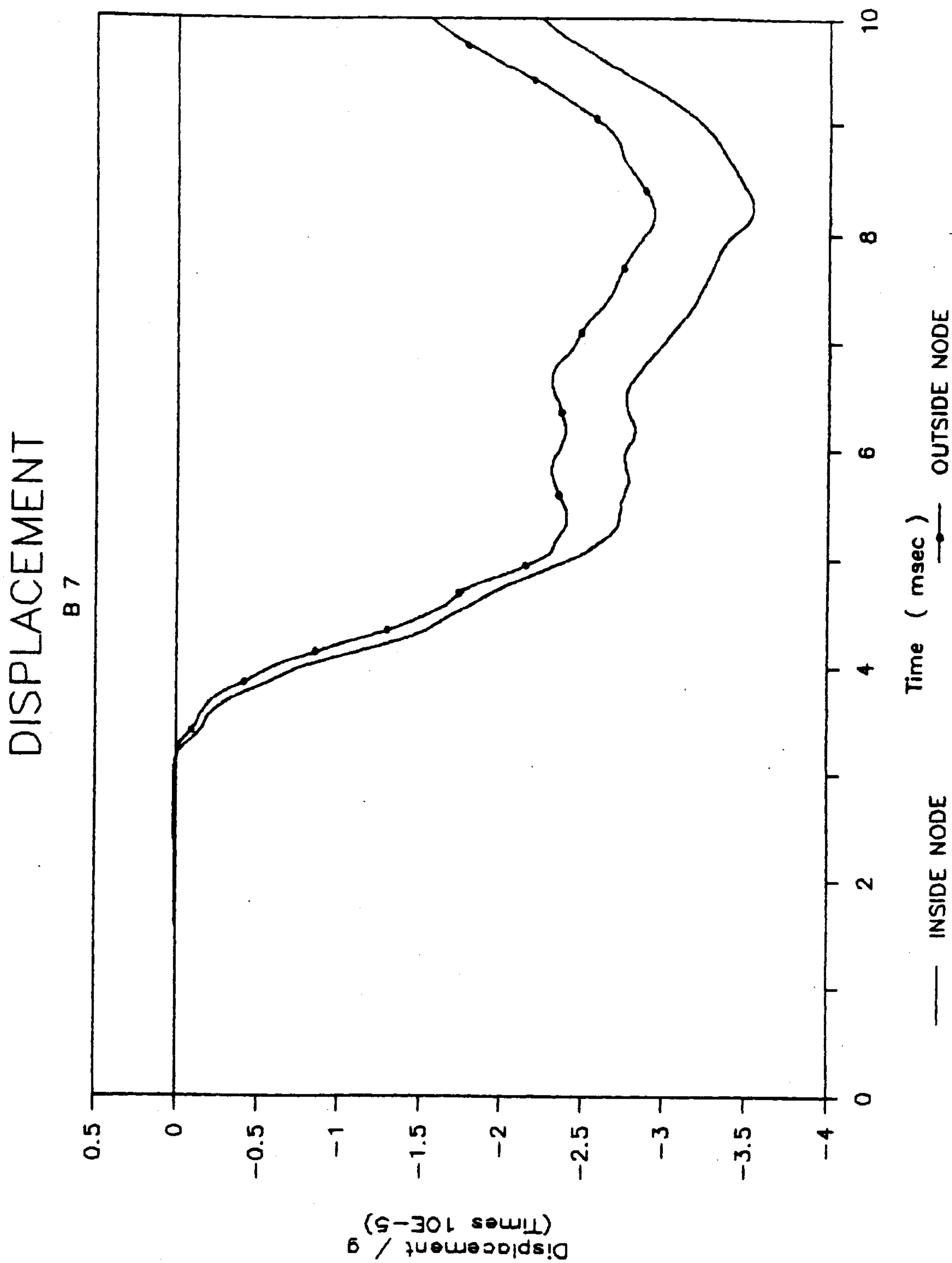

DISPLACEMENT
B 7
0.5
0
-0.5
-1
-1.5
-2
-2.5
-3
-3.5
-4
Displacement / g
(Times 10E-5)
0
2
4
6
8
10
Time (msec)
INSIDE NODE
OUTSIDE NODE

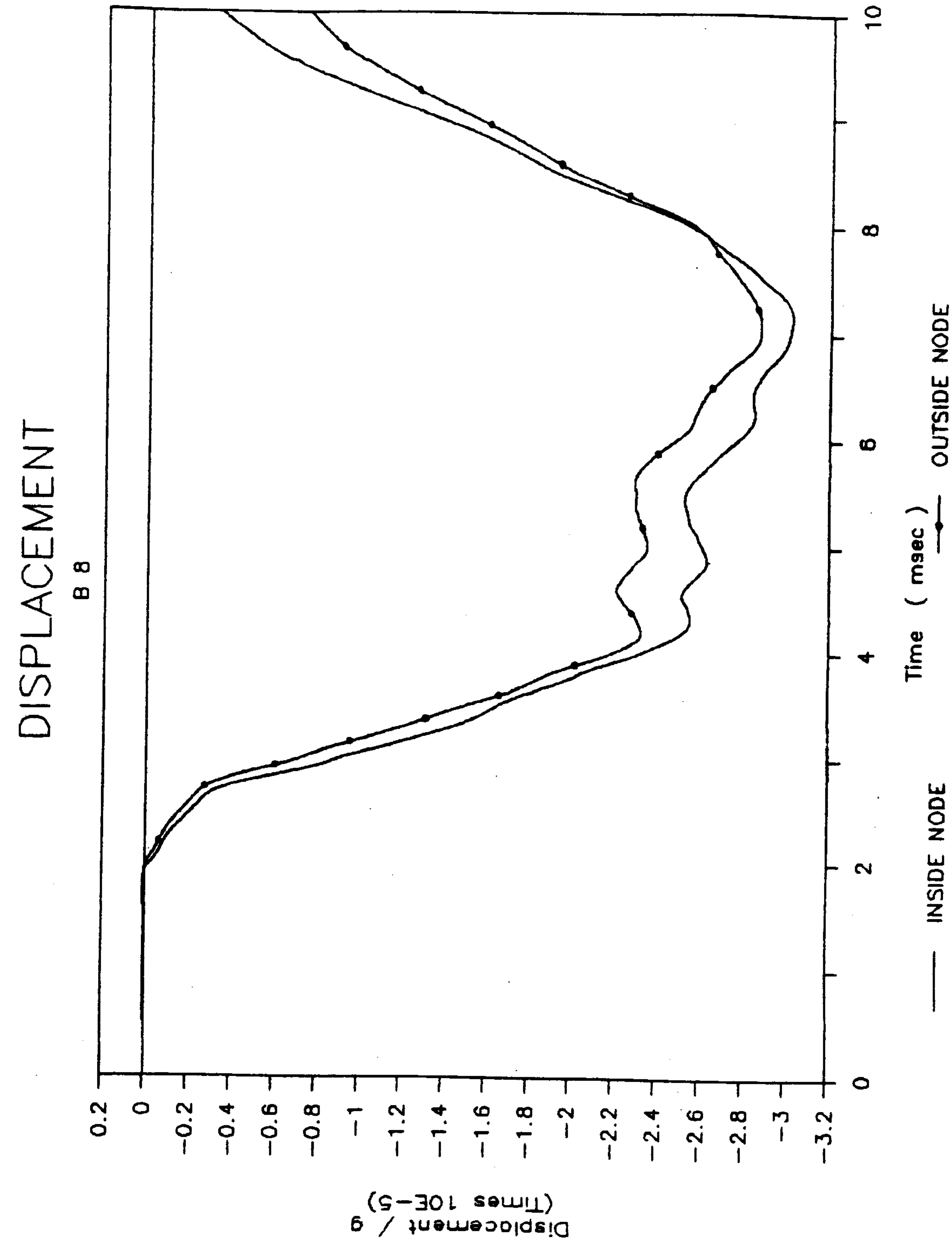

DISPLACEMENT
B 8
Displacement / g
(Times 10E-5)
0.2
0
-0.2
-0.4
-0.6
-0.8
-1
-1.2
-1.4
-1.6
-1.8
-2
-2.2
-2.4
-2.6
-2.8
-3
-3.2
0
2
4
6
8
10
Time (msec)
INSIDE NODE
OUTSIDE NODE

DISPLACEMENT

ST 1

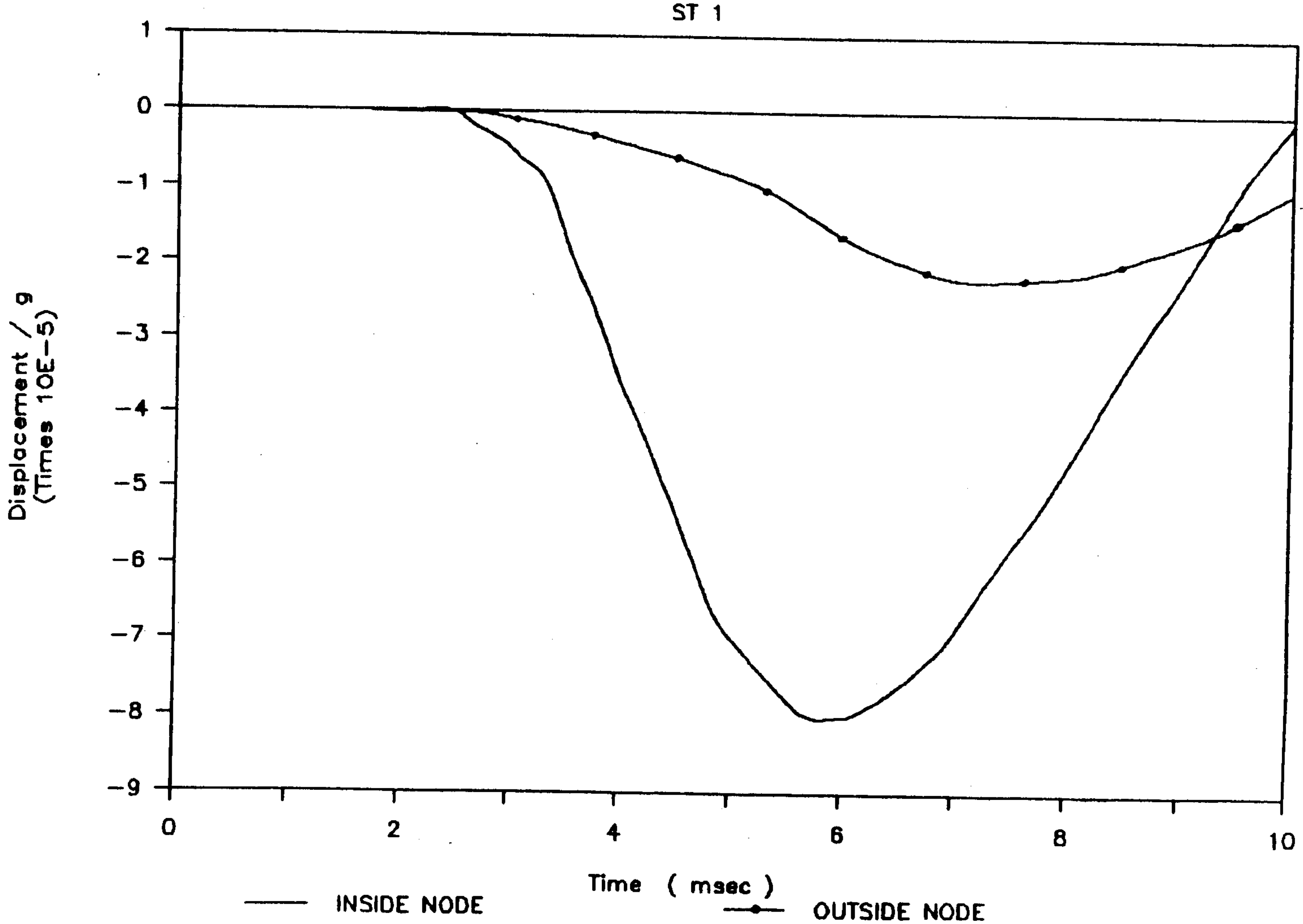

DISPLACEMENT

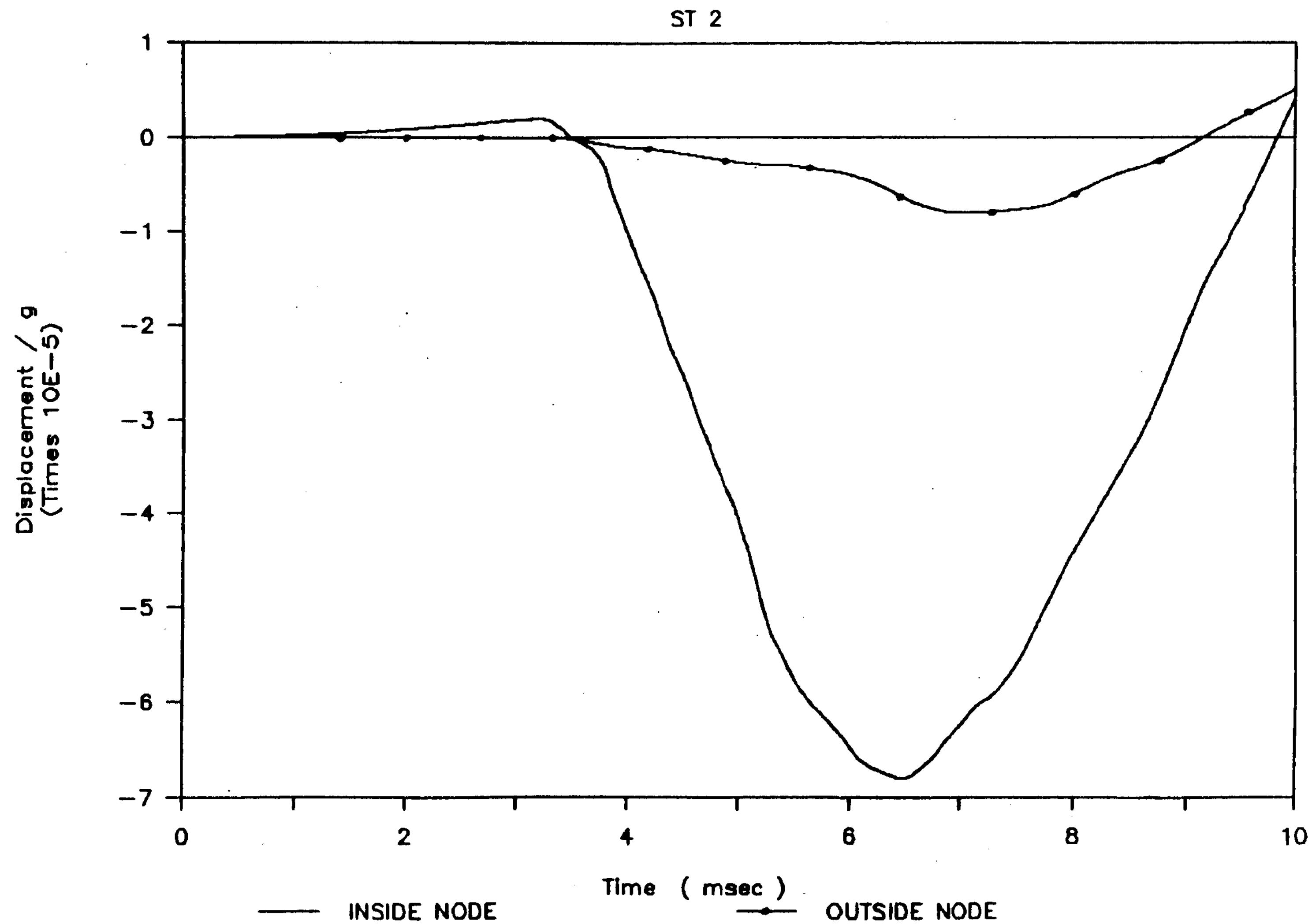

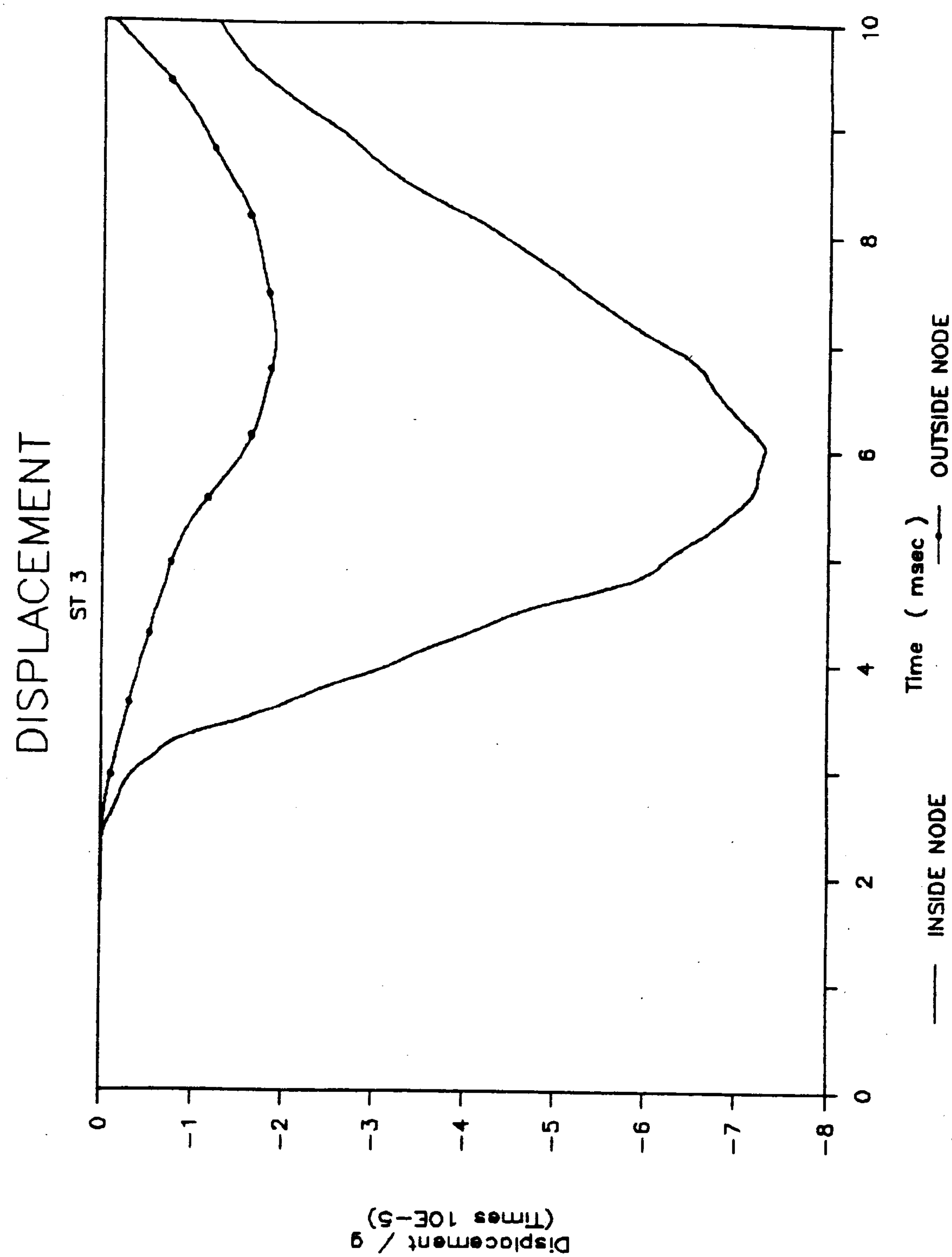
DISPLACEMENT
ST 3
Time (msec)
INSIDE NODE
OUTSIDE NODE
Displacement / g
(Times 10E-5)
0
-1
-2
-3
-4
-5
-6
-7
-8
0
2
4
6
8
10

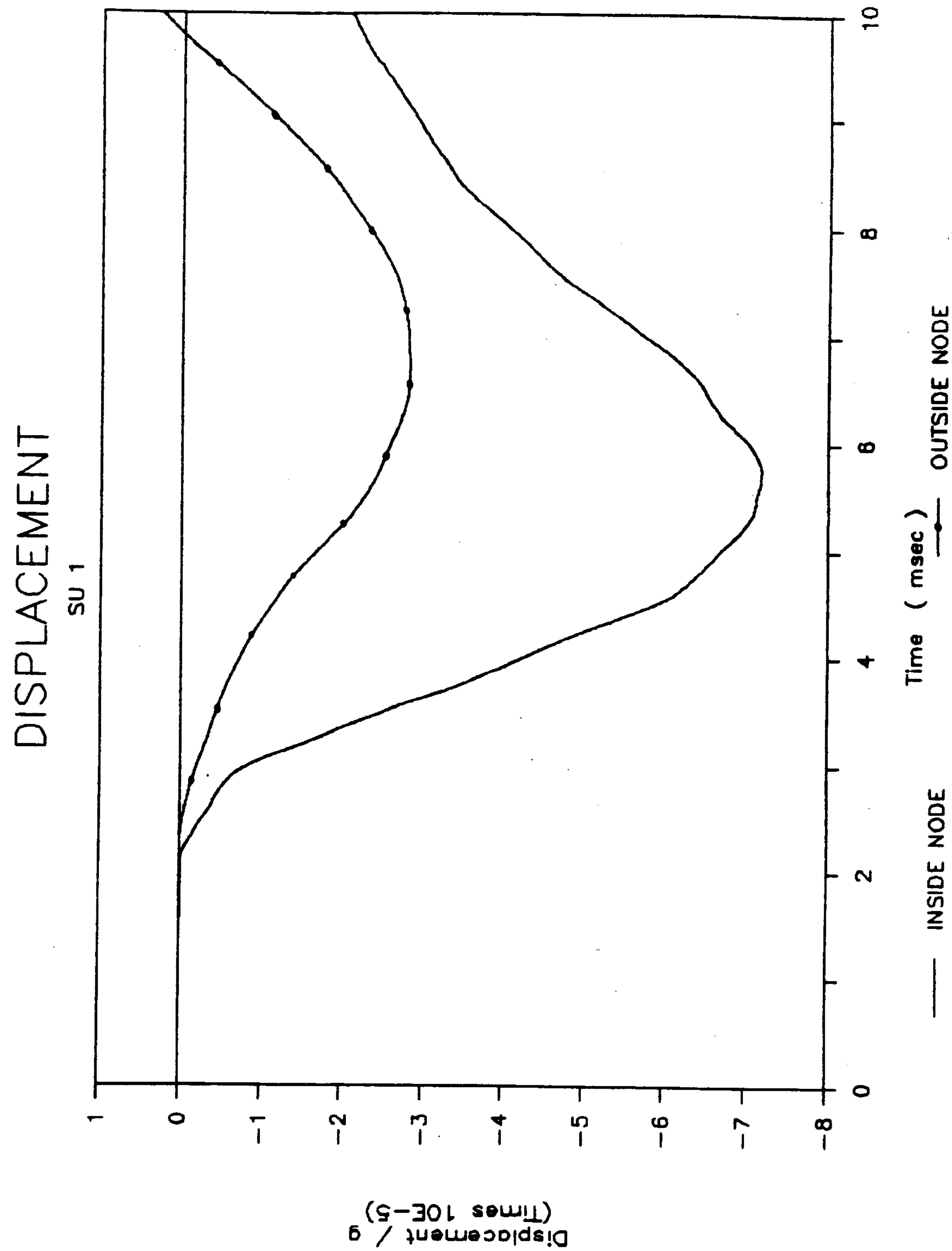
DISPLACEMENT
SU 1
Displacement / g
(Times 10E-5)
1
0
-1
-2
-3
-4
-5
-6
-7
-8
0
2
4
6
8
10
Time (msec)
INSIDE NODE
OUTSIDE NODE

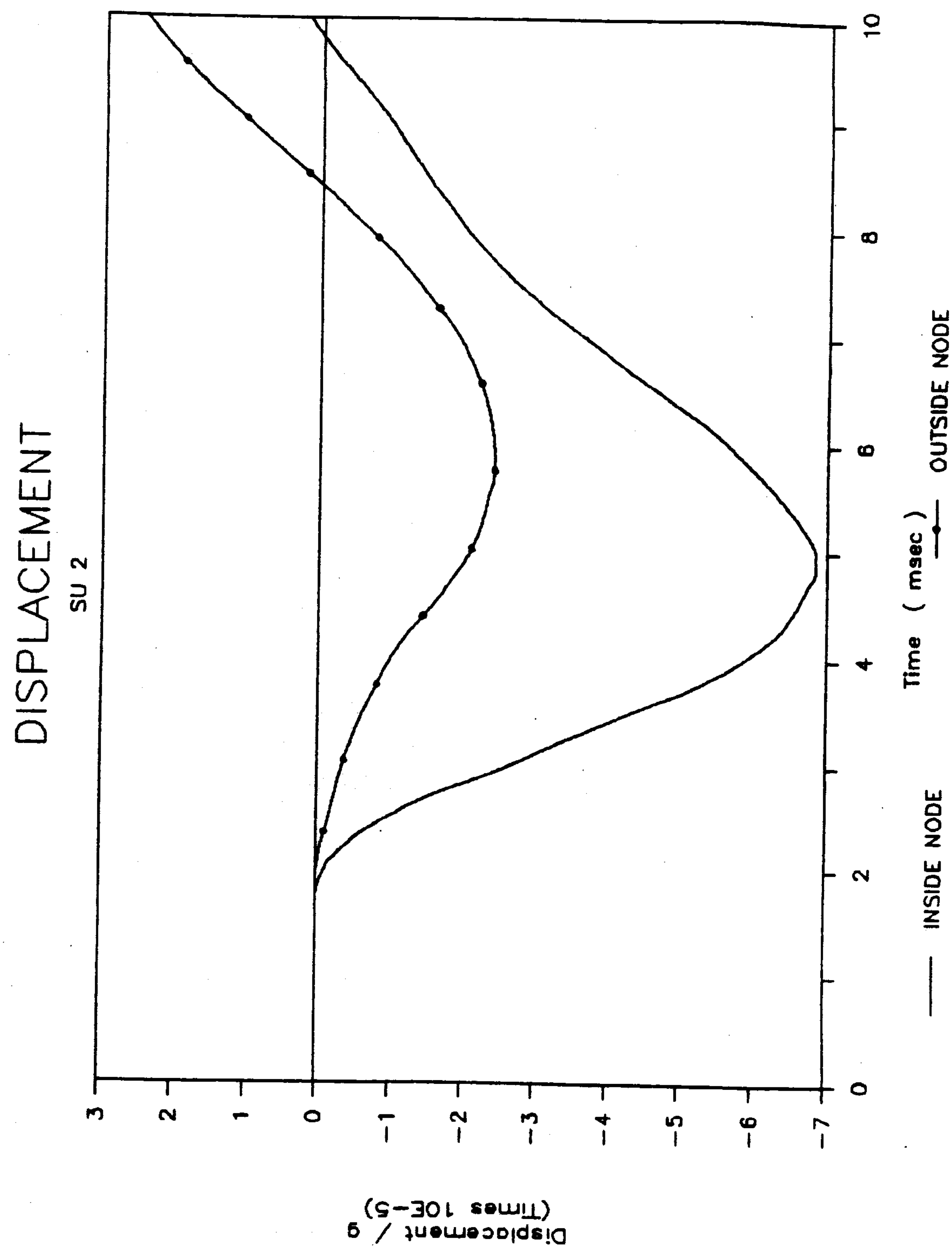
DISPLACEMENT
SU 2
Displacement / g
(Times 10E-5)
3
2
1
0
-1
-2
-3
-4
-5
-6
-7
0
2
4
6
8
10
Time (msec)
INSIDE NODE
OUTSIDE NODE

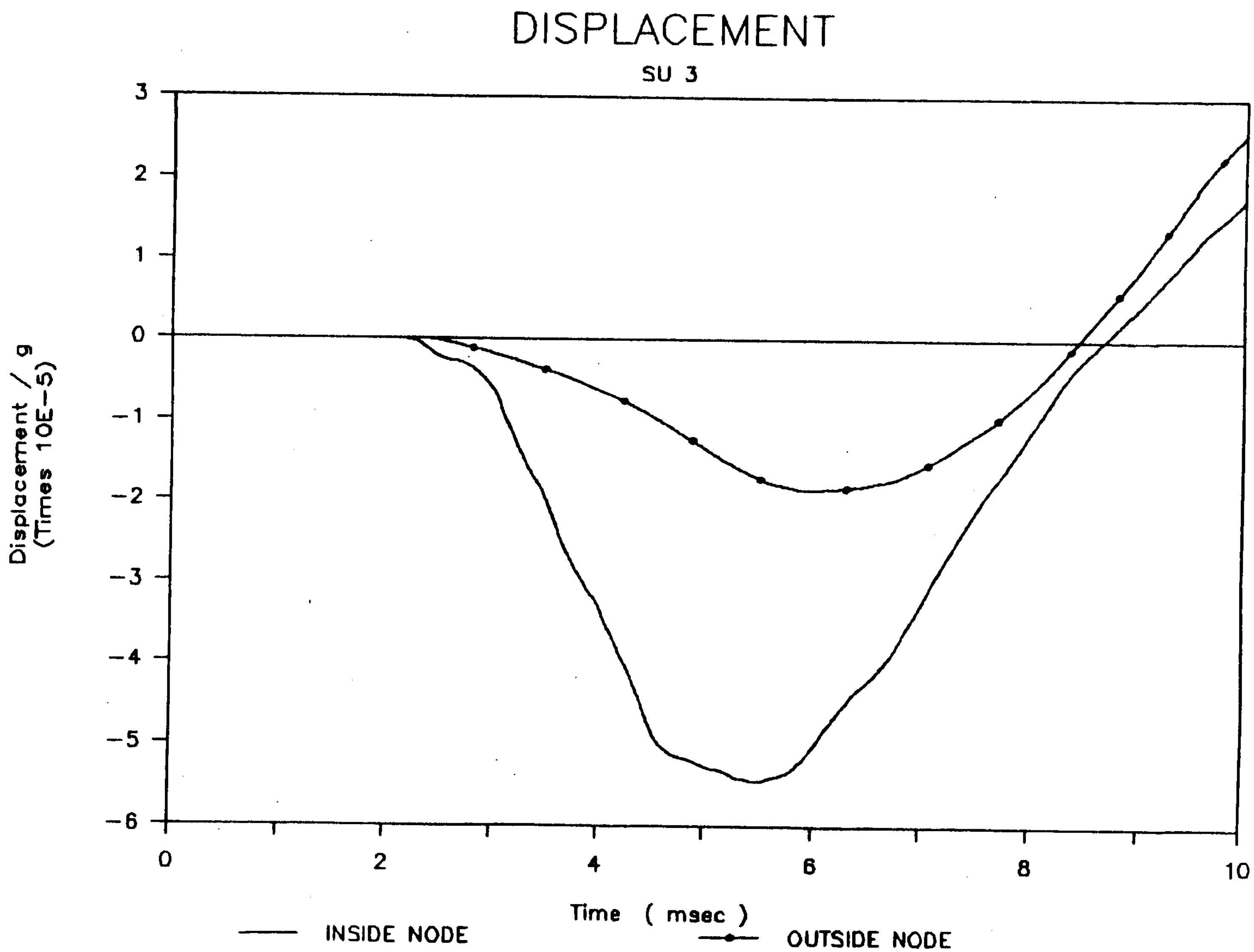

DISPLACEMENT
SU 3
Displacement / g
(Times 10E-5)
3
2
1
0
-1
-2
-3
-4
-5
-6
0
2
4
6
8
10
Time (msec)
INSIDE NODE
OUTSIDE NODE

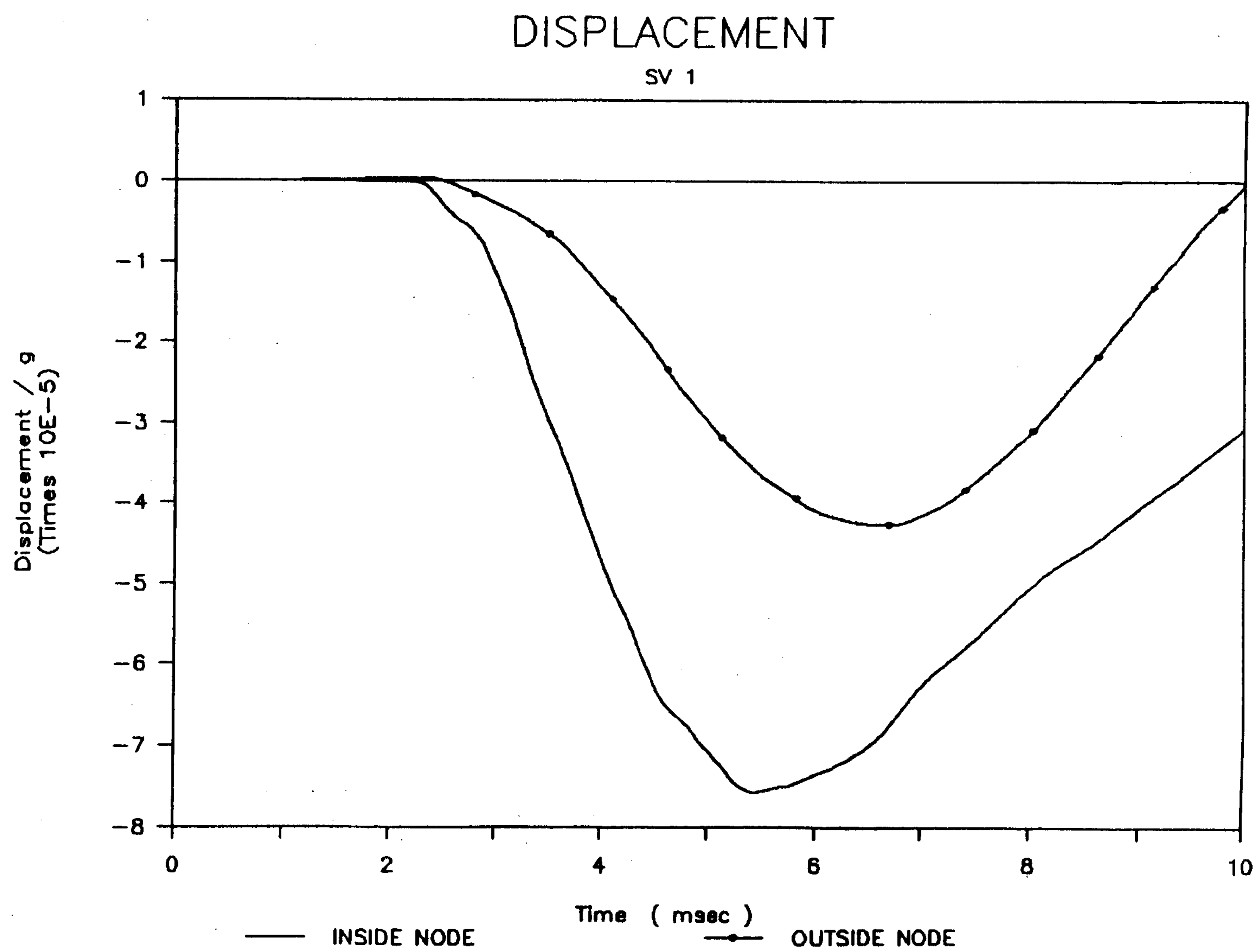

DISPLACEMENT
SV 1
Displacement / g
(Times 10E-5)
1
0
-1
-2
-3
-4
-5
-6
-7
-8
0
2
4
6
8
10
Time (msec)
INSIDE NODE
OUTSIDE NODE

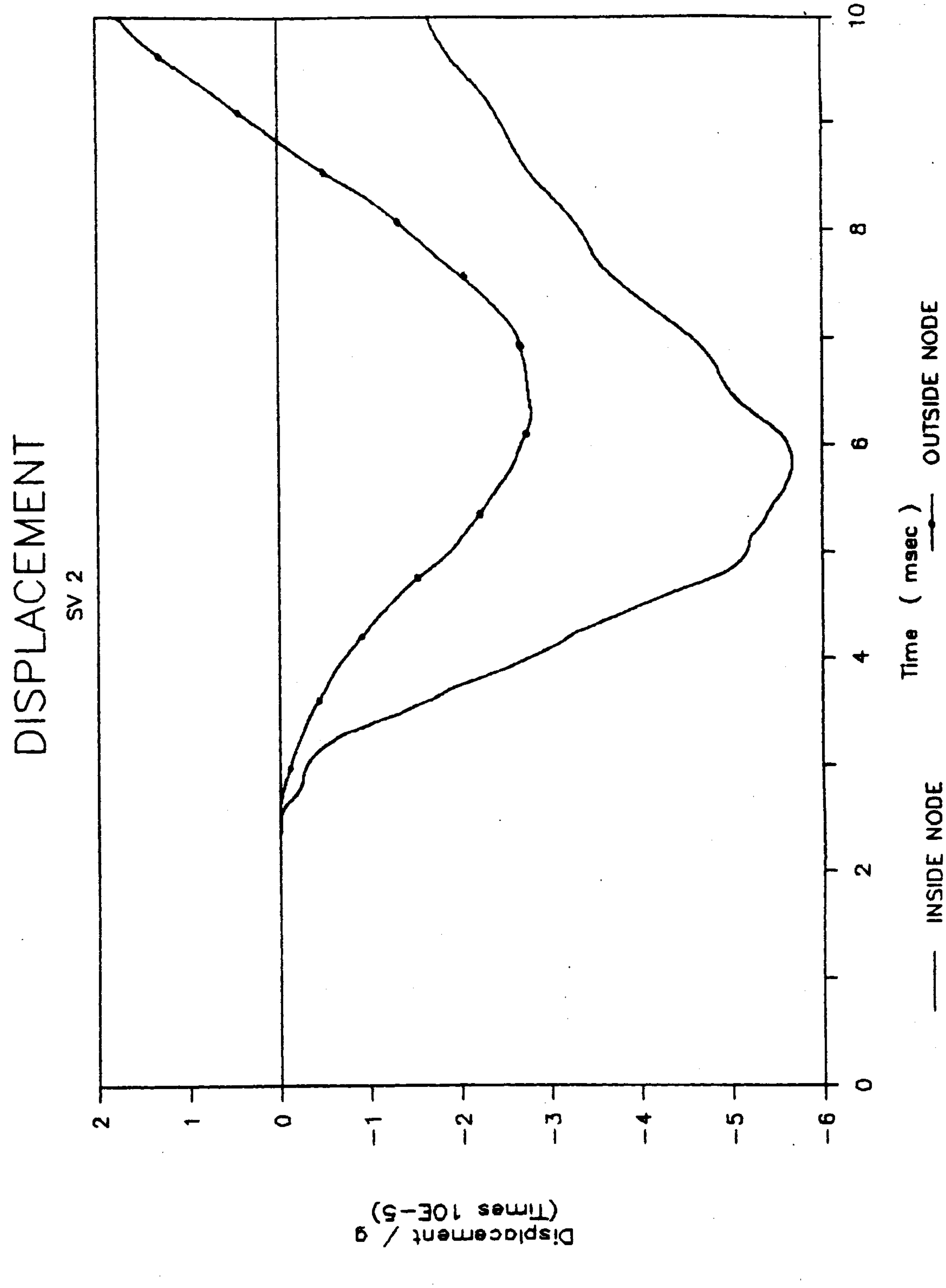
DISPLACEMENT
SV 2
Displacement / g
(Times 10E-5)
2
1
0
-1
-2
-3
-4
-5
-6
0
2
4
6
8
10
Time (msec)
INSIDE NODE
OUTSIDE NODE

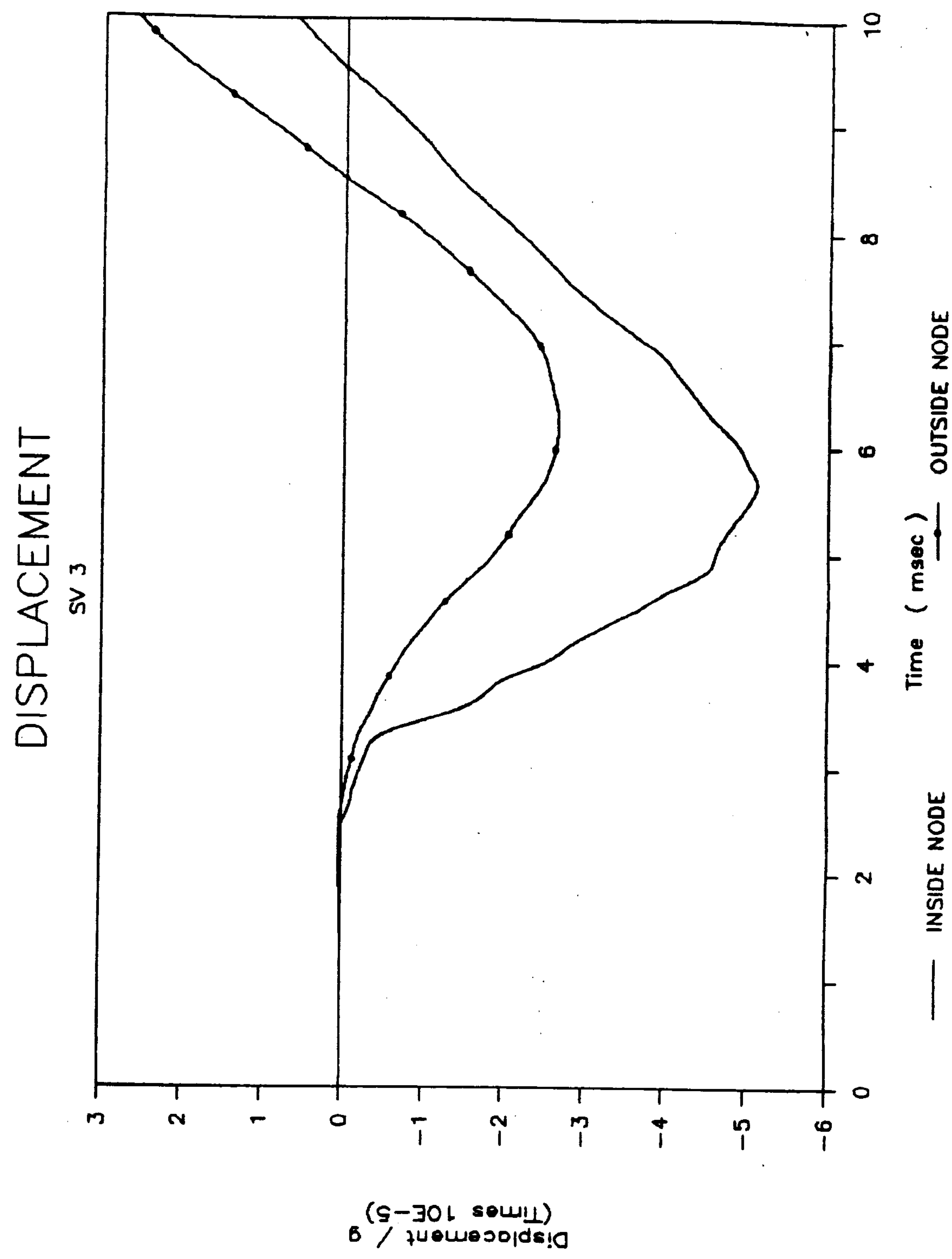
DISPLACEMENT
SV 3
Displacement / g
(Times 10E-5)
Time (msec)
INSIDE NODE
OUTSIDE NODE
3
2
1
0
-1
-2
-3
-4
-5
-6
0
2
4
6
8
10

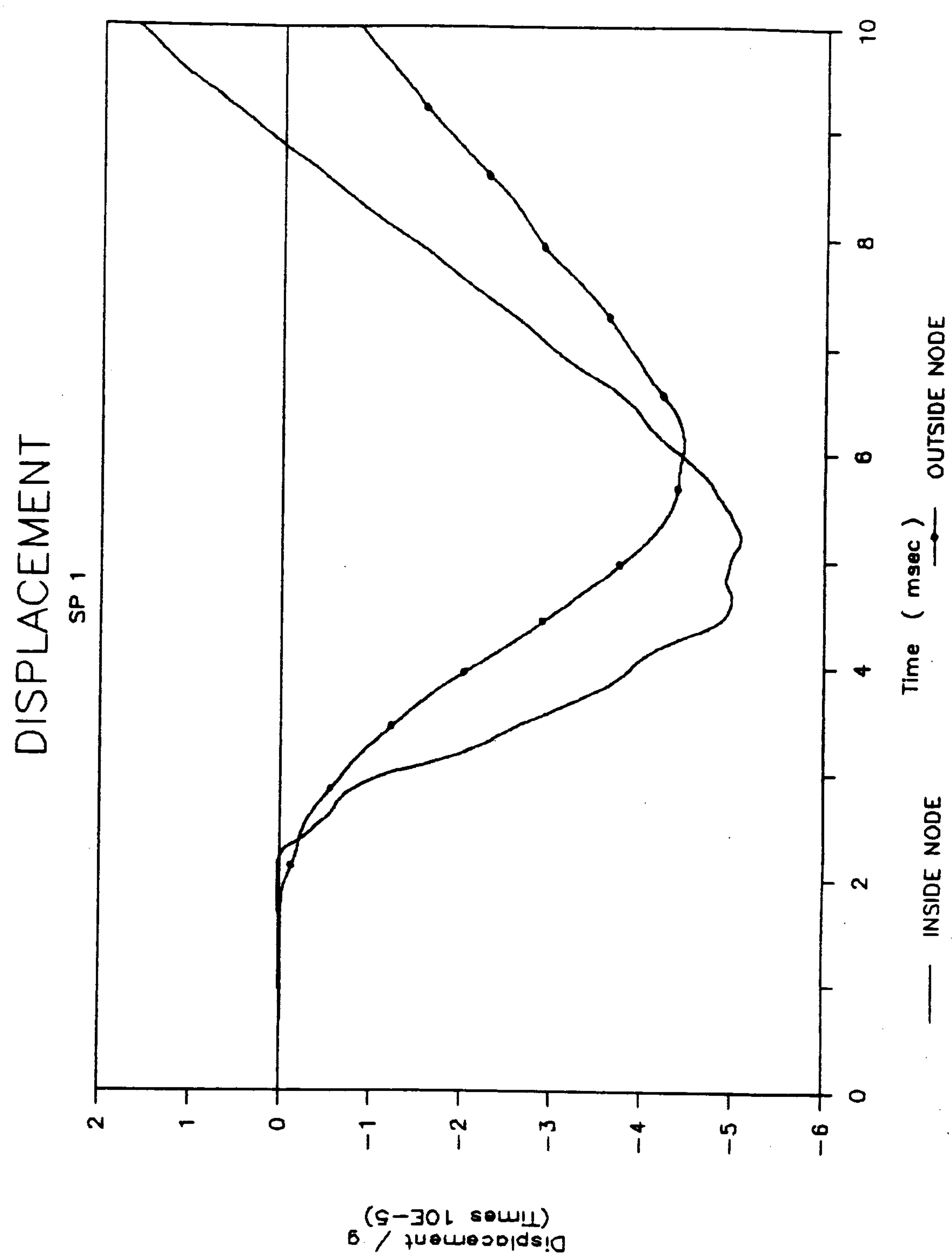

DISPLACEMENT
SP 1
Displacement / g
(Times 10E-5)
2
1
0
-1
-2
-3
-4
-5
-6
0
2
4
6
8
10
Time (msec)
INSIDE NODE
OUTSIDE NODE

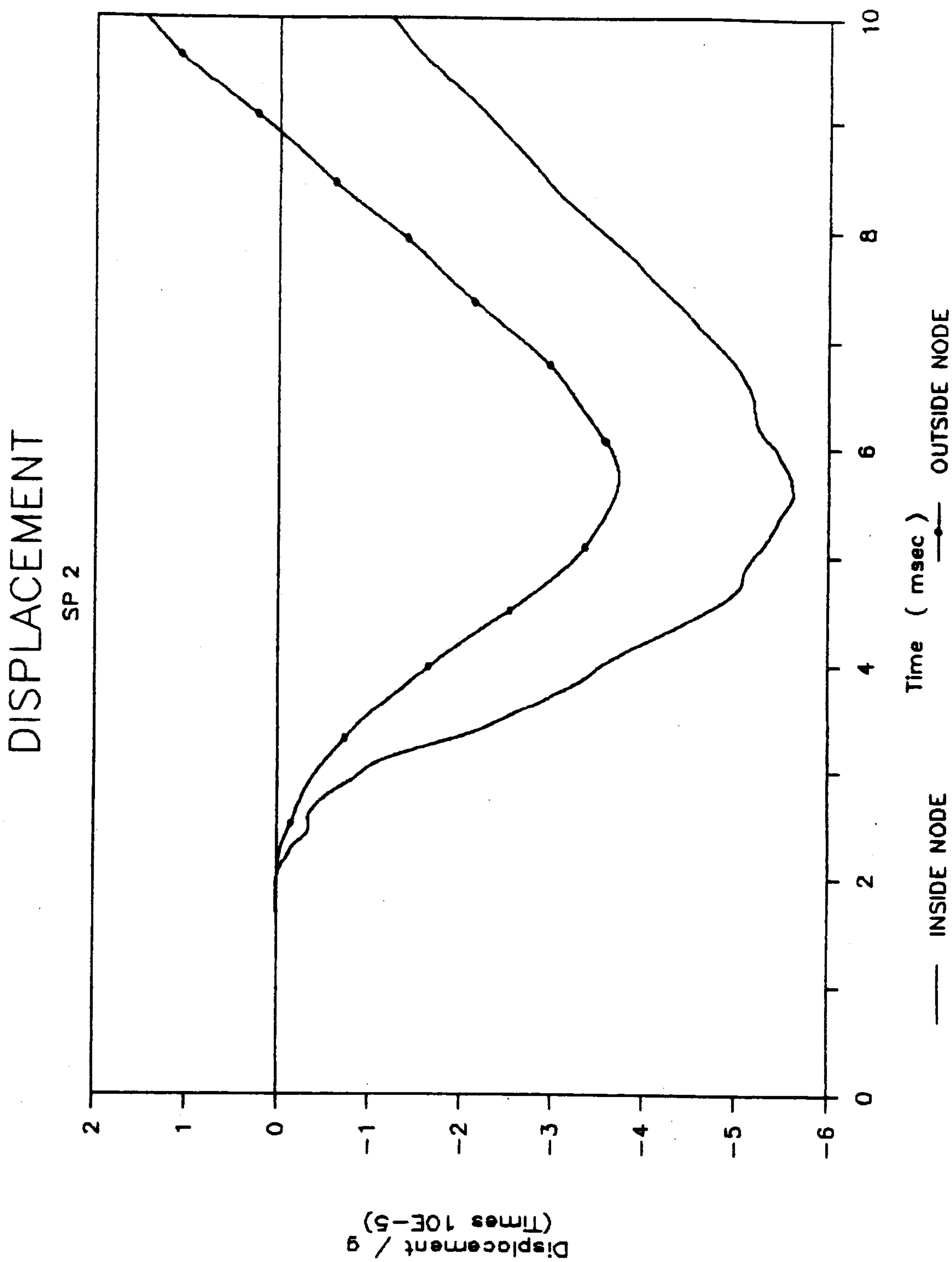
DISPLACEMENT
SP 2
Displacement / g
(Times 10E-5)
2
1
0
-1
-2
-3
-4
-5
-6
0
2
4
6
8
10
Time (msec)
INSIDE NODE
OUTSIDE NODE

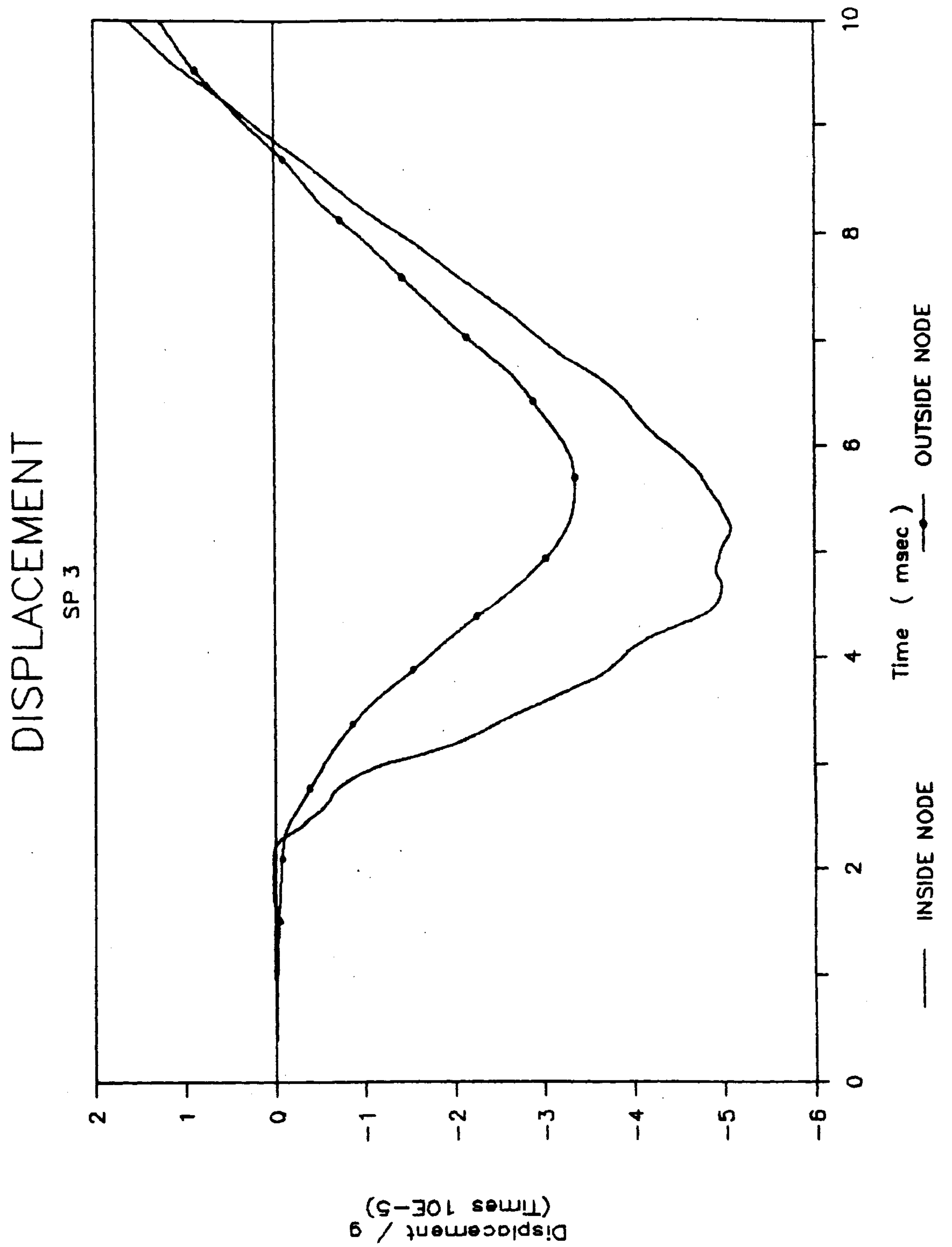
DISPLACEMENT
SP 3
Displacement / g
(Times 10E-5)
2
1
0
-1
-2
-3
-4
-5
-6
0
2
4
6
8
10
Time (msec)
INSIDE NODE
OUTSIDE NODE

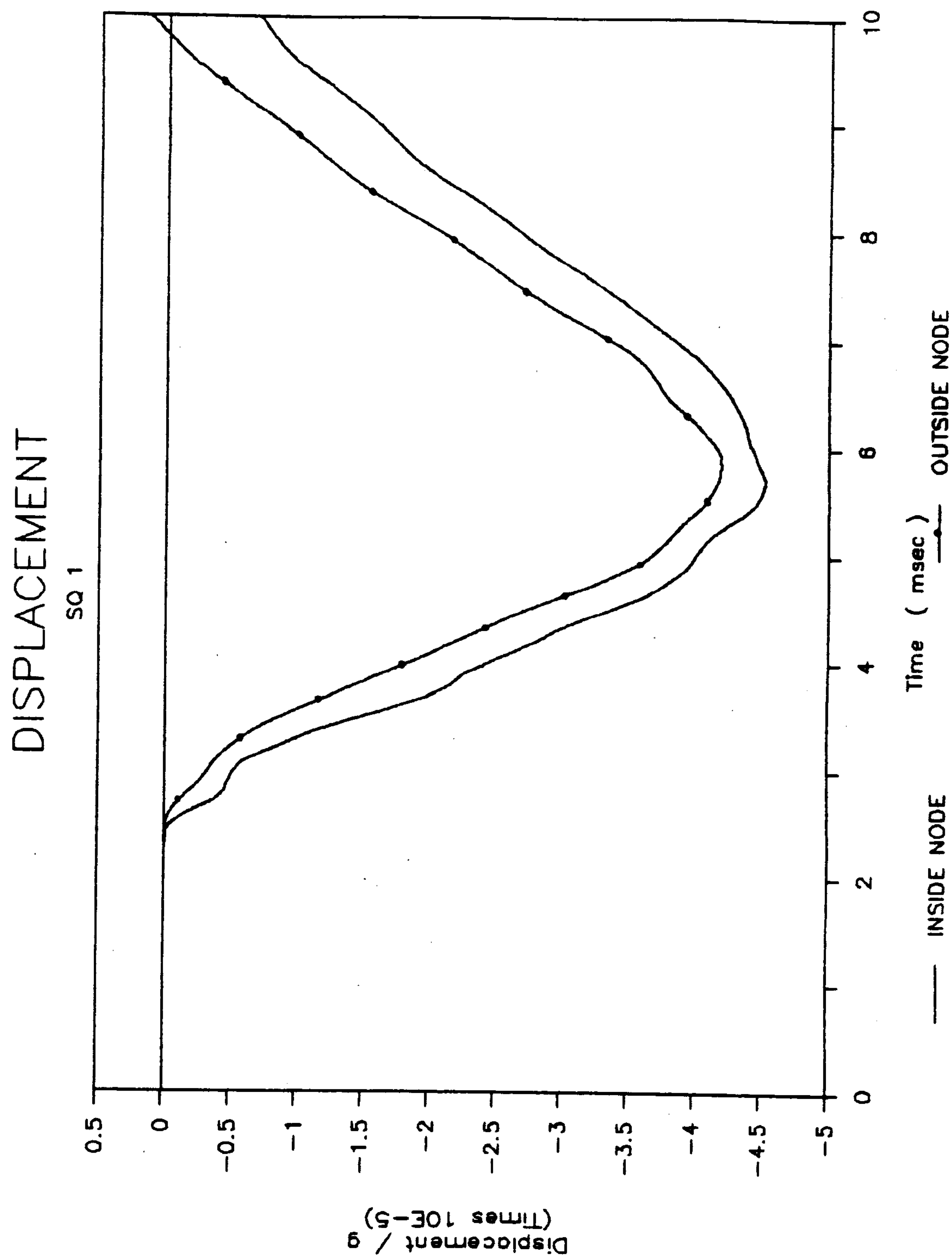
DISPLACEMENT
SQ 1
Displacement / g
(Times 10E-5)
0.5
0
-0.5
-1
-1.5
-2
-2.5
-3
-3.5
-4
-4.5
-5
0
2
4
6
8
10
Time (msec)
INSIDE NODE
OUTSIDE NODE

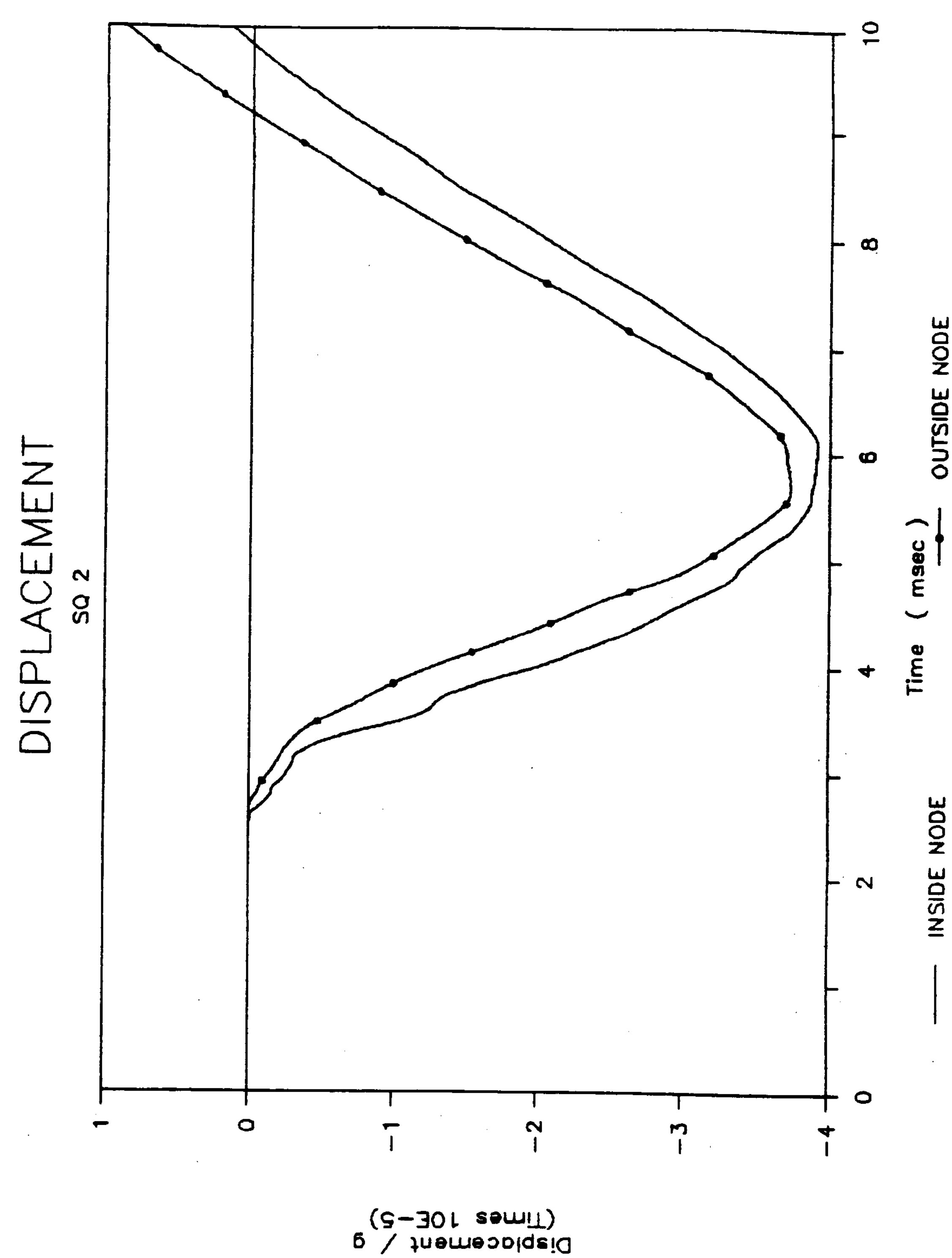

DISPLACEMENT
SQ 2
Displacement / g
(Times 10E-5)
1
0
-1
-2
-3
-4
0
2
4
6
8
10
Time (msec)
INSIDE NODE
OUTSIDE NODE

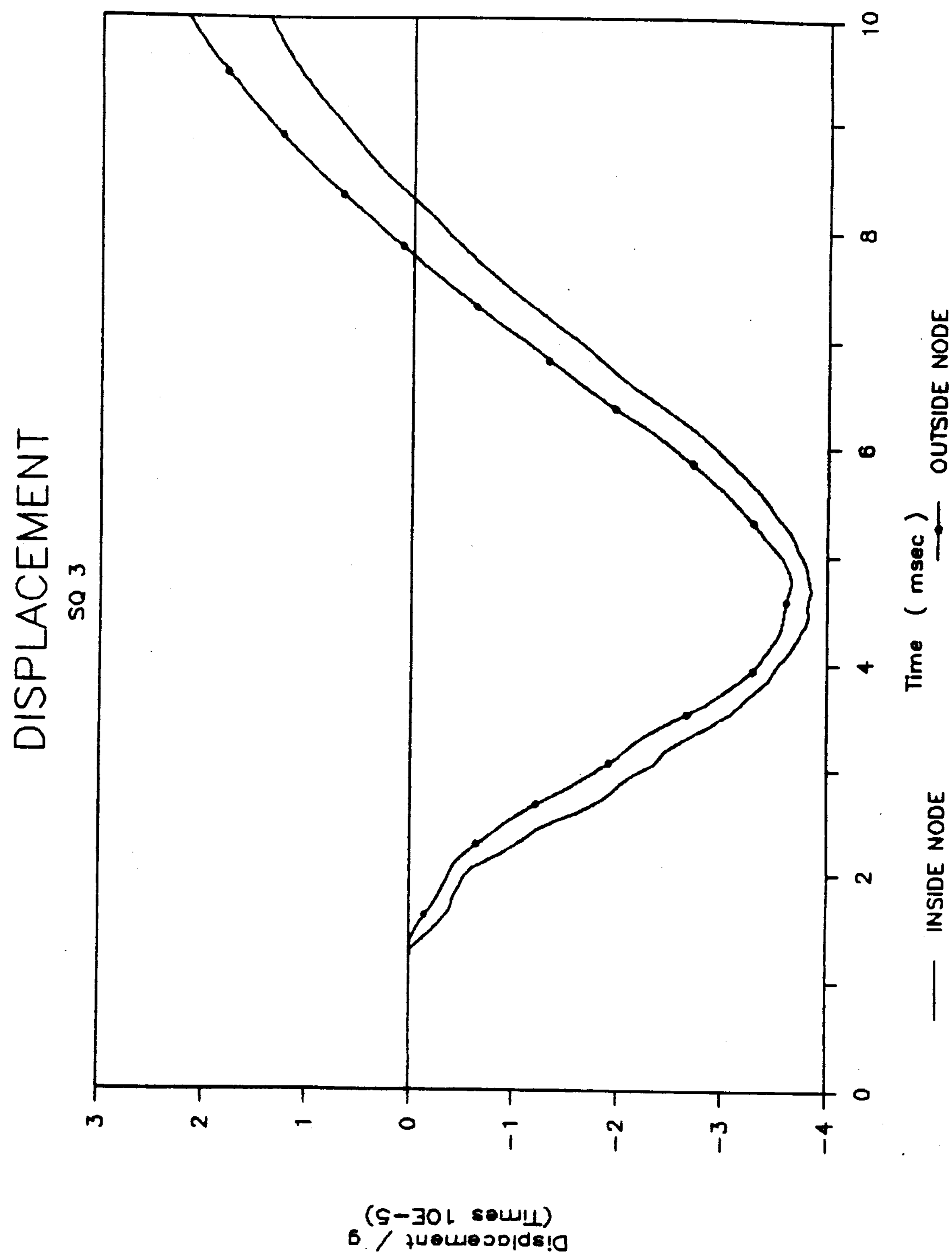

DISPLACEMENT
SQ 3
Displacement / g
(Times 10E-5)
3
2
1
0
-1
-2
-3
-4
0
2
4
6
8
10
Time (msec)
INSIDE NODE
OUTSIDE NODE

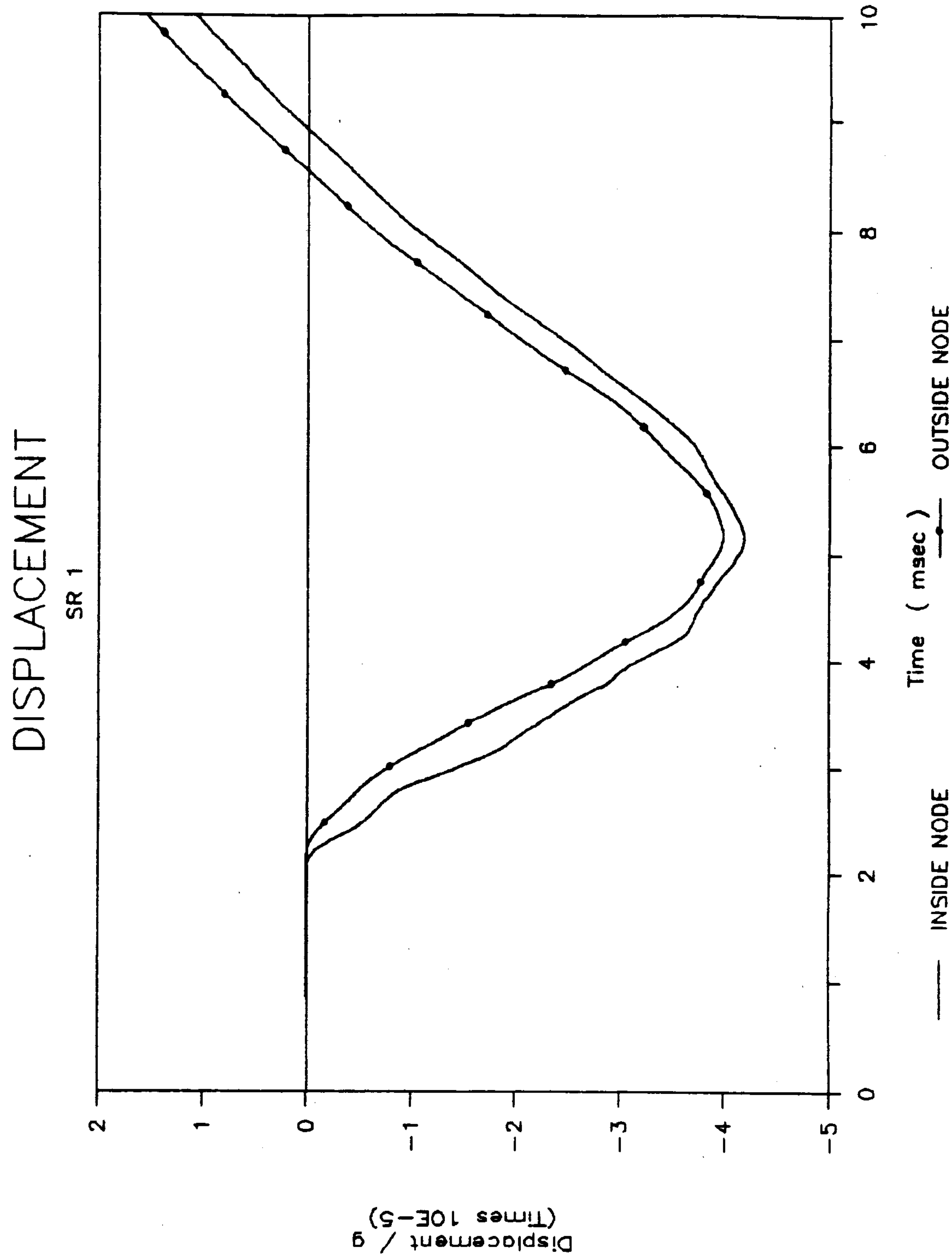
DISPLACEMENT
SR 1
Displacement / g
(Times 10E-5)
2
1
0
-1
-2
-3
-4
-5
0
2
4
6
8
10
Time (msec)
INSIDE NODE
OUTSIDE NODE

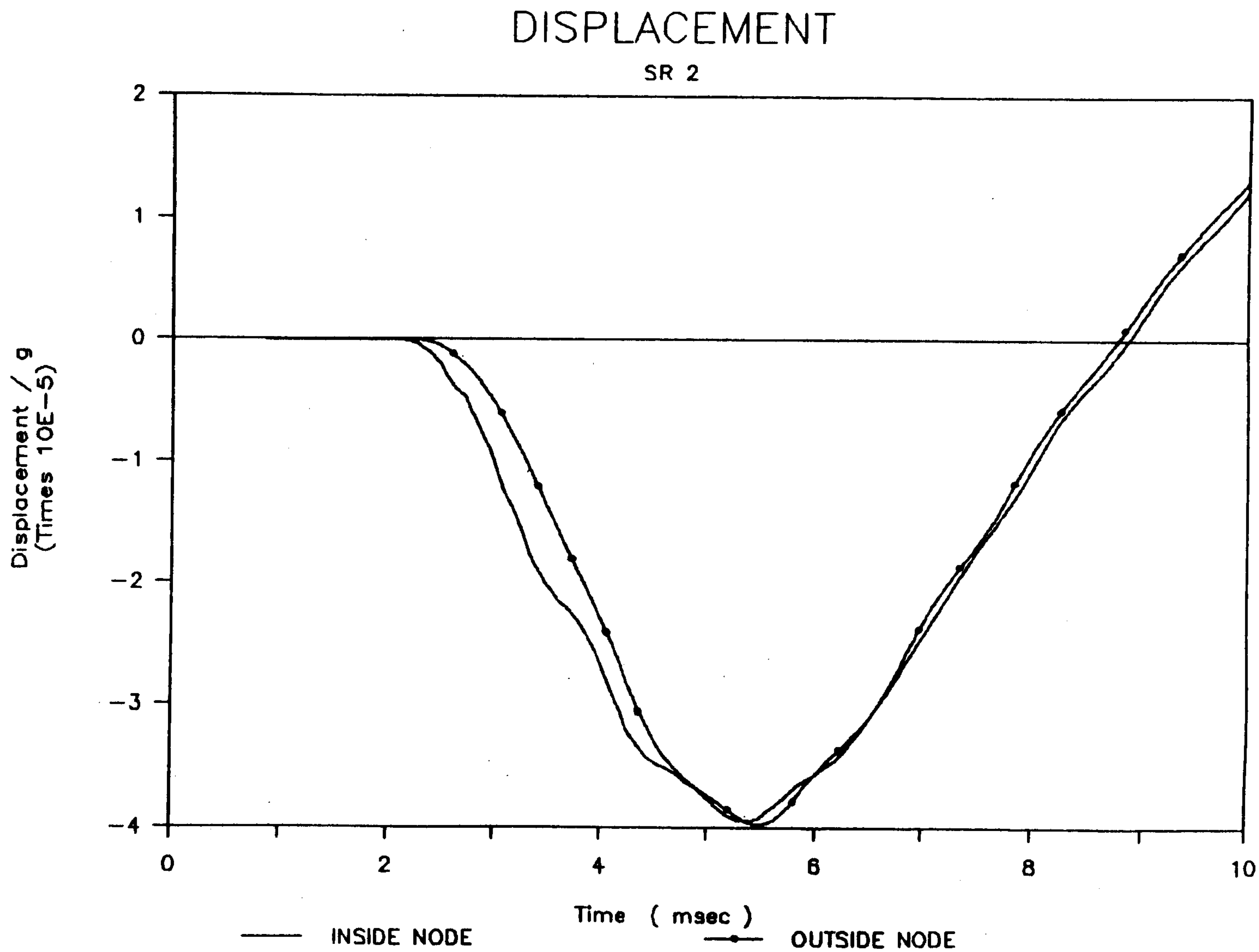

DISPLACEMENT
SR 2
Displacement / g
(Times 10E−5)
2
1
0
−1
−2
−3
−4
0
2
4
6
8
10
Time (msec)
INSIDE NODE
OUTSIDE NODE

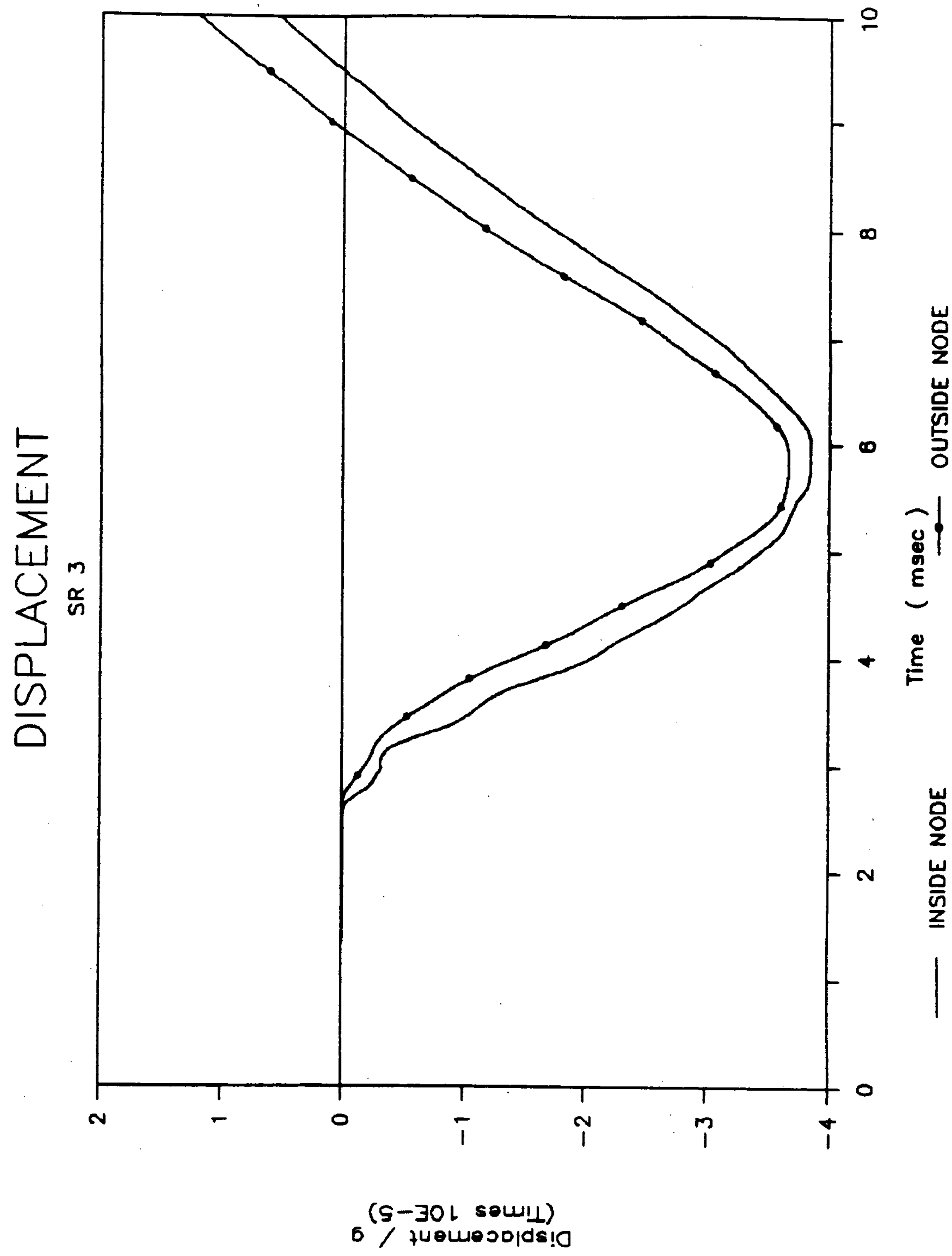
DISPLACEMENT
SR 3
Displacement / g
(Times 10E-5)
2
1
0
-1
-2
-3
-4
0
2
4
6
8
10
Time (msec)
INSIDE NODE
OUTSIDE NODE

APPENDIX C

Power Spectrum - Frequency Plots

The plots in the Appendix are the ones from the following tests:

B 1	: Inside Node, Outside Node	;	B 5	:	Inside Node, Outside Node
B 2	: "	;	B 6	:	"
B 3	: "	;	B 7	:	"
B 4	: "	;	B 8	:	"
ST 1	: Inside Node, Outside Node	;	SP 1	:	Inside Node, Outside Node
ST 2	: "	;	SP 2	:	"
ST 3	: "	;	SP 3	:	"
SU 1	: Inside Node, Outside Node	;	SQ 1	:	Inside Node, Outside Node
SU 2	: "	;	SQ 2	:	"
SU 3	: "	;	SQ 3	:	"
SV 1	: Inside Node, Outside Node	;	SR 1	:	Inside Node, Outside Node
SV 2	: "	;	SR 2	:	"
SV 3	: "	;	SR 3	:	"

U 1 : Inside Node, Outside Node

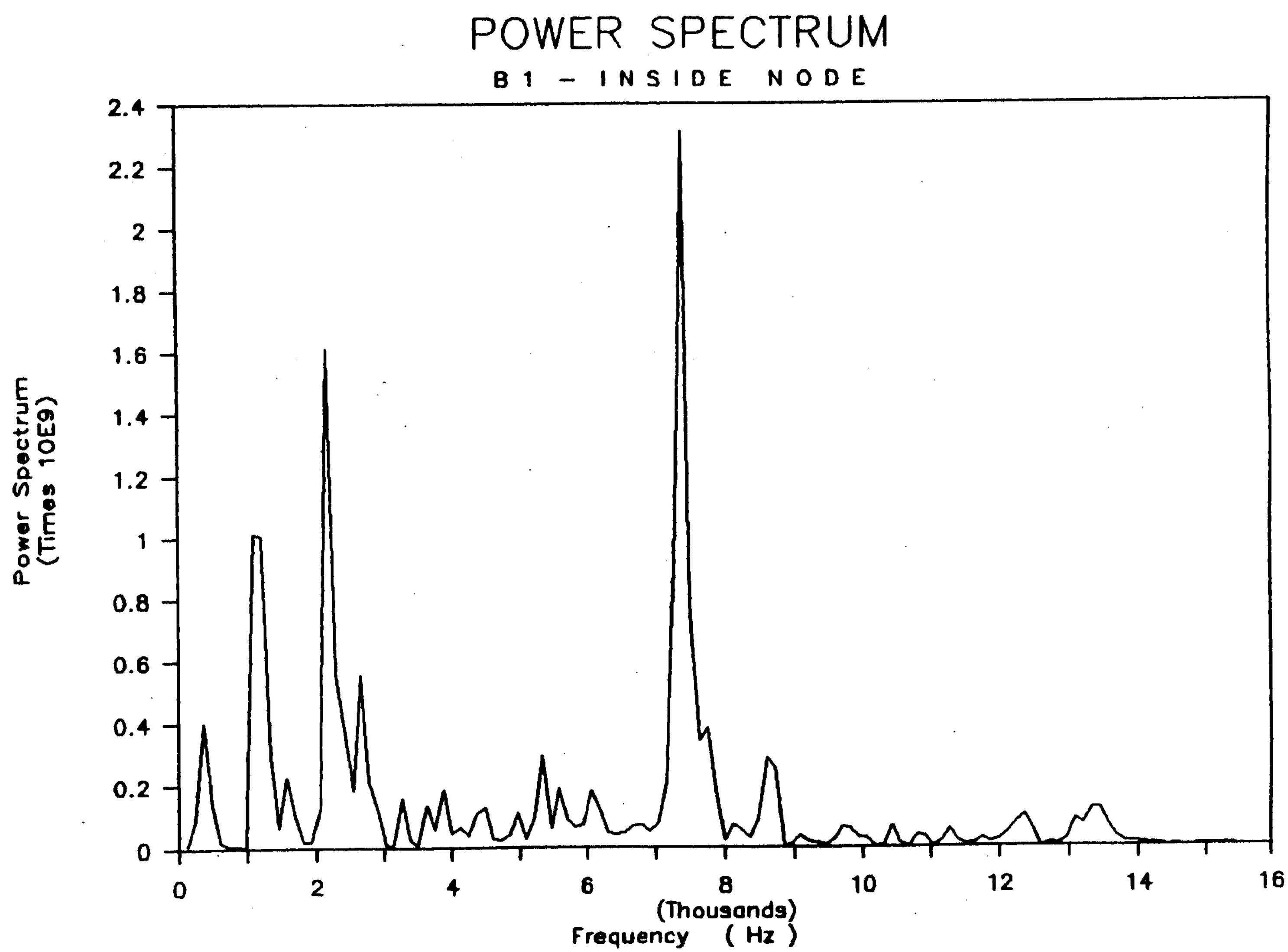
POWER SPECTRUM
B 1 – INSIDE NODE
Power Spectrum
(Times 10E9)
2.4
2.2
2
1.8
1.6
1.4
1.2
1
0.8
0.6
0.4
0.2
0
0
2
4
6
8
10
12
14
16
(Thousands)
Frequency (Hz)

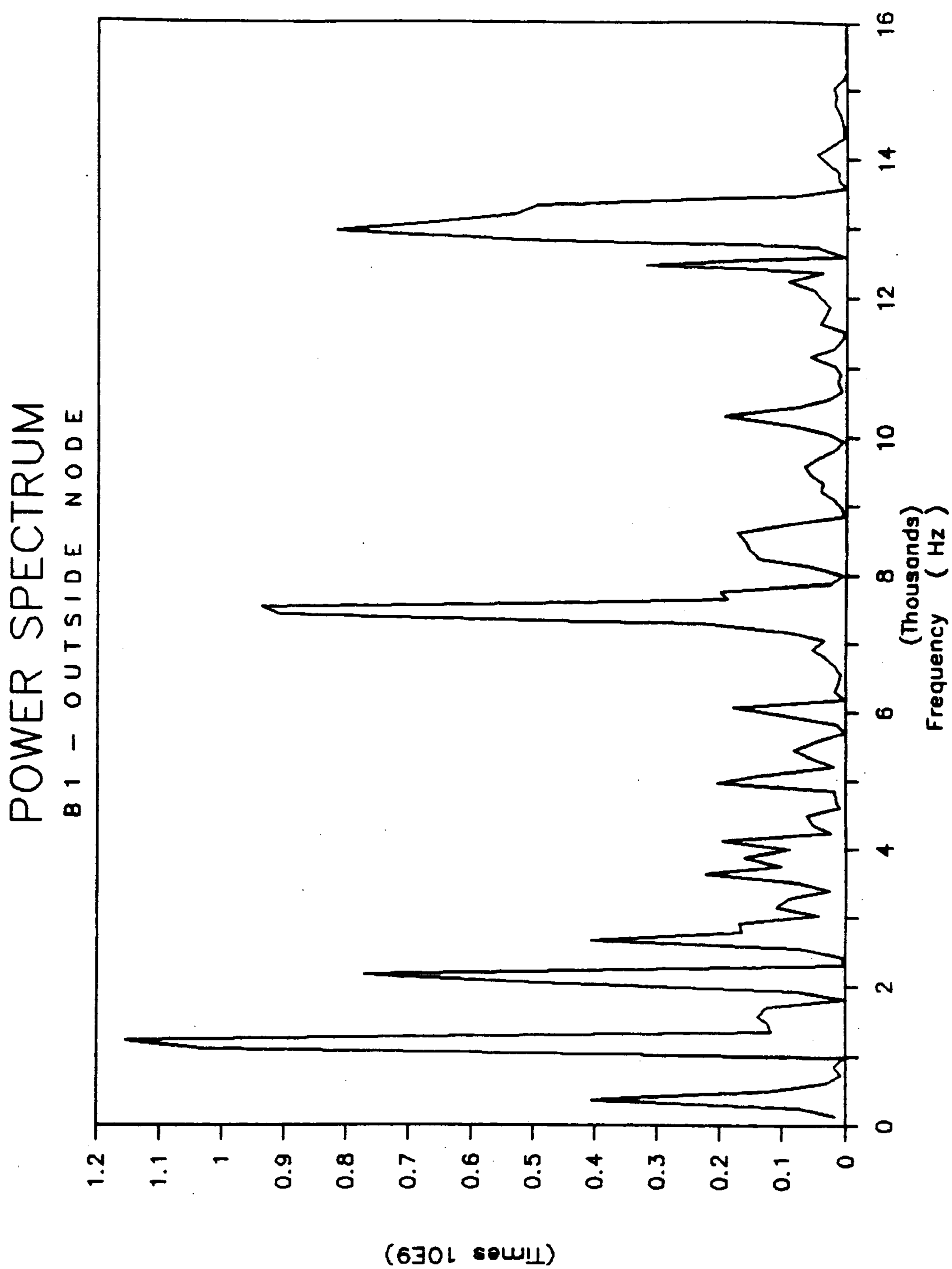

POWER SPECTRUM
B1 - OUTSIDE NODE
Power Spectrum
(Times 10E9)
Frequency
(Thousands)
(Hz)

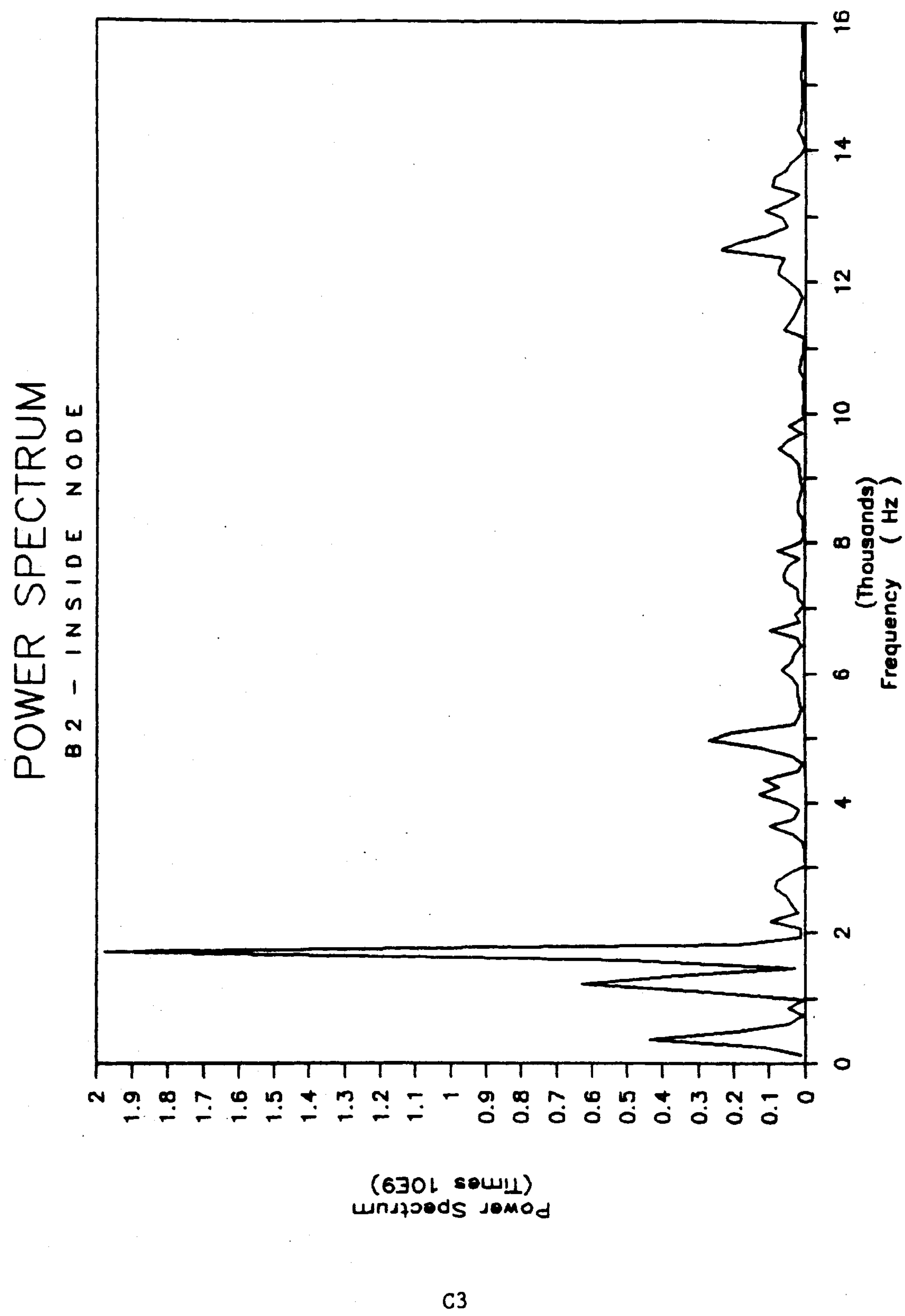

POWER SPECTRUM
B2 - INSIDE NODE
Power Spectrum
(Times 10E9)
2
1.9
1.8
1.7
1.6
1.5
1.4
1.3
1.2
1.1
1
0.9
0.8
0.7
0.6
0.5
0.4
0.3
0.2
0.1
0
0
2
4
6
8
10
12
14
16
(Thousands)
Frequency (Hz)

POWER SPECTRUM

B2 - OUTSIDE NODE

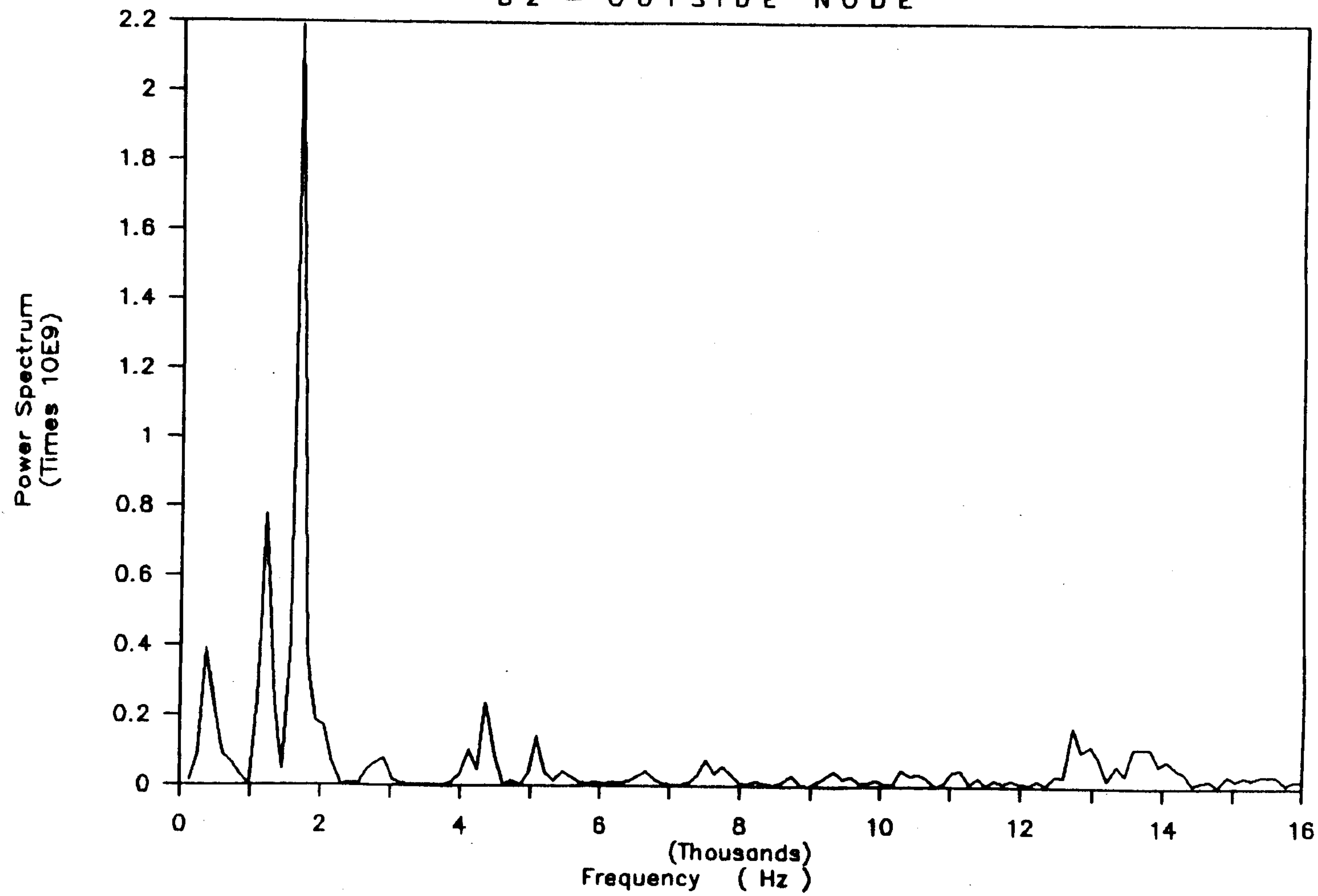

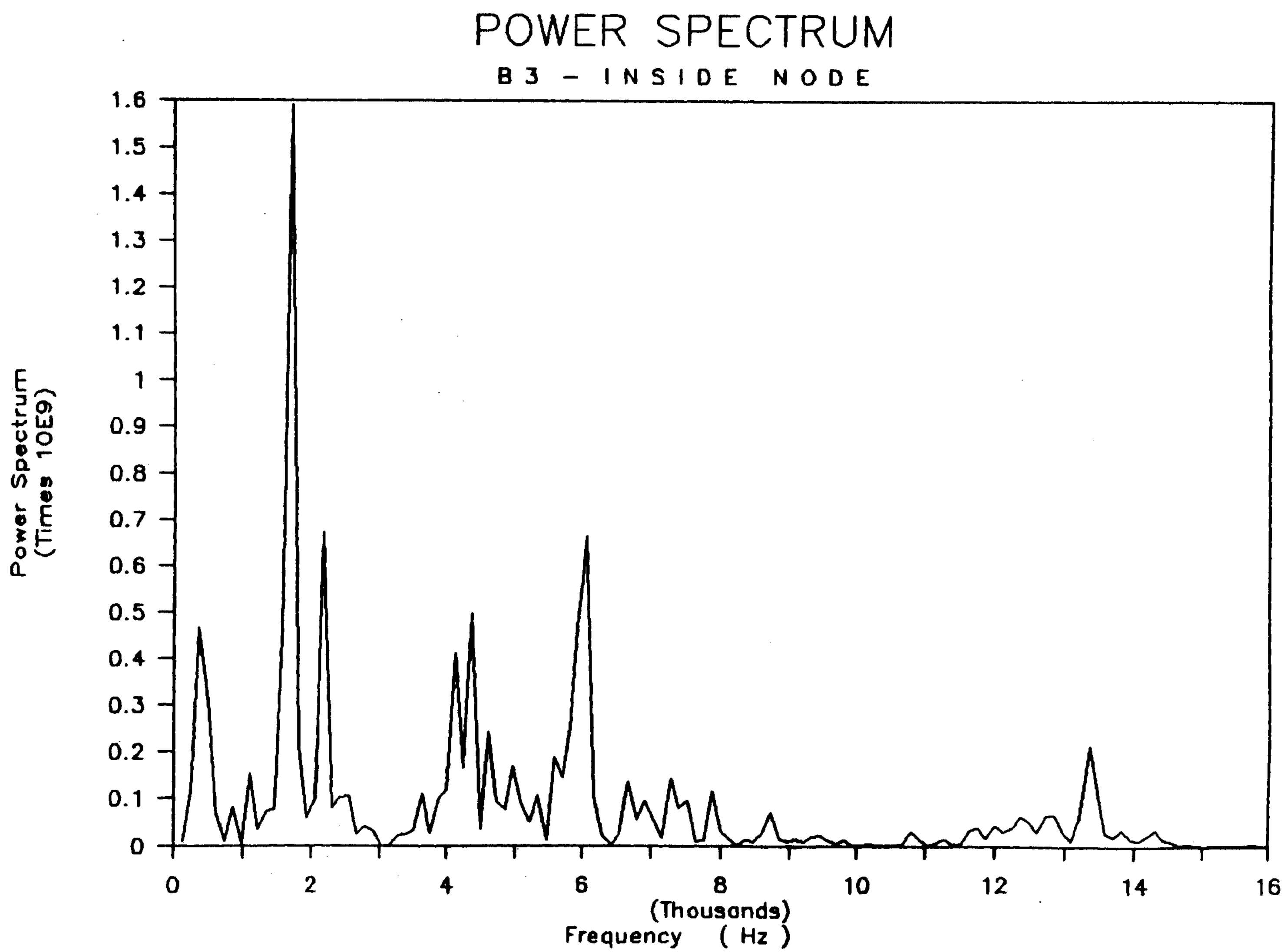

POWER SPECTRUM
B 3 - INSIDE NODE
Power Spectrum
(Times 10E9)
1.6
1.5
1.4
1.3
1.2
1.1
1
0.9
0.8
0.7
0.6
0.5
0.4
0.3
0.2
0.1
0
0
2
4
6
8
10
12
14
16
(Thousands)
Frequency (Hz)

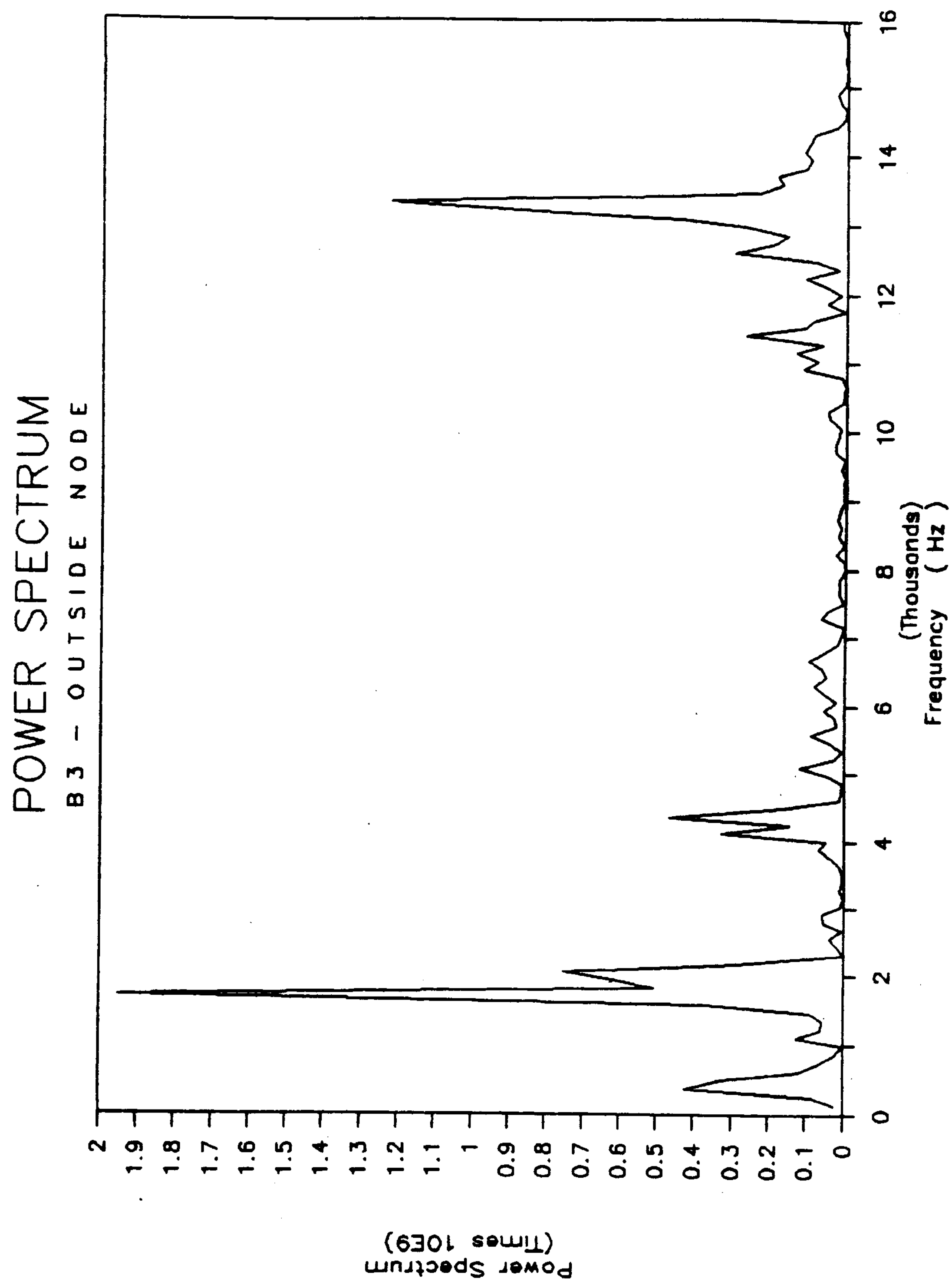
POWER SPECTRUM
B3 - OUTSIDE NODE
Power Spectrum
(Times 10E9)
2
1.9
1.8
1.7
1.6
1.5
1.4
1.3
1.2
1.1
1
0.9
0.8
0.7
0.6
0.5
0.4
0.3
0.2
0.1
0
0
2
4
6
8
10
12
14
16
(Thousands)
Frequency (Hz)

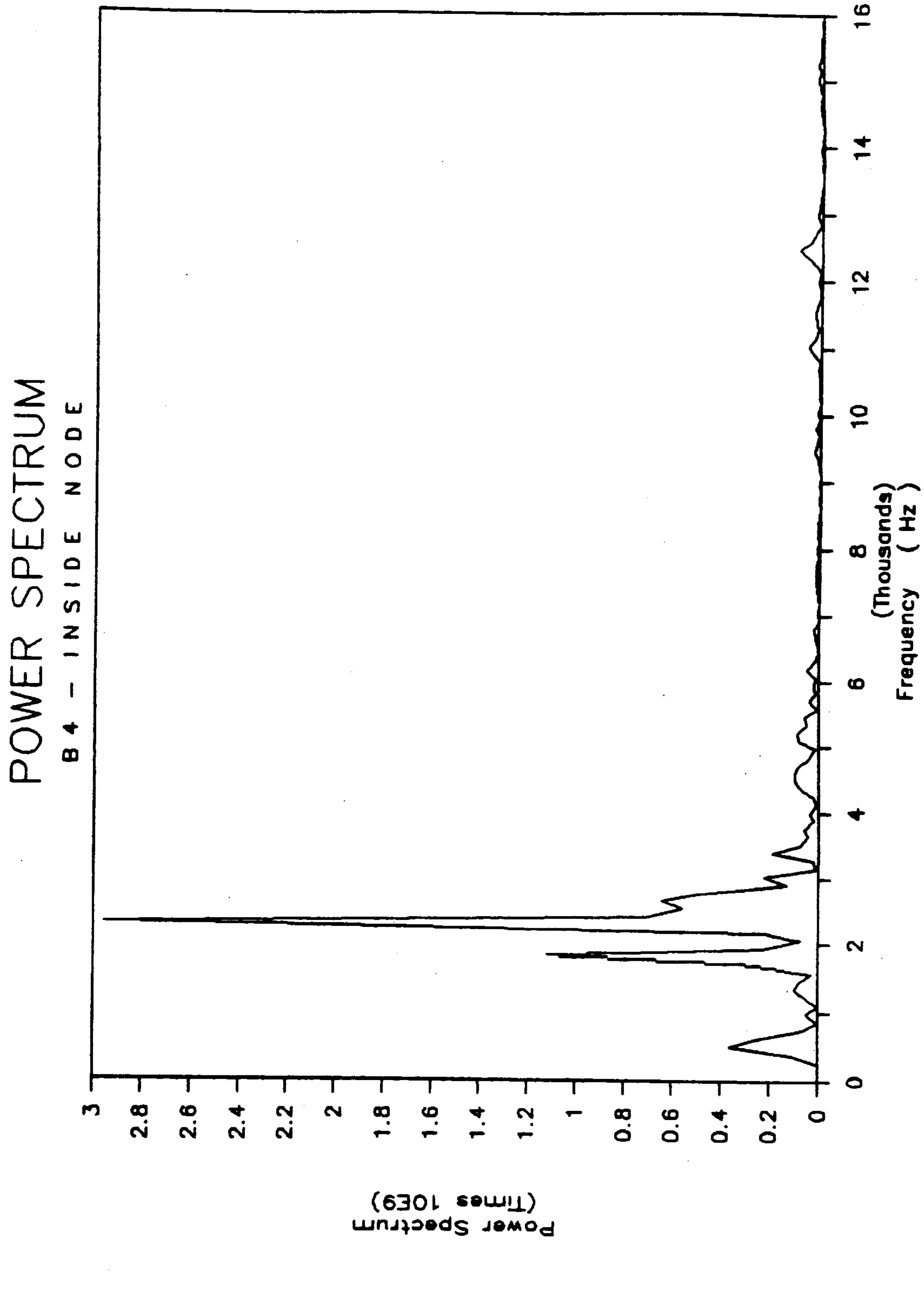
POWER SPECTRUM
B4 - INSIDE NODE
Power Spectrum
(Times 10E9)
3
2.8
2.6
2.4
2.2
2
1.8
1.6
1.4
1.2
1
0.8
0.6
0.4
0.2
0
0
2
4
6
8
10
12
14
16
Frequency (Thousands)
(Hz)

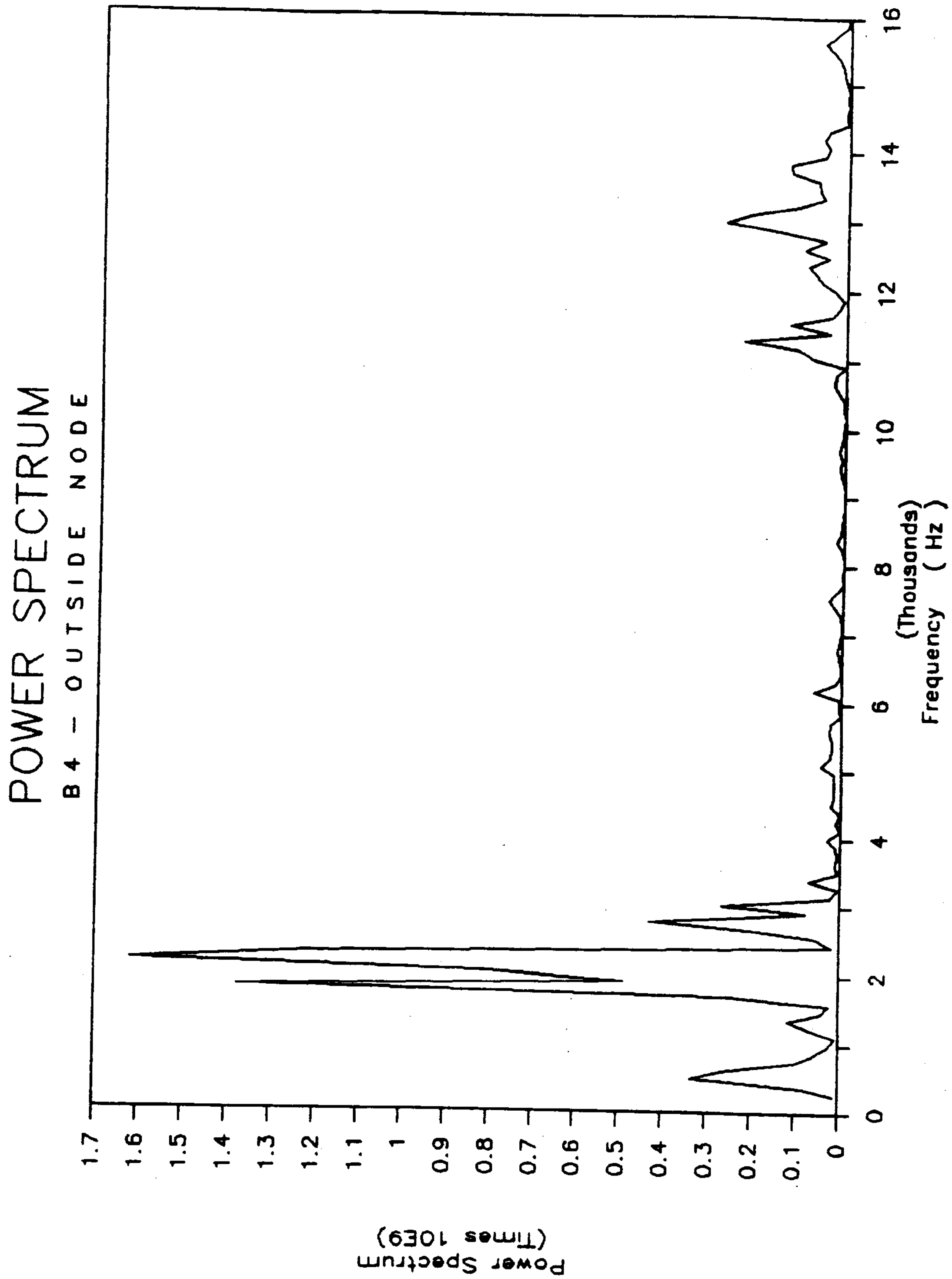
POWER SPECTRUM
B 4 – OUTSIDE NODE
Power Spectrum
(Times 10E9)
0
0.1
0.2
0.3
0.4
0.5
0.6
0.7
0.8
0.9
1
1.1
1.2
1.3
1.4
1.5
1.6
1.7
0
2
4
6
8
10
12
14
16
(Thousands)
Frequency (Hz)

POWER SPECTRUM

B5 - INSIDE NODE

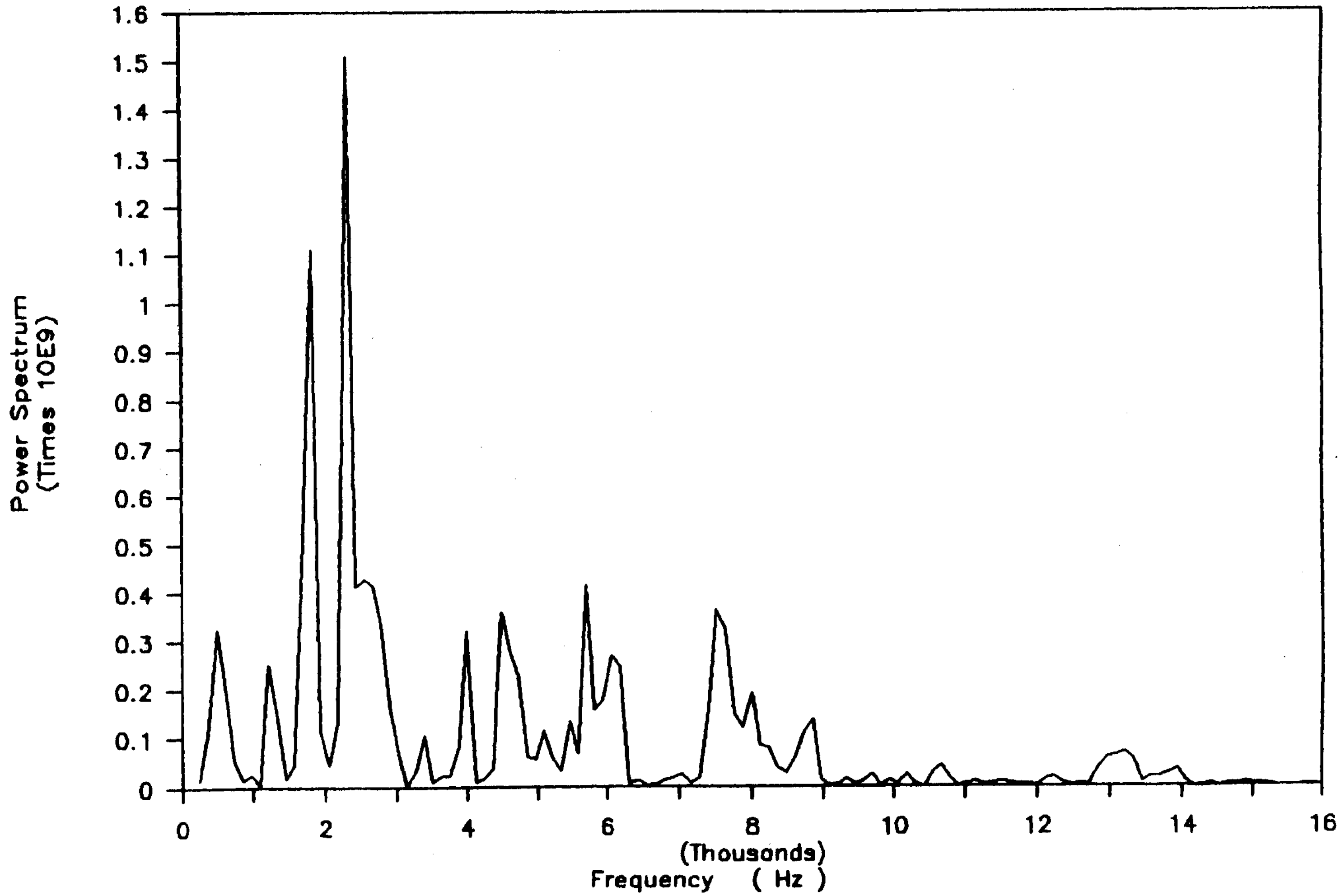

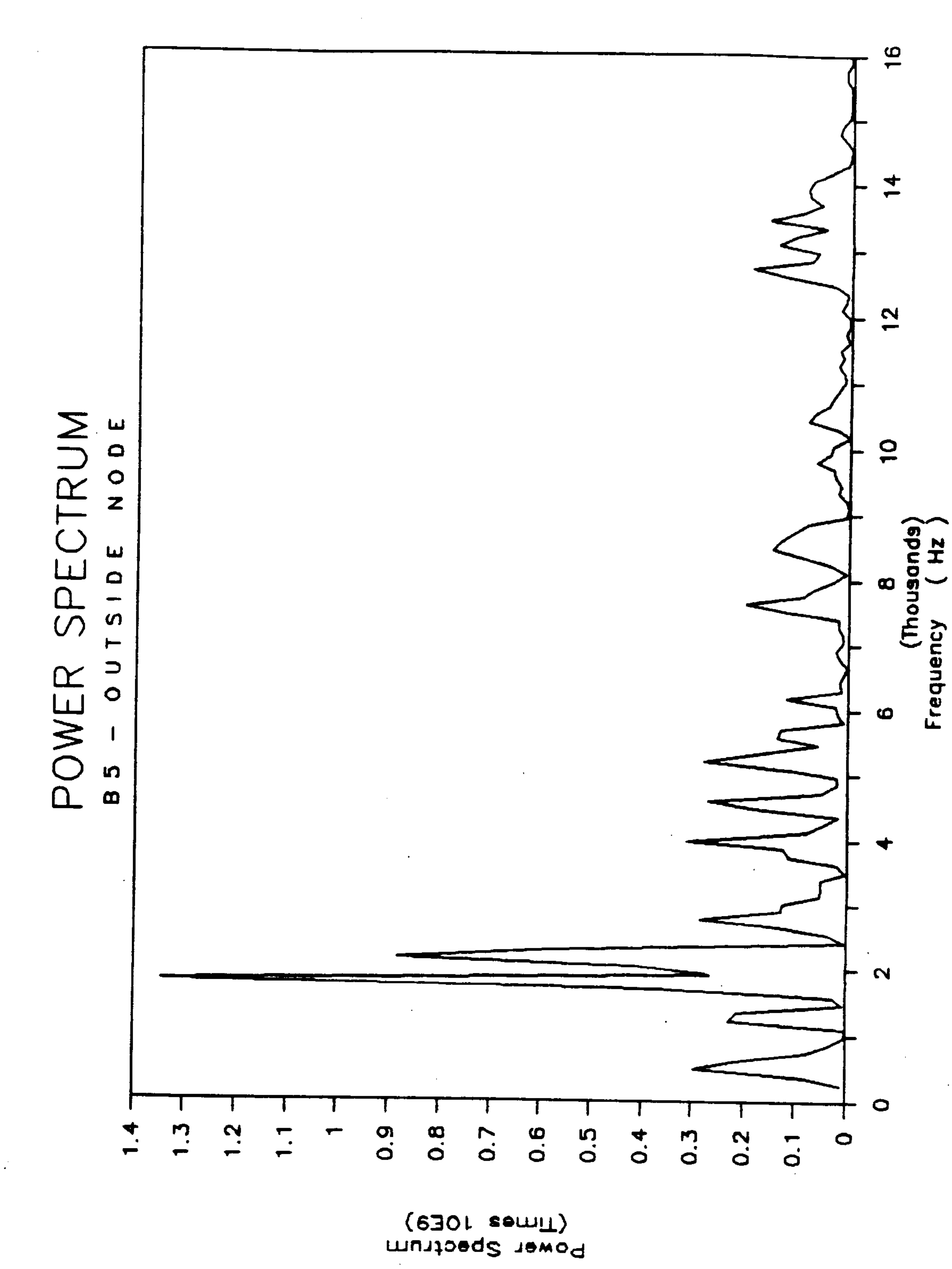
POWER SPECTRUM
B5 - OUTSIDE NODE
Power Spectrum
(Times 10E9)
1.4
1.3
1.2
1.1
1
0.9
0.8
0.7
0.6
0.5
0.4
0.3
0.2
0.1
0
0
2
4
6
8
10
12
14
16
(Thousands)
Frequency (Hz)

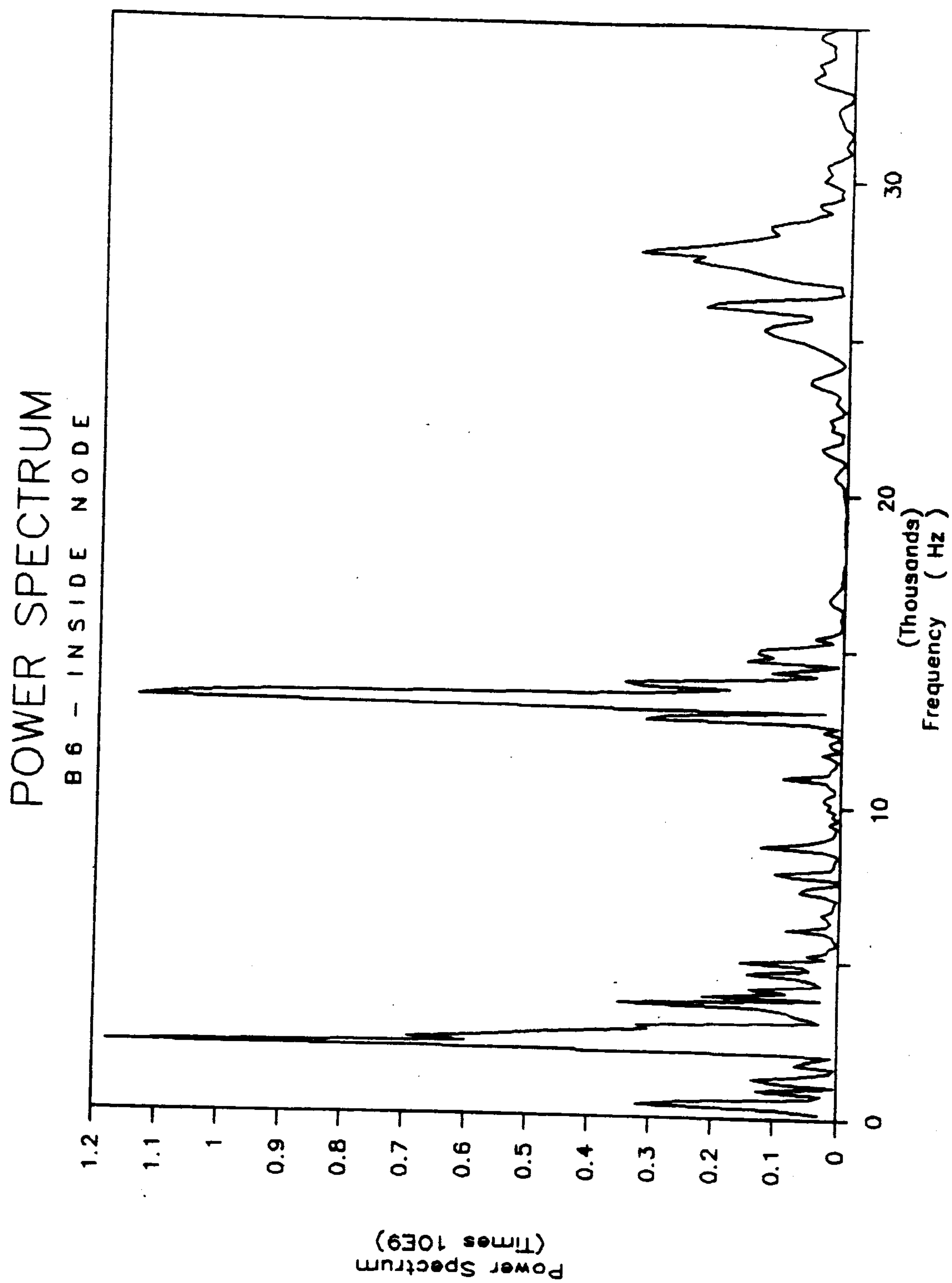
POWER SPECTRUM
B6 - INSIDE NODE
Power Spectrum
(Times 10E9)
Frequency (Hz)
(Thousands)
0
0.1
0.2
0.3
0.4
0.5
0.6
0.7
0.8
0.9
1
1.1
1.2
0
10
20
30

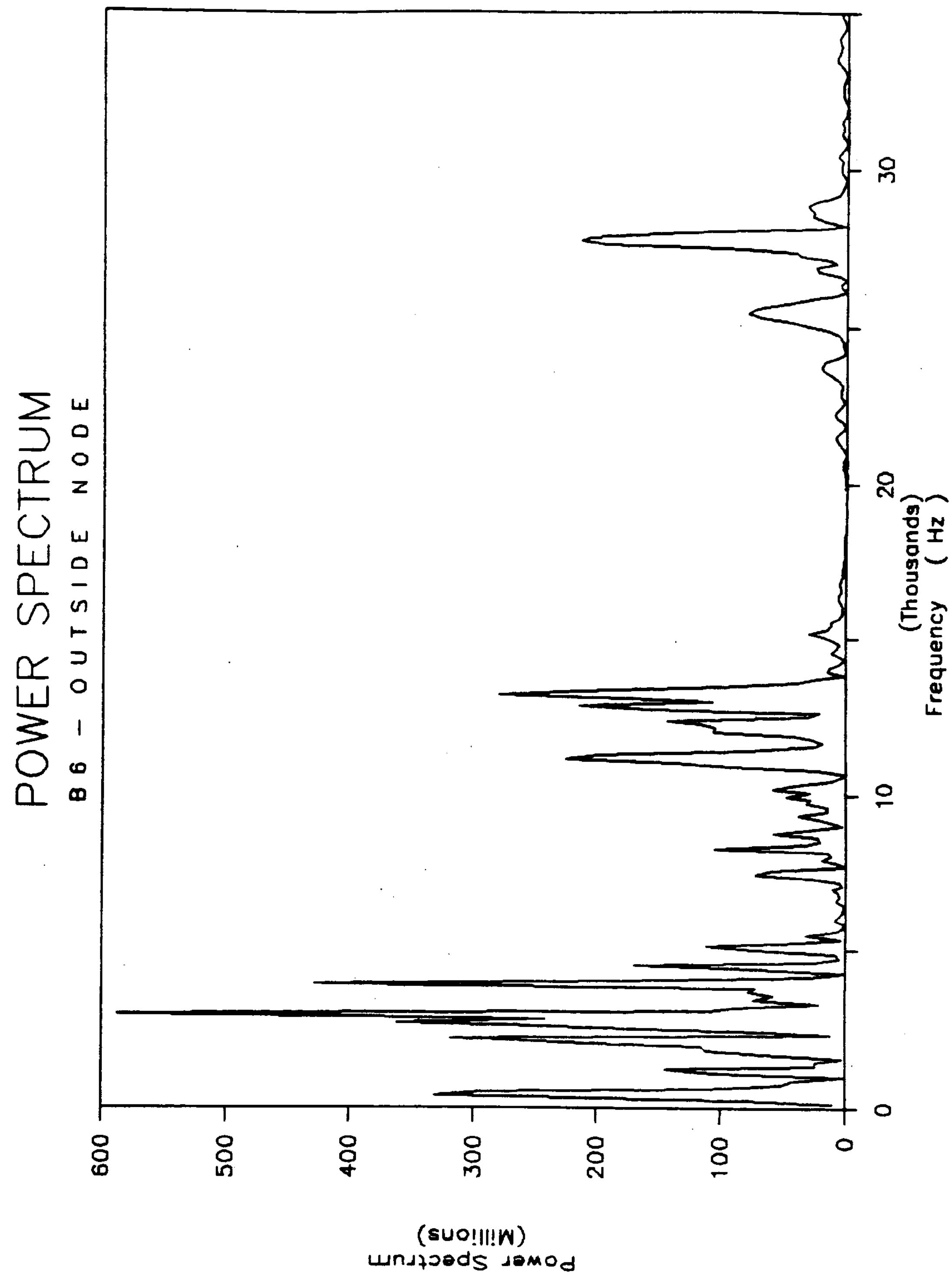
POWER SPECTRUM
B6 - OUTSIDE NODE
Power Spectrum
(Millions)
600
500
400
300
200
100
0
0
10
20
30
(Thousands)
Frequency (Hz)

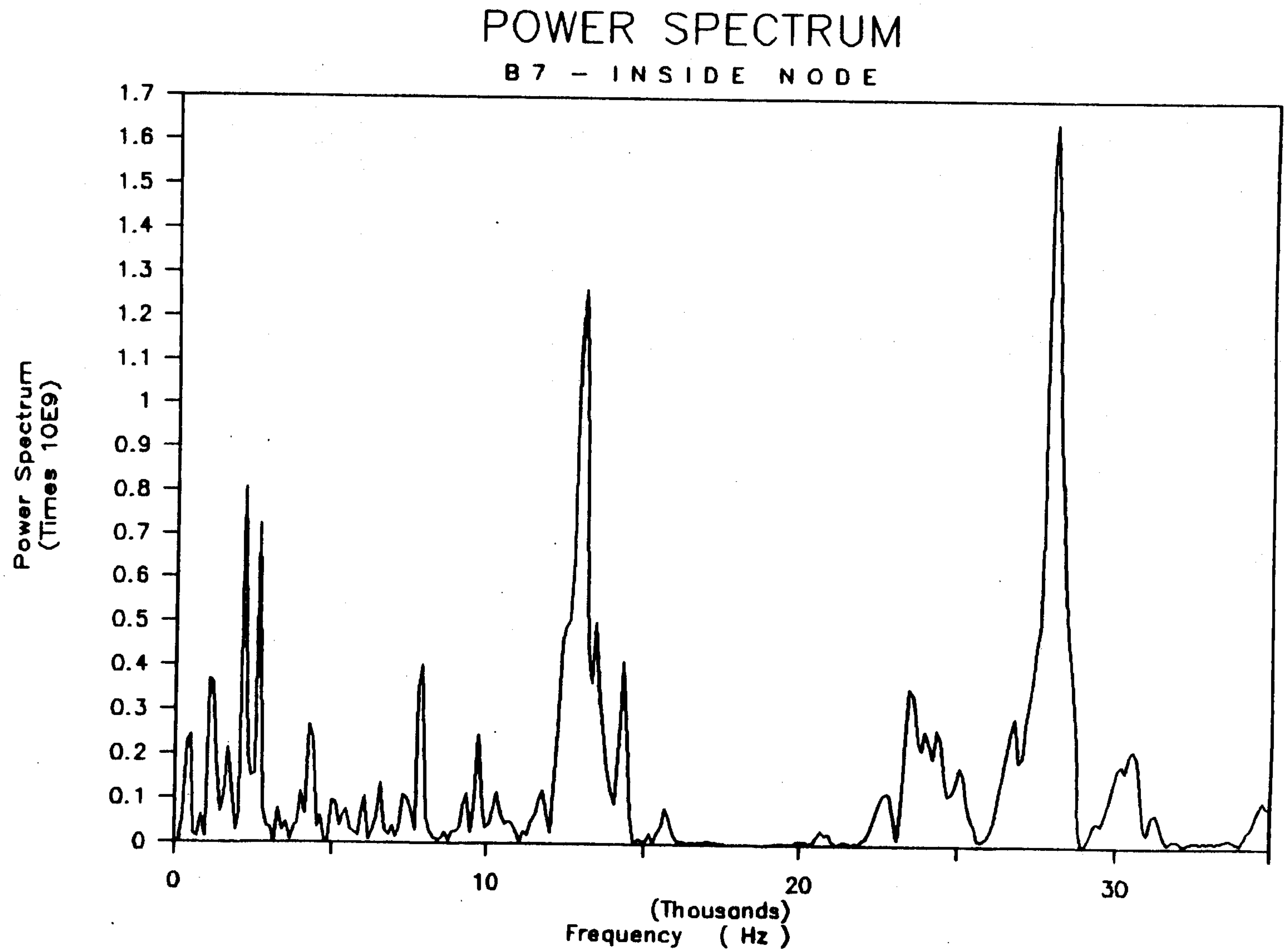
POWER SPECTRUM
B7 - INSIDE NODE
Power Spectrum
(Times 10E9)
1.7
1.6
1.5
1.4
1.3
1.2
1.1
1
0.9
0.8
0.7
0.6
0.5
0.4
0.3
0.2
0.1
0
0
10
20
30
(Thousands)
Frequency (Hz)

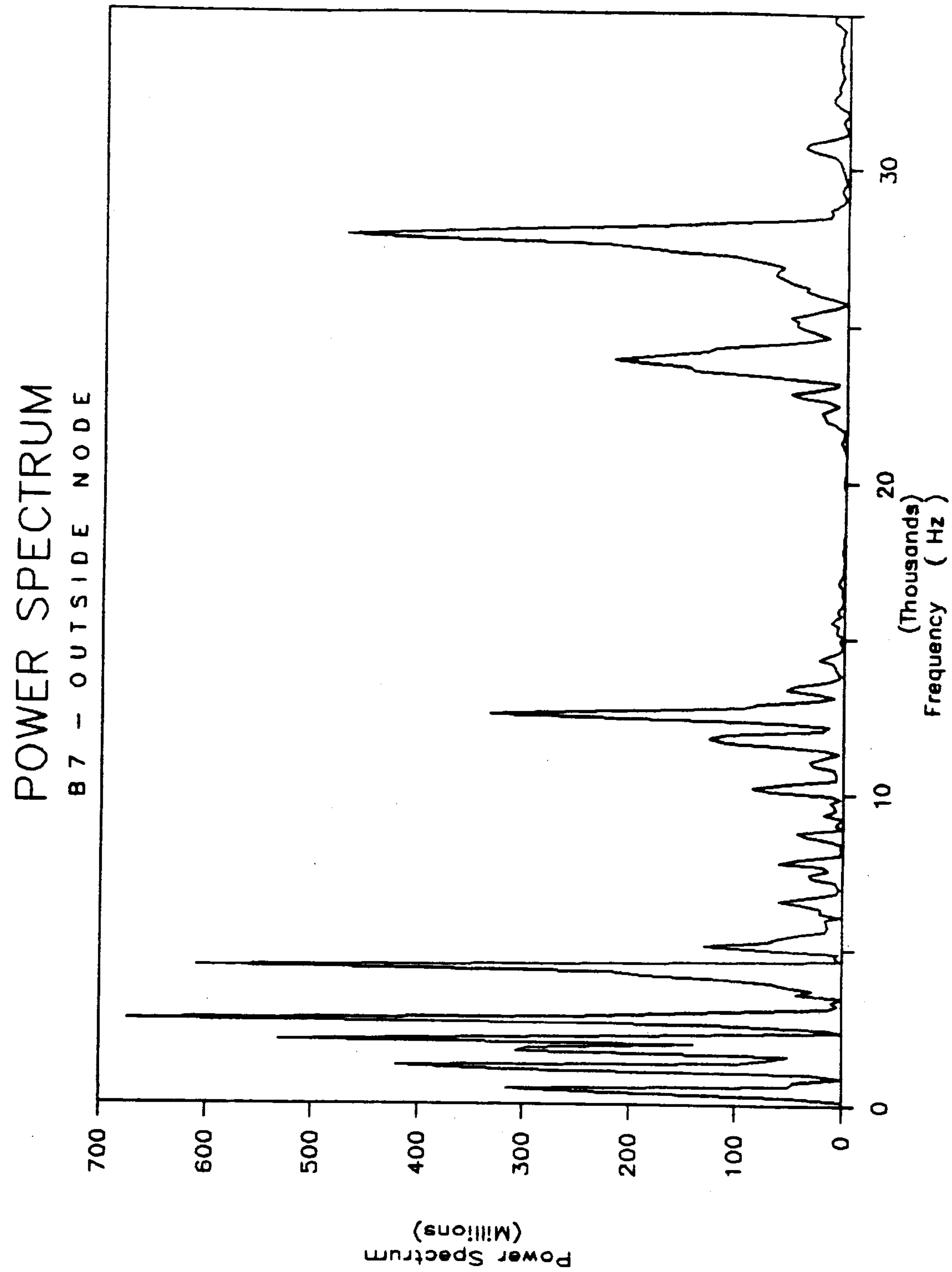
POWER SPECTRUM
B 7 - OUTSIDE NODE
Power Spectrum
(Millions)
0
100
200
300
400
500
600
700
0
10
20
30
(Thousands)
Frequency (Hz)

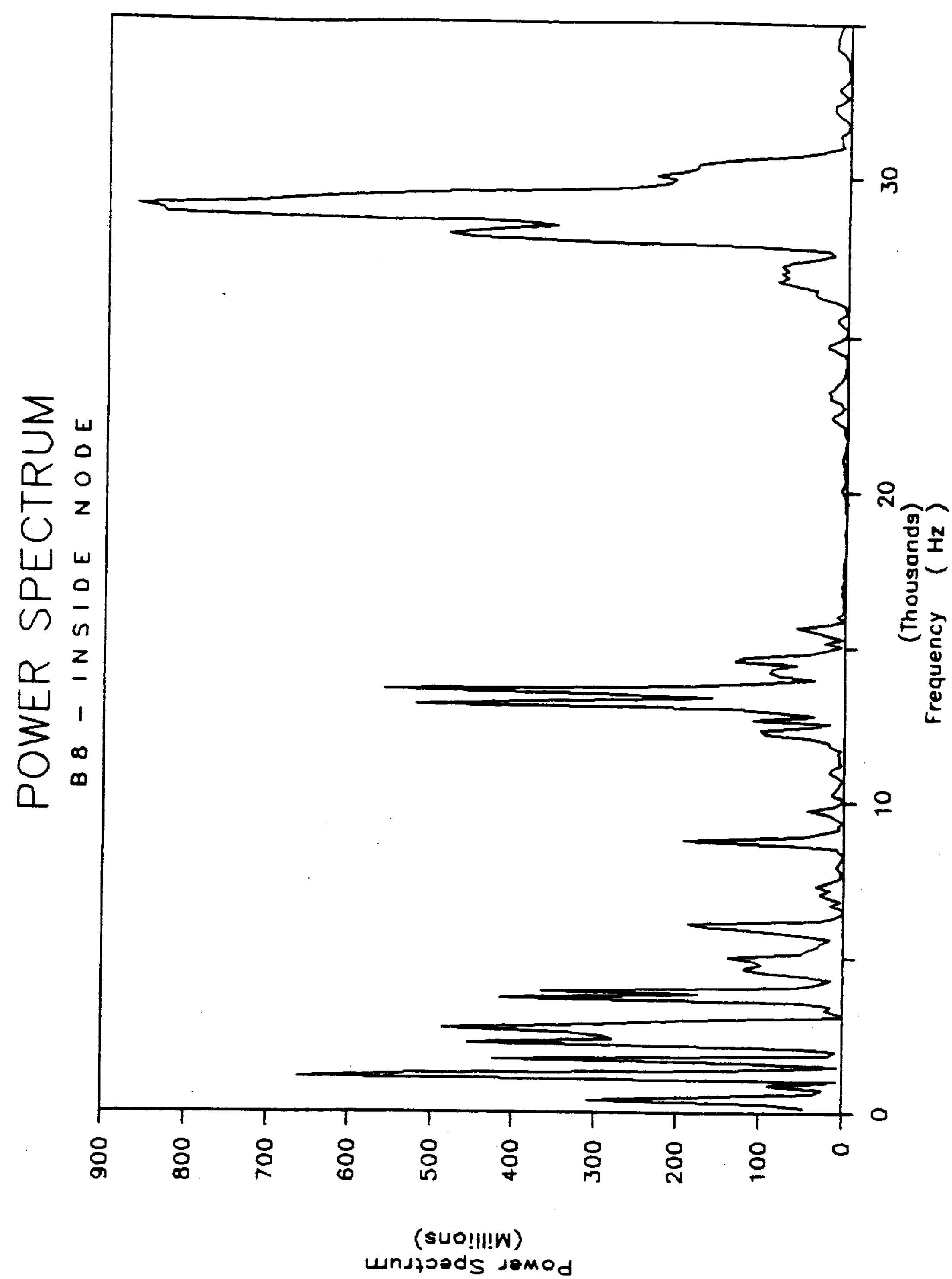
POWER SPECTRUM
B8 - INSIDE NODE
Power Spectrum
(Millions)
900
800
700
600
500
400
300
200
100
0
0
10
20
30
(Thousands)
Frequency (Hz)

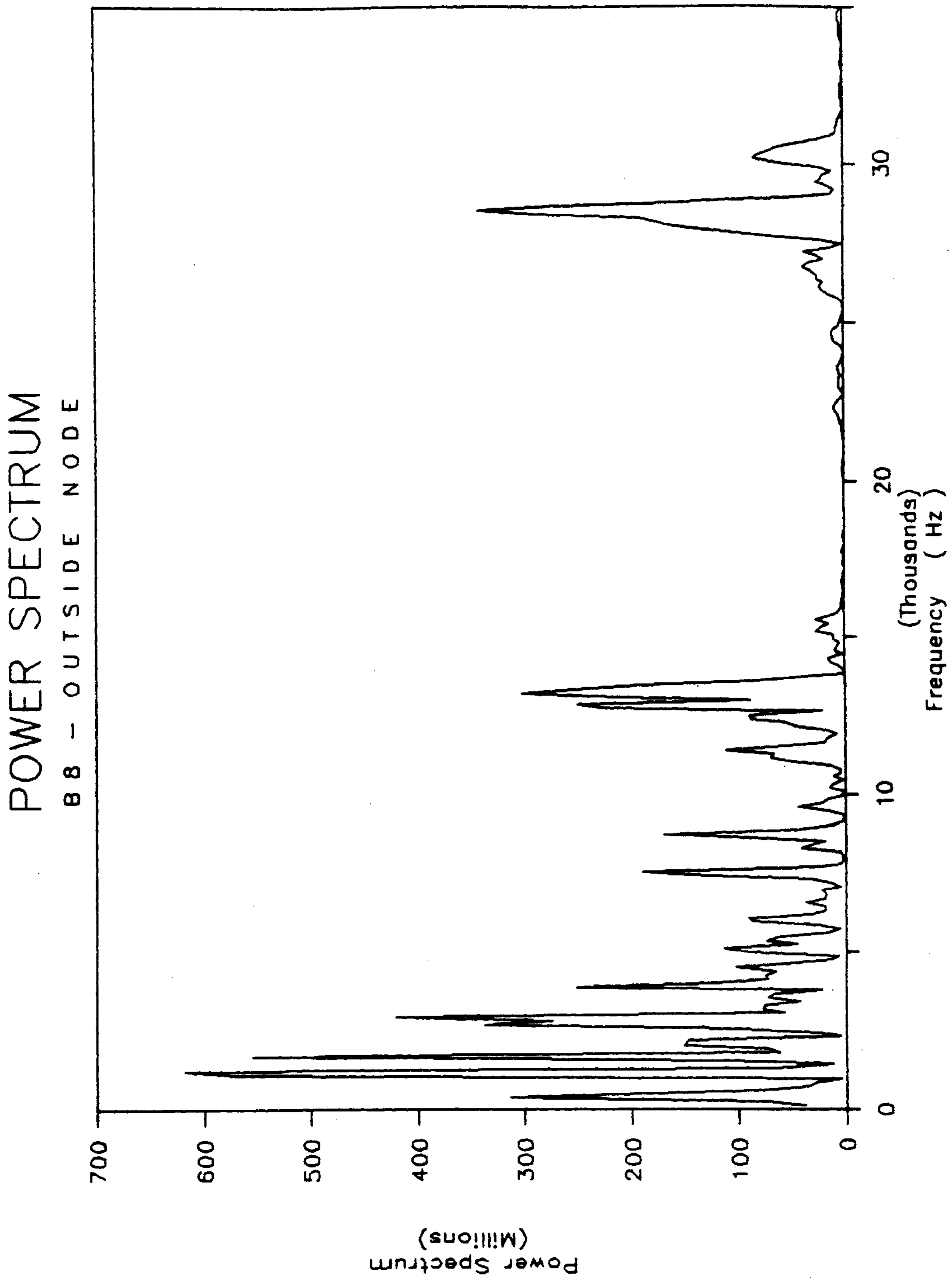
POWER SPECTRUM
BB - OUTSIDE NODE
Power Spectrum
(Millions)
700
600
500
400
300
200
100
0
0
10
20
30
(Thousands)
Frequency (Hz)

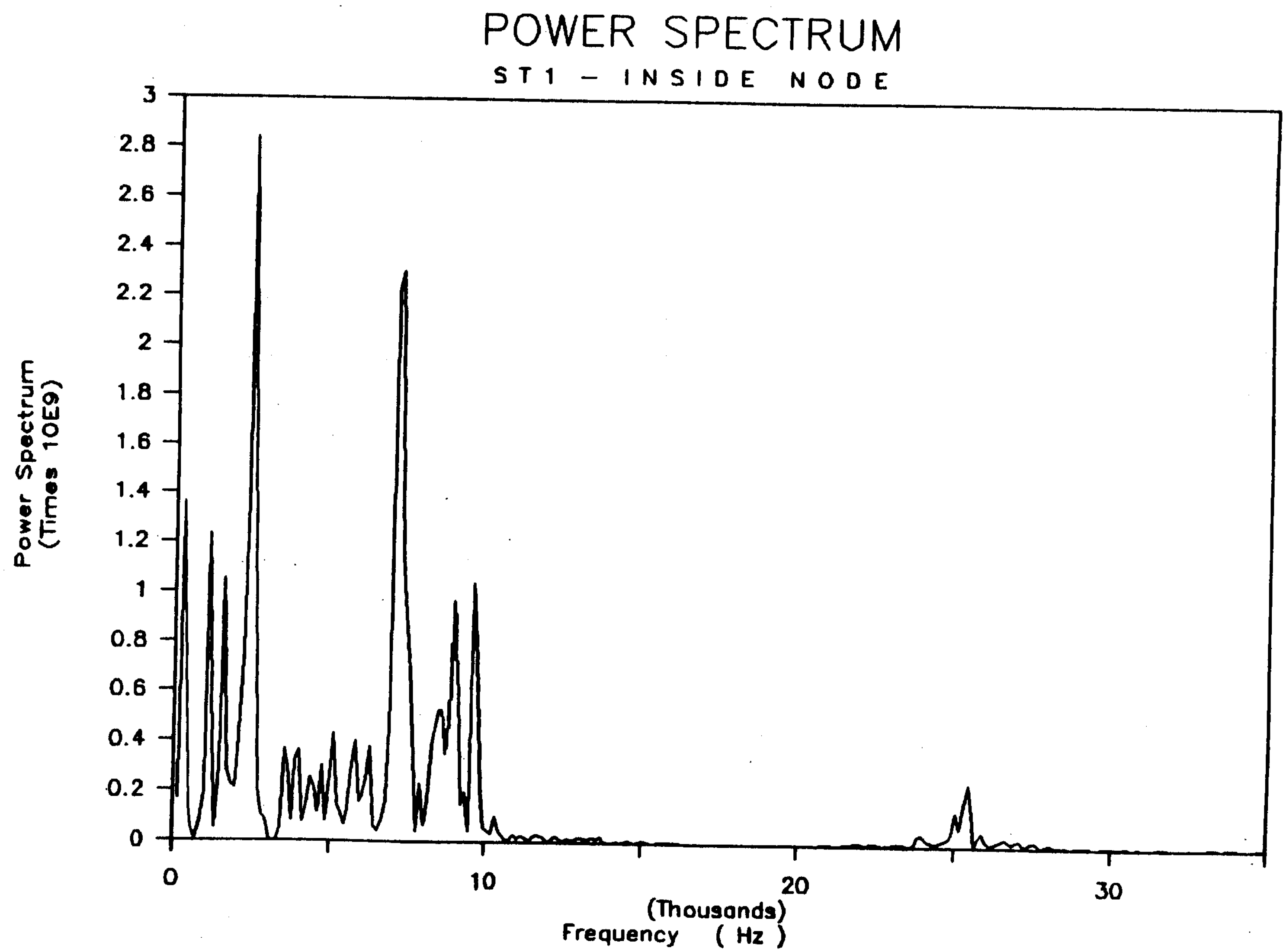
POWER SPECTRUM
ST1 - INSIDE NODE
Power Spectrum
(Times 10E9)
3
2.8
2.6
2.4
2.2
2
1.8
1.6
1.4
1.2
1
0.8
0.6
0.4
0.2
0
0
10
20
30
(Thousands)
Frequency (Hz)

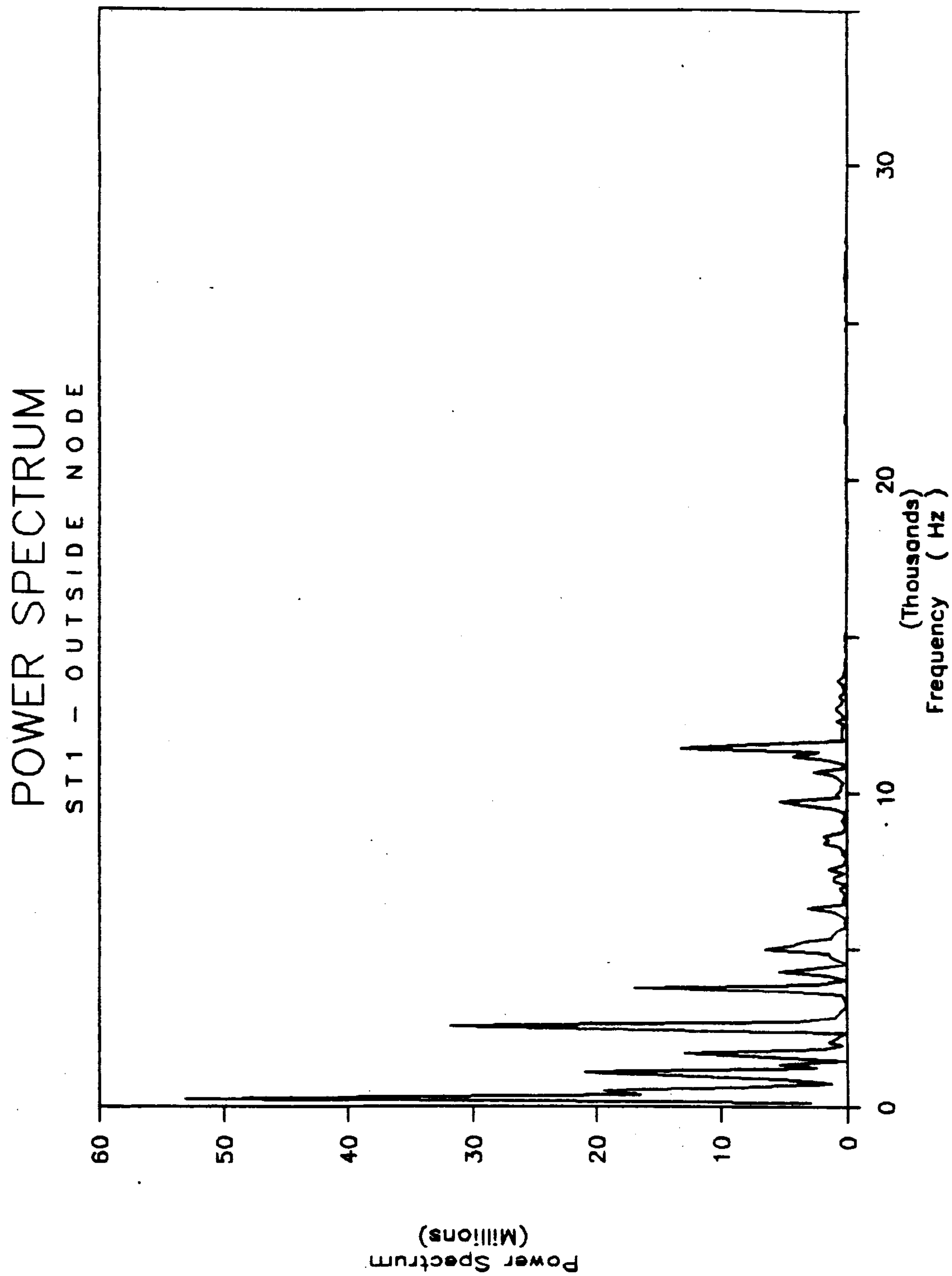
POWER SPECTRUM
ST1 - OUTSIDE NODE
Power Spectrum
(Millions)
0
10
20
30
40
50
60
Frequency (Hz)
(Thousands)
0
10
20
30

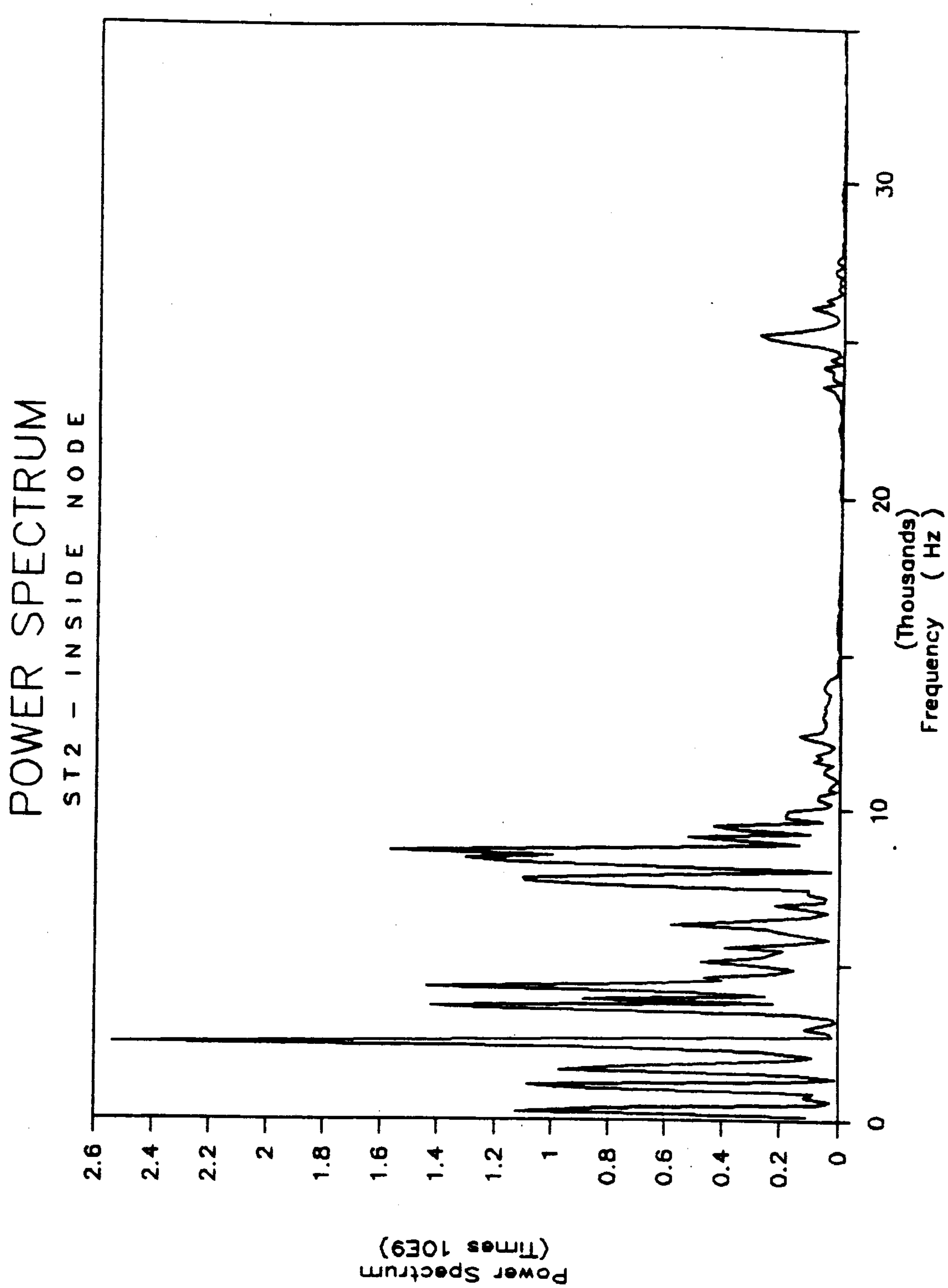

POWER SPECTRUM
ST2 - INSIDE NODE
Power Spectrum
(Times 10E9)
2.6
2.4
2.2
2
1.8
1.6
1.4
1.2
1
0.8
0.6
0.4
0.2
0
0
10
20
30
(Thousands)
Frequency (Hz)

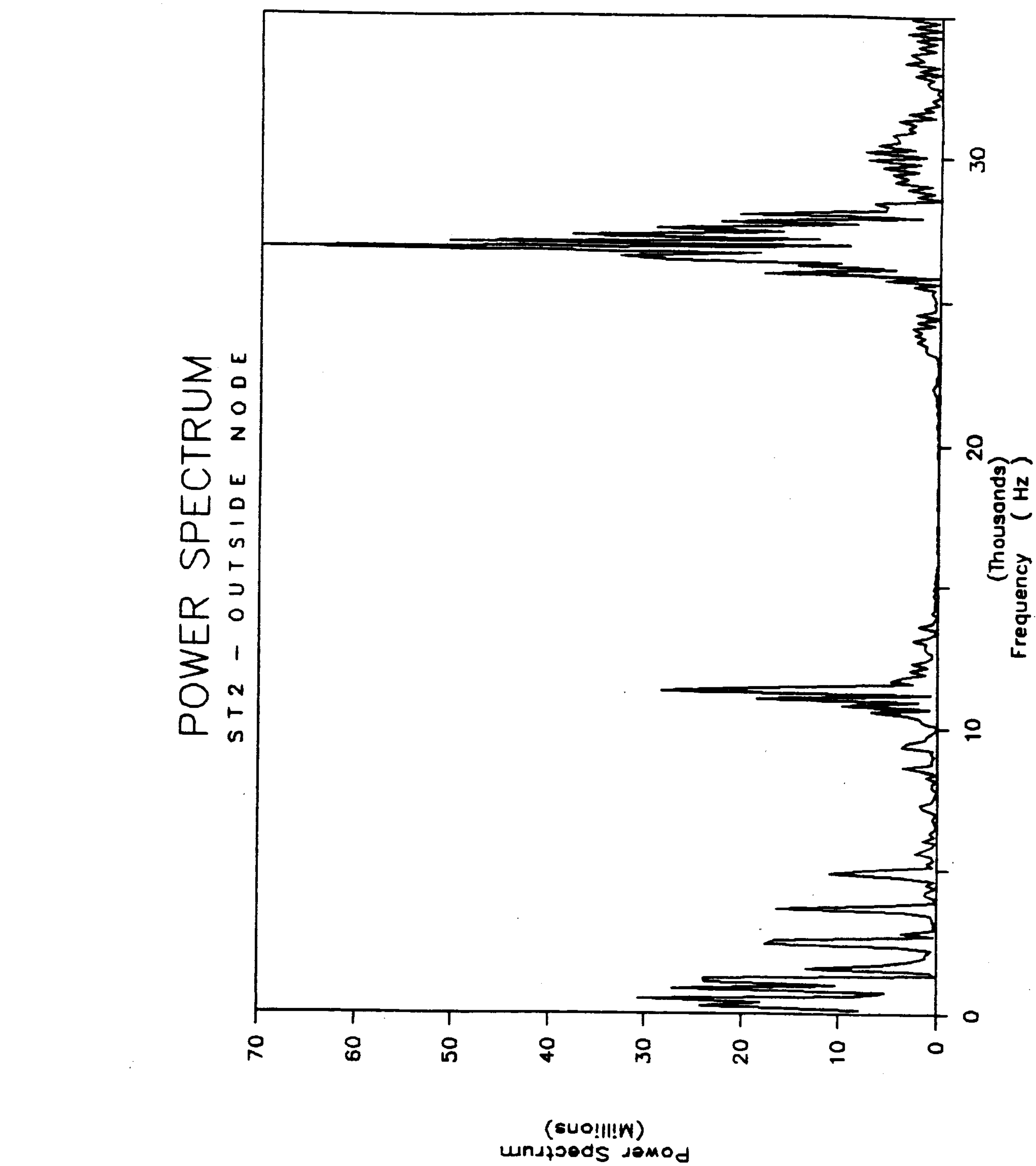

POWER SPECTRUM
ST2 - OUTSIDE NODE
Power Spectrum
(Millions)
0
10
20
30
40
50
60
70
0
10
20
30
Frequency (Hz)
(Thousands)

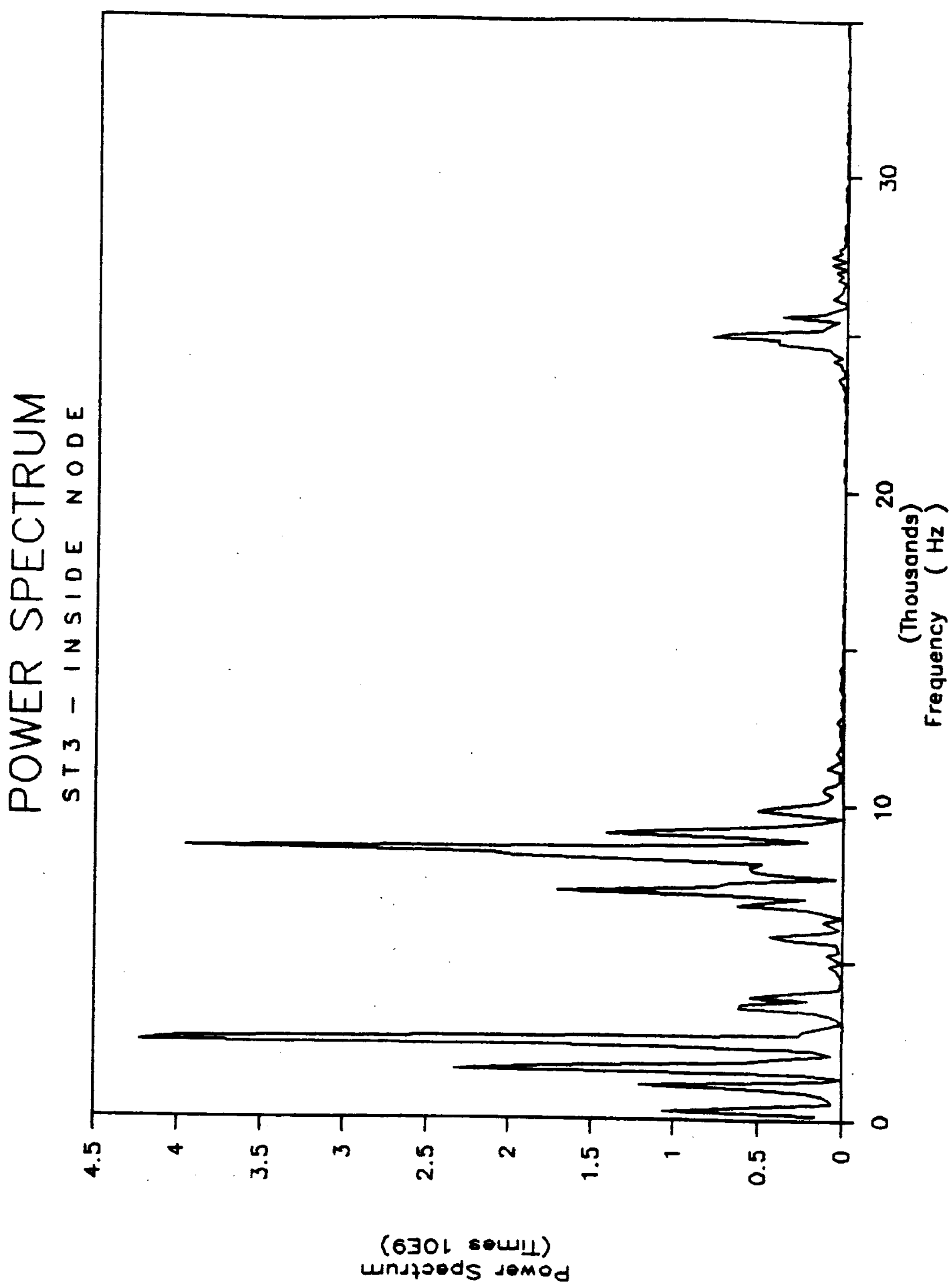
POWER SPECTRUM
ST3 - INSIDE NODE
Power Spectrum
(Times 10E9)
Frequency (Hz)
(Thousands)
0
0.5
1
1.5
2
2.5
3
3.5
4
4.5
0
10
20
30

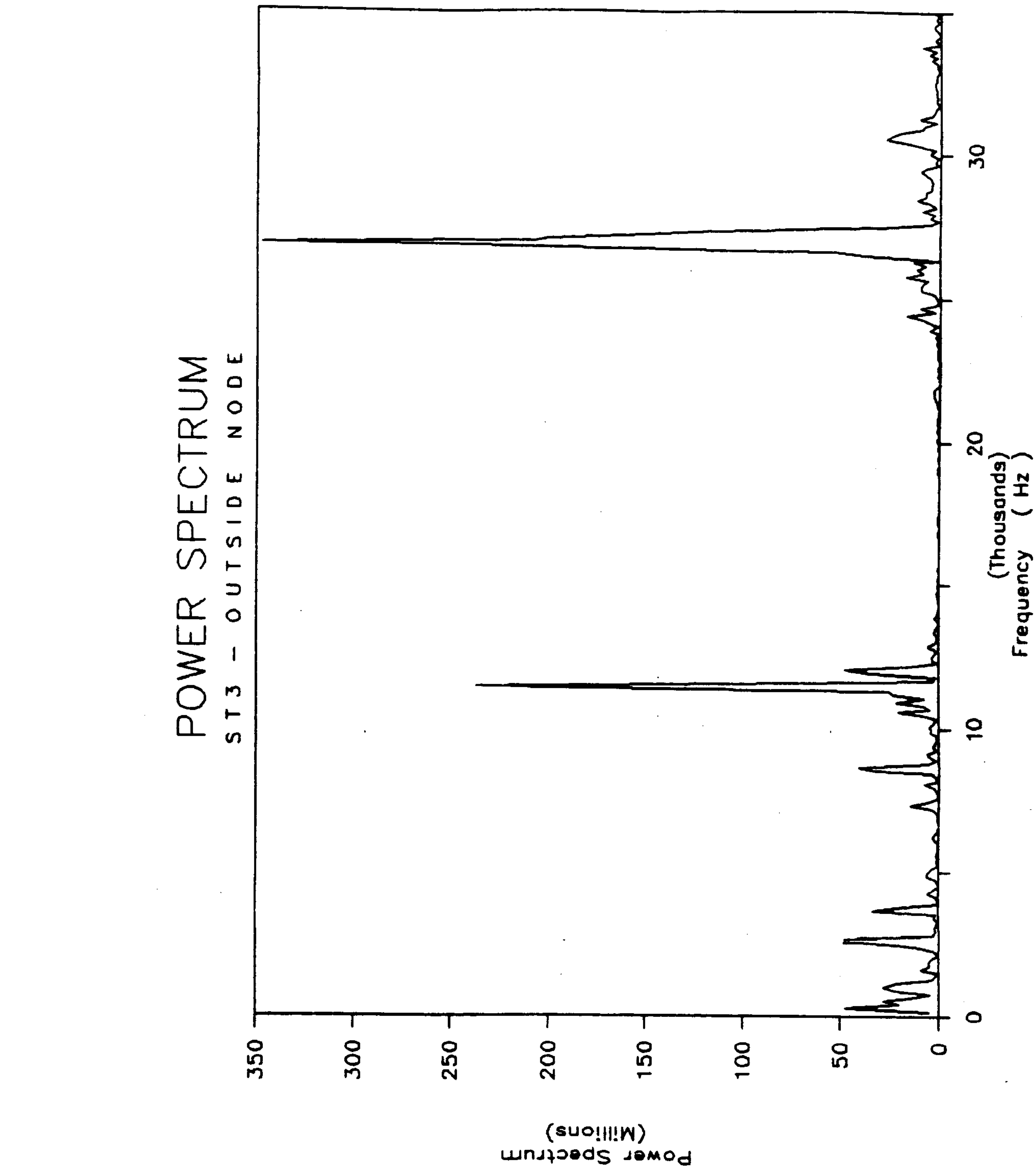
POWER SPECTRUM
ST3 - OUTSIDE NODE
Power Spectrum
(Millions)
350
300
250
200
150
100
50
0
0
10
20
30
(Thousands)
Frequency (Hz)

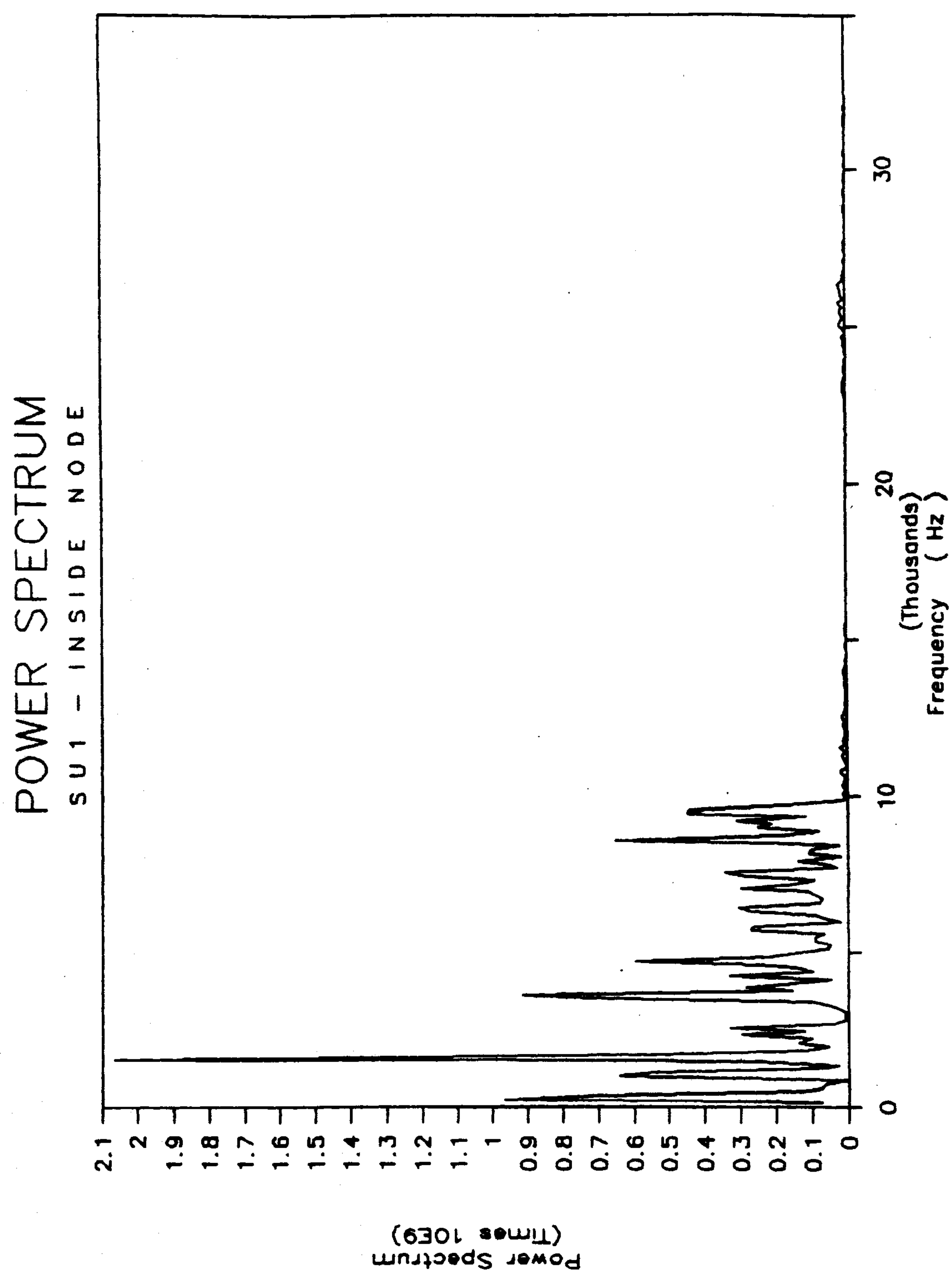
POWER SPECTRUM
SU1 - INSIDE NODE
Power Spectrum
(Times 10E9)
2.1
2
1.9
1.8
1.7
1.6
1.5
1.4
1.3
1.2
1.1
1
0.9
0.8
0.7
0.6
0.5
0.4
0.3
0.2
0.1
0
0
10
20
30
(Thousands)
Frequency (Hz)

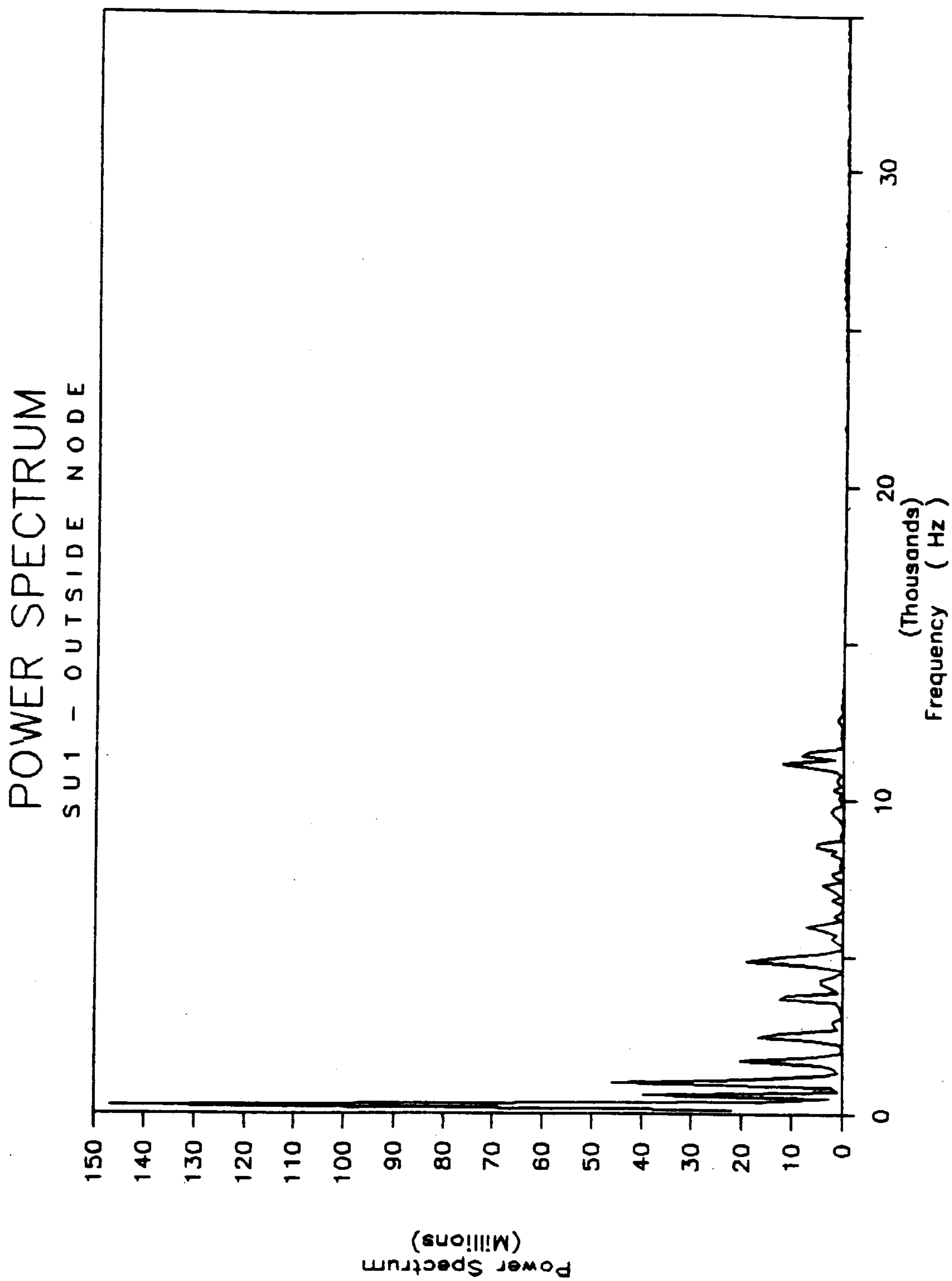
POWER SPECTRUM
SU1 - OUTSIDE NODE
Power Spectrum
(Millions)
150
140
130
120
110
100
90
80
70
60
50
40
30
20
10
0
0
10
20
30
(Thousands)
Frequency (Hz)

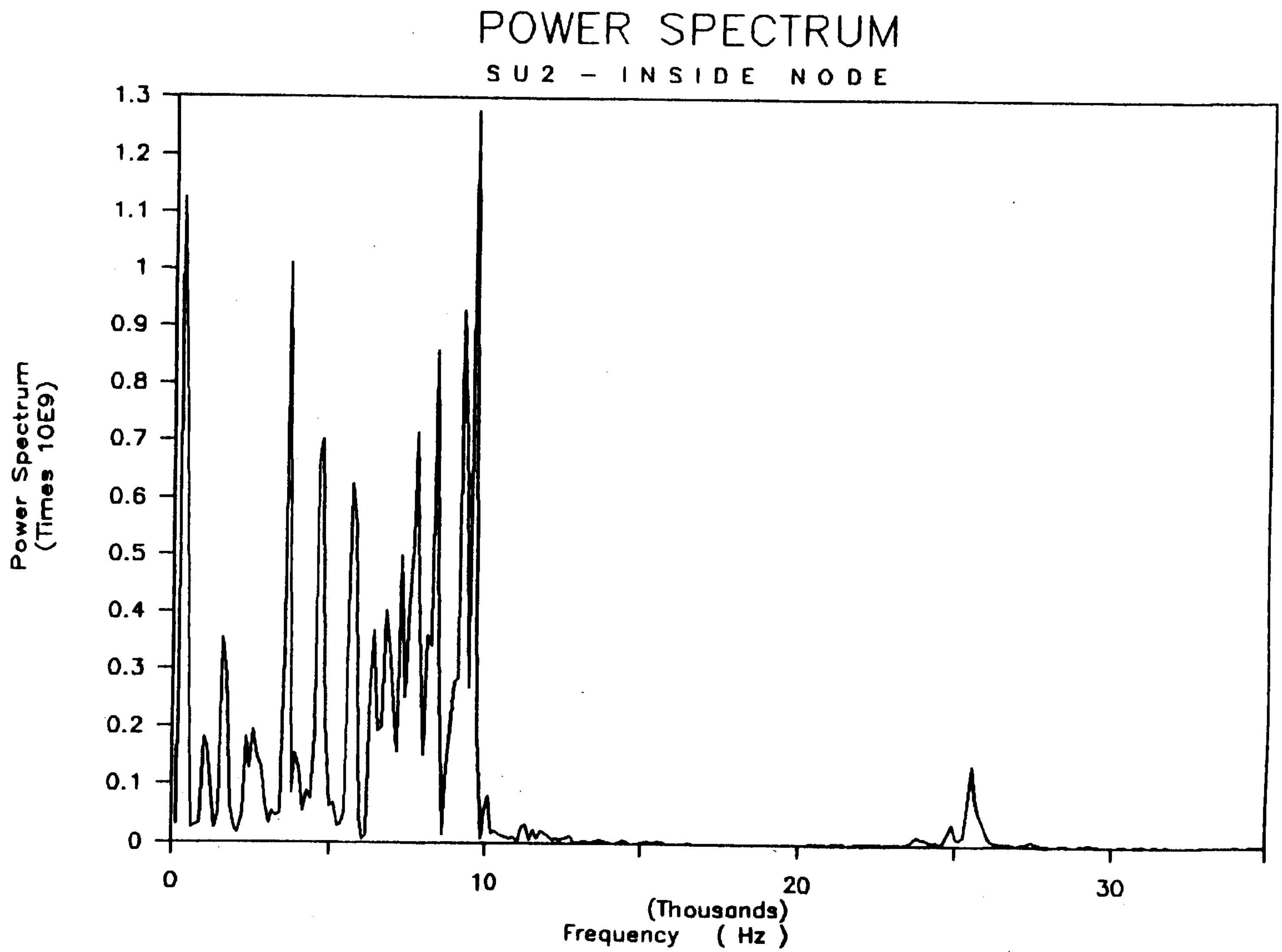
POWER SPECTRUM
SU2 - INSIDE NODE
Power Spectrum
(Times 10E9)
1.3
1.2
1.1
1
0.9
0.8
0.7
0.6
0.5
0.4
0.3
0.2
0.1
0
0
10
20
30
(Thousands)
Frequency (Hz)

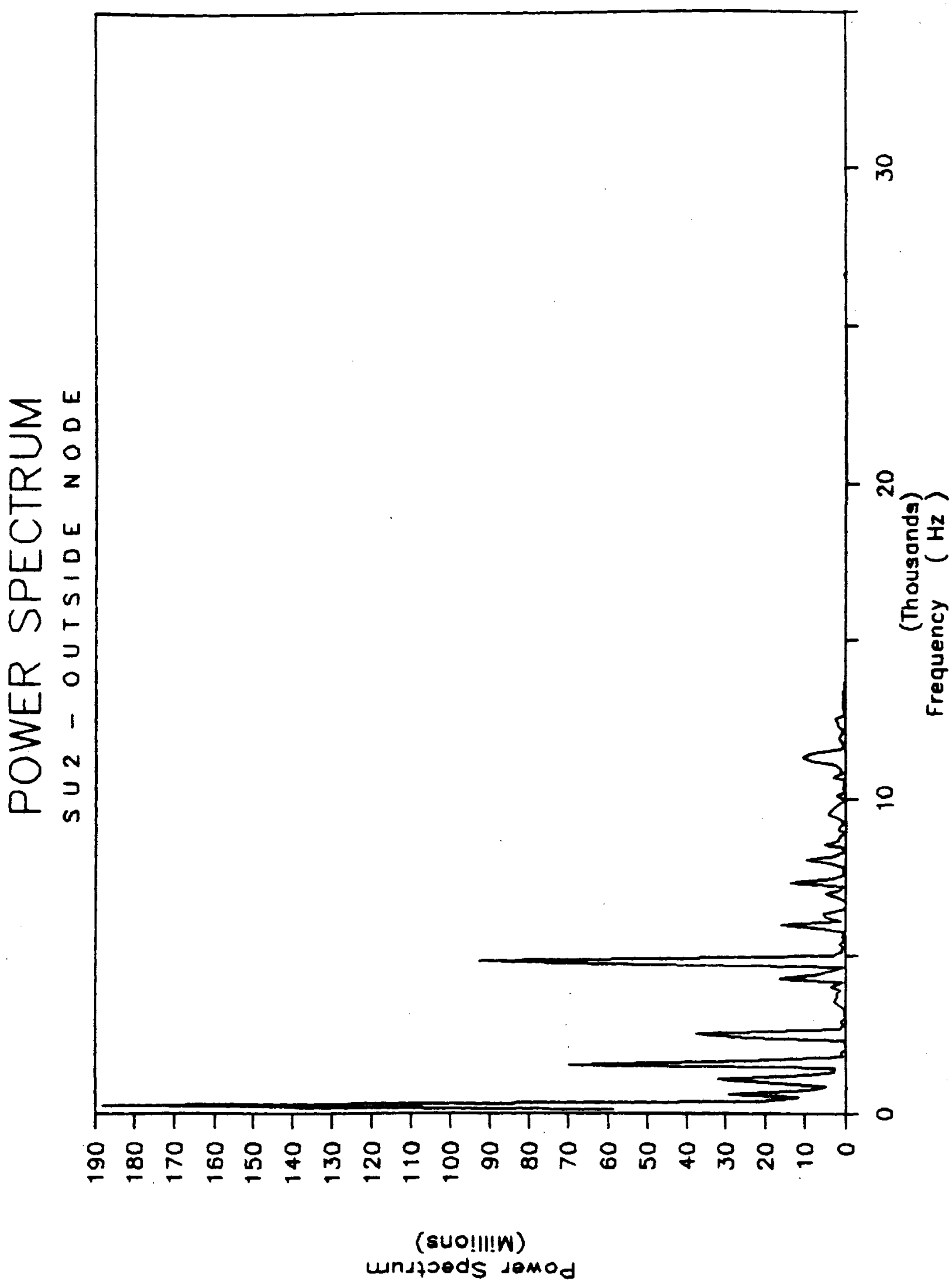
POWER SPECTRUM
SU2 - OUTSIDE NODE
Power Spectrum
(Millions)
190
180
170
160
150
140
130
120
110
100
90
80
70
60
50
40
30
20
10
0
Frequency (Hz)
(Thousands)
0
10
20
30

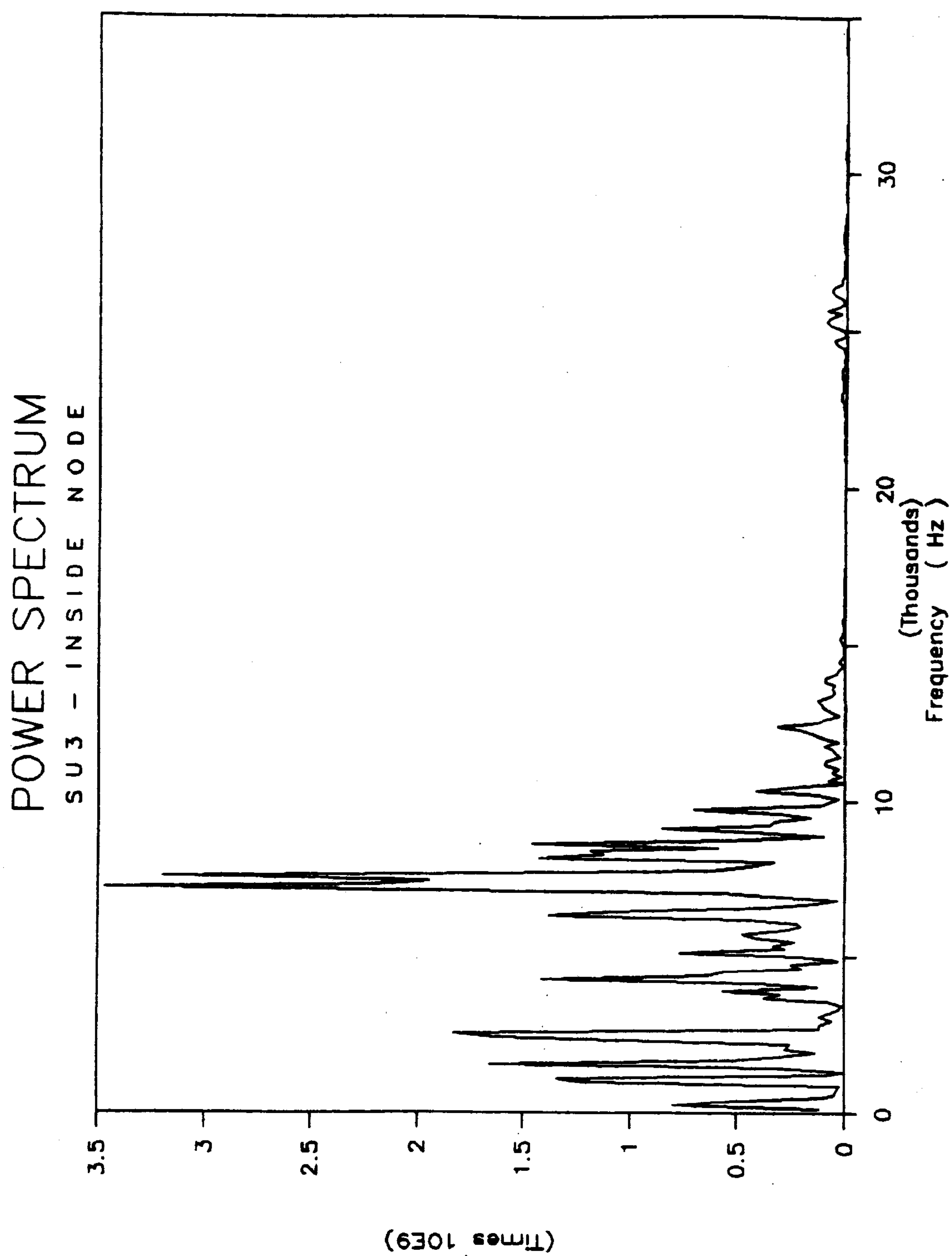
POWER SPECTRUM
SU3 - INSIDE NODE
Power Spectrum
(Times 10E9)
0
0.5
1
1.5
2
2.5
3
3.5
Frequency (Hz)
(Thousands)
0
10
20
30

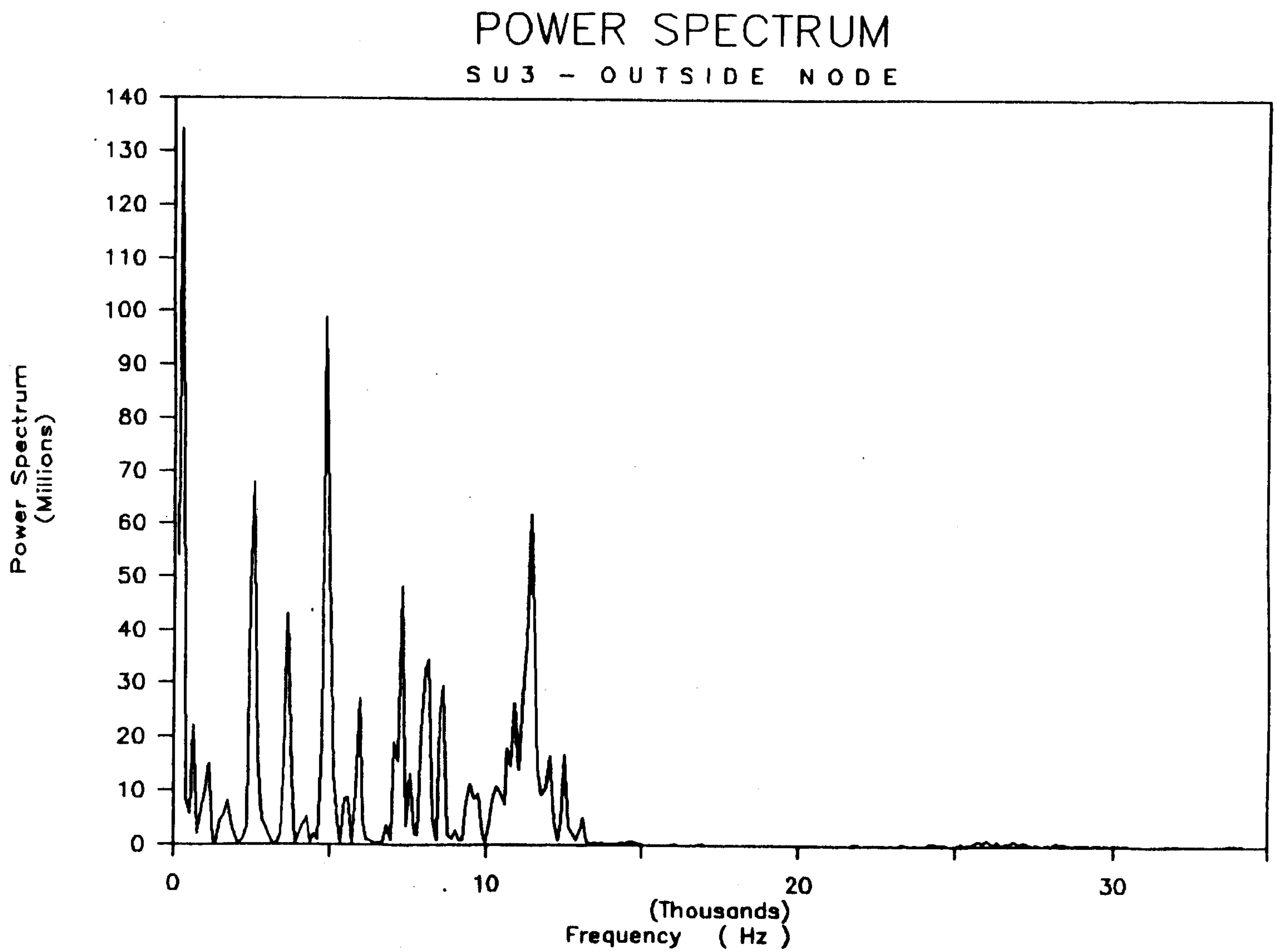
POWER SPECTRUM
SU3 - OUTSIDE NODE
Power Spectrum (Millions)
140
130
120
110
100
90
80
70
60
50
40
30
20
10
0
0
10
20
30
(Thousands)
Frequency (Hz)

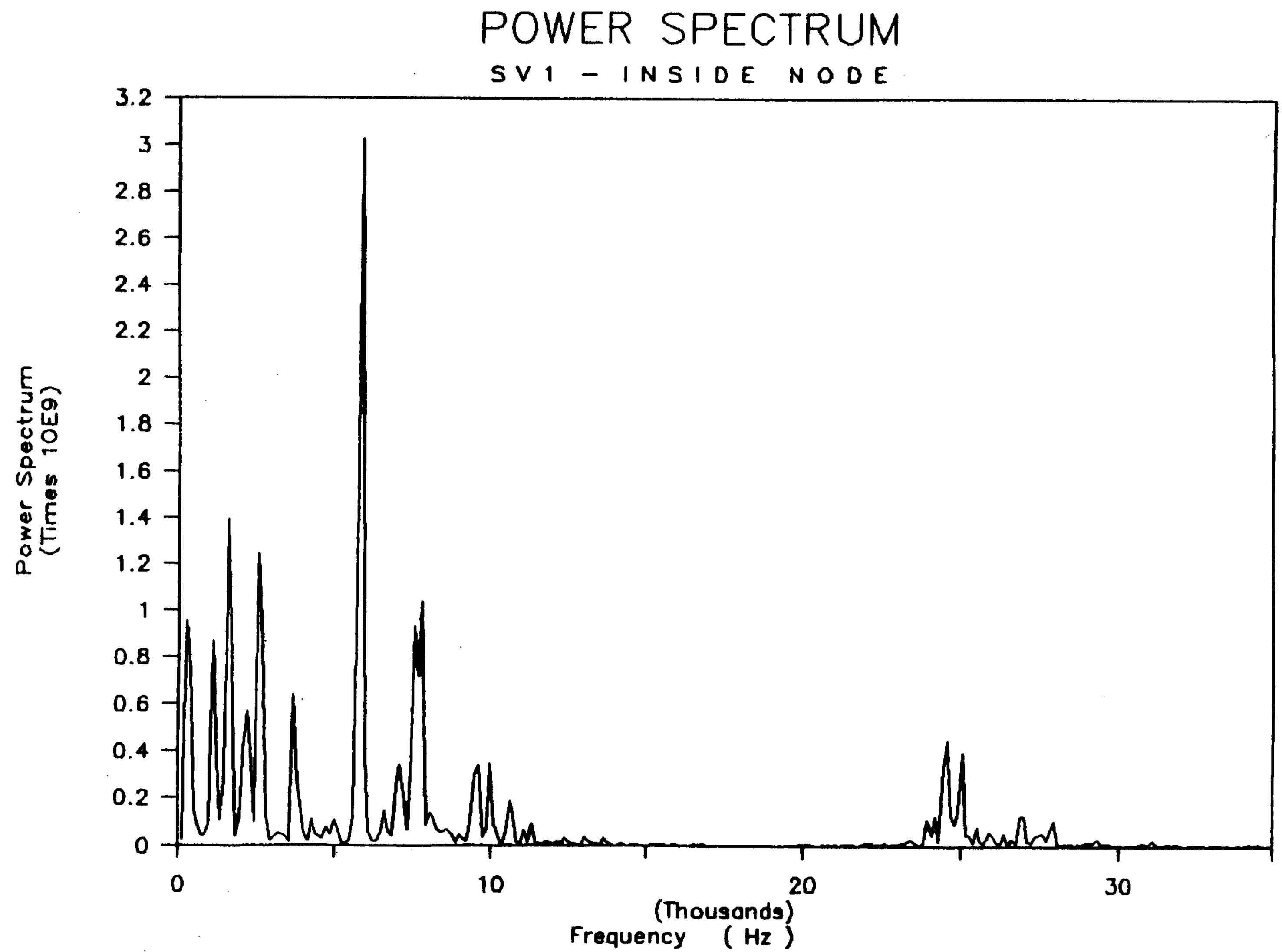
POWER SPECTRUM
SV1 – INSIDE NODE
Power Spectrum
(Times 10E9)
3.2
3
2.8
2.6
2.4
2.2
2
1.8
1.6
1.4
1.2
1
0.8
0.6
0.4
0.2
0
0
10
20
30
(Thousands)
Frequency (Hz)

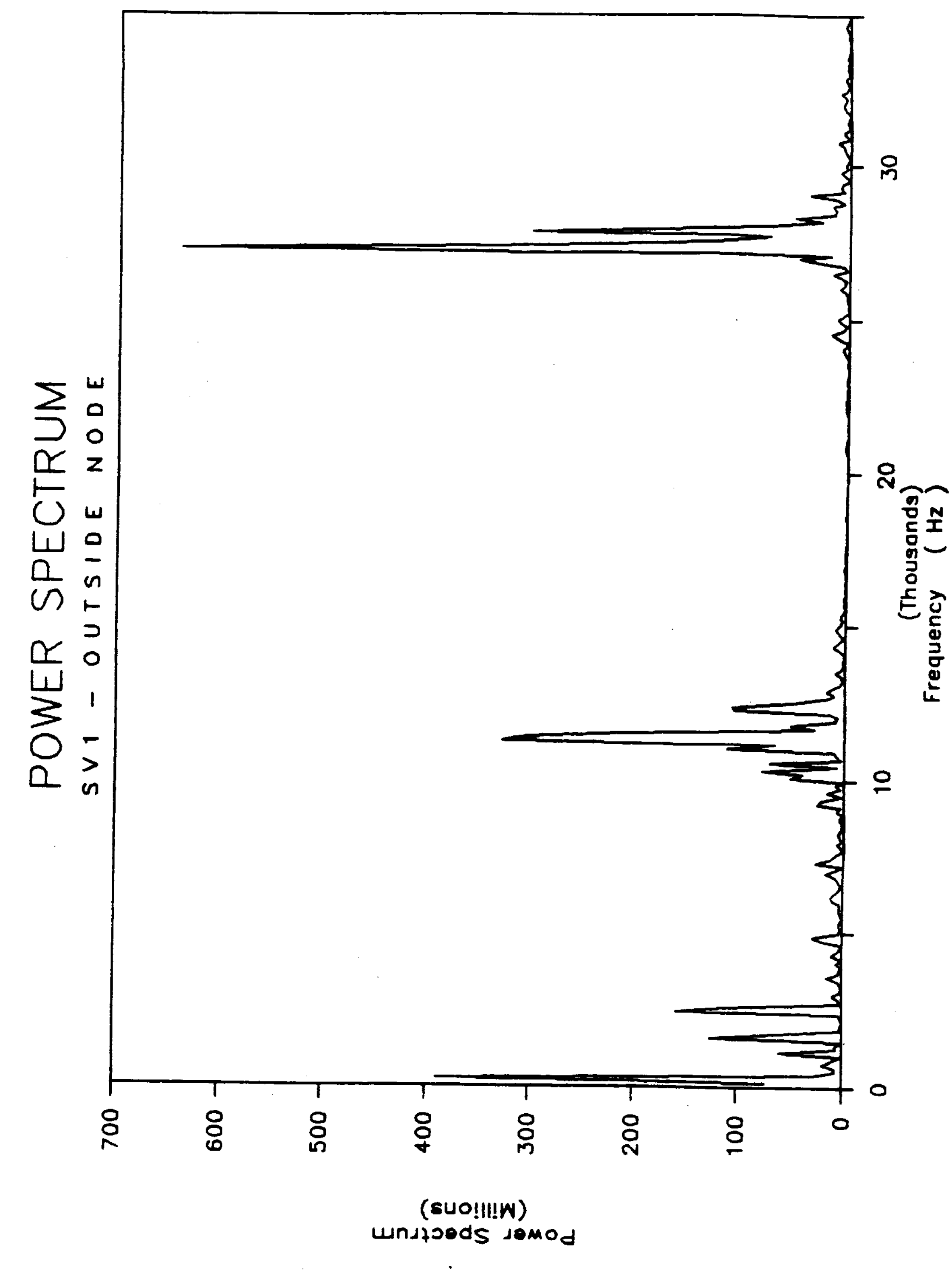
POWER SPECTRUM
SV1 - OUTSIDE NODE
Power Spectrum
(Millions)
0
100
200
300
400
500
600
700
0
10
20
30
(Thousands)
Frequency (Hz)

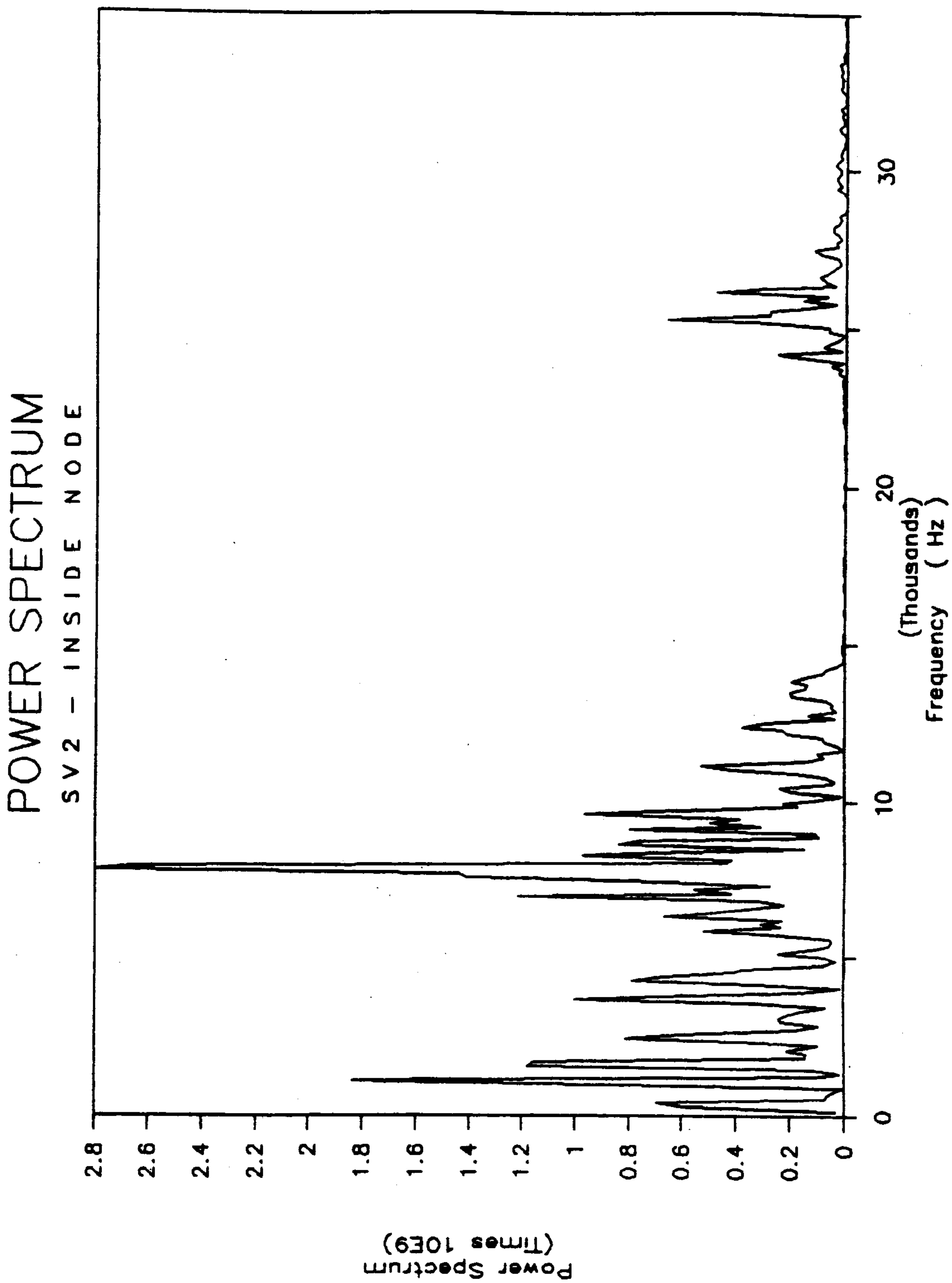
POWER SPECTRUM
SV2 - INSIDE NODE
Power Spectrum
(Times 10E9)
2.8
2.6
2.4
2.2
2
1.8
1.6
1.4
1.2
1
0.8
0.6
0.4
0.2
0
0
10
20
30
(Thousands)
Frequency (Hz)

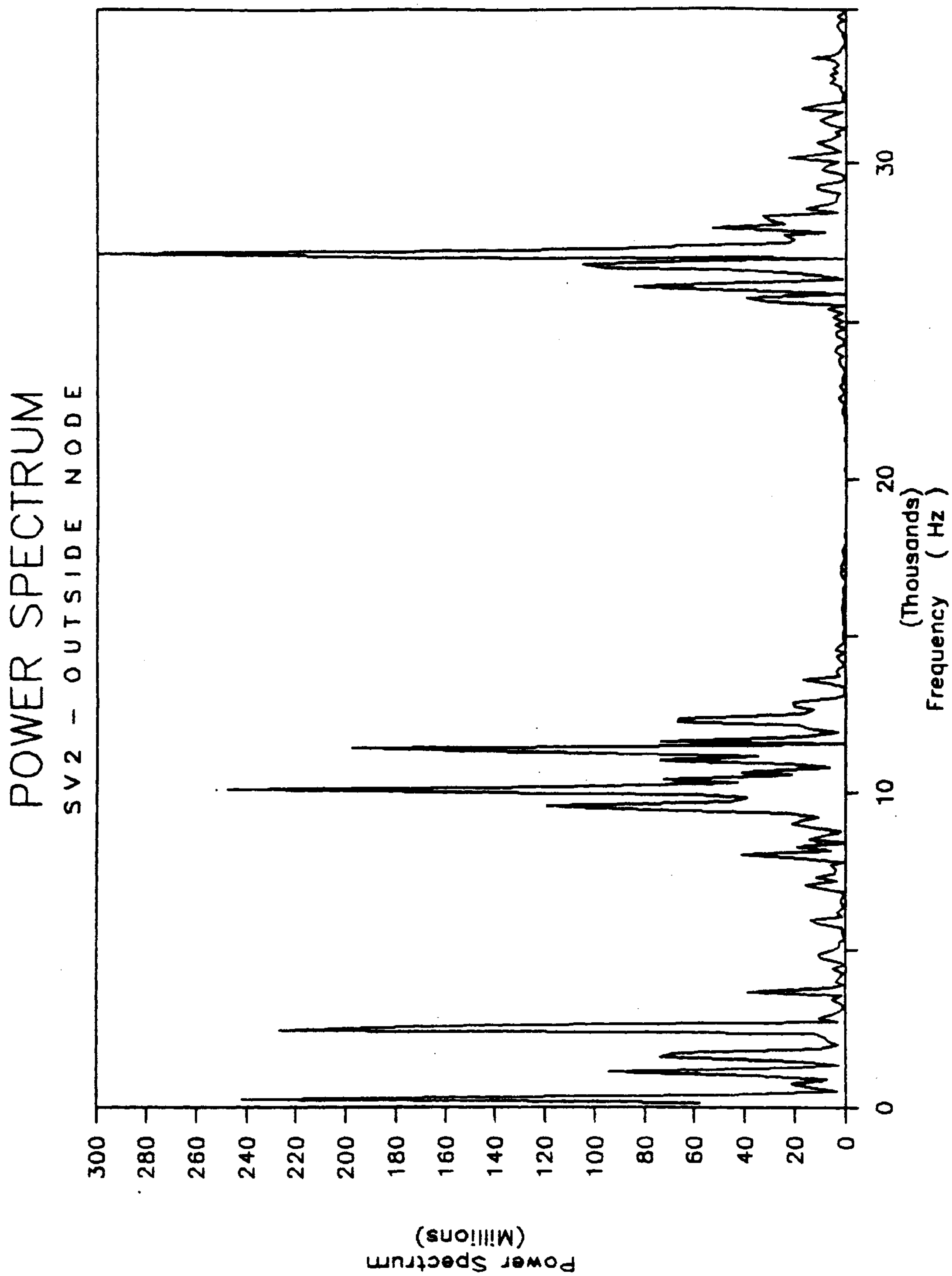
POWER SPECTRUM
SV2 - OUTSIDE NODE
Power Spectrum
(Millions)
300
280
260
240
220
200
180
160
140
120
100
80
60
40
20
0
0
10
20
30
(Thousands)
Frequency (Hz)

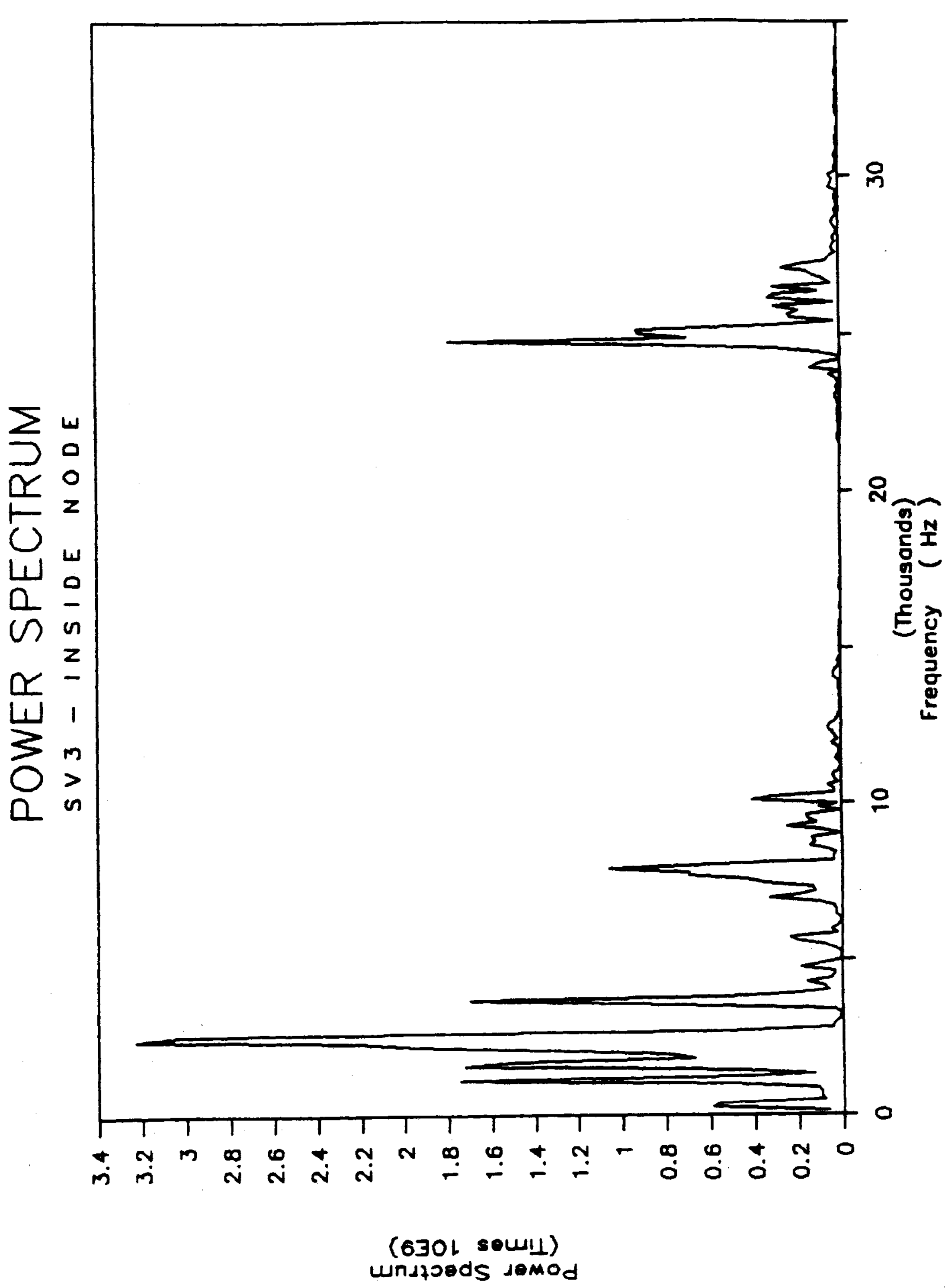
POWER SPECTRUM
SV3 - INSIDE NODE
Power Spectrum
(Times 10E9)
0
0.2
0.4
0.6
0.8
1
1.2
1.4
1.6
1.8
2
2.2
2.4
2.6
2.8
3
3.2
3.4
0
10
20
30
(Thousands)
Frequency (Hz)

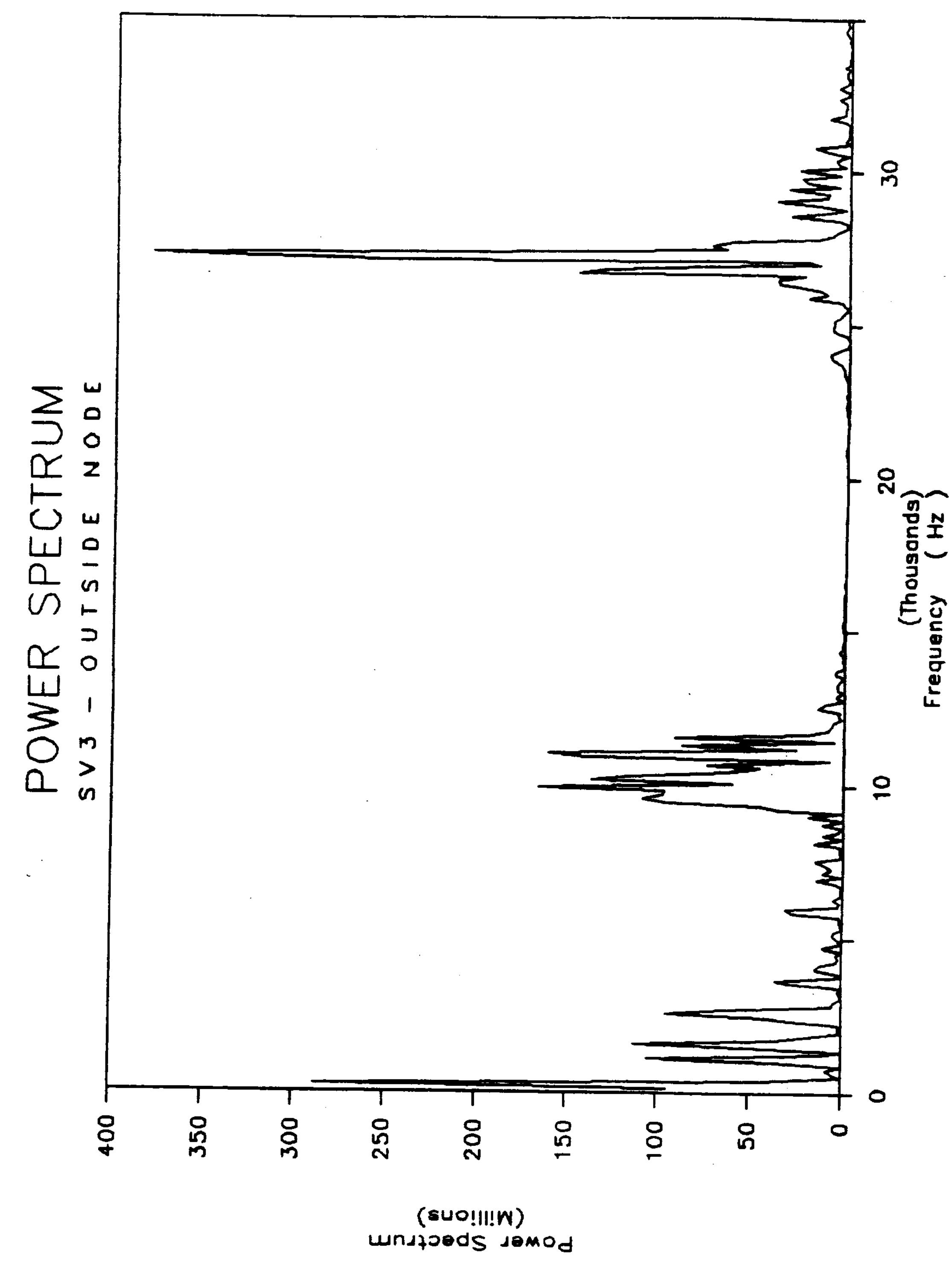
POWER SPECTRUM
SV3 - OUTSIDE NODE
Power Spectrum
(Millions)
400
350
300
250
200
150
100
50
0
0
10
20
30
Frequency (Hz)
(Thousands)

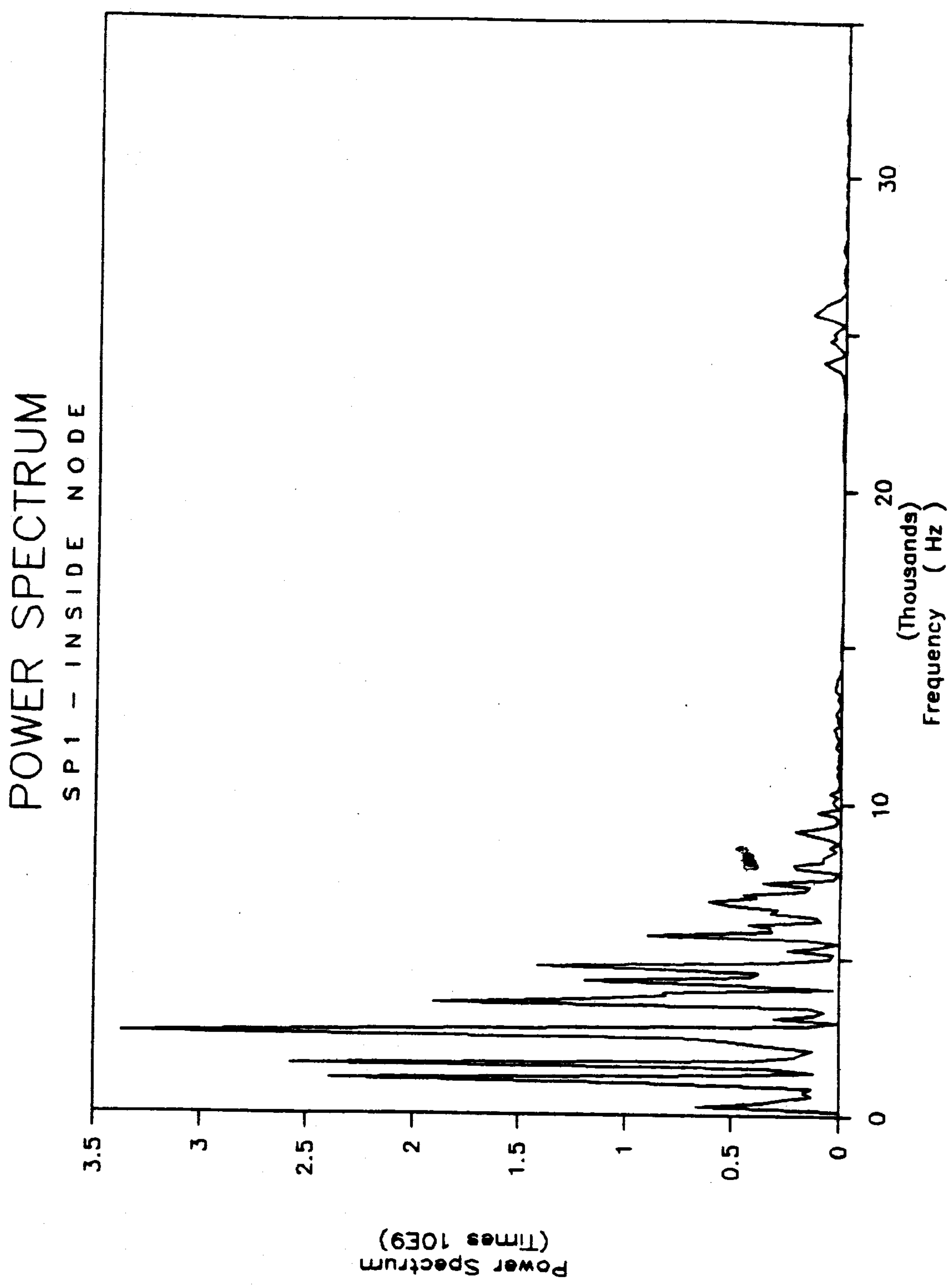
POWER SPECTRUM
SP1 - INSIDE NODE
Power Spectrum
(Times 10E9)
Frequency (Hz)
(Thousands)
0
0.5
1
1.5
2
2.5
3
3.5
0
10
20
30

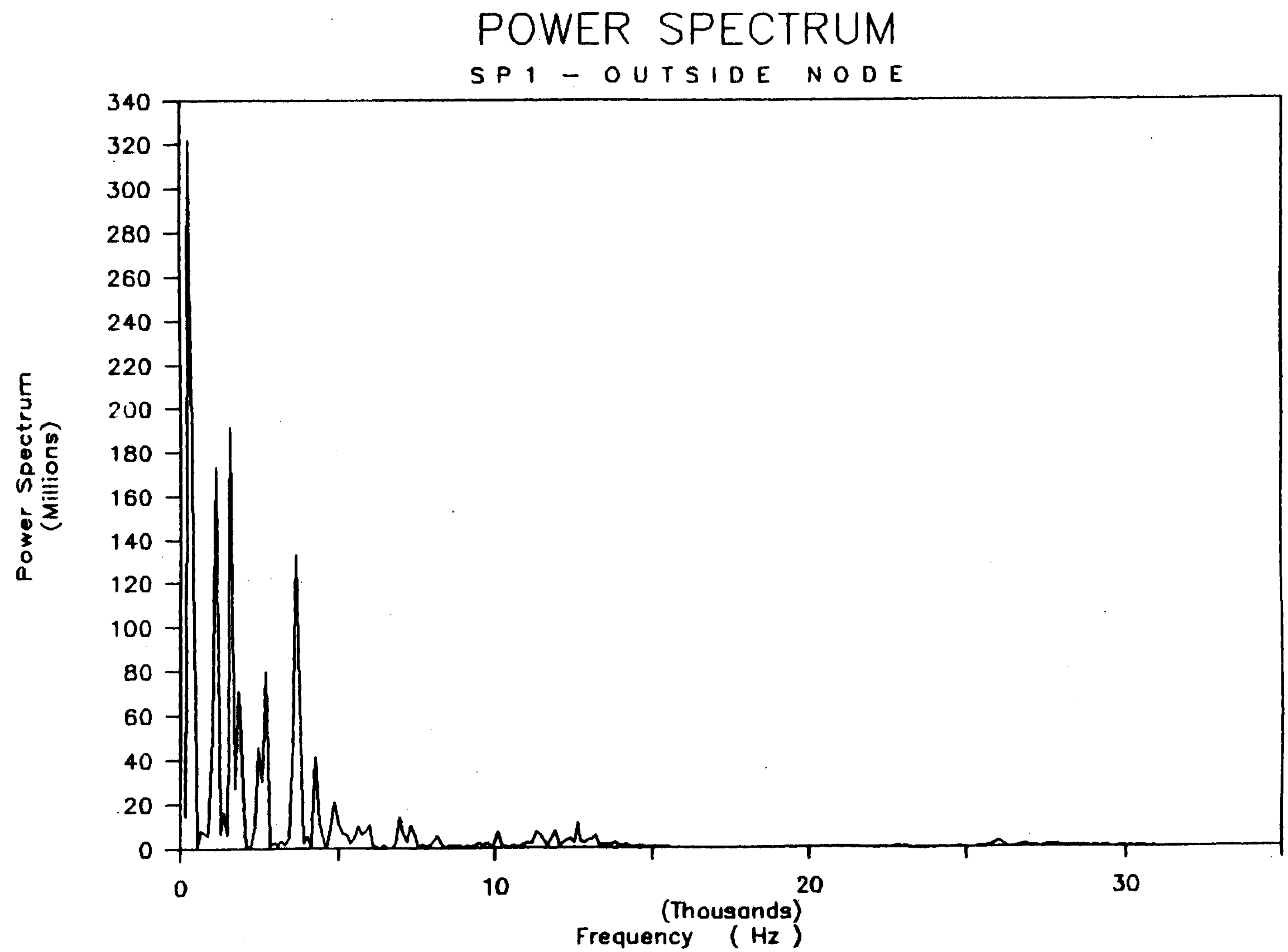
POWER SPECTRUM
SP1 - OUTSIDE NODE
Power Spectrum
(Millions)
340
320
300
280
260
240
220
200
180
160
140
120
100
80
60
40
20
0
0
10
20
30
(Thousands)
Frequency (Hz)

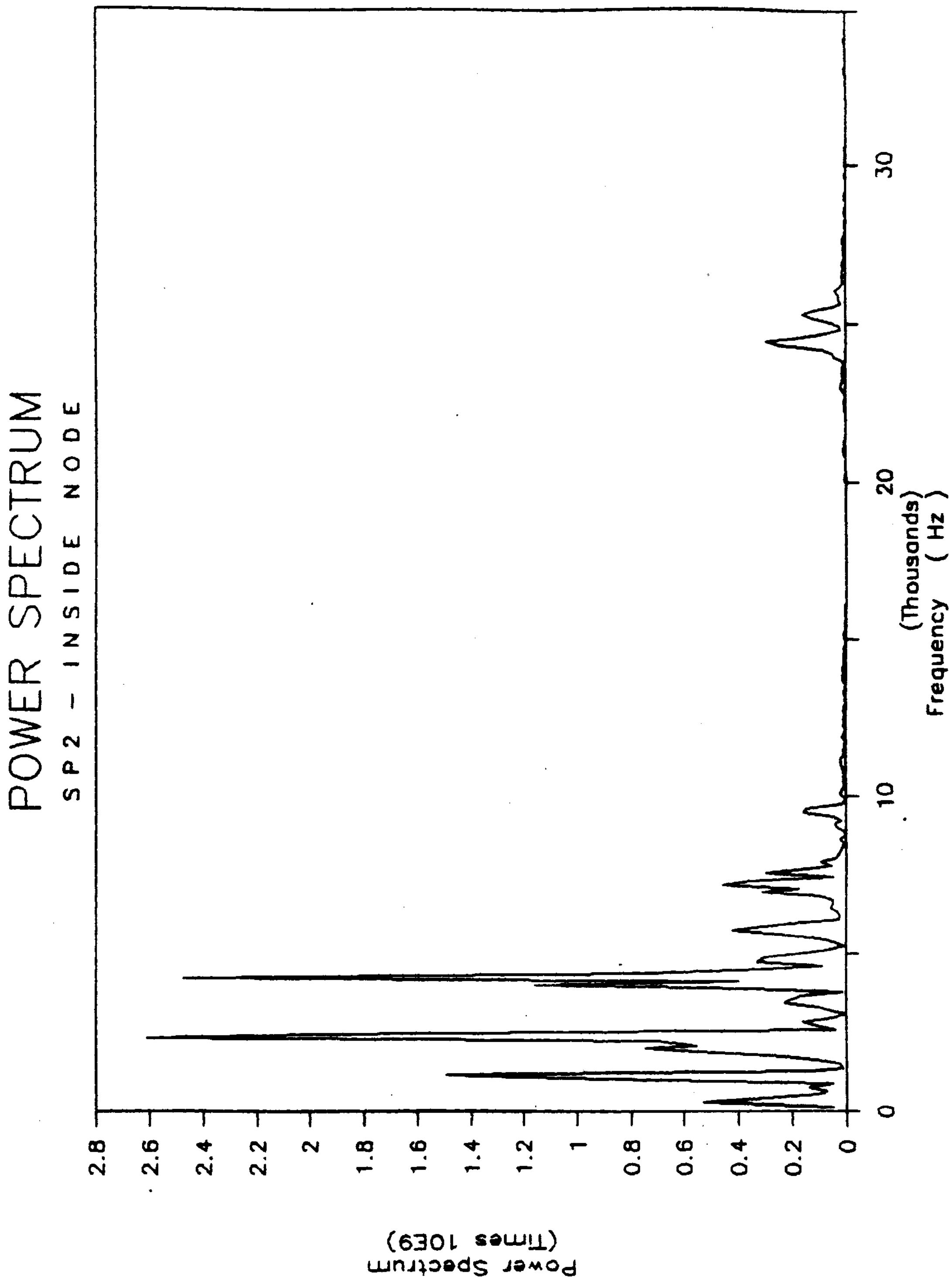
POWER SPECTRUM
SP2 - INSIDE NODE
Power Spectrum
(Times 10E9)
2.8
2.6
2.4
2.2
2
1.8
1.6
1.4
1.2
1
0.8
0.6
0.4
0.2
0
0
10
20
30
(Thousands)
Frequency (Hz)

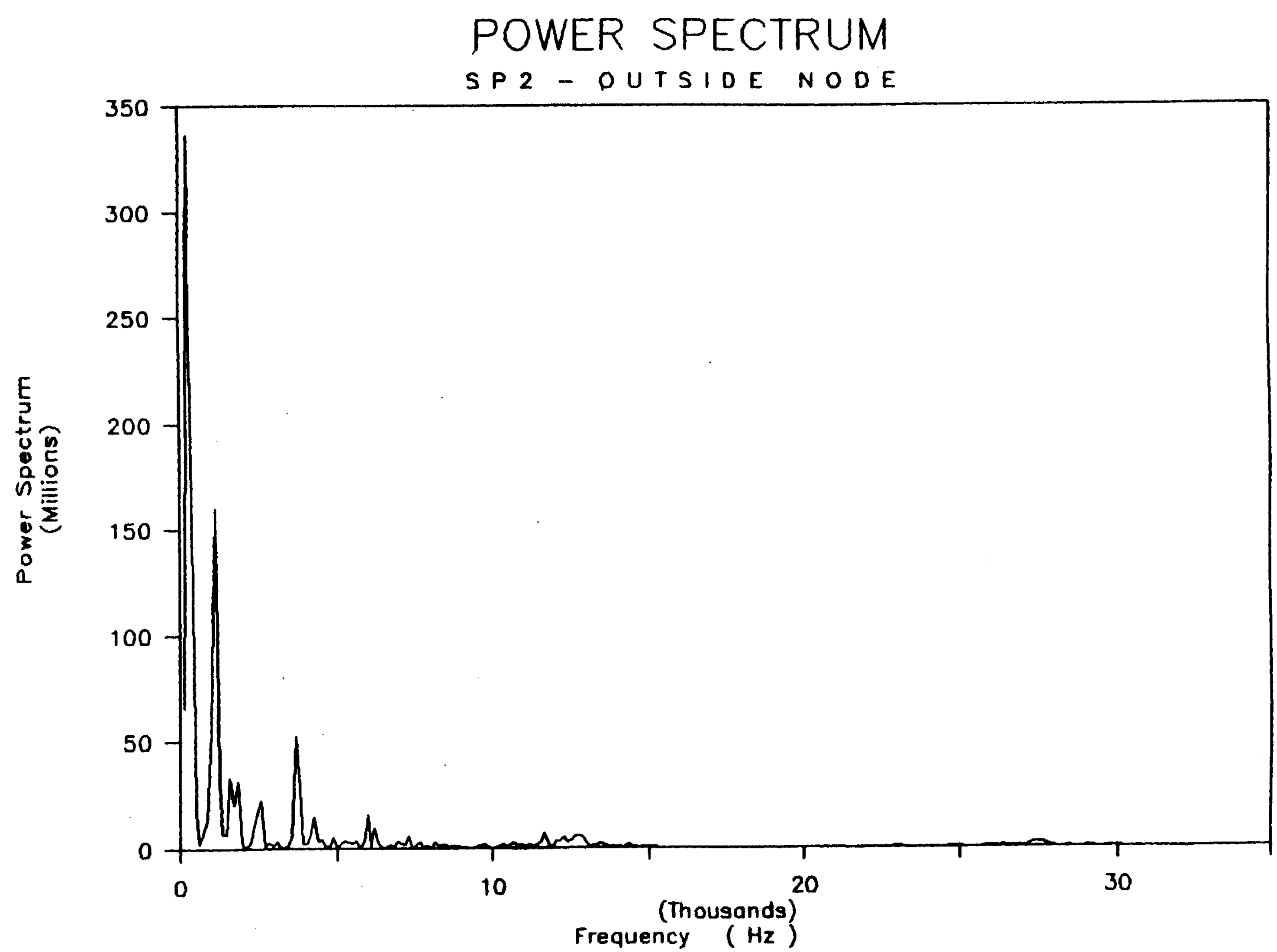
POWER SPECTRUM
SP2 - OUTSIDE NODE
Power Spectrum (Millions)
350
300
250
200
150
100
50
0
0
10
20
30
(Thousands)
Frequency (Hz)

POWER SPECTRUM

SP3 – INSIDE NODE

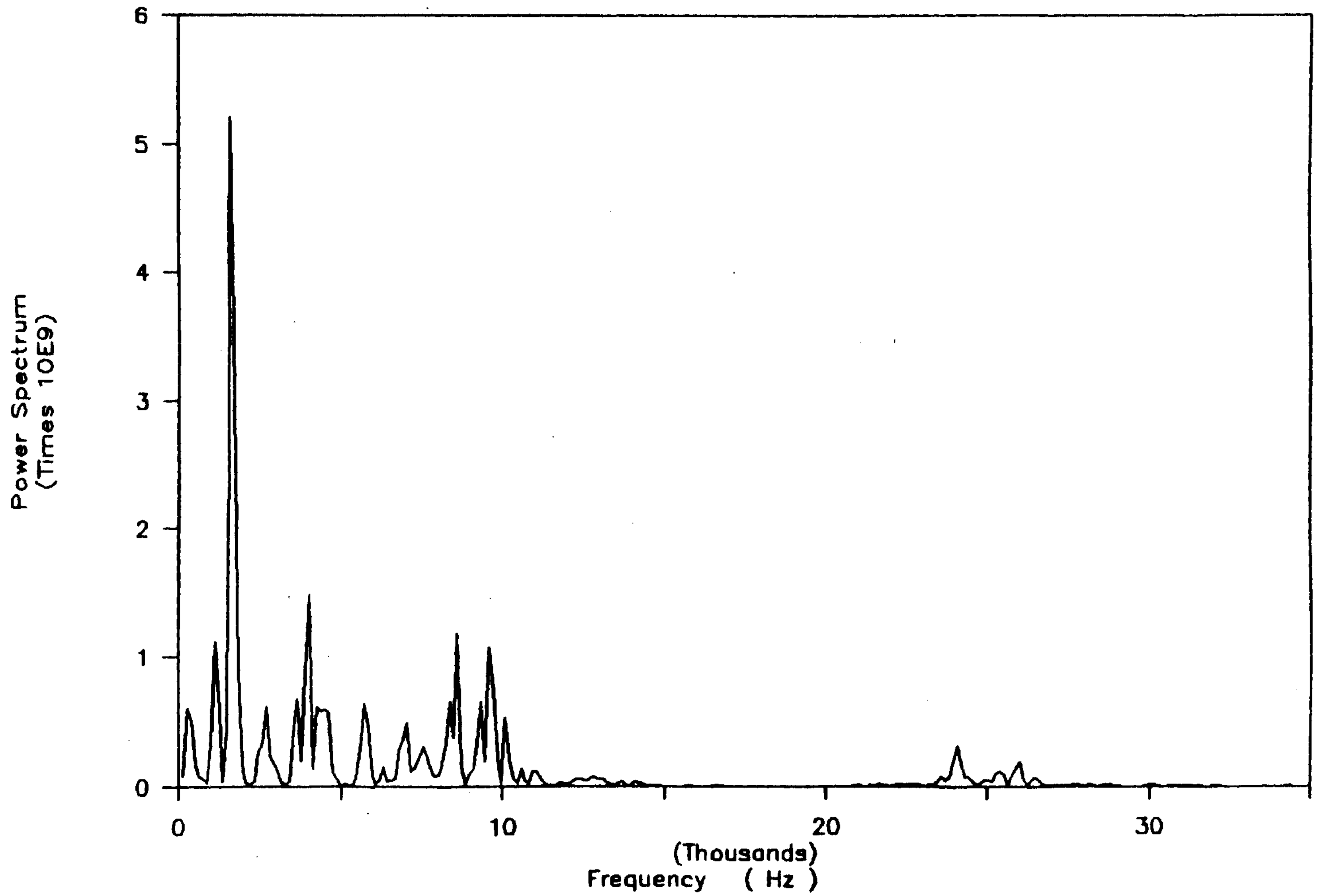

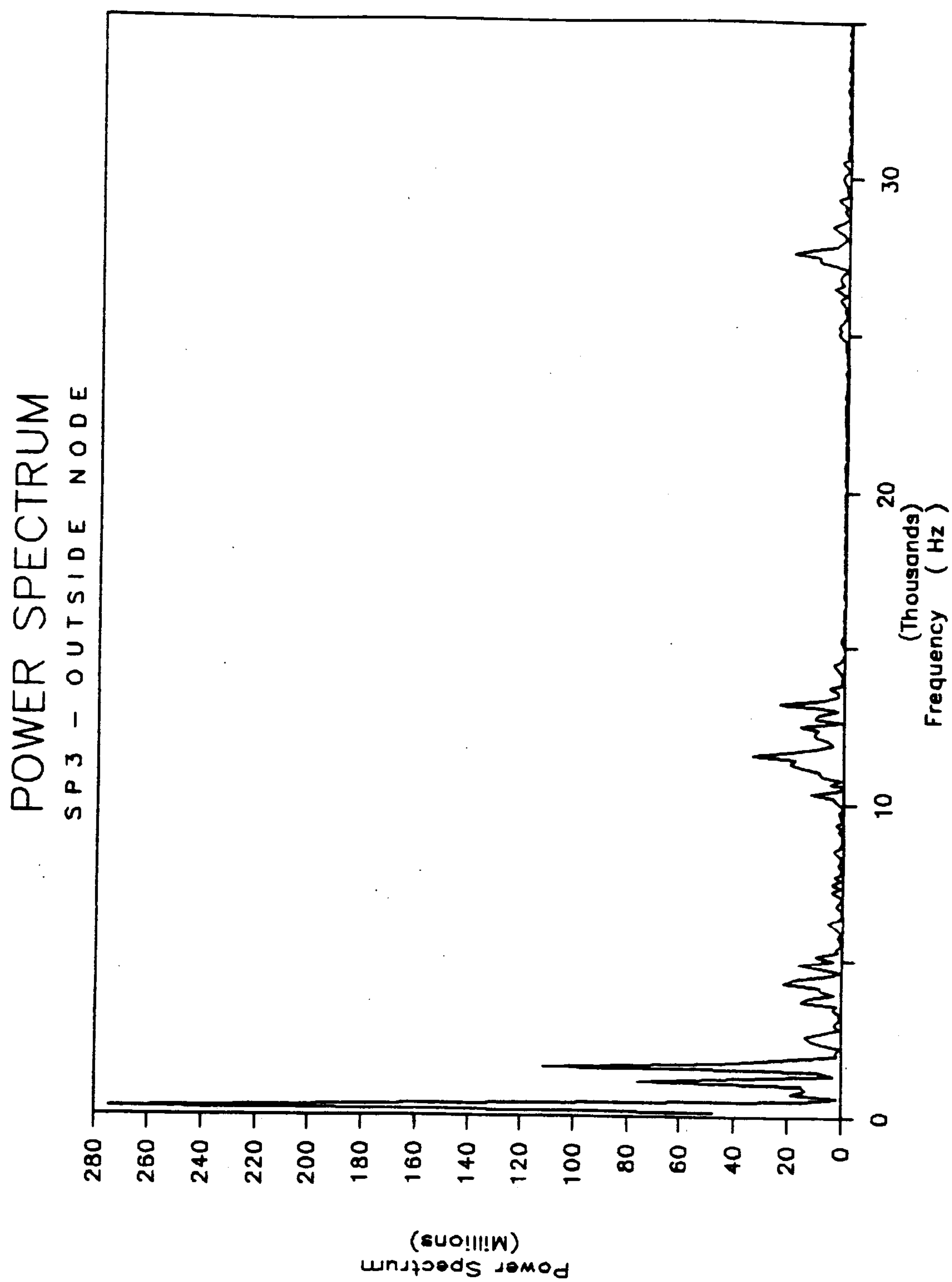
POWER SPECTRUM
SP3 - OUTSIDE NODE
Power Spectrum
(Millions)
0
20
40
60
80
100
120
140
160
180
200
220
240
260
280
Frequency (Hz)
(Thousands)
0
10
20
30

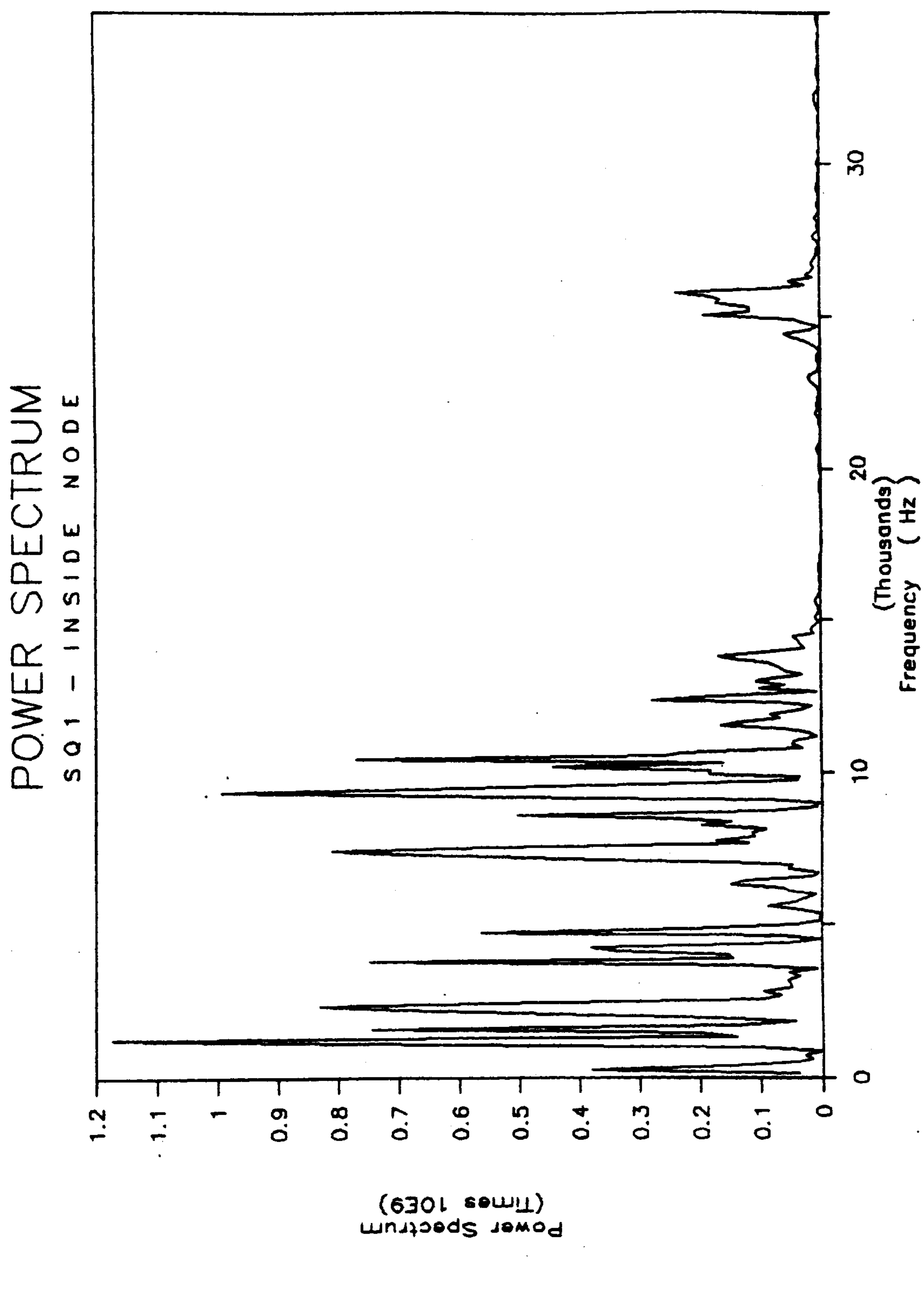

POWER SPECTRUM
SQ1 - INSIDE NODE
Power Spectrum
(Times 10E9)
1.2
1.1
1
0.9
0.8
0.7
0.6
0.5
0.4
0.3
0.2
0.1
0
0
10
20
30
(Thousands)
Frequency (Hz)

POWER SPECTRUM

SQ1 – OUTSIDE NODE

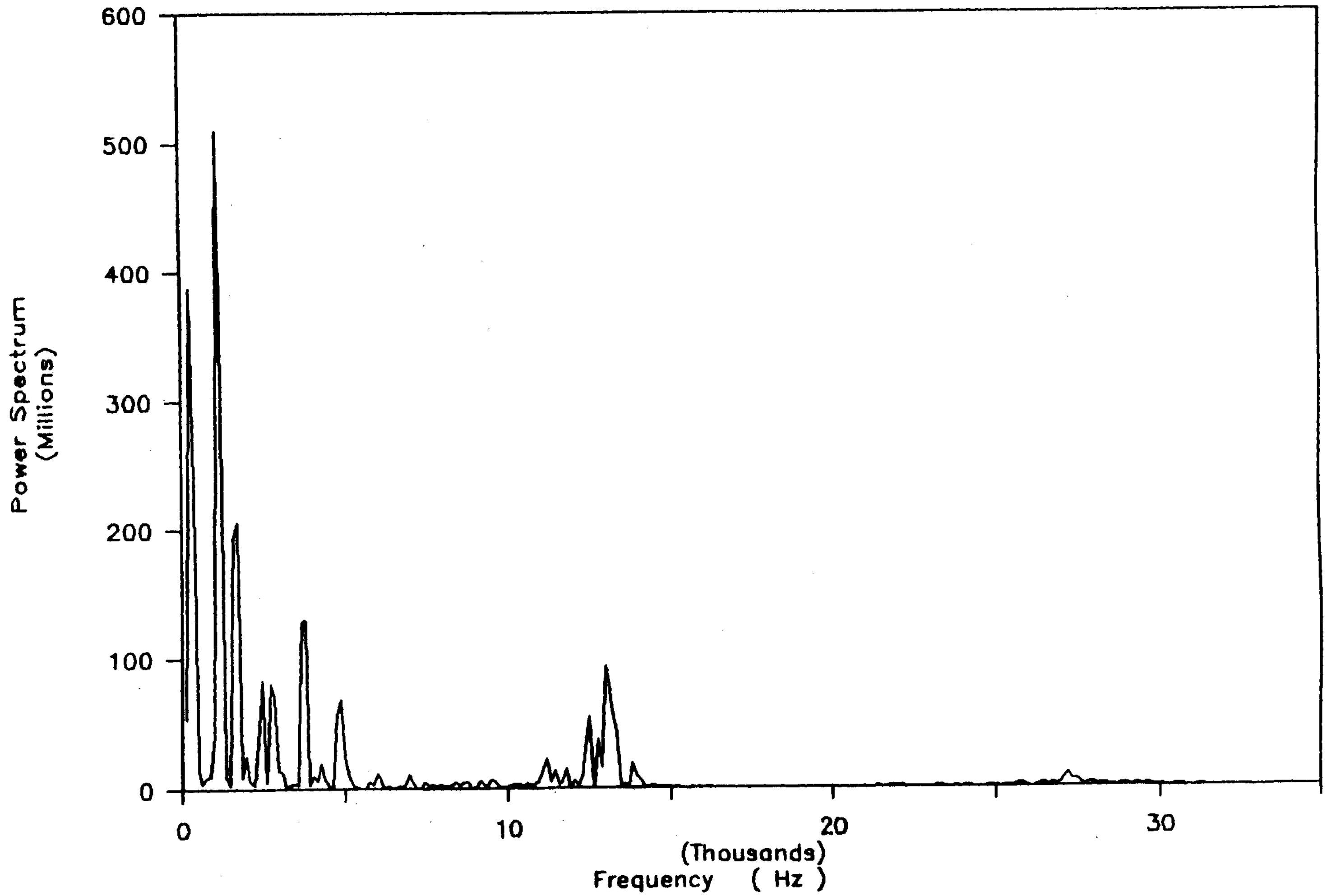

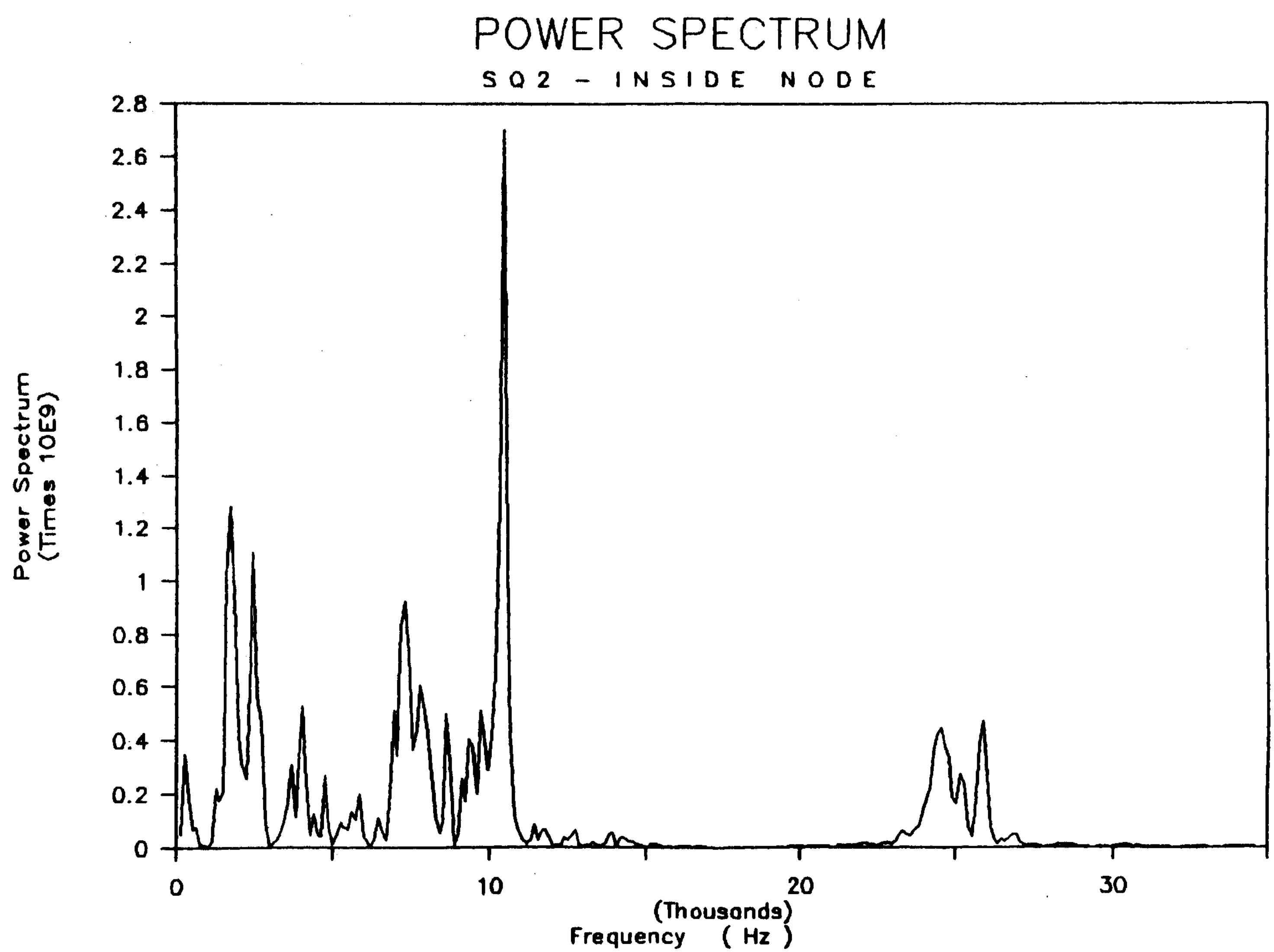
POWER SPECTRUM
SQ2 - INSIDE NODE
Power Spectrum
(Times 10E9)
2.8
2.6
2.4
2.2
2
1.8
1.6
1.4
1.2
1
0.8
0.6
0.4
0.2
0
0
10
20
30
(Thousands)
Frequency (Hz)

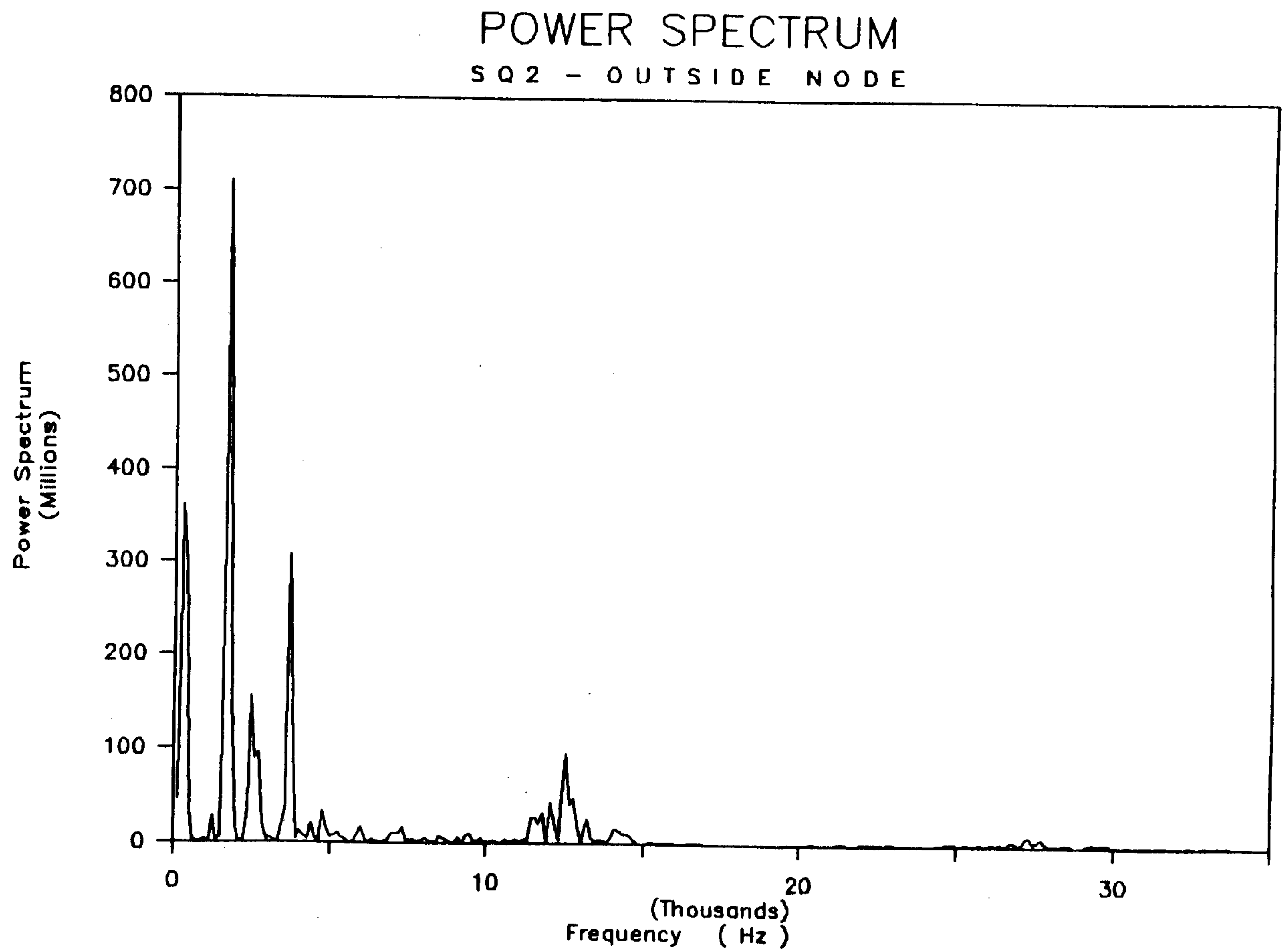
POWER SPECTRUM
SQ2 - OUTSIDE NODE
Power Spectrum
(Millions)
800
700
600
500
400
300
200
100
0
0
10
20
30
(Thousands)
Frequency (Hz)

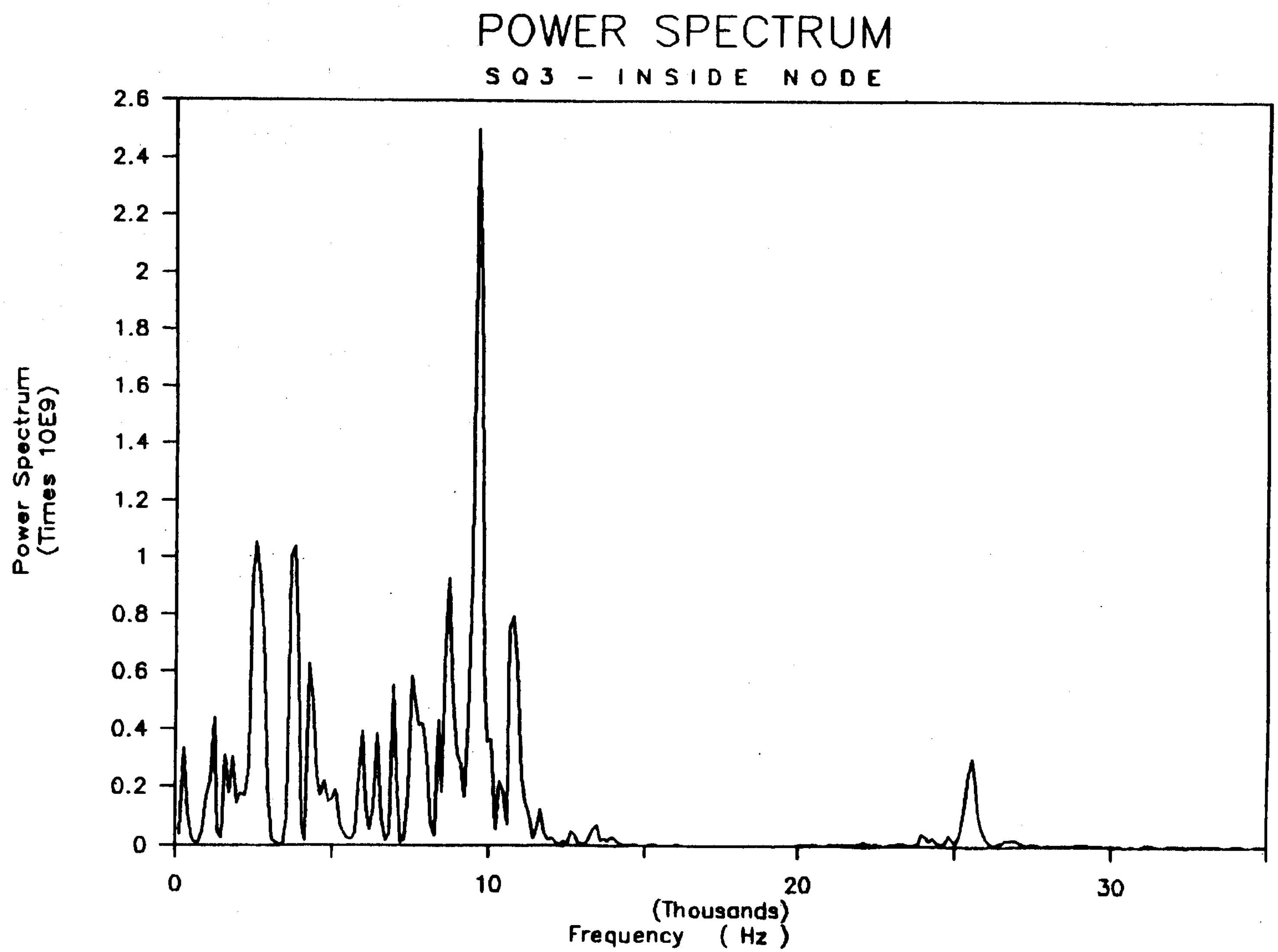
POWER SPECTRUM
SQ3 – INSIDE NODE
Power Spectrum
(Times 10E9)
2.6
2.4
2.2
2
1.8
1.6
1.4
1.2
1
0.8
0.6
0.4
0.2
0
0
10
20
30
(Thousands)
Frequency (Hz)

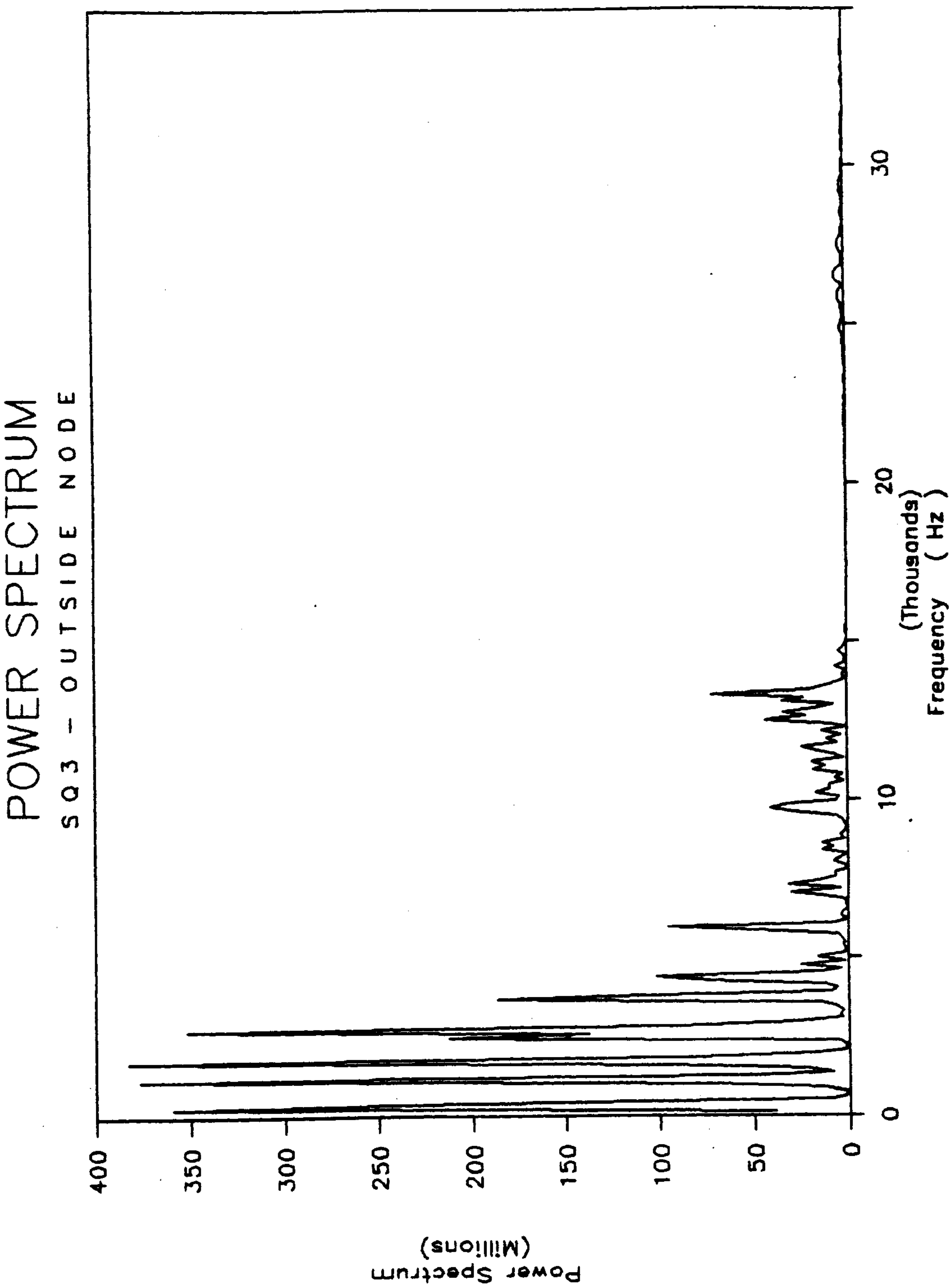

POWER SPECTRUM
SQ3 - OUTSIDE NODE
Power Spectrum
(Millions)
400
350
300
250
200
150
100
50
0
0
10
20
30
(Thousands)
Frequency (Hz)

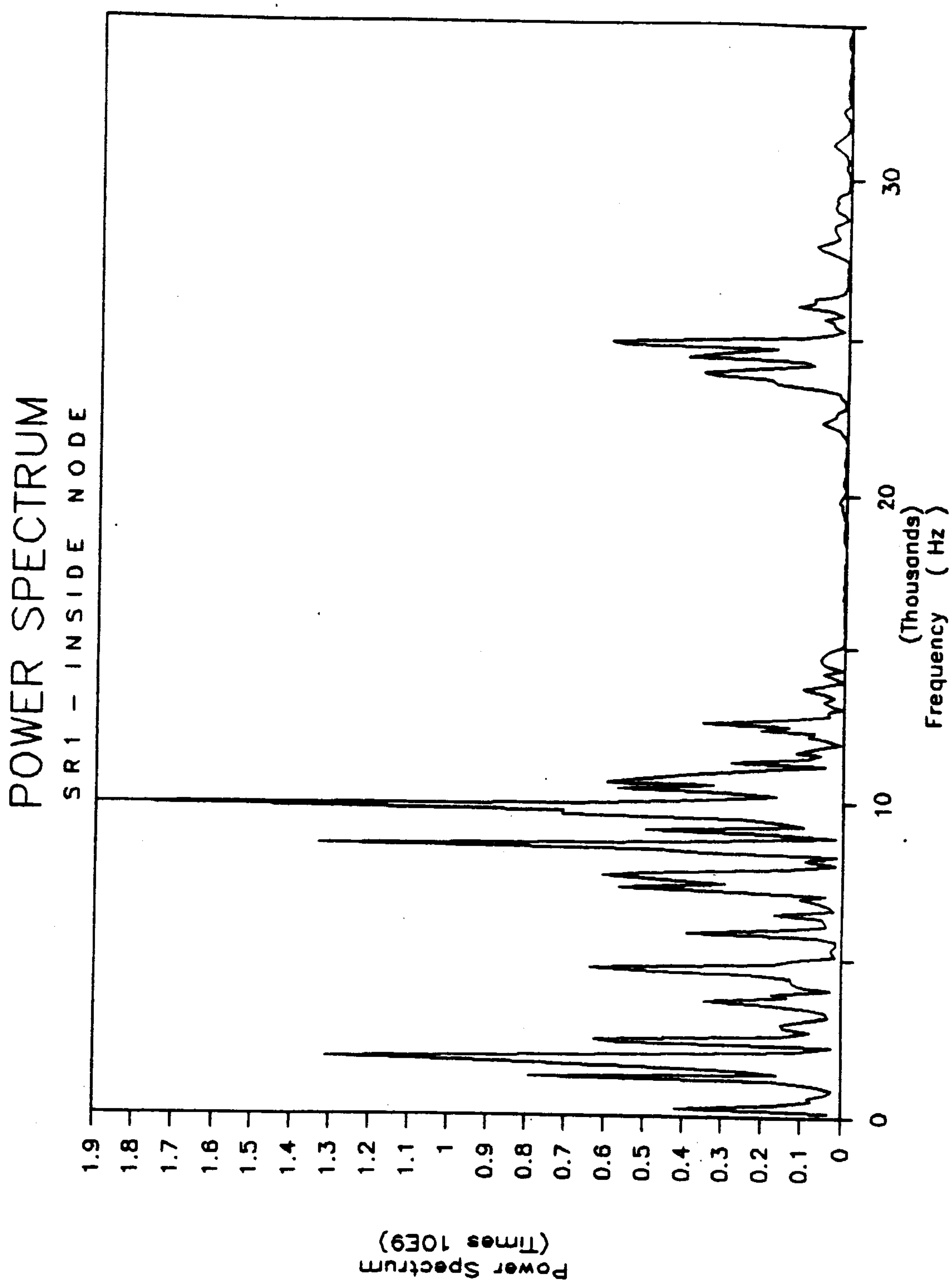
POWER SPECTRUM
SR1 - INSIDE NODE
Power Spectrum
(Times 10E9)
Frequency (Hz)
(Thousands)
0
10
20
30
0
0.1
0.2
0.3
0.4
0.5
0.6
0.7
0.8
0.9
1
1.1
1.2
1.3
1.4
1.5
1.6
1.7
1.8
1.9

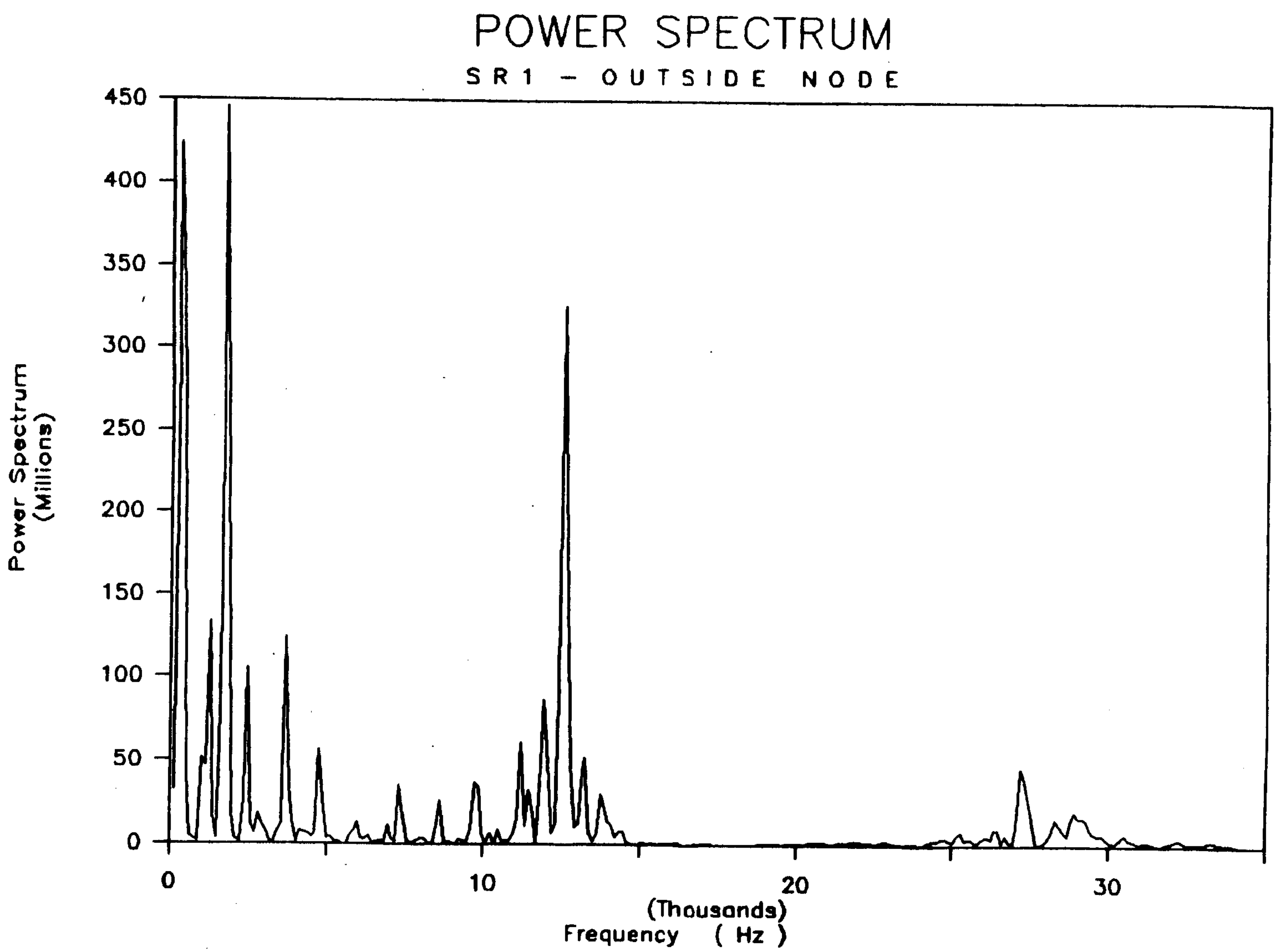
POWER SPECTRUM
SR1 - OUTSIDE NODE
Power Spectrum
(Millions)
450
400
350
300
250
200
150
100
50
0
0
10
20
30
(Thousands)
Frequency (Hz)

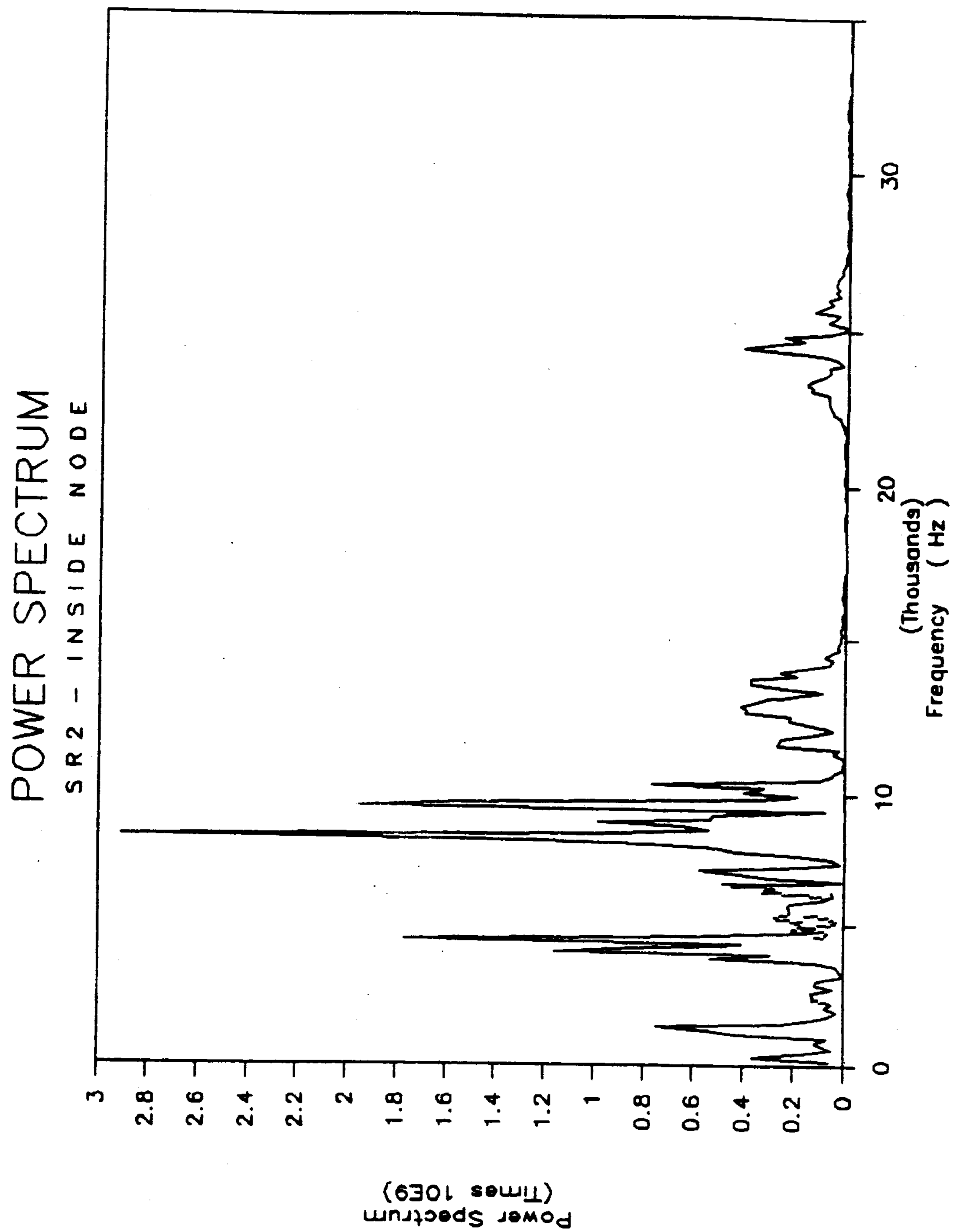
POWER SPECTRUM
SR2 - INSIDE NODE
Power Spectrum
(Times 10E9)
3
2.8
2.6
2.4
2.2
2
1.8
1.6
1.4
1.2
1
0.8
0.6
0.4
0.2
0
0
10
20
30
(Thousands)
Frequency (Hz)

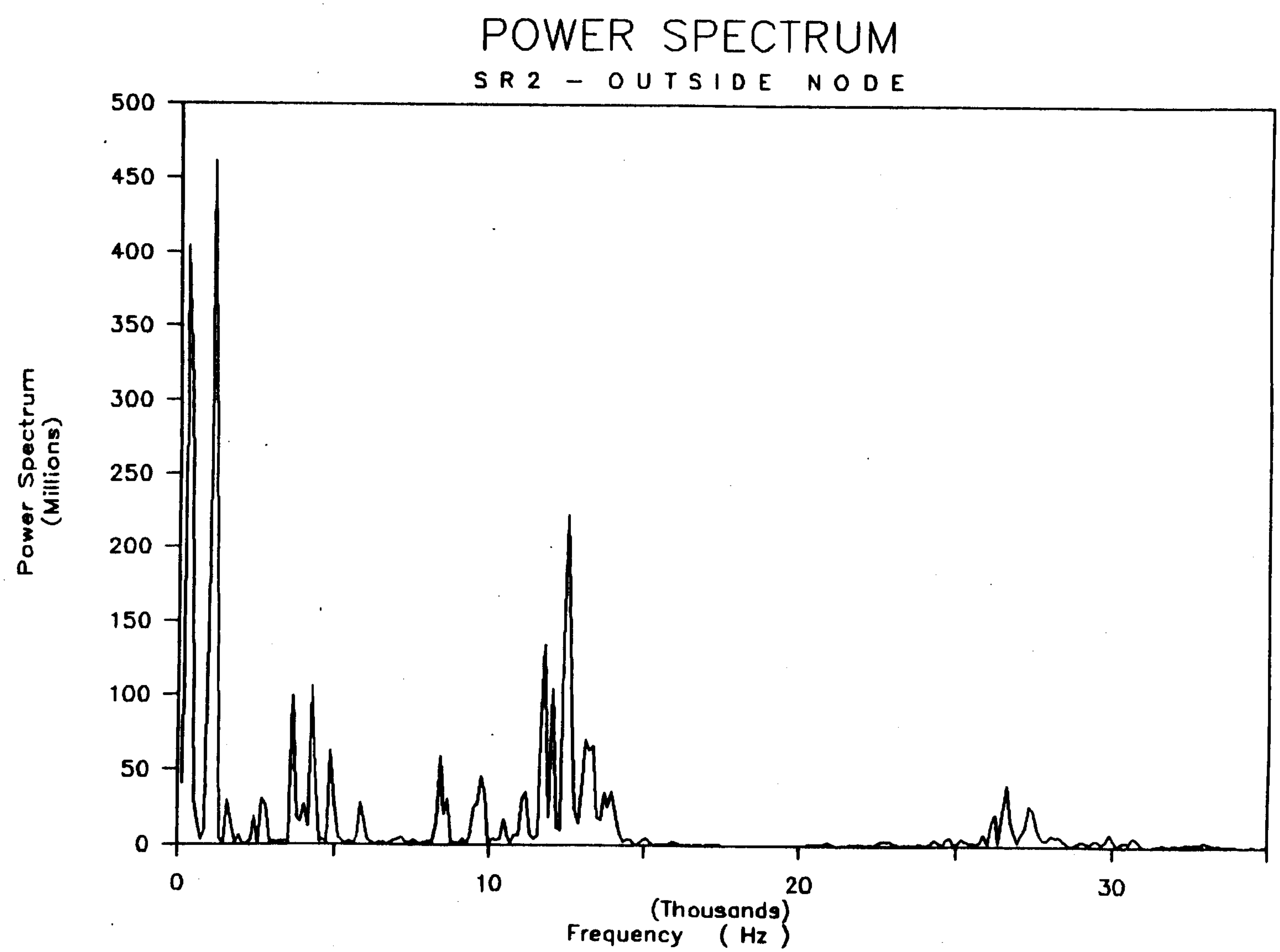

POWER SPECTRUM
SR2 – OUTSIDE NODE
Power Spectrum
(Millions)
500
450
400
350
300
250
200
150
100
50
0
0
10
20
30
(Thousands)
Frequency (Hz)

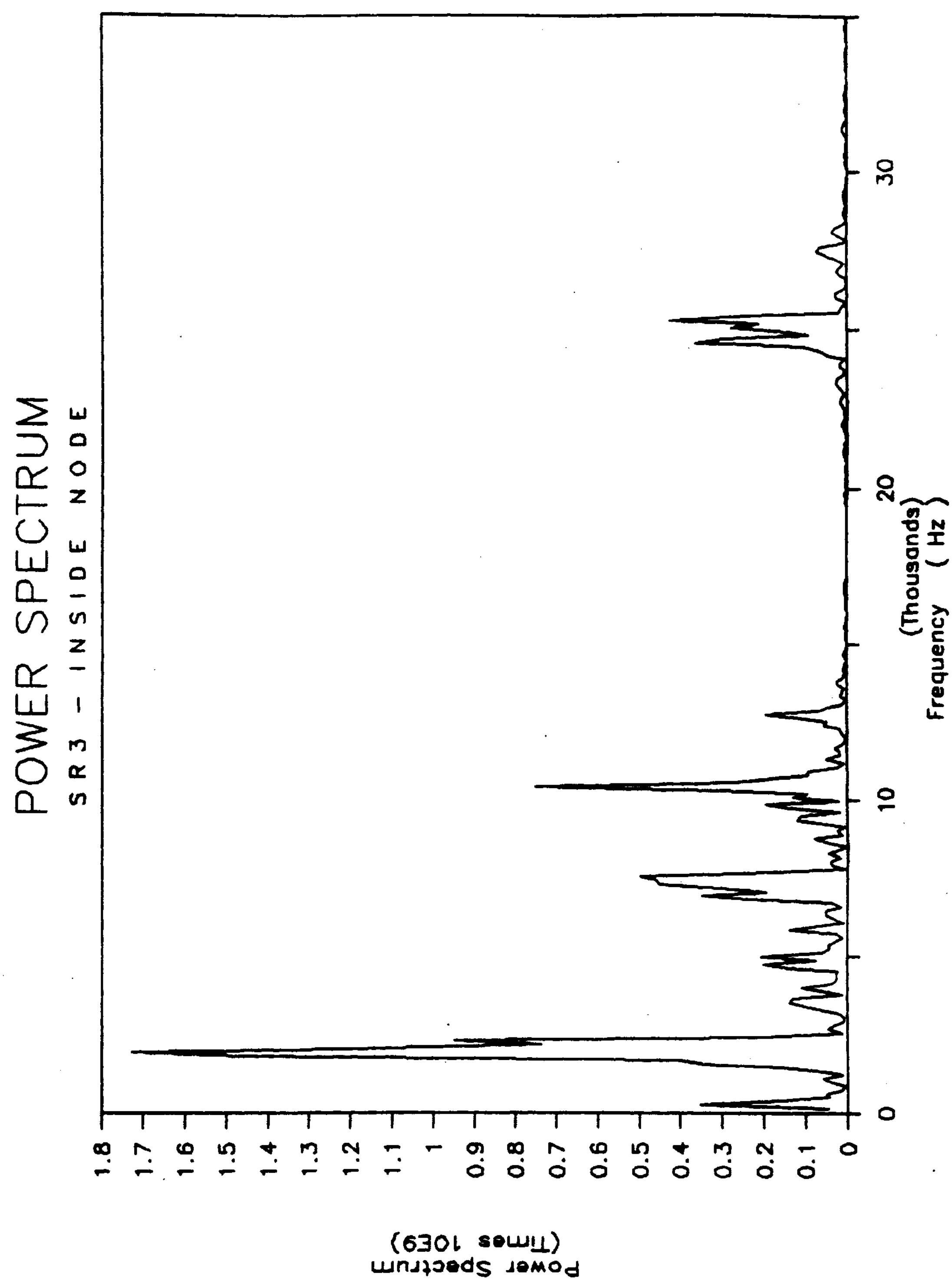
POWER SPECTRUM
SR3 - INSIDE NODE
Power Spectrum
(Times 10E9)
1.8
1.7
1.6
1.5
1.4
1.3
1.2
1.1
1
0.9
0.8
0.7
0.6
0.5
0.4
0.3
0.2
0.1
0
0
10
20
30
Frequency
(Thousands)
(Hz)

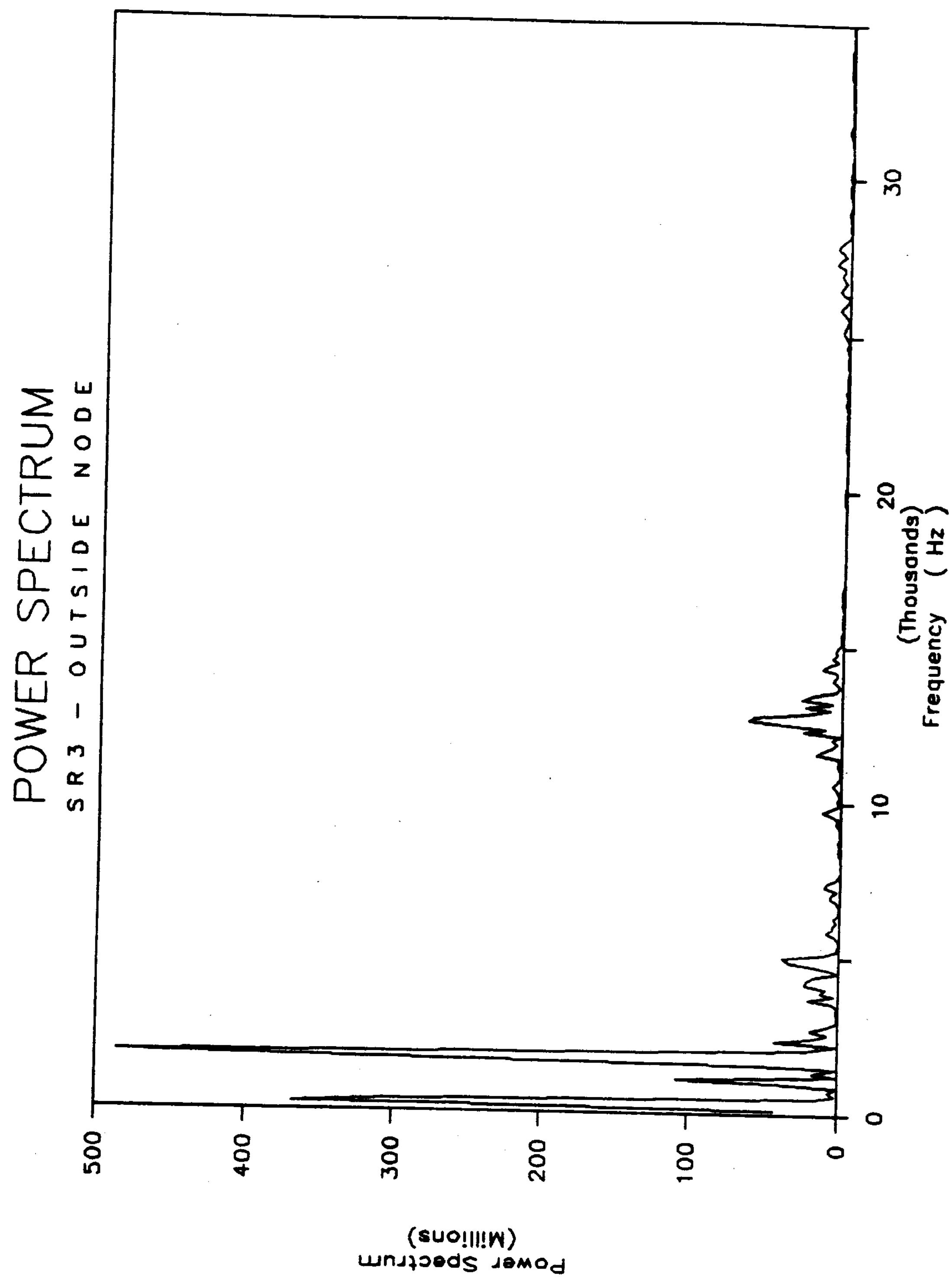
POWER SPECTRUM
SR3 - OUTSIDE NODE
Power Spectrum
(Millions)
500
400
300
200
100
0
0
10
20
30
(Thousands)
Frequency (Hz)

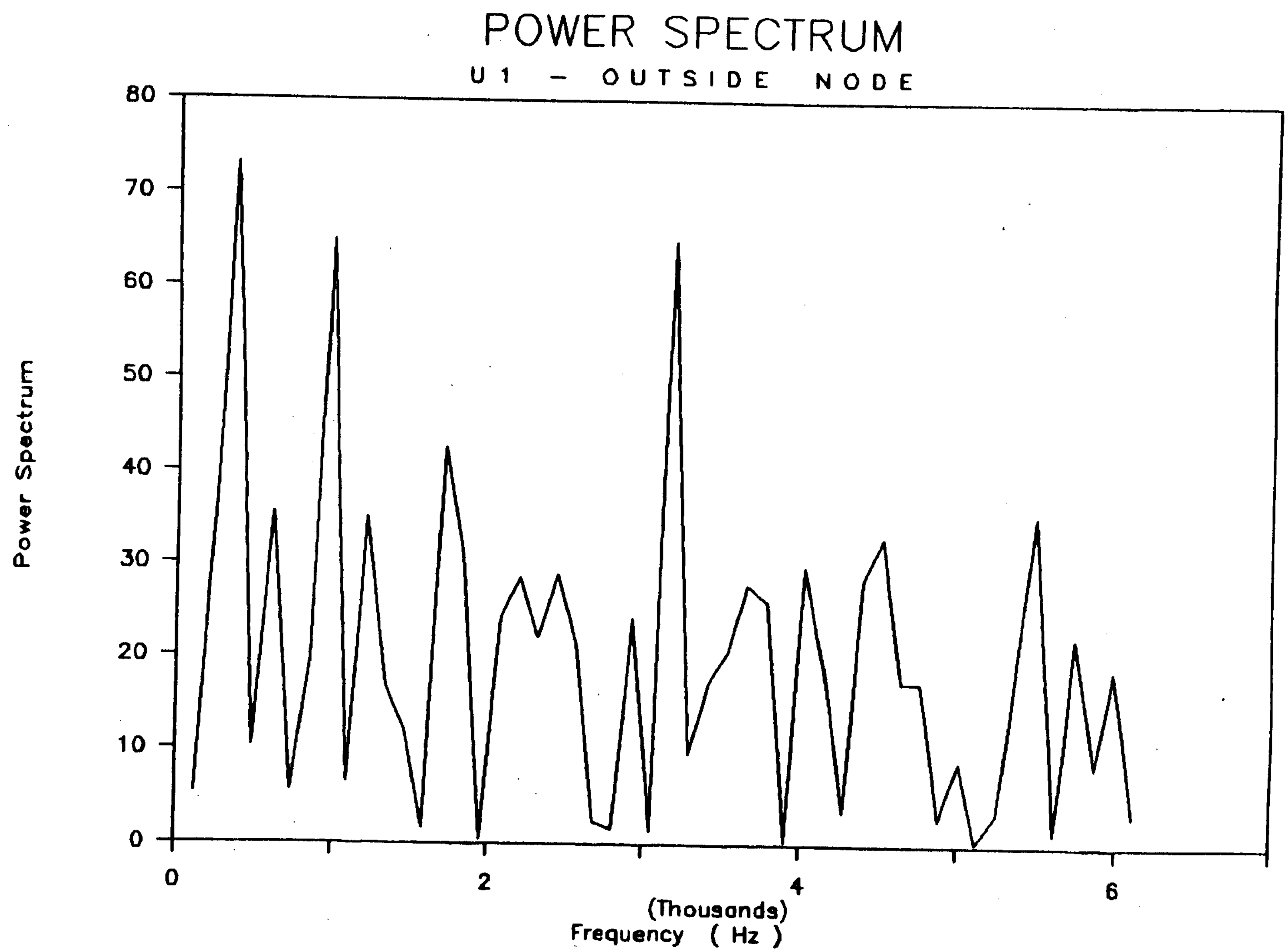
POWER SPECTRUM
U1 - OUTSIDE NODE
Power Spectrum
80
70
60
50
40
30
20
10
0
0
2
4
6
(Thousands)
Frequency (Hz)

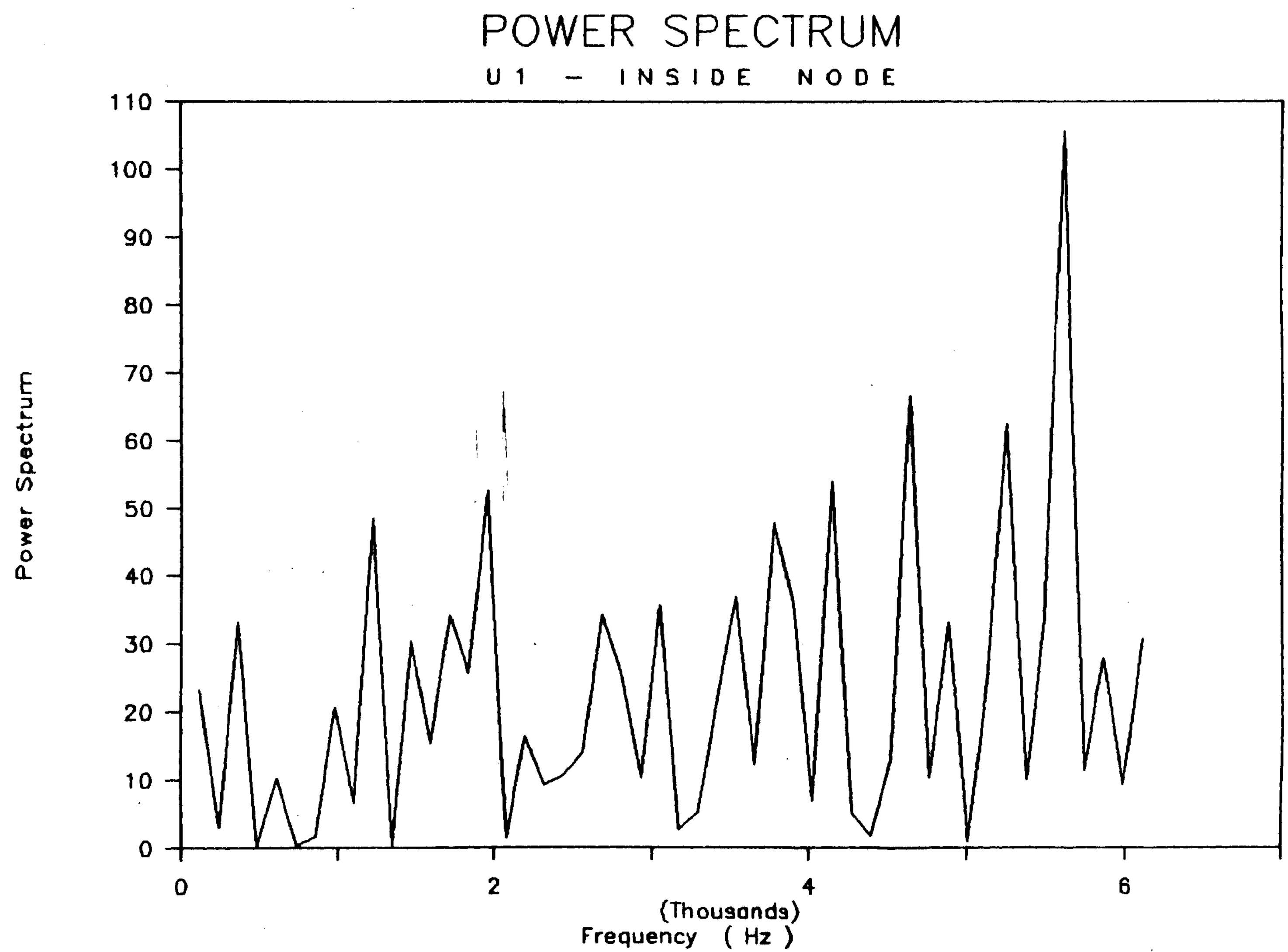
POWER SPECTRUM
U1 – INSIDE NODE
Power Spectrum
110
100
90
80
70
60
50
40
30
20
10
0
0
2
4
6
(Thousands)
Frequency (Hz)

APPENDIX D

Tables: Maximum in Power Spectrum and corresponding Frequency

The Tables in the Appendix are the ones from the following tests:

B 1	: Inside Node, Outside Node	;	B 5	: Inside Node, Outside Node
B 2	: "	;	B 6	: "
B 3	: "	;	B 7	: "
B 4	: "	;	B 8	: "
ST 1	: Inside Node, Outside Node	;	SP 1	: Inside Node, Outside Node
ST 2	: "	;	SP 2	: "
ST 3	: "	;	SP 3	: "
SU 1	: Inside Node, Outside Node	;	SQ 1	: Inside Node, Outside Node
SU 2	: "	;	SQ 2	: "
SU 3	: "	;	SQ 3	: "
SV 1	: Inside Node, Outside Node	;	SR 1	: Inside Node, Outside Node
SV 2	: "	;	SR 2	: "
SV 3	: "	;	SR 3	: "
BS 1	: Inside Node, Outside Node			
BS 2	: "			
BS 3	: "			

TEST : B1IN

Max #	Frequency (Hz)	Power Spectrum
1	366	404006944
2	1098	1009392576
3	1586	223795840
4	2196	1611124864
5	2684	555711808

Magnitude of the main peaks in the Power Spectrum plot and Frequency at which they occur.

TEST : B1OUT

Max #	Frequency (Hz)	Power Spectrum
1	366	406527360
2	1220	1152787328
3	2196	771856448
4	2684	405164448
5	3660	222684848

Magnitude of the main peaks in the Power Spectrum plot and Frequency at which they occur.

TEST : B2IN

Max #	Frequency (Hz)	Power Spectrum
1	366	436534176
2	1220	628534592
3	1708	1976213632

Magnitude of the main peaks in the Power Spectrum plot and Frequency at which they occur.

TEST : B2OUT

Max #	Frequency (Hz)	Power Spectrum
1	366	388728672
2	1220	773360576
3	1708	2188972544
4	4392	233416208

Magnitude of the main peaks in the Power Spectrum plot and Frequency at which they occur.

TEST : B3IN

Max #	Frequency (Hz)	Power Spectrum
1	366	467400576
2	1708	1588370944
3	2196	672191424
4	4148	409640992
5	4392	497068768
6	4636	242765312

Magnitude of the main peaks in the Power Spectrum plot and Frequency at which they occur.

TEST : B3OUT

Max #	Frequency (Hz)	Power Spectrum
1	366	423932832
2	1708	1947858176
3	2074	748397120
4	4148	325875552
5	4392	464750048

Magnitude of the main peaks in the Power Spectrum plot and Frequency at which they occur.

TEST : B4IN

Max #	Frequency (Hz)	Power Spectrum
1	366	363641664
2	1708	1113722496
3	2196	2957961472
4	2562	638576256
5	2928	218874000

Magnitude of the main peaks in the Power Spectrum plot and Frequency at which they occur.

TEST : B4OUT

Max #	Frequency (Hz)	Power Spectrum
1	366	333303008
2	1708	1377624192
3	2074	1618066304
4	2684	432038944
5	2928	263250656

Magnitude of the main peaks in the Power Spectrum plot and Frequency at which they occur.

TEST : B5IN

Max #	Frequency (Hz)	Power Spectrum
1	366	324687168
2	1098	251563984
3	1708	1110973824
4	2196	1511236224
5	2440	424901568
6	3904	317742048
7	4392	357990848

Magnitude of the main peaks in the Power Spectrum plot and Frequency at which they occur.

TEST : B5OUT

Max #	Frequency (Hz)	Power Spectrum
1	366	297123328
2	1098	227851536
3	1708	1345008896
4	2074	882355008
5	2684	284814144
6	3904	312486272
7	4514	271071904

Magnitude of the main peaks in the Power Spectrum plot and Frequency at which they occur.

TEST : B6IN

Max #	Frequency (Hz)	Power Spectrum
1	366	321620576
2	2196	1179138432
3	2440	693159040
4	2928	321184000
5	3660	352789504
6	3904	216047216

Magnitude of the main peaks in the Power Spectrum plot and the Frequency at which they occur.

TEST : B6OUT

Max #	Frequency (Hz)	Power Spectrum
1	366	331169760
2	2196	317847392
3	2684	361805856
4	2928	586952832
5	3904	428695328

Magnitude of the main peaks in the Power Spectrum plot and the Frequency at which they occur.

TEST : B7IN

Max #	Frequency (Hz)	Power Spectrum
1	488	244953776
2	1098	367843840
3	1708	213697056
4	2196	808263680
5	2684	723341120
6	4270	264671520

Magnitude of the main peaks in the Power Spectrum plot and the Frequency at which they occur.

TEST : B7OUT

Max #	Frequency (Hz)	Power Spectrum
1	488	316533376
2	1220	420957792
3	1708	306886496
4	2074	531778016
5	2684	674299200
6	4392	609475328

Magnitude of the main peaks in the Power Spectrum plot and the Frequency at which they occur.

TEST : B8IN

Max #	Frequency (Hz)	Power Spectrum
1	366	308815008
2	1098	661261056
3	1708	423577408
4	2196	453778464
5	2684	485257312
6	3660	415327136
7	3904	364424224

Magnitude of the main peaks in the Power Spectrum plot and the Frequency at which they occur.

TEST : B8OUT

Max #	Frequency (Hz)	Power Spectrum
1	366	313411008
2	1220	617780544
3	1708	555806016
4	2684	336857344
5	2928	420793184
6	3904	251669776

Magnitude of the main peaks in the Power Spectrum plot and the Frequency at which they occur.

TEST : ST1IN

Max #	Frequency (Hz)	Power Spectrum
1	244	1365679232
2	1098	1234105344
3	1586	1053075008
4	2440	2839922688
5	3538	369143648
6	4026	362176224
7	4392	252942272
8	4758	298577472

Magnitude of the main peaks in the Power Spectrum plot and the Frequency at which they occur.

TEST : ST1OUT

Max #	Frequency (Hz)	Power Spectrum
1	244	53148684
2	488	19450504
3	1098	20974196
4	1342	5359778
5	1708	12941211
6	2074	1355685
7	2562	31807490
8	3782	16919910
9	4270	5351515

Magnitude of the main peaks in the Power Spectrum plot and the Frequency at which they occur.

TEST : ST2IN

Max #	Frequency (Hz)	Power Spectrum
1	244	1123824000
2	732	119929344
3	1098	1080235776
4	1586	970240704
5	2440	2539303936
6	2928	115421072
7	3660	1421992192
8	3904	887312704
9	4270	1439097088
10	4636	461796416

Magnitude of the main peaks in the Power Spectrum plot and the Frequency at which they occur.

TEST : ST2OUT

Max #	Frequency (Hz)	Power Spectrum
1	244	24209370
2	488	30698276
3	854	27120594
4	1220	23929596
5	1586	13194389
6	2440	17498548
7	2806	3491533
8	3660	16313095
9	4880	10908088

Magnitude of the main peaks in the Power Spectrum plot and the Frequency at which they occur.

TEST : ST3IN

Max #	Frequency (Hz)	Power Spectrum
1	244	1069813760
2	1098	1207082624
3	1586	2322523904
4	2440	4226160896
5	3538	615272448
6	3904	539937664
7	4880	72300640

Magnitude of the main peaks in the Power Spectrum plot and the Frequency at which they occur.

TEST : ST3OUT

Max #	Frequency (Hz)	Power Spectrum
1	244	47128156
2	488	27448256
3	976	27701534
4	1586	8891145
5	1830	4885983
6	2562	47899408
7	3416	2010893
8	3660	33196058
9	4270	5080981
10	4880	6107917

Magnitude of the main peaks in the Power Spectrum plot and the Frequency at which they occur.

TEST : SU1IN

Max #	Frequency (Hz)	Power Spectrum
1	244	966926016
2	976	642547840
3	1586	2065247616
4	2074	134416784
5	2318	297165216
6	2562	327010144
7	3660	913473088
8	3904	283713952
9	4270	329035168
10	4758	596384448

Magnitude of the main peaks in the Power Spectrum plot and the Frequency at which they occur.

TEST : SU1OUT

Max #	Frequency (Hz)	Power Spectrum
1	244	146903488
2	610	39660504
3	976	45899108
4	1708	20290292
5	2440	16727928
6	2928	1703729
7	3660	12396636
8	4270	4238947
9	4880	19039450

Magnitude of the main peaks in the Power Spectrum plot and the Frequency at which they occur.

TEST : SU2IN

Max #	Frequency (Hz)	Power Spectrum
1	244	1125359488
2	976	181265312
3	1586	354799616
4	2318	180904576
5	2562	193896464
6	3172	53317480
7	3660	1010905856
8	3904	154434944
9	4270	87644816
10	4758	702429312

Magnitude of the main peaks in the Power Spectrum plot and the Frequency at which they occur.

TEST : SU2OUT

Max #	Frequency (Hz)	Power Spectrum
1	244	188130208
2	610	29277726
3	1098	32089332
4	1586	69843416
5	1952	1108805
6	2562	37366084
7	2928	1120251
8	3538	2472251
9	3782	2062609
10	4026	3407484
11	4270	16306217
12	4880	92841544

Magnitude of the main peaks in the Power Spectrum plot and the Frequency at which they occur.

TEST : SU3IN

Max #	Frequency (Hz)	Power Spectrum
1	244	794329792
2	1098	1336846080
3	1586	1657621504
4	2074	273663488
5	2562	1825969408
6	3050	116969080
7	3660	372853312
8	3904	562582528
9	4270	1409365376
10	4758	244992048

Magnitude of the main peaks in the Power Spectrum plot and the Frequency at which they occur.

TEST : SU3OUT

Max #	Frequency (Hz)	Power Spectrum
1	244	134125464
2	610	22137264
3	1098	14904301
4	1708	7978847
5	2562	67844128
6	3660	43151628
7	4270	4973242
8	4514	1917615
9	4880	99136032

Magnitude of the main peaks in the Power Spectrum plot and the Frequency at which they occur.

TEST : SV1IN

Max #	Frequency (Hz)	Power Spectrum
1	244	954775744
2	1098	866776064
3	1586	1385488384
4	2196	568230016
5	2562	1238057344
6	3660	635888192

Magnitude of the main peaks in the Power Spectrum plot and the Frequency at which they occur.

TEST : SV1OUT

Max #	Frequency (Hz)	Power Spectrum
1	244	389366688
2	732	17899320
3	1098	58736260
4	1342	5974528
5	1586	124244656
6	2440	157633808
7	2928	7723854
8	3538	14014242
9	4026	4821405
10	4270	9135825
11	4880	27117430

Magnitude of the main peaks in the Power Spectrum plot and the Frequency at which they occur.

TEST : SV2IN

Max #	Frequency (Hz)	Power Spectrum
1	366	695727360
2	1098	1835042432
3	1586	1181405952
4	2074	208220896
5	2440	811552128
6	3050	234689408
7	3660	1002351296
8	4270	786498816

Magnitude of the main peaks in the Power Spectrum plot and the Frequency at which they occur.

TEST : SV2OUT

Max #	Frequency (Hz)	Power Spectrum
1	244	241678208
2	732	21441264
3	1098	94012968
4	1586	73880624
5	2440	227022432
6	2806	10304348
7	3416	5238790
8	3660	38605696
9	4026	3376425
10	4392	5126121
11	4880	10170752

Magnitude of the main peaks in the Power Spectrum plot and the Frequency at which they occur.

TEST : SV3IN

Max #	Frequency (Hz)	Power Spectrum
1	244	588377856
2	1098	1747737728
3	1586	1727666816
4	2440	3230816256
5	3660	1698278272
6	4270	152282848
7	4758	181781696

Magnitude of the main peaks in the Power Spectrum plot and the Frequency at which they occur.

TEST : SV3OUT

Max #	Frequency (Hz)	Power Spectrum
1	244	288163360
2	732	8065860
3	1098	105479440
4	1586	112773840
5	2562	94942432
6	3294	1432387
7	3660	35399120
8	4026	14163745
9	4514	3155005
10	4758	9914428

Magnitude of the main peaks in the Power Spectrum plot and the Frequency at which they occur.

TEST : SP1IN

Max #	Frequency (Hz)	Power Spectrum
1	244	664127040
2	732	165814384
3	1098	2388368896
4	1586	2578663936
5	2562	3372720128
6	3050	300880672
7	3538	1906981248
8	3904	819724864
9	4270	1189817216
10	4758	1409755776

Magnitude of the main peaks in the Power Spectrum plot and the Frequency at which they occur.

TEST : SP1OUT

Max #	Frequency (Hz)	Power Spectrum
1	244	321926304
2	1098	173664192
3	1586	191439216
4	1830	70644136
5	2440	45273876
6	2684	79469456
7	3660	132885864
8	4270	41074648
9	4880	20208672

Magnitude of the main peaks in the Power Spectrum plot and the Frequency at which they occur.

TEST : SP2IN

Max #	Frequency (Hz)	Power Spectrum
1	244	529093536
2	732	135985120
3	1098	1493427840
4	1952	745980544
5	2318	2612300032
6	2806	157266592
7	3416	225884720
8	4026	1158543104
9	4270	2476697856
10	4758	330825024

Magnitude of the main peaks in the Power Spectrum plot and the Frequency at which they occur.

TEST : SP2OUT

Max #	Frequency (Hz)	Power Spectrum
1	244	336538240
2	1098	159976816
3	1586	32815164
4	1830	31109836
5	2562	22174410
6	3660	52594748

Magnitude of the main peaks in the Power Spectrum plot and the Frequency at which they occur.

TEST : SP3IN

Max #	Frequency (Hz)	Power Spectrum
1	244	600473984
2	1098	1118632064
3	1586	5210422784
4	2684	612485184
5	3660	672027520
6	4026	1481367040
7	4270	607025856
8	4514	590483136

Magnitude of the main peaks in the Power Spectrum plot and the Frequency at which they occur.

TEST : SP3OUT

Max #	Frequency (Hz)	Power Spectrum
1	244	274360608
2	1098	75838344
3	1586	111809392
4	4270	21126232

Magnitude of the main peaks in the Power Spectrum plot and the Frequency at which they occur.

TEST : SQ1IN

Max #	Frequency (Hz)	Power Spectrum
1	244	381335168
2	732	27755636
3	1220	1173202176
4	1586	744223104
5	2318	831194944
6	2806	95775528
7	3172	55605720
8	3416	51717004
9	3782	748776512
10	4270	381766880
11	4758	562000064

Magnitude of the main peaks in the Power Spectrum plot and the Frequency at which they occur.

TEST : SQ1OUT

Max #	Frequency (Hz)	Power Spectrum
1	244	387648096
2	1098	509758944
3	1708	205839440
4	1952	24340112
5	2440	83281808
6	2684	80444904
7	3782	128638704
8	4880	67890408

Magnitude of the main peaks in the Power Spectrum plot and the Frequency at which they occur.

TEST : SQ2IN

Max #	Frequency (Hz)	Power Spectrum
1	244	347297088
2	1220	217335168
3	1708	1282509184
4	2440	1109396608
5	3660	305885152
6	4026	523428256
7	4758	267463344

Magnitude of the main peaks in the Power Spectrum plot and the Frequency at which they occur.

TEST : sq2out

Max #	Frequency (Hz)	Power Spectrum
1	244	361532640
2	1220	26856054
3	1708	709687424
4	2440	155000560
5	2684	95150136
6	3660	307159360
7	4758	33445230

Magnitude of the main peaks in the Power Spectrum plot and Frequency at which they occur.

TEST : SQ3IN

Max #	Frequency (Hz)	Power Spectrum
1	244	335919744
2	1220	439666048
3	1586	311528352
4	1830	307348576
5	2562	1051992000
6	3782	1039643136
7	4270	628640448
8	4758	219321056

Magnitude of the main peaks in the Power Spectrum plot and the Frequency at which they occur.

TEST : SQ3OUT

Max #	Frequency (Hz)	Power Spectrum
1	244	359539072
2	1098	377178432
3	1708	382465184
4	2440	212722912
5	2684	351675680
6	3660	186229808
7	4392	101203088
8	4758	25032008

Magnitude of the main peaks in the Power Spectrum plot and the Frequency at which they occur.

TEST : SR1IN

Max #	Frequency (Hz)	Power Spectrum
1	244	418906560
2	610	82388224
3	1220	790435648
4	1830	1311241344
5	2440	625076928
6	2928	151778688
7	3660	343331456
8	3904	173631376
9	4758	637612800

Magnitude of the main peaks in the Power Spectrum plot and the Frequency at which they occur.

TEST : SR1OUT

Max #	Frequency (Hz)	Power Spectrum
1	244	424121856
2	976	51689584
3	1220	133808160
4	1708	445383360
5	2440	105546504
6	3660	124133088
7	4758	56479344

Magnitude of the main peaks in the Power Spectrum plot and the Frequency at which they occur.

TEST : SR2IN

Max #	Frequency (Hz)	Power Spectrum
1	244	364870368
2	732	112109448
3	1220	745283392
4	1830	72086896
5	2074	58911080
6	2318	121036824
7	2562	126479944
8	2806	111119600
9	3660	530636704
10	3904	1156518784
11	4270	1764038016

Magnitude of the main peaks in the Power Spectrum plot and the Frequency at which they occur.

TEST : SR2OUT

Max #	Frequency (Hz)	Power Spectrum
1	244	404634048
2	1098	461484128
3	1586	29483022
4	2684	30333034
5	3660	99279152
6	4026	26627934
7	4270	105668360
8	4880	62558660

Magnitude of the main peaks in the Power Spectrum plot and the Frequency at which they occur.

TEST : SR3IN

Max #	Frequency (Hz)	Power Spectrum
1	244	352165408
2	610	49444088
3	1098	55303036
4	1952	1726887808
5	2318	951127872
6	2684	44106156
7	3538	136005840
8	4026	108661096
9	4758	201204144

Magnitude of the main peaks in the Power Spectrum plot and the Frequency at which they occur.

TEST : SR3OUT

Max #	Frequency (Hz)	Power Spectrum
1	244	367923360
2	1098	107557744
3	1830	485500768
4	2318	42201220
5	4148	21754586

Magnitude of the main peaks in the Power Spectrum plot and the Frequency at which they occur.

TEST : BS1IN

Max #	Frequency (Hz)	Power Spectrum
1	366	558928576
2	1098	62048968
3	1708	517824064
4	2196	690801088
5	2806	166433728
6	3294	145567504
7	3904	164592416
8	4148	68179696
9	4392	88140560
10	4636	154953792

Magnitude of the main peaks in the Power Spectrum plot and the Frequency at which they occur.

TEST : BS1OUT

Max #	Frequency (Hz)	Power Spectrum
1	366	554439808
2	1220	70831112
3	1708	563843584
4	1952	774974784
5	2440	152283120
6	2806	160817392
7	3416	34229352
8	3904	284485152
9	4514	67064744

Magnitude of the main peaks in the Power Spectrum plot and the Frequency at which they occur.

TEST : BS2IN

Max #	Frequency (Hz)	Power Spectrum
1	366	687603520
2	732	177725760
3	1098	87742280
4	1708	110840144
5	2928	962477888
6	3294	123088800
7	3904	102725432
8	4148	25342946
9	4392	180509008
10	4636	164796160

Magnitude of the main peaks in the Power Spectrum plot and the Frequency at which they occur.

TEST : BS2OUT

Max #	Frequency (Hz)	Power Spectrum
1	366	665983488
2	1098	85545824
3	1708	101274664
4	2196	84620400
5	2440	150312416
6	2928	1130213760
7	3904	227191008
8	4148	148257504
9	4392	220511456

Magnitude of the main peaks in the Power Spectrum plot and the Frequency at which they occur.

TEST : BS3IN

Max #	Frequency (Hz)	Power Spectrum
1	366	537469888
2	732	49836148
3	1220	1880386688
4	1708	812451968
5	2196	144270544
6	2440	87442312
7	2684	349038592
8	2928	109324976
9	3294	255951968
10	3660	554695168
11	4148	870824192
12	4514	2378280192

Magnitude of the main peaks in the Power Spectrum plot and the Frequency at which they occur.

TEST : BS3OUT

Max #	Frequency (Hz)	Power Spectrum
1	366	547839360
2	1220	2157023744
3	1708	868856576
4	1952	239680896
5	2440	33453520
6	2684	252408000
7	3172	512684576
8	3782	248076432
9	4148	462249984
10	4392	4644845056

Magnitude of the main peaks in the Power Spectrum plot and the Frequency at which they occur.